UNIVERSITY OF CALIFORNIA, SAN DIEGO

Biomass structure and environmental relationships for phytoplankton communities in the southern California Current and adjacent ocean ecosystems

A dissertation submitted in partial satisfaction of the requirements for the degree Doctor of Philosophy

in

Oceanography

by

Andrew Grant Taylor

Committee in charge:

Michael R. Landry, Chair
Katherine Barbeau
Maarten J. Chrispeels
Peter J. S. Franks
Ralf Goericke
Mark D. Ohman

2014

The Dissertation of Andrew Grant Taylor is approved, and it is acceptable in quality and form for publication on microfilm and electronically:

_____

_____

_____

_____

_____

_____
Chair

University of California, San Diego

2014

DEDICATION

This dissertation is dedicated to my grandfather, John E. Taylor. I never got the chance to meet him, but it is because of his strong work ethic, sacrifice and drive to provide for his wife and three children, devotion to provide a higher-level education for all of his kids, and furthermore, instilling these core values into the family that I find myself in the place I am today. For everything he has done, I am eternally grateful.

TABLE OF CONTENTS

LIST OF FIGURES

Chapter 1

Chapter 2

Chapter 3

Chapter 4

LIST OF TABLES

Chapter 1

Chapter 2

Chapter 3

Chapter 4

ACKNOWLEDGEMENTS

Without question, the first person I must acknowledge is my advisor, Michael Landry. Mike's expansive knowledge of oceanography, scientific thought and understanding, insight into tackling complex problems, love of teaching and helping others, and his truly caring and respectful personality have made it an honor and a pleasure to work with him as both a graduate student and staff reach associate over the past nine years. When I first met Mike, I was in the last quarter of my undergraduate degree, and he had just moved to Scripps Institution of Oceanography. I took his Introduction to Biological Oceanography course for three reasons. First, it met one of my requirements to complete my degree. Second, I did have a genuine interest in the subject. Third, and most importantly at the time, it fit into my already busy class schedule. One day I stopped by into his office hours just to chat and get to know my professor, not knowing how this one chance encounter would alter my career path and my life. As we talked, he found out my background in microbiology and my experience with epifluorescence microscopy. He told me he just purchased a new microscope system and had this idea of using automated digital microscopy for analyzing marine microbial samples, but he needed a tech to figure it out. He offered me a job as a staff research associate, and I took it. To keep a long story short, that is how I got to where I am today. The path has been long, the road has been winding, but the rewards and results have made it all worthwhile. Mike's patience for his students and staff, his genuine love of teaching and research, his unselfish joy of seeing other people succeed, his open door policy, the level of respect he carries for

those he works with, and his reverence for the scientific process are what set him apart. These are the qualities that mark the distinction between an advisor and a *great* advisor/boss/colleague and friend.

I also must acknowledge my committee, Peter Franks, Ralf Goericke, Mark Ohman, Katherine Barbeau and Maarten Chrispeels, whom have helped make this dissertation possible. These wonderful scientists and colleagues have all been kind and gracious, helpful and guiding, understanding and influential, each in their own and unique way. Their advice, feedback and suggestions have provided while writing up this dissertation are what has molded this into a reality. Through the last minute committee meetings, reviews and suggestions on manuscripts, smiles at laughs while on month-long research cruises (0200 CTD casts; coffee while looking at profiles and making sampling decisions; jokes and smiles in the galley during dinner), tough teaching as my professors (*Arabidopsis thaliana*, oxygen utilization rates with depth, identifying zooplankton)…for all of their time and work, I am forever grateful. Oceanography is one of those special disciplines where (sometimes) we get to, or are forced to, spend *a lot* of time with colleagues in the close quarters of a research vessel. This level of personal interaction sets this field of research apart from the rest.

Elizabeth (Pooh) Venrick, has been my colleague in microscopy, plankton and the California Current Ecosystem. When I first started working for Mike as a lab tech, and had absolutely no idea about who/what/where/when/how to get things done at SIO, Pooh was always there to help and guide me in the right direction. Moreover, she helped me become a professional microscopist. While our methods differ (light

microscopy vs. digital epifluorescence microscopy) she was still able to provide more help and advice than I could ever learn from a book or journal article. How many to count? She had a good answer. What is this organism I have found here? She could always tell me, or at least pinpoint the genus and send me on the correct path of investigation. Her research into the plankton of the California Current set the stage my work is built upon. She is a pioneer of Oceanography in so many ways. I will be forever grateful to her for sharing her knowledge and experience. (By the way, *Happy Birthday* to you, Pooh! You know what I am talking about.)

My family has been an incredible resource of love and support throughout my life. To my mother, I thank you for teaching me how fun science and learning can be. You supported my inquisitive nature and fostered a child who just wanted to learn how everything in the world works. No matter how strange of an 'experiment' I thought up you allowed me to do it. Not many mothers would let their son dissect his dead gold fish before flushing it, just so he could see how a fish works. And, it takes an extraordinary mother to let her son dig up the dead hamster we buried in the back yard to see its skeleton; and then burry it back for him while he is puking after learning the hard way it can take years to decompose to bones, and that the decomposition process smells retched! When I wanted to take apart, mechanical things in the house, to learn how they function you would always let me, and you didn't get *too* angry if I was unable to put it back together again.

To my father, I thank you for all of your support as a child and throughout my college years. Your generosity and sacrifice made my higher education possible. You

also had a huge impact in teaching me appreciate and love the natural world. I will always remember the summers spent as a junior ranger in many of the national parks we would visit, and I enjoyed the many long hikes we would take so see amazing places and natural wonders. Thank you for forcing me to study as a kid when I didn't want too. Remember me sitting in grandma's kitchen and crying because I didn't want to do my math homework? Well, I'm now glad you forced me to do it.

My fellow lab mates, you have been a huge part of my graduate career and I am thankful for all of their help along the way. Dan and John, you two were the most amazing lab techs and friends. Thanks for making the long months at sea more enjoyable. It was so nice to have wonderful roommates on the ship and someone to help pass the time. Also, thanks for your excellent work with making slides and analyzing microscopy samples! Mike, Moira, Ally P., Nacho and Lorena, we go back to the beginning and shared a lot of long cruises and 0200 CTD casts, it was always an adventure. To the amazing post docs we've had in our lab over the years, Lorena, André and Eun Jin, I thank you all for help, guidance and advice you shared with me while I was a student. To our newest lab members, Ally F. and Bellineth, we haven't worked together too long, but I have enjoyed your company and getting to know you better. And lastly, to the student workers who have spent time in our lab, Daniel and Emy, I thank you for your friendship and for all of your help along the way.

And my Scripps friends outside of my lab, thank you for the good times that kept me sane! Allain and Christian, what can I say? We always have fun and it was always an escapade. Taco Tuesday, late night discussions in the grotto, fun times out

on the town and adventures at the Double Tree in Costa Rica. It was always exciting and I never knew what would transpire. Let us always keep in touch and keep hanging out.

Lastly, Angela, the love of my life, I am forever thankful that I have found you! You are the most amazing and loving person, intelligent beyond belief and have the most incredible insight into everything. It was complete serendipity how we found each other, especially when neither of us was looking. But, I guess the universe does smile upon us once in awhile. You have only been with me for the last portion of my graduate work, which is probably the hardest time, but you have always been fully understanding and supportive. You have helped to give me the strength and drive to finish. I am appreciative of everything!

Chapter 1, in full, has been published in Deep-Sea Research II: Topical Studies in Oceanography: Taylor, A.G., Landry, M.R., Selph, K.E., Yang, E.- J., 2011. "Biomass, size structure and depth distributions of the microbial community in the eastern equatorial Pacific." Deep-Sea Res. II 58, 342-357. The dissertation author was the primary investigator and author of this paper.

Chapter 2, in full, has been published in Journal of Plankton Research: Taylor, A.G., Goericke, R., Landry, M.R., Selph, K.E., Wick, D.A., Roadman, M.J., 2012. "Sharp gradients in phytoplankton community structure across a frontal zone in the

California Current Ecosystem." J. Plankton Res 34, 778-789. The dissertation author was the primary investigator and author of this paper.

Chapter 3, in full, has been submitted for publication of the material as it may appear in Deep-Sea Research II: Topical Studies in Oceanography: Taylor, A.G., Landry, M.R., Selph, K.E., Wokuluk, J.J., 2013. "Temporal and spatial patterns of microbial community biomass and composition in the southern California Current Ecosystem." Deep-Sea Res. II. The dissertation author was the primary investigator and author of this paper.

Chapter 4, in full, is currently in preparation for submission to Limnology and Oceanography: Taylor, A.G., Landry, M.R. "Patterns and variability in phytoplankton size structure, biomass and community composition across the southern California Current and adjacent ocean ecosystems." The dissertation author was the primary investigator and author of this paper.

VITA AND PUBLICATIONS

EDUCATION

2014 Doctor of Philosophy, University of California, San Diego

2013 Master of Science, University of California, San Diego

2004 Bachelor of Science, University of California, San Diego

PUBLICATIONS

Taylor, A.G. and Landry, M.R. (in prep) Patterns and variability in phytoplankton community size structure and composition with trophic state across the southern California Current and adjacent ocean ecosystems.

Taylor, A.G., Landry, M.R., Selph, K.E. and Yang, E.J. (2011) Biomass, size structure and depth distributions of the microbial community in the eastern equatorial Pacific. *Deep-Sea Res. II* 58, 342-357.

Taylor, A.G., Goericke, R., Landry, M.R., Selph, K.E., Wick, D.A. and Roadman, M.J. (2012) Sharp gradients in phytoplankton community structure across a frontal zone in the California Current Ecosystem. *J. Plankton Res.* 34, 778-789.

Taylor, A.G., Landry, M.R., Selph, K.E., and Wokuluk, J.J. (in review) Temporal and spatial patterns of microbial community biomass and composition in the southern California Current Ecosystem. *Deep-Sea Research II*.

Chekalyuk, A.M., Landry, M.R., Goericke, R., Taylor, A.G. and Hafez, M. (2012) Laser fluorescence analysis of phytoplankton across a frontal zone in the California Current Ecosystem. *J. Plankton Res.* 34, 761-777.

Li, Q.P., Franks, J.S., Landry, M.R., Goericke, R. and Taylor, A.G. (2010) Modeling phytoplankton growth rates and chlorophyll to carbon ratios in California coastal and pelagic ecosystems. *J. Geophys. Res.* 115, 1-12.

Brzezinski, M.A., Baines, S.B., Balch, W.M., Beucher, C.P., Chai, F., Dugdale, R.C., Krause, J.W., Landry, M.R., Marchi, A., Measures, C.I., Nelson, D.M., Parker, A.E., Poulton, A.J., Selph, K.E., Strutton, P.G., Taylor, A.G. and Twining, B.S. (2011) Co-limitation of diatoms by iron and silicic acid in the equatorial Pacific. *Deep-Sea Research II* 58, 493-511.

Parker, A.E., Wilkerson, F.P., Dugdale, R.C., Marchi, A.M., Hogue, V.E., Landry, M.R. and Taylor, A.G. (2011) Spatial patterns of nitrogen uptake and phytoplankton in the equatorial upwelling zone (110°W-140°W) during 2004 and 2005. *Deep-Sea Research II* 58, 417-433.

Selph, K.E., Landry, M.R., Taylor, A.G., Yang, E.J., Measures, C.I., Yang, J., Stukel, M.R., Christensen, S. and Bidigare, R.R. (2011) Spatially-resolved taxon-specific phytoplankton production and grazing dynamics in relation to iron distributions in the Equatorial Pacific between 110 and 140°W. *Deep-Sea Research II* 58, 358-377.

Landry, M.R., Selph, K.E., Taylor, A.G., Decima, M., Balch, W.M. and Bidigare, R.R. (2011) Phytoplankton growth, grazing and production balances in the HNLC equatorial Pacific. *Deep-Sea Research II* 58, 524-535.

Krause, J.W., Brzezinski, M.A., Landry, M.R., Baines, S.B., Nelson, D.M., Selph, K.E., Taylor, A.G. and Twining, B.S. (2010) The effects of biogenic silica detritus, zooplankton grazing, and diatom size structure on silicon cycling in the euphotic zone of the eastern equatorial Pacific. *Limnol. Oceanogr.* 55, 2608-2622.

Samo, T.J., Pedler, B.E., Ball, I.G., Pasulka, A.L., Taylor, A.G., Aluwihare, L.I., Azam, F., Goericke, R. and Landry, M.R. (2012) Microbial distribution and activity across a water mass frontal zone in the California Current Ecosystem. *J. Plankton Res.* 34, 802-814.

Pasulka, A.L., Landry, M.R., Taniguchi, D.A.A., Taylor, A.G., and Chruch, M.J. (2013). Temporal dynamics of phytoplankton and heterotrophic protists at station ALOHA. *Deep-Sea Research II* http://dx.doi.org/10.1016/j.dsr2.2013.01.007.

TEACHING EXPERIENCE

Teaching Assistant; Introduction to Oceanography (SIO134), UCSD undergraduate course. Winter 2012.

Teaching Assistant; California Coastal Oceanography (SIO101), UCSD undergraduate course. Fall 2013.

SELECTED MEETING PRESENTATIONS

Taylor, A. G. (2010) Using high-throughput digital microscopy to study sharp frontal transitions of microbial communities in the southern CCE. CICESE and Universidad Autonoma de Baja California, Ensenada, Mexico. (Invited talk).

Taylor, A. G., Landry, M. R., Selph, K. E. and Wick, D. A. (2010) Sharp frontal transitions of microbial communities in the southern California Current. Ocean Sciences Meeting, Portland, OR.

Taylor, A. G., Landry, M. R. and Selph, K. E. (2008) Contrasting coastal and offshore phytoplankton communities within the California Current Ecosystem. Ocean Sciences Meeting, Orlando, FL.

SEA-GOING RESEARCH PARTICIPATION

2012, August	CCE-LTER (California Current Ecosystem, Long Term Ecological Research project), Process cruise, R/V Melville
2011, June/July	CCE-LTER, Process cruise, R/V Melville
2010, June/July	Costa Rica Dome FluZiE project, R/V Melville
2009, April	CCE-LTER student cruise, R/V New Horizon
2008, October	CCE-LTER, Process cruise, R/V Melville
2007, April	CCE-LTER, Process cruise, R/V Thomas G. Thompson
2006, May	CCE-LTER, Process cruise, R/V Knorr
2005, September	Equatorial Pacific Biocomplexity project, eastern equatorial Pacific, R/V Roger Revelle
2005, January	CCE-LTER/CalCOFI, CalCOFI cruise, R/V New Horizon
2004, November	CCE-LTER/CalCOFI, Inaugural CCE cruise, R/V Roger Revelle

ABSTRACT OF THE DISSERTATION

Biomass structure and environmental relationships for phytoplankton communities in the southern California Current and adjacent ocean ecosystems

by

Andrew Grant Taylor

Doctor of Philosophy in Oceanography

University of California, San Diego 2014

Professor Michael R. Landry, Chair

The biomass, composition and size-structure of phytoplankton communities directly control many key ocean processes, such as ocean carbon cycling, food web length, trophic transfer efficiencies and biogeochemical processes. Phytoplankton communities are structured through complex interactions of bottom-up (physical processes; nutrient, light, trace metal availability) and top-down (biological processes; grazing, viral lyses, mortality) forcing that are constantly working in concert. In this dissertation I address the biomass structure and environmental relationships for

phytoplankton communities in the southern California Current and adjacent ocean ecosystems. I begin by examining the microbial communities in the eastern Equatorial Pacific (EEP), a high-nitrate, low-chlorophyll open-ocean upwelling region, where I developed and first applied an advanced digital epifluorescence microscopy system. By combing results obtained from epifluorescence microscopy with flow cytometry (FCM) I am able to obtain a fairly complete picture of the composition, biomass and size-structure of the entire microbial community throughout the euphotic zone. My finding from the EEP show that upwelling modestly alters the phytoplankton community size-structure, giving areas with enhanced diatom and dinoflagellate biomass and also increases in nano- and pico-phytoplankton. Then I applied these same methods to investigate changes in the microbial community across a strong frontal zone in the California Current Ecosystem (CCE) where the most striking features were a sharp transition between the phototrophic bacteria *Prochlorococcus* (PRO) and *Synechococcus* (SYN) and a very large (~7 fold) increase in micro-sized (>20 μm) biomass directly at the front. Lastly, I compiled data on microbial communities from four disparate regions of the central to eastern North Pacific Ocean in order to investigate interregional commonalities and differences, and to test hypothesized relationships between phytoplankton size structure and total phytoplankton biomass along trophic gradients. Here I show that there are coherent patterns and variability in the phytoplankton community size-structure and composition that are clear across a wide range of trophic states and ecosystem types.

INTRODUCTION

Marine microbial food webs

Microscopic phytoplankton comprise the base of oceanic food webs. These unicellular, photosynthetic organisms comprise only one to three precent of global primary producer biomass, but are responsible for about half of the total global primary production (Falkowski et al., 2000). The structure and composition of phytoplankton communities directly affects food web length and trophic transfer efficiencies, with regions higher in nutrients supporting larger phytoplankton and, therefore, fewer trophic steps to higher level consumers such as fish and seabirds (Ryther, 1969; Fenchel, 1988; Iverson, 1990). Additionally, many key processes of marine biogeochemistry and ocean carbon cycling, such as primary production, new production, carbon export from the euphotic zone and trace-element limitation, are strongly related to the size structure, composition and biomass of phytoplankton communities (Eppley and Peterson, 1979; Longhurst, 1991; Falkowski, 1993; Falkowski et al., 2000; Turner, 2002; Behrenfeld et al., 2006).

Because the phytoplankton base is central to understanding and modeling many processes in marine ecosystems, but often difficult to measure directly, many attempts have been made to assess phytoplankton community biomass, structure and production based on a few key, remotely sensed parameters, such as water temperature and total chlorophyll *a* (TChl) (Platt, 1986; Morel and Berthon, 1989; Behrenfeld and Falkowski, 1997; Behrenfeld et al., 2005; Perez et al., 2005). While much progress

has been made field data sets are relatively sparse for quantitatively testing or refining the information made from such approaches.

The structure and composition of phytoplankton communities is greatly influenced both by physical/chemical (bottom-up, macro- and micro-nutrient/light limitation) and by biological/trophic (top-down, grazing) forces (Tilman et al., 1982; Hecky and Kilham, 1988; Hutchins and Bruland, 1998; Calbet and Landry, 2004). While it is understood that both of these processes work in concert to organize the phytoplankton community, the mechanisms of these interactions are less well known. Several hypotheses have emerged to better explain how these two forces, and the complex mechanisms involved, interact to structure community biomass and composition. The step-addition hypothesis of Chisholm (1992) and Thingstad (1998) envisions the community response to increasing nutrient inventory (N), or increasing trophic state, as creating new niches for larger cells to be added to a stable foundation of smaller cells. This theory assumes that the smallest and most efficient competitor for nutrient uptake is a constant component of the plankton community biomass above some threshold level of N. As nutrients increase, biomass is added to the community in the form of the next smallest and efficient competitor. For each new organism (or size class) added, growth rate increases with N until a maximum rate is achieved. Thereafter, they achieve a steady state balance with the grazers of that size class, and new nutrients provide the resource niche for adding larger forms. An alternative to the step-addition hypothesis is the recent rising tide hypotheses of Barber and Hiscock (2006). The rising tide predicts that all phytoplankton size classes will increase in

response to improved nutrient conditions for growth, but large cells will show a disproportionate increase.

Methods of assessing microbial community structure

To more fully understand the environmental relationships and mechanisms involved in structuring phytoplankton communities, one must be able to make direct measurements of microbial biomass, size-structure and composition. To conduct my research for this dissertation, I used two complementary approaches for assessing the microbial community biomass and composition: an advanced digital epifluorescence microscopy system that I developed and flow cytometric (FCM) analysis of the smallest populations, such as photosynthetic bacteria. Since early days of oceanography, traditional bright field microscopy has been the standard for examining phytoplankton (Utermöhl, 1958). To this day, this settled-volume inverted microscopy method provides the best approach for identifying larger plankton at the species or genus levels. Moreover, the Utermöhl method is still the standard for identifying and estimating the biomass of more delicate organisms, such as ciliates, that cannot be enumerated by more aggressive preservation and concentration methods. Traditional bright field microscopy, however, has some drawbacks. For example, it is very labor intensive and requires many hours to process just one sample. Also, identification of plankton to the species level requires substantial expertise and training. This method is also not well suited to counting very small cells (< ~5 μm),

and it is very difficult to distinguish pigmented cells (autotrophs) from non-pigmented cells (heterotrophs), or previously living cells from detritus.

As microbial interactions were beginning to command attention in plankton research in the late 1970's and early 1980's, epifluorescence microscopy was introduced to better resolve and enumerate smaller components of the community, including recently discovered *Synechococcus*, and to distinguish heterotrophic bacteria and small flagellate grazers from primary produces of similar size (Hobbie et al., 1977; Davis and Sieburth, 1982; Haas, 1982; Caron, 1983; Sherr and Sherr, 1983). At least for eukaryotic cells, epifluorescence microscopy also has the advantage of being able to distinguish autotrophic from heterotrophic cells based on the presence or absence of chlorophyll *a* autofluorescence. Using different pore-size filters (8-µm and 0.8-µm) and magnifications (200x and 630x) on a compound epifluorescence microscope, it is possible to enumerate and measure cells ranging from < 1 to > 400 µm. Furthermore, with the addition DNA specific stains, such as 4',6-diamidno-2-phenylindole (DAPI), it is possible to distinguish living cells from detritus and, thus, get a more accurate count of the actual living biomass. However, epifluorescence microscopy does sacrifice the ability to identify most cells at the species level. Additionally, it is not suited for counting more delicate organisms, such as ciliates, which can be destroyed by the preservation and filtration steps involved. Therefore, epifluorescence microscopy and traditional light microscopy have mixed advantages and disadvantages that complement one another.

With the development of digital imaging devices, ocean researchers were quick to adapt digital cameras to epifluorescence microscopy to produce digital micrographs (Sieracki et al., 1985; Verity and Sieracki, 1993). This marriage of technologies has two important advantages for the enumeration and measurement of cells over counting and measuring by eye. First, it allows for more precise and sophisticated measurements of cell dimensions than simply estimating cell lengths and widths using an ocular grid. For example, measurements from a digital image can be made as precise as 0.1-μm $pixel^{-1}$ at 630x magnification, as opposed to estimating that a cell is ~2.3 'boxes' long from a grid. Additionally, digital imaging produces high-quality, high-fidelity records of sample contents that will not degrade over time, allowing one to go-back and reanalyze samples if needed to check consistency of identification over time, or to expanded analyses in new directions. There are, however, some important issues associated with digital epifluorescence microscopy, such as the 'halo-effect' in defining cell boundaries, the use of geometric formulas to estimate cell biovolume, and the use of biovolume to carbon conversions. Nevertheless, the benefits are substantial.

Advanced digital epifluorescence microscopy takes the imaging of samples a big step further by fully automating the acquisition of images and semi-automating the analysis of the images (Taylor et al., 2011, 2012, 2013). This is accomplished by using a computer controlled microscope that automatically scans the microscope slide, focuses on a preset number of random positions, and shifts between three or more fluorescence channels per position. Additionally, an extended depth of focus (EDF)

step is employed that takes several (5-10) z-plane images through the sample for each channel, from which totally in-focus image fields from each position can be reconstructed (Fig. 3.2). Automated acquisition is combined with semi-automated image analysis to produce a vast amount of data on phytoplankton community biomass, size-structure and composition in a high-throughput manner.

Despite its strengths, digital microscopy is not well suited for assessing the biomass contributions of the some of the smaller microbes, especially the phototrophic bacteria, *Prochlorococcus* (PRO), whose chlorophyll autofluorescence rapidly fades making it indistinguishable from the typically more abundant heterotrophic bacteria. Since the late 1980's and early 1990's, it has therefore become standard practice to use another advanced technology, flow cytometry (FCM), to enumerate autotrophic (including PRO and *Synechococcus* (SYN)) and heterotrophic prokaryotes (Olson *et al.*, 1985; Chisholm *et al.*, 1988, 1992; Monger and Landry, 1993). Such components can comprise 80% or more of the total community biomass in some oligotrophic regions, and consequently play an important role in the primary production, carbon cycling and nutrient remineralization in the oceans (Azam et al., 1983; Campbell et al., 1994). Therefore, the data provided from FCM on the biomass of prokaryotic organisms complement digital microscopy by filling an important piece of the total community biomass, size structure and composition puzzle. By combining these two complementary methods, I have been able to get a fairly complete picture of marine microbial communities in terms of carbon biomass, size-structure and composition.

Dissertation outline

The overarching goals of this dissertation are to understand the environmental relationships and mechanisms involved in structuring phytoplankton communities, to test existing hypotheses that explain these relationships, and to develop, where appropriate, new mechanistic hypotheses to explain the patterns we see. My research was conducted over a six-year period (2004 to 2010) from four areas and research programs in the central to eastern North Pacific Ocean: the California Current Ecosystem, Long Term Ecological Research (CCE-LTER) program off of southern California (Ohman et al. 2013); the Hawaii Ocean Time-series (HOT) program at ocean station ALOHA (Karl and Lukas); the Equatorial Biocomplexity (EB) project in the eastern equatorial Pacific between 110° and 140°W (Nelson and Landry 2011), and the FLUx and Zinc Experiment (FLUZiE; Stukel et al. 2013) in the Costa Rica Dome (CRD). Each of these disparate regions is distinct in its oceanic forcing and biogeochemistry, and therefore offers a different perspective for examining the environmental relationships that determine patterns of biomass, size-structure and composition of microbial communities.

While the composition of phytoplankton communities may differ in each region, reflecting the local biogeochemistry and bottom-up forcing unique to each ecosystem, some clear patterns of community size-structure and succession of compositional groups are evident across all areas studied. Common patterns derive from underlying mechanisms that shape the structure and function of the food web across diverse marine environments. Understanding these relationships and

mechanisms can help bridge the gap between empirical studies of phytoplankton ecology and large-scale ocean modeling.

In Chapter 1, entitled "Biomass, size structure and depth distributions of the microbial community in the eastern equatorial Pacific", I developed and first applied advanced digital epifluorescence microscopy system during two cruises in the eastern Equatorial Pacific (EEP). During this study I investigated the structure and distributions of phytoplankton communities in the EEP, a region of relative high-nitrate, low-chlorophyll (HNLC) constancy. The EEP is an area of active upwelling where the equatorial undercurrent shoals upward as it travels from west to east across the Pacific, injecting nutrients and iron into the base of the euphotic zone. My findings from this study indicate that this upwelling modestly alters the phytoplankton community size-structure, giving areas with enhanced diatom and dinoflagellate biomass and also increases in nano- and pico-phytoplankton. While physical processes have an effect on the phytoplankton community in some parts of the EEP, such as active upwelling areas and the passing of tropical instability waves, the region as a whole is fairly consistent, with integrated autotrophic biomass varying only 2-fold throughout the region and total community composition and carbon to chlorophyll *a* ratios being very consistent throughout the water column. Although the US Joint Global Ocean Flux Studies (JGOFS) program studied the region in the early 1990's, it lacked a systemic investigation of the phytoplankton by microscopic methods. Mine was the first to provide a comprehensive assessment of phytoplankton community

components including depth profiles of standing stocks and composition taken at over 30 stations in the region. The paper based on this chapter has been published in Deep-Sea Research II: Topical Studies in Oceanography (Taylor, A.G., Landry, M.R., Selph, K.E., Yang, E.- J., 2011).

In Chapter 2, entitled "Sharp gradients in phytoplankton community structure across a frontal zone in the California Current Ecosystem", I investigated the sharp transitions of phytoplankton communities across a strong frontal system in the California Current Ecosystem (CCE). The CCE is a highly productive coastal upwelling system that includes many diverse sub-regions, from coastal eutrophic to offshore oligotrophic. The area is also greatly influenced by strong frontal gradients and mesoscale-scale eddies that alter phytoplankton community biomass composition and size structure. During a research cruise in October 2009, I investigated the gradients and "hot spots" in the plankton community across ~25 km of a strong frontal zone in the CCE. The most striking result was the sharp transition between the phototrophic bacteria *Prochlorococcus* (PRO) and *Synechococcus* (SYN), with PRO dominating the picophytoplankton (A-Pico) biomass in the warm oligotrophic waters south of the front and SYN dominating the A-Pico biomass in the cool eutrophic waters north of the front. Both PRO and SYN were almost absent directly at the front. Another striking feature of the phytoplankton community biomass and size-structure across the frontal zone was the very large (~7 fold) increase in micro-sized (>20 μm) diatom biomass directly at the front. This increase in large and actively growing cells

is consistent with nutrient enrichment caused by physical forcing and nutrient injection directly at the front, as opposed to simply the convergent flow of communities from either side of the front. The community size structures and compositions to the north and south of the front were similar, although, higher biomass was found in the upwelling waters to the north and lower biomass was found in the oligotrophic waters to the south. The paper based on this chapter has been published in Journal of Plankton Research (Taylor, A.G., Goericke, R., Landry, M.R., Selph, K.E., Wick, D.A., Roadman, M.J., 2012).

In Chapter 3, entitled "Temporal and spatial patterns of microbial community biomass and composition in the southern California Current Ecosystem", I investigated the biomass, composition and size-structure of microbial communities within the southern CCE region from ten 'cardinal' stations on the California Cooperative Oceanic Fisheries Investigations (CalCOFI) grid during 25 quarterly cruises from 2004 to 2010. I found patterns between phytoplankton communities that followed a gradient from inshore to offshore, and northern to southern transect lines. Inshore communities were dominated by large micro-size (20 – 200 μm) diatoms and dinoflagellates, had higher overall biomass, lower functional group evenness and showed distinct seasonal cycles. Offshore communities were dominated by smaller size-class cells, lower overall biomass, greater functional group evenness and were more stable over seasonal cycles. An interesting finding of the study was the variability of autotrophic carbon-to-chlorophyll *a* ratios (AC:Chl *a*) as a function of

nitracline depth. Over the entire region AC:Chl *a* ratios in the mixed layer ranged from 40 to 80, increasing with the depth of the nitracline. There was also a very consistent relationships between total living microbial carbon (MC) and particulate organic carbon (POC), with MC comprising about half of POC. The paper based on this chapter has been submitted for publication to Deep-Sea Research II: Topical Studies in Oceanography (Taylor, A.G., Landry, M.R., Selph, K.E., Wokuluk, J.J.).

In Chapter 4, entitled "Patterns and variability in phytoplankton size structure, biomass and community composition across the southern California Current and adjacent ocean ecosystems", I combined data on the microbial communities from four regions of the central to eastern North Pacific Ocean to investigate interregional commonalities and differences, and to test hypothesized relationships between phytoplankton size structure and total phytoplankton biomass along trophic gradients. My findings in this study showed that the patterns and variability in the phytoplankton community size-structure and composition were clear across a wide range of trophic states and ecosystem types. Furthermore, the phytoplankton community biomass showed distinct size-class and compositional patterns with increasing trophic state. All size classes increase with increasing total phytoplankton biomass initially; however, pico-autotrophs decrease with further enrichment in both relative and absolute terms. I link this decline in pico-autotrophic biomass to a increased biomass and turnover rate of heterotrophic bacteria, which enhances grazing pressure on small prey. The biomass increase of larger micro-autotroph cells is rapid and monotonic, resulting in dominance of this size class at high trophic states. Changes in composition of taxonomic groups within size-classes give insight into structural

changes that occur with increasing trophic richness, while inter-regional differences reflect nutrient differences unique to each system. Understanding these patterns and their underlying mechanisms can help bridge the gap between empirical studies of phytoplankton ecology and large-scale ocean modeling. The paper based on this chapter is currently in preparation for submission to Limnology and Oceanography (Taylor, A.G., Landry, M.R.).

References

Azam, F., Fenchel, T., Field, J.G., Gray, J.S., Meyer-Reil, L.A., Thingstad, F., 1983. The ecological role of water-column microbes in the sea. Marine Ecology Progress Series 10, 257-263.

Barber, R.T., Hiscock, M.R., 2006. A rising tide lifts all phytoplankton: growth response of other phytoplankton taxa in diatom-dominated blooms. Global Biogeochemical Cycles 20, GB4S03. doi:10.1029/2006GB002726.

Behrenfeld, M.J., O'Malley, R.T., Siegel, D.A., McClain, C.R., Sarmiento, J.L., Feldman, G.C., Milligan, A.J., Falkowski, P.G., Letelier, R.M., Boss, E.S., 2006. Climate-driven trends in contemporary ocean productivity. Nature 444, 752-755.

Behrenfeld, M.J., Boss, E., Siegel, D.A., Shea, D.M., 2005. Carbon-based ocean productivity and phytoplankton physiology from space. Global Biogeochemical Cycles 19, 1-14.

Behrenfled, M.J., Falkowski, P.G., 1997. Photosynthetic rates derived from satellite-based chlorophyll concentration. Limnology and Oceanography 42, 1-20.

Calbet, A., Landry, M.R., 2004. Phytoplankton growth, microzooplankton grazing, and carbon cycling in marine systems. Limnology and Oceanography 49, 51-57.

Campbell, L., Nolla, H.A., Vaulot, D., 1994. The importance of Prochlorococcus to community structure in the central North Pacific Ocean. Limnology and Oceanography 39, 954-961.

Caron, D.A., 1983. Technique for enumeration of heterotrophic and phototrophic nanoplankton, using epifluorescence microscopy, and comparison with other procedures. Applied Environmental Microbiology 46, 491-498.

Chisholm, S.W., 1992. Phytoplankton size. In: Falkowski, P. G., Woodhead, A. D. (Eds.), Primary Productivity and Biogeochemical Cycles in the Sea. Plenum, New York, pp. 213-237.

Chisholm, S.W., Frankel, S.L., Goericke, R., Olson, R.J., Palenick, B., Waterbury, J.B., West-Johnsrud, L., Zettler, E.R., 1992. Prochlorococcus marinus nov. gen. nov. sp.: an oxyphototrophic marine prokaryote containing divinyl chlorophyll a and b. Archives of Microbiology 157, 297-300.

Chisholm, S.W., Olson, R.J., Zettler, E.R., Goericke, R., Waterbury, J.B., Welschmeyer, N.A., 1988. A novel free-living prochlorophyte abundant in the oceanic euphotic zone. Nature 334, 340-343.

Davis, P.G., Sieburth, J.M., 1982. Differentiation of the photosynthetic and heterotrophic populations of nano-plankters by epifluorescence microscopy. Ann. Inst. Oceanogr., (Paris) 58(Supl.), 249-259.

Eppley, R.W., Peterson, B.J., 1979. Particulate organic matter flux and planktonic new production in the deep ocean. Nature 282, 677-680.

Falkowski, P., Scholes, R.J., Boyle, E., Canadell, J., Canfield, D., Elser, J., Gruber, N., Hibbard, K., Hogberg, P., Linder, S., Mackenzie, F.T., Morre III, B., Pedersen, T., Rosenthall, Y., Seitzinger, S., Smetacek, V., Steffen, W., 2000. The global carbon cycle: a test of our knowledge of earth as a system. Science 290, 291-296.

Falkowski, P.G., 1993. The role of phytoplankton photosynthesis in global biogeochemical cycles. Photosynthesis Research 39, 235-258.

Fenchel, T., 1988. Marine plankton food chains. Ann. Rev. Syst. 19, 19-38.

Haas, L.W., 1982. Improved epifluorescent microscopic technique for observing planktonic micro-organisms. Ann. Inst. Oceanogr. (Paris) 58(Suppl.), 261-266.

Hickey, B., 1979. The California Current System – hypotheses and facts. Prog. Oceanogr. 8, 191-279.

Hobbie, J.E., Daley, R.J., Jasper, A., 1977. Use of nuclepore filters for counting bacteria by fluorescence microscopy. Applied and Environmental Microbiology 33, 1225-1228.

Hutchins, D.A., Bruland, K.W., 1998. Iron-limited diatom growth and Si:N uptake ratios in a coastal upwelling regime. Nature 393, 561-564.

Iverson, R.L., 1990. Control of marine fish production. Limnology and Oceanography 35, 1593-1604.

Karl, D.M., Lukas, R., 1996. The Hawaii Ocean Time-series (HOT) program: Background, rationale and field implementation. Deep-Sea Research II 43, 129-156.

Longhurst, A.R., 1991. Role of the marine biosphere in the global carbon cycle. Limnology and Oceanography 36, 1507-1526.

Monger, B.C., Landry, M.R., 1993. Flow cytometric analysis of marine bacteria with Hoechst 33342. Applied Environmental Microbiology 59, 905-911.

Morel, A., Berthon, J-F., 1989. Surface pigments, algal biomass profiles, and potential production of the euphotic layer: relationships reinvestigated in view of remote-sensing applications. Limnology and Oceanography 34, 1545-1562.

Nelson, D.M., Landry, M.R., 2011. Regulation of phytoplankton production and upper-ocean biogeochemistry in the eastern equatorial Pacific: Introduction to results of the Equatorial Biocomplexity project. Deep-Sea Res. II 58, 277-283.

Ohman, M.D., Barbeau, K.A., Franks, P.J.S., Goericke, R., Landry, M.R., Miller, A.J., 2013. Ecological transitions in a coastal upwelling ecosystem. Oceanography 26, 210-219.

Olson, R.J., Vaulot, D., Chisholm, S.W., 1985. Marine phytoplankton distributions measured using shipboard flow cytometry. Deep-Sea Research 32, 1273-1280.

Perez, V., Fernandez, E., Maranon, E., Serret, P., Garcia-Soto, C., 2005. Seasonal and interannual variability of chlorophyll a and primary production in the Equatorial Atlantic: in situ and remote sensing observations. Journal of Plankton Research 27, 189-197.

Platt, T., 1986. Primary production of the ocean water column as a function of surface light intensity: algorithms for remote sensing. Deep-Sea Research 33, 149-163.

Ryther, J.H., 1969. Photosynthesis and fish production in the sea. The production of organic matter and its conversion to higher forms of life vary throughout the world ocean. Nature 166, 72-78.

Sherr, E.B., Sherr, B.F., 1983. Enumeration of heterotrophic microprotozoa by epifluorescence microscopy. Estuarine Coastal Shelf Science 16, 1-7.

Sieracki, M.E., Johnson, P.W., Sieburth, J. McN., 1985. Detection, enumeration, and sizing of planktonic bacteria by image-analyzed epifluorescence microscopy. Applied Environmental Microbiology 49, 799-810.

Stukel, M.R., Décima, M., Selph, K.E., Taniguchi , D.A.A., Landry, M.R., 2013. The role of *Synechococcus* in vertical flux in the Costa Rica upwelling dome. Progress in Oceanography, http://dx.doi.org/10.1016/j.pocean.2013.04.003.

Taylor, A.G., Landry, M.R., Selph, K.E., Yang, E.J., 2011. Biomass, size structure and depth distributions of the microbial community in the eastern equatorial Pacific. Deep-Sea Res. II 58, 342-357.

Taylor, A.G., Goericke, R., Landry, M.R., Selph, K.E., Wick, D.A., Rodman, M.J., 2012. Sharp gradients in phytoplankton community structure across a frontal zone in the California Current Ecosystem. Journal of Plankton Research 34, 778-789, doi:10.1093/plankt/fbs036

Taylor, A.G., Landry, M.R., Selph, K.E., Wokuluk, J.J., In review. Temporal and spatial patterns of microbial community biomass and composition in the southern California Current Ecosystem. Deep-Sea Res. II.

Thingstad, T.F., 1998. A theoretical approach to structuring mechanisms in the pelagic food web. Hydrobiologia 363, 59-72.

Tilman, D., Kilham, S.S., Kilham, P., 1982. Phytoplankton community ecology: the role of limiting nutrients. Ann. Rev. Ecol. Syst. 13, 349-372.

Turner, J.T., 2002. Zooplankton fecal pellets, marine snow and sinking phytoplankton blooms. Aquat. Microb. Ecol. 27, 57-102.

Utermöhl, H., 1958. Zur vervoll kommung der quantitativen phytoplankton-methodik. Mitt. Int. Ver. Theor. Angew. Limnol. 9, 1-38.

Verity, P.G., Sieracki, M.E., 1993. Use of color image analysis and epifluorescence microscopy to measure plankton biomass. In Kemp, P. F., Sherr, B. F., Sherr, E. B. and Cole, J. J. (eds), Handbook of Methods in Aquatic Microbial Ecology. Lewis Publishers, Boca Raton, FL, pp. 327-388.

CHAPTER 1

Biomass, size structure and depth distributions of the microbial community in the eastern equatorial Pacific

Andrew G. Taylor, Michael R. Landry, Karen E. Selph, Eun Jin Yang

Abstract

We investigated the biomass, size structure and composition of microbial communities over a broad area of the eastern equatorial Pacific (4°N-4°S, 110-140°W) during cruises in December 2004 (EB04) and September 2005 (EB05). Vertical-profile samples were collected at 30 stations at depths extending from the surface to the 0.1% light level, and each sample was analyzed quantitatively by flow cytometry and epifluorescence microscopy. Autotrophic biomass averaged 14.8 ± 4.2 (1 s.d.) µg C L^{-1} for the euphotic zone, with dinoflagellates comprising 39%, *Prochlorococcus* 28%, other flagellates 18%, *Synechococcus* 7.5%, and diatoms 6.3%. Nanoplankton accounted for 46% of autotroph biomass, while pico- and microphytoplankton comprised 39 and 16%, respectively. C:Chl *a*veraged 64 ± 14 for the euphotic zone, with a mean mixed-layer value of 78 ± 20 and a minimum of 36 ± 15 at the 1% light level. Heterotrophic biomass averaged 7.0 ± 1.2 µg C L^{-1} for prokaryotes, 1.6 ± 0.9 µg C L^{-1} for dinoflagellates, 1.5 ± 1.1 µg C L^{-1} for other flagellates, and 2.1 ± 0.4 µg C L^{-1} for ciliates. Euphotic zone integrated biomass varied 2-fold, 1.2 to 2.5 g C m^{-2},

among stations, decreasing west to east with the gradient in euphotic zone concentrations of dissolved iron. Overall, community biomass and the contributions of functional groups displayed remarkable constancy over our study area, but some patterns were evident, such as the enhancement of picophytoplankton in the leading (upwelling) edges of tropical instability waves and larger diatoms in the trailing (downwelling) edges. *Prochlorococcus*, in particular, exhibited more variability than expected, given its generally assumed role as a stable background species in the tropical oceans, and was positively associated with the areas of enhanced autotrophic carbon and Chl *a*. With corrections for different methodological assumptions taken into account, our EB05 estimates of mixed-layer community biomass are 27-35% higher than values for JGOFS studies in 1992.

Introduction

The eastern equatorial Pacific (EEP) is an open-ocean upwelling region that is well known for its high-nitrate, low-chlorophyll (HNLC) characteristics, iron (Fe) fertilization response, and global significance as a source of CO2 to the atmosphere (Murray et al., 1994; Coale et al., 1996; Feely et al., 2002, 2006). The EEP is a region of zonal and meridional gradients of dissolved iron (Fe), strong currents, propagating waves, and El Niño-Southern Oscillation (ENSO) perturbations (Flament et al., 1996; Kaupp et al., 2010; Strutton et al, 2010). Yet it is also paradoxically viewed as a tightly regulated chemostat-like system that exhibits a very modest level of biological variability (Frost and Franzen, 1992; Dugdale and Wilkerson, 1998). What we know about the variability of biological communities in the EEP is however very limited. Intensive process studies along the 140°W transect in 1992 by the US Joint Global Ocean Flux Study (JGOFS), for example, provided only sparse information about community composition at a few depths and a few stations (Stoecker et al., 1996; Verity et al., 1996), while the spatial survey by Chavez et al. (1996) was restricted to surface waters and provided no physical context to assess spatial relationships.

A number of investigations have dealt with microbial communities in the equatorial Pacific (Price et al., 1994; Iriarte and Fryxell 1995; Kirchman et al., 1995; Vørs et al., 1995; Stoecker et al., 1996; Verity et al., 1996; Mackey et al., 2002; Brown et al., 2003; Yang et al., 2004), though most have focused on taxonomic subsets or size classes of the total community. Of the studies that have taken a more comprehensive approach (Chavez et al., 1996; Ishizaka et al., 1997; Brown et al.,

2003), Chavez et al. (1991, 1996) are the most spatially extensive within the EEP region, but sampling was only from the upper mixed-layer and abundances of *Prochlorococcus* were indirectly estimated. Brown et al. (2003) was the first to analyze community structure on a full transect of depth profiles across the equator (8°N to 8°S, 180°), but was located well west of the JGOFS study area (110-140ºW) in the EEP. Similarly, Ishizaka et al.'s (1997) analysis of community size structure from bacteria to mesozooplankton was located out of the JGOFS region, did not include direct assessment of *Prochlorococcus* and made no distinction between autotrophic and heterotrophic dinoflagellates. Lastly, a few studies are notable in having integrated analyses of microbial community biomass and composition with growth and grazing process experiments in the equatorial Pacific (Chavez et al., 1991, 1996; Verity et al., 1996; Landry et al., 2000, 2003), but the data set is small (~40 experiments) and the approaches quite different.

The present study is part of a larger experimental investigation of the controls on phytoplankton biomass and production in the EEP, for which we revisited the JGOFS region between 110° and 140°W on cruises in December 2004 and September 2005. We sampled the microplankton community through the euphotic zone to the 0.1% light level at 30 stations, which represents for this region a unique depth-resolved data set on autotrophic and heterotrophic biomass, size structure and composition. In addition, each of the present analyses from 8 depths/station and 30 stations is associated with experimental taxon-specific assessments of growth and grazing rates (Selph et al., 2010). Consequently, the present community biomass

analysis is part of the most comprehensive and spatially extensive study of plankton community structure, depth relationships, and process rates in EEP to date. Here we assess for the first time the magnitudes and variabilities of depth-integrated standing stocks over the broad domain of our study region, and relate them to environmental gradients and disturbance features. Where data can be compared in the surface mixed layer, we ask whether the stock levels show evidence of a change since JGOFS studies in 1992, as might be expected from the strengthening of trade winds since the late 1990s (McPhaden and Zhang, 2004; Feely et al., 2006). Lastly, these data also provide a community biomass context for companion studies of growth, grazing and production processes (Décima et al., 2010; Landry et al., 2010; Selph et al., 2010).

Materials and Methods

Sampling

We investigated the spatial variability of plankton community structure and biomass in the eastern equatorial Pacific during two cruises of the R/V Roger Revelle. Samples were collected from 9-24 December 2004 (EB04) on a meridional transect along 110ºW from 4°N to 4°S and on a zonal transect along the equator from 110° to 140°W (Fig. 1.1). Samples were collected from 8-24 September 2005 (EB05) on a meridional transect along 140°W from 4°N to 2.5°S and on a zonal transect along 0.5ºN from 140° to 123.5°W. At each of the 30 stations sampled, seawater was collected at eight depths during pre-dawn (typically 0300, local time) CTD casts. For

each station, we sampled the surface water (1-2 m) and depths corresponding to the penetration of 53, 31, 13, 7.6, 5.0, 0.8, and 0.1% of surface irradiance. Sampling depths were determined from the relationship between beam c light transmission and PAR, calibrated with mid-day CTD profiles (Balch et al., 2010). At all stations and depths, a similar suite of samples was collected for chlorophyll a and for microbial community analyses by flow cytometry and epifluorescence microscopy.

Chlorophyll a analyses

Samples (280 ml) for Chl *a* analyses were filtered onto 25-mm Gelman GF/F filters and extracted in 10 ml of 90% acetone for 24 h at -20˚C. Fluorometric analyses of chlorophyll a were made with a Turner Designs AU-10 fluorometer using equations calibrated against a pure chlorophyll a standard (Holm-Hansen et al., 1963).

Picoplankton analyses by flow cytometry

Picoplankton abundances of *Prochlorococcus* (PRO), *Synechococcus* (SYN) and non-pigmented prokaryotes (H-Bact) were determined using a shore-based flow cytometer. These samples (2 ml) were preserved with 0.5% paraformaldehyde (v/v, final concentration) frozen in liquid nitrogen, and subsequently stored at -80°C. Prior to analysis, batches of thawed samples were stained with Hoechst 33342 (1 μg ml^{-1}, v/v, final concentration) at room temperature in the dark for 1 h (Campbell and Vaulot, 1993; Monger and Landry, 1993). Aliquots (100 μl) were analyzed using a Beckman-Coulter EPICS Altra flow cytometer with a Harvard Apparatus syringe

pump for volumetric sample delivery. Simultaneous (co-linear) excitation of the plankton was provided by two argon ion lasers, tuned to 488 nm (1 W) and the UV range (200 mW). The optical filter configuration distinguished populations on the basis of chlorophyll a (red fluorescence, 680 nm), phycoerythrin (orange fluorescence, 575 nm), DNA (blue fluorescence, 450 nm), and forward and 90° side scatter signatures. Calibration beads (0.5- and 1.0-µm yellow-green beads and 0.5-µm UV beads) were used in each sample to standardize fluorescence and scatter parameters. Raw data (listmode files) were processed using the software FlowJo (Treestar Inc., www.flowjo.com). PRO and SYN abundances from flow cytometry (FCM) analyses were converted to biomass estimates using mixed-layer estimates of 32 and 101 fg C $cell^{-1}$, respectively (Garrison et al., 2000; Brown et al., 2008). These cell biomass values correspond to mean equivalent spherical diameters (ESD) of 0.65 and 0.95 µm, respectively, for PRO and SYN, assuming cell carbon densities of 0.22 pg C μm^{-3}. They are comparable also to those (35 and 100 fg C cell-1, respectively) used in a recent synthesis of microbial community structure in the equatorial Pacific (Landry and Kirchman, 2002).

Microscopical assessment of nano- and microplankton

Aliquots of 50 and 500 ml were collected for analyses of nano- and microplankton by digitally enhanced epifluorescence microscopy. The 50-ml nanoplankton samples were preserved with paraformaldehyde (0.5% final concentration) and stained with proflavin (0.33% w/v). The 500-ml microplankton

samples were preserved with 260 µl of alkaline Lugol's solution followed by 10 ml of buffered formalin and 500 µl of sodium thiosulfate (modified protocol from Sherr and Sherr, 1993), and then stained with proflavin (0.33% w/v). Preserved samples were allowed to fix at room temperature for at least one hour prior to filtration. Samples were then filtered onto black 0.8-µm (50 ml) or 8.0-µm (500 ml) Nuclepore filters overlaying 20-µm Millipore backing filters to facilitate even cell distributions. During filtration, the samples were drawn down until ~5 ml remained in the filtration tower. Concentrated DAPI (50 mg ml-1) was then added and allowed to sit briefly (5 s) before filtering the remaining sample until dry. Filters were mounted onto glass slides with immersion oil and cover slips.

Slides were imaged and digitized with a Zeiss AxioVert 200M inverted epifluorescence microscope equipped with a fully motorized stage and controlled by Zeiss AxioVision software. Digital images were captured with a Zeiss AxioCam HRc color CCD digital camera, using the auto exposure function to prevent over exposure. The fluorescence signal for each image was normalized to the exposure time, as there is a strong linear relationship between the two; although, no attempt was made to calibrate the fluorescence signal to any type of reference standard. Slides were viewed at either 630X (50-ml aliquots) or 200X (500-ml aliquots), and at least 20 random fields per slide were imaged. Each field image consisted of three- to four different fluorescent channels: Chl *a*, DAPI, FITC (50- and 500-ml aliquots), and phycoerythrin (50-ml aliquots only). The separate channel images for each field were composited into 24-bit RGB images for analysis.

Counting and sizing of eukaryotes of >1.5-µm cell lengths was semi-automated with ImagePro software. For each slide (50- and 500-ml aliquots) more than 300 cells were counted whenever possible. Seen as bright spots against a dark background, individual cells were selected and outlined in three pre-processing steps, automated using VBA script within the ImagePro software. All pre-processing steps to outline objects to be counted were performed on the green channel, corresponding to fluorescence of proflavin-stained cell protein, extracted as an 8-bit gray scale image from the original 24-bit RGB image. First, a fast Fourier transform (FFT) was applied to remove background noise and irregularities, making it easier to segment cells from the background. Second, a Laplace filter was applied to find the actual cell edges and reduce the halo effect common to epifluorescence images. Third, cells were segmented from the background, leaving an image with the segmented cells outlined. Images that did not appear to segment well and images of poor quality were discarded. The outline created after pre-processing was then applied back to the original 24-bit RGB image to collect measurements from all channels. Manual interaction was then required to split connected cells, delete artifacts, and add cells that were too dim to be segmented from the background automatically.

For the EB04 cruise, cells were identified and grouped manually into six plankton functional groups (heterotrophic flagellates, autotrophic flagellates, diatoms, heterotrophic dinoflagellates, autotrophic dinoflagellates and prymnesiophytes). Autotrophs were distinguished from heterotrophic cells by the presence of chlorophyll, seen as red autofluorescence under blue light excitation. For EB05, prymnesiophytes

were included in counts of autotrophic flagellates (A-Flag), and dinoflagellates (A-Dino) and A-Flag were distinguished by a multi-layer perceptron neural network model using NeuroSolutions software (NeuroDimensions, www.nd.com) after diatoms were identified manually. The MLP neural network model was trained with a back propagation algorithm using a data set of >22,000 manually identified cells from EB05 stations 5, 9, 15 and 23.

In addition to functional groupings, all cells were binned into five size categories (<5, 5-10, 10-20, 20-40 and >40 μm) based on measurement of the longest cell axis. Length (L) and width (W) measurements were converted to biovolumes (BV; μm3) by applying the geometric formula of a prolate sphere (BV = 0.524 L W H). For the unmeasured dimension of cell height (H), we used H = W for diatoms (95% pennate types) and H = 0.5 W for flagellates (94% of dinoflagellates were athecate). The rationale for this difference is described below. Carbon (C; pg cell-1) biomass was computed from BV from the equations of Menden-Deuer and Lessard (2000): $C = 0.216 \times BV^{0.939}$ for non-diatoms, and $C = 0.288 \times BV^{0.811}$ for diatoms.

The issue of cell height arose because previous assessments of microbial community biomass in the equatorial Pacific by Chavez et al. (1991, 1996) have utilized H:W assumptions ranging from 0.5-1.0 for different categories of flagellates. We used two types of size inferences from subsets of our samples to determine how the H:W ratio should be applied in our case. For very small flagellates, the Menden-Deuer and Lessard (2000) equations give estimates of cellular carbon density (0.22-0.23 pg C μm-3) that are approximately the same as those used for autotrophic

prokaryotes. To quantify relative carbon densities on our slides, we compared the normalized cell-integrated green fluorescence (proflavin protein binding) of our smallest size category of autotrophic flagellates (<1.8 µm ESD) to *Synechococcus* cells in the same samples. Carbon densities were found to be the same on average when the height H of the flagellate cells was 0.51 W. For larger flagellates on the 8-µm filters, we used the capabilities of our microscope to optically section individual cells and create 3D representations of biovolume (Z-stacked topographic images), from which we derived H:W relationships of 0.57 ± 0.19 (1 s.d.; unless otherwise stated, all ± terms represent one standard deviation) (n = 120) using digital analysis and 0.45 ± 0.11 (n=43) using a more subjective manual assessment of depth of focus. We conclude from these analyses that the flagellates in our samples (i.e., cells with flexible membranes) generally flattened on the filters during the slide preparation process, and that a H:W ratio of 0.5 could be reasonably applied in BV estimates for both small and large cells. A more quantitative analysis of this issue and its implications for microbial carbon biomass assessments in the oceans is needed, but is beyond the scope of the present study.

On EB04, additional samples were collected for analysis of ciliates, which were sub-optimally preserved and rarely observed in the fields counted on slides. Aliquots of 250 ml were preserved with acid Lugol's solution (final concentration 5%) and stored at room temperature in the dark. Sub-samples of 100 ml were settled in Uttermöhl sedimentation chambers for at least 24 h and counted and measured with a Zeiss inverted microscope. BV calculations were based on measured dimensions and

the closest geometric shapes for individual cells. To convert cell biovolume estimates to carbon, we used 0.19 μg C μm^{-3} for naked ciliates (Putt and Stoecker, 1989) and the equation, C (pg) = 44.5 + 0.053 lorica volume (μm^3), for loricate ciliates (Verity and Langdon, 1984).

Contour plots

Contour plots were generated using Ocean Data View (Schlitzer, 2006). A VG gridding algorithm was used for variable resolution in a rectangular grid where grid spacing varies accordingly to data density.

Results

Hydrographic and nutrient environments

Detailed descriptions of the physical and nutrient environments during our two cruises are given by Strutton et al. (2010), Dugdale et al. (2010), Kaupp et al. (2010) and Selph et al. (2010). The basic features of the system are summarized briefly below as context for our euphotic zone sampling of the microplankton community. Euphotic zone depth, defined as the depth of penetration of 0.1% surface irradiance, varied from 96 to 112 m on the equatorial transect during EB04 and from 94 to 101 m along 0.5ºN on EB05. Euphotic depths were shallowest on the western end (140°W) of these zonal transects. On N-S meridional transects, euphotic depths varied from

120 to 131 m along 110°W (EB04) and from 95 to 130 m along 140°W (EB05), deepening away from the equator.

Consistent with its HNLC (high nitrate, low chlorophyll) regional designation, surface concentrations of dissolved nitrate + nitrite (N+N) were high, typically 5-7 μM in surface waters, with lower values of 2-4 μM only at 0°, 120°W (EB04) and 0.5°N, 132.5°W (EB05) (Dugdale et al., 2010). The principal source of new nitrogen and iron to the euphotic zone in the EEP is the Equatorial Undercurrent (EUC) (Johnson et al., 2002). The EUC was usually evident between 0.5°S and 0.5°N, and the top of the EUC, seen as the depth of enhanced concentration of dissolved aluminum and >100 cm sec^{-1} eastward flow, shoaled from ~110 m at 140°W (0.1% light level) to 90 m at 110°W (Kaupp et al., 2010). Nitracline depth also shoaled to the east, rising from ~ 90 to 60 m from 140° to 110°W (Dugdale et al., 2010). Mixed-layer Fe concentrations varied opposite to the trends in EUC and nitracline depth and decreased in a W-E gradient. The highest dissolved Fe concentrations (>0.34 nM) were found in the west at 0°, 140°W, while in the east at 110ºW mixed-layer Fe concentrations were at undetectable levels (<0.08 nM) (Kaupp et al., 2010). Therefore, as the EUC shoaled in its eastward flow it appears to have been largely stripped of dissolved Fe content by biological processes, resulting in greater optical clarity of the water-column (reduced particulate concentration) and a deepening of the euphotic zone.

Relative to the very low euphotic zone concentrations of Fe at 0°, 110ºW (EB04), the shallowest depth at which Fe exceeded 0.15 nM shoaled along the 110°W meridional transect from >120 m at the equator to ~70 m at 3°S and 4°N (Selph et al.,

2010). However, at the 140ºW transect (EB05) Fe concentrations decreased sharply on either side of the upwelling region (>0.5 nM) between 1°S and the equator; nonetheless concentrations were higher than 0.2 nM in surface waters throughout the transect area from 4°N to 3°S. Therefore, the eastward decrease in Fe concentration between 140 and 110°W was a significant feature of the growth environment for phytoplankton during our study, even for stations removed from the direct effect of the EUC at the equator.

Distributions of Chl *a* and total autotrophic biomass

Depth-averaged euphotic-zone concentrations of Chl *a* varied by a factor of 2.8 (0.14-0.39 μg Chl *a* L^{-1}) in our study region (Table 1.1), with a value of 0.24 ± 0.6 μg Chl *a* L^{-1}. On the EB04 equatorial transect, mixed-layer Chl *a* was highest in the west, from 135-140°W, and concentrations decreased toward the east (Fig. 1.2a). However, a strong subsurface Chl *a* maximum was evident at 110°W between 50 and 75 m (Fig. 1.2a, d). On the 0.5°N transect for EB05, the area of elevated Chl *a* concentration (>0.3 mg Chl *a* L^{-1}) from 123.5 to 130.5°W (Fig. 1.2b) coincided with the occurrence of a Tropical Instability Wave (TIW) (Selph et al., 2010; Strutton et al., 2010). The enhanced Chl *a* between the equator and 1°S on the 140°W transect (Fig. 1.2c) was the location of active upwelling and high Fe concentration. Consistent with the E-W gradient in iron, Chl *a* values were generally lower along the 110°W transect than at comparable latitudes along the 140°W transect. The 110°W transect was further

distinguished by well-developed subsurface Chl *a* maxima (>0.25 mg Chl *a* L^{-1}), especially at the equator and at 3-4°N (Fig. 1.2d).

Depth-averaged euphotic-zone estimates of autotrophic biomass ranged 2.5-fold, from 10 to 25 μg C L^{-1}, with a mean concentration of 14.9 ± 4.1 μg C L^{-1} for the study region (Table 1.1). The EB05 transect along 140°W had the highest autotrophic carbon values (AC) (18.3 μg C L^{-1}), while mean concentrations were lowest (12.6 μg C L^{-1}) in the east at 110°W (Fig. 1.2c and d). Along the 140°W transect, the highest mixed-layer values of AC (>30 μg C L^{-1}) were located in the area of active upwelling around 1°S (Fig. 1.2c). Although distributions of autotrophic carbon have some features in common with Chl *a*, the carbon profiles are somewhat more uniform in appearance. Specifically, they do not show a corresponding significant response to the TIW during EB05 (Fig. 1.2b), nor are carbon values enhanced in the deep Chl *a* maxima seen along the 110°W transect during EB04 (e.g., Fig 2d).

The mean euphotic-zone integrated ratio of autotrophic carbon to chlorophyll a (C:Chl) was 64 ± 14 for the study area (Table 1.1). Vertical profiles of C:Chl had similar characteristics at all stations, with a mean mixed-layer value of 78 ± 20 and a minimum of 36 ± 15 at the 0.8% light level (Fig. 1.3). Between the 0.8 and 0.1% light levels C:Chl *a* estimates increased by ~50% (mean value of 53). This observed increase, however, might be due to a calculation artifact if cells in the lower euphotic zone are degrading and therefore have substantially lower C:BV than our assumed conversion factors. The highest station estimates of C:Chl (>92; 2 standard deviations above the mean) were found at 4°S, 110° on EB04 and at the equator, 140°W on

EB05. The four lowest station ratios of C:Chl (43-45; >1 standard deviation below the mean) occurred along the 0.5°N transect during EB05, with the TIW-influence area between 125 and 131ºW accounting for three of them (Table 1.1, Fig. 1.2b).

Biomass estimates of phototrophic and heterotrophic prokaryotes

Biomass estimates of the phototrophic bacteria, *Prochlorococcus* (PRO) and *Synechococcus* (SYN), averaged 5.6 µg C L^{-1} over the full euphotic zone (station range = 1.6 to 10.5 µg C L^{-1}) (Table 1.1), accounting for 37% (range 16 to 65%) of total autotrophic biomass. The mean biomass and abundance ratios, respectively, of PRO to SYN were 4:1 and 12:1. Biomass of SYN, averaging 1.5 µg C L^{-1} (range = 0.4 to 2.9 µg C L^{-1}; Table 1.1), was relatively evenly distributed on all four transects and largely confined to the upper 50 m of the water column. The highest areas of SYN biomass were between 125.7 and 127.8°W on the 0.5ºN transect (>3.5 µg C L^{-1} in the upper 25 m), and between the equator and 1°S on the 140°W transect (>2.5 µg C L^{-1} in the upper 45 m). The lowest SYN concentrations were on the 110ºW transect (average = 0.7 µg C L^{-1}). Similar high and low biomass features appear prominently in transect contour plots for PRO (Fig. 1.4). The area of high mixed-layer (>8 µg C L^{-1}, upper 30 m) biomass at 127.8°W on the 0.5°N transect (EB05) is the region of TIW influence (Fig. 1.4b), and the active upwelling area just south of the equator at 140ºW (Fig. 1.4c) had the highest PRO biomass levels (11.5 µg C L^{-1}) sampled during our study. PRO concentrations in the mixed layer were generally lower (3-5 µg C L^{-1}) along the equator during EB04 (Fig. 1.4a), with the 110°W transect showing a local

minimum (~2 μg C L^{-1}) at the equator, increasing symmetrically to the north and south (Fig. 1.4d).

Heterotrophic bacteria (H-Bact) averaged 7 μg C L^{-1} over the euphotic zone, almost double the mean biomass of total heterotrophic flagellates (including heterotrophic dinoflagellates) and 58% of total heterotrophic biomass at the stations where ciliates were included in the analyses (Table 1.2). Biomass distributions of H-Bact were similar to the trends for total autotrophs, giving a strong positive relationship between the two measurements (R^2= 0.63, $p<0.0001$; logarithmic regression) (Fig. 1.5).

Size-class distributions of autotrophic biomass

On average, nano-sized phytoplankton (A-Nano; 2-20 μm) comprised the highest proportion (mean = 46%) of total autotrophic biomass, with A-Pico (< 2 μm) and A-Micro (20-200 μm) cells comprising 39 and 16%, respectively (Table 1.1). A-Pico biomass was strongly dominated by phototrophic bacteria (Table 1.1); thus, A-Pico contours in Figure 1.6 show similar distributions and features to those in Figure 1.4. All size classes were elevated in the upwelling area on the 140°W transect between the equator and 1°S (Fig. 1.6c). On the EB04 equatorial transect (Fig. 1.6a), A-Micro differed from smaller phytoplankton in displaying a pronounced eastward decreasing gradient, a consequence of not having elevated concentrations between 110 and 120°W like smaller cells. A-Micro also differed in having a local biomass minimum in the TIW-influenced area of the 0.5°N transect on EB05 (Fig. 1.6b). A-

Nano distributions were intermediate between pico- and micro-size classes, displaying most of the local high and low features seen for the smaller cells, but with more uniform distributions along each transect. However, A-Nano biomass levels along the 0.5°N transect of EB05 was notably about a factor of two lower than on other transects.

Biomass distributions of heterotrophic flagellates

Depth-averaged biomass estimates of heterotrophic flagellates (H-Flag) from epifluorescence microscopy ranged slightly more than 5-fold, from 1.5 to 8.0 μg C L^{-1}, with a mean concentration of 3.2 μg C L^{-1} for the study region (Table 1.2). This component of the community includes heterotrophic dinoflagellates (H-Dino) and H-Flag, which contributed 1.64 versus 1.54 μg C L^{-1}, respectively, on average to total heterotrophic biomass. It does not however include the biomass contribution of ciliated protists, which is considered separately below (Section 3.6). Nano-sized heterotrophic flagellates (H-Nano, 2-20 μm) comprised the majority (mean = 72%) of the biomass, while H-Pico (<2 μm) and H-Micro (20-200 μm) cells accounted for 4 and 24%, respectively (Table 1.2). Along all transects, H-Nano distributions were similar to A-Nano, although slightly less uniform. This is most apparent on both meridional transects, where H-Nano concentrations were higher and extended deeper into the water column south of the equator at 140°W and north of the equator at 110°W (Fig. 1.7c,d). H-Nano biomass was elevated in the upwelling region between 1°S and the equator along the 140°W transect, while H-Micro biomass did not display

a pronounced maximum in this same region (Fig. 1.7c). Biomass distributions of H-Nano and H-Micro along the EB04 equatorial transect followed the same eastward decreasing gradients as autotrophic cells of comparable size (Fig. 1.7a). Both H-Nano and H-Micro had pronounced, but vertically separate, biomass maxima in the TIW-influenced area of the 0.5°N transect on EB05 (Fig. 1.7b). H-Micro biomass in the TIW-influenced area of the 0.5°N transect (mean = 1.6 μg C L^{-1}) was more than double the average on other transects (0.6 μg C L^{-1}) (Table 1.2).

Integrated community composition, biomass and size structure

For the 30 stations at which flow cytometric and epifluorescence (EPI) microscopical assessments of community biomass can be combined, the euphotic zone integrated values varied by 2-fold, ranging from 1.2 to 2.5 g C m-2, with a mean concentration of 1.8 g C m^{-2} (Table 1.4). Adding the 8-station average for ciliate biomass (0.2 g C m^{-2}) to other stations where inverted microscopy measurements were not made increases the average to 1.9 g C m^{-2}. The percentages of community biomass for each functional group identified were also fairly consistent across the study area; although compositional variability was greater than total integrated biomass, largely due to divergent responses of the different community components in the TIW area on the 0.5°N transect (Table 1.4). Biomass contributions of each phototrophic functional group to the total phytoplankton community are shown for the EB04 110°W meridional and equatorial zonal transects in Figure 1.8. Similar patterns (not shown) were also found for the EB05 140°W meridional and 0.5°N zonal

transects. Photosynthetic dinoflagellates (A-Dino) dominated the phytoplankton community, comprising 39%, on average (range 17 to 62%), of total integrated autotrophic biomass (Table 1.3). PRO (mean = 28%), A-Flag (18%, including prymnesiophytes), SYN (7.5%), and diatoms (6.3%) followed in order of their mean contributions to total autotrophs (Table 1.3).

The average integrated biomass for A-Dino was 0.54 g C m^{-2} for the study region (Table 1.4), 77% residing in the nano size class. The highest depth-integrated values for A-Dino biomass (0.9 g C m^{-2}), in the upwelling area between 1°S and the equator on the 140°W transect, reflected a large increase in >20-µm cells (Fig. 1.9c, Table 1.4). Biomass of > 20-µm A-Dino was also elevated along the EB04 equatorial transect from 127 to 140ºW (Fig. 1.9a). Along the 140°W meridional transect, vertical distributions of A-Dinos showed biomass maxima in the upper mixed layer, decreasing gradually with depth. Along the 110°W meridional transect, however, concentrations decreased rapidly below the mixed layer (Fig. 1.10d). Biomass of >20-µm A-Dinos was also elevated in the TIW-influenced area of the 0.5°N transect around 130.5°W (Fig. 1.9b).

Among the groups identified, diatoms comprised, on average, the smallest percentage (6.3%) of phytoplankton community biomass in the study area, but they also exhibited more variability (an 18-fold range, from 0.9 to 16.5%; Table 1.4) than other groups. The variability in biomass can be attributed to changes of size-class structure of the diatom community, as opposed to changes in diatom community abundance. Diatoms <20-µm showed relatively little variation in integrated biomass.

In contrast, >20-µm diatoms had distinct areas of high biomass, with the highest concentrations along the equator at 125.3ºW and 140°W (0.19 g C m^{-2}) and in the TIW-influenced area on the EB05 0.5°N transect at 132.5°W (0.22 g C m^{-2}) (Fig. 1.9a,b).

At the 8 stations along the equatorial transect of EB04 where ciliates (CIL) were analyzed by inverted microscopy, they averaged 2.1 ± 0.36 µg C L^{-1} and 220 ± 38 mg C m^{-2} for the euphotic zone, accounting for 47 ± 5.6 % of the total biomass of heterotrophic protists. Aloricate (i.e., naked) forms consistently dominated ciliate biomass (93 ± 5%; n = 64) at all stations and depths analyzed. Ciliate biomass estimates from inverted microscopy averaged 2.0 ± 0.8 times greater than estimates for H-Dino taxa by the same method. Thus, ciliates dominated the H-Micro size category, at least for this subset of EB04 stations, consistent with most H-Dino biomass residing in nano-sized cells. For the 8 stations where biomass estimates include ciliates, the depth-integrated ratio of autotrophic to heterotrophic carbon biomass (AC:HC) averaged 1.2 ± 0.16. Even without ciliates considered, comparably low ratios were found along the 0.5ºN transect on EB05, averaging only 1.1 (range 1.0 to 1.2).

Mean biomass profiles

Mean profiles of carbon biomass (± 95% confidence limits) are plotted in Figure 1.11 as a function of light depth for component groups of the EEP microbial community. While surface concentrations of Chl *a* extend relatively deep in the

euphotic zone, or are often exceeded by deep maximum values (Fig. 1.2), autotrophic carbon falls off sharply as a rule below the 10% Io light depth. Diatom biomass, on average, is highest at high light levels close to the surface and declines fairly uniformly with depth below. A-Dino biomass, which dominates the depth pattern for total autotrophs, is more uniformly high or increasing with depth in the upper third of the euphotic zone, with a sharper break at 10% Io. We did not account in our analyses for larger cell size of the deep populations of *Prochlorococcus*, which would increase their biomass at 1% light depth and below by 50 to 100% (Binder et al., 1996), and we may have also overestimated substantially (Fig. 1.3) the carbon biomass of degrading eukaryotic phytoplankton in our 0.1% Io samples. Therefore, PRO could be the dominant contributor to autotroph C at 0.1% Io. This would be consistent with DVChl *a*, the signature photosynthetic pigment of PRO, only exceeding MVChl *a* in the 0.1% Io samples (Selph et al., 2010).

Relative to autotrophs, surface concentrations of heterotrophic protists extend deeper in the euphotic zone, only declining to about half of surface values at the 0.1% light depth (Fig. 1.11). H-Dino, H-Flag and ciliates can be all be seen as significant contributors to protistan grazer biomass, with H-Flag and H-Dino sharing co-dominance of the H-Nano size class and CIL dominating the H-Micro.

Discussion

Community biomass comparisons

Previous studies of microbial community biomass, size structure, composition and carbon to chlorophyll a ratios have established a baseline of estimates for the upper euphotic zone in the eastern equatorial Pacific (EEP) region. Unfortunately, these studies are not easy to compare directly among themselves and with the present results because they involve substantial differences in measured variables, technologies (analysis by eye versus digitally enhanced images), geometric biovolume (BV) calculations and BV conversions to carbon equivalents. Nevertheless, by taking these differences into account when comparing the present study to historical estimates we can make some broad observations on how they relate and assess whether differences in microbial community abundance may have occurred over time.

To establish a climatological mean estimate of autotrophic carbon for the EEP region we use data reported by Chavez et al. (1996) and Brown et al. (2003), the most spatially extensive and complete previous studies in the equatorial Pacific. Chavez et al. (1996) reported mean estimates of autotrophic carbon in mixed-layer samples of 23.3 μg L^{-1} (n = 23 samples) during normal upwelling condition in September-December 1992, 18.6 μg C L^{-1} (n = 24) during El Niño conditions in March-May 1992, and 16.1 μg C L^{-1} (n = 20) for a suite of historical cruises between 1988 and 1990. The climatology of the area for autotroph biomass is therefore 19.4 μg C L^{-1}, which compares to estimates of 24.3 ± 4.4 μg L^{-1} (n = 53 samples) for the upper 50 m from Brown et al. (2003) and an average of 19.0 ± 6.4 μg C L^{-1} (n =120) for the upper

1/3rd of the euphotic zone in the present study. However, we need to take methodological differences between the studies into account and apply appropriate conversion factors to the historical data before we can begin to compare them quantitatively.

Chavez et al. (1996), for example, converted their indirect estimates of PRO cell abundance to carbon using a factor (24 fg C $cell^{-1}$) that is substantially lower than presently accepted values. Given the mean upper euphotic estimate of 5.5 ± 2.9 µg C L^{-1} for PRO in our samples, correcting for the lower cellular C estimates of Chavez et al (1996) should increase their autotroph biomass estimates by ~1.4 µg C L^{-1} on average. By the same token, their estimates of carbon values were elevated relative to ours by using H:W assumptions of 0.75 for athecate dinoflagellates and 1.0 for other autotrophic flagellates. We accounted for these systematic differences by applying appropriate factors to their Table 4 biomass estimates by taxonomic group, and also by reducing eukaryote biomass by an additional 10% to represent the mean offset in moving BV-corrected carbon estimates from Eppley et al. (1970) equations to the Menden-Deuer and Lessard (2000) calculations. With all of these changes, the mean mixed-layer estimates (5°N to 5°S) of autotrophic C for the EqPac Survey 1 and Survey II cruises from Chavez et al. (1996) are lowered to 15.6 and 17.5 µg C L^{-1}, respectively. Applying similar corrections to the tabulated estimates in Brown et al. (2003) give a mean value of 16.2 µg C L^{-1} for 0-50 m autotrophs collected from 4°N to 4°S at 180° under cold-tongue conditions. The grand weighted average from these previous studies is 16.4 µg C L^{-1}. Our estimates for the upper euphotic zone during

the mild El Niño condition of EB04, 16.2 ± 3.5 μg C L^{-1}, is right on this historical average. The average for ENSO-neutral conditions on EB05, 22.2 ± 7.6 μg C L^{-1}, is about 35% higher. A similar reanalysis of heterotrophic protist biomass from Chavez et al. (1996), to conform to the present methodological assumptions, yields biomass estimates 4.6 and 4.7 μg C L^{-1} for the 1992 Survey I and II cruises, respectively. Again, our EB04 estimate for heterotrophic protists (4.8 μg C L^{-1}) is very close to the historical values, while the EB05 values with ciliates added (nominally 7.5 μg C L^{-1}) are substantially higher.

Our upper-layer biomass estimate for heterotrophic protists from EPI microscopy is 4.2 ± 2.1 μg C L^{-1}. The average for EB05 (5.0 ± 2.5 μg C L^{-1}) is more than double that for EB04 (2.3 ± 0.8 μg C L^{-1}). The ciliate analysis for EB04 adds 2.5 ± 0.7 μg C L^{-1} to total mixed-layer estimates of heterotrophic protists for this cruise (i.e., mean = 4.8 μg C L^{-1}). If we assume comparable ciliate abundance during EB05, the average for that cruise increases by 50% to 7.5 μg C L^{-1}. Chavez et al. (1996) reported values of 6.5, 5.6 and 4.0 μg C L^{-1} for 1992 normal upwelling, 1992 El Niño and 1988-1990 cruises, respectively. Their EPI analyses explicitly included ciliates, which averaged 1.3-1.5 μg C L^{-1} for the two survey cruises in 1992, with mean abundance estimates of 2.1-3.0 ciliates mL^{-1}. These ciliate biomass values are somewhat lower than ours, but, given the very different approaches used, the Chavez et al (1996) abundances are reassuringly similar to our estimate of 2.6 ± 1.0 cells mL^{-1}. In contrast, Verity et al. (1996) reported extremely low densities (0.07 ± 0.04 ciliates mL^{-1}) and biomass estimates (0.2 ± 0.1 μg C L^{-1}) from inverted microscopical

analyses of formalin-preserved samples from 1992. This large discrepancy from Verity et al. (1996) and the present study would seem to suggest that most of their ciliates were lost during collection or preservation. We conclude from these comparisons that ciliates make substantially larger contributions to the consortium of protistan grazers in the equatorial Pacific than suggested by the Verity et al. (1996) study.

In a companion study, Décima et al. (2010) found that mesozooplankton biomass was 26% higher during EB05 relative to EB04, and that standing stocks compared on a comparable basis averaged 80-90% higher than collections made on the corresponding EqPac El Niño and upwelling cruises in 1992. This led Décima et al. (2010) to suggest that conditions had changed to support higher standing stocks of zooplankton since the early 1990's, similar and proportional to the documented decadal increase in mesozooplankton in the North Pacific Subtropical Gyre (NPSG) observed in monthly net sampling at Stn. ALOHA (Sheridan and Landry, 2004). The present study provides some evidence for, but falls short of fully supporting, the notion that the growth environments for mesozooplankton have been enhanced, both in the EEP and NPSG, by their linked response to increasing trade wind strength since the late 1990s (Feely et al., 2006). At the stations sampled, our community biomass assessments for EB05 are 29% higher than previous estimates for the region compared on the same basis. However, the EB04 results show no enhancement relative to historical values, which may or may not be because the stations sampled on this cruise were mostly on the low side (110°W) of the W-E biomass gradient. Regardless,

whatever mechanism supported higher standing stocks of mesozooplankton during our study, it clearly did not involve proportionally higher biomass levels of the lower trophic levels, as compared here to historical estimates for the equatorial region.

Carbon:chlorophyll ratios

For the area from 4°N to 4°S, Chavez et al. (1996) provide mixed-layer values of C:Chl, taken from plotted points in their Figure 15, of 97 ± 30 for the 1992 El Nino conditions (Survey I cruise) and 154 ± 56 for 1992 normal upwelling (Survey II). For the same latitudinal range at 180° in 1996, the C:Chl ratios of Brown et al. (2003) average 99 ± 18 for the upper 50 m of the water column. These ratio estimates decrease in proportion to the calculated changes in autotrophic carbon above, giving new estimates of 81 for Survey I, 116 for Survey II (Chavez et al., 1996), and 67 for Brown et al. (2003). Our mean mixed-layer C:Chl of 78 ± 20 is lower than all previous estimates based on microscopical analyses of the plankton community in the equatorial Pacific, but is intermediate among historical values where the calculation of autotrophic biomass derives from the same assumptions.

Our euphotic-zone integrated estimate of C:Chl (64 ± 14) is substantially lower than those from previous microscopy-based studies in the equatorial Pacific. However, it is relatively close to the commonly used value of 58 from Eppley et al. (1992), which comes from the slope of the regression of POC versus Chl *a*. On face value, Eppley's (1992) method would seem to provide an upper limit for the C:Chl *a* ratio of autotrophs, since Chl *a* is specific to phytoplankton while C comes from many

sources. However, POC measurements individually provide weak constraints to the C:Chl *a* estimate, leaving the regression analysis subject to bias by variability in the other contributors to C. In the present study, for example, autotroph carbon accounts for substantially less than half of the typical POC values of 50-100 μg C L^{-1} (Eppley et al., 1992; B. Balch, pers com.).

While the convergence of microscopical and regression-based estimates of C:Chl for the equatorial Pacific is encouraging, the application of this variable to interpreting the dynamics of the region demands some caution. There is a clear depth-dependency to this ratio (Fig. 1.3), reflecting physiological and community adaptations in the opposing gradients of light and nutrients (Fe). Mixed-layer values of 78 ± 20 would therefore be the most appropriate ratio to use for assessing mean carbon equivalents of ocean color images from satellites. The ratio also displays substantial variability, even within the mixed layer where the measurement precision is relatively good and 3 independent samples are analyzed per station. High values exceed 100 in the vicinity of the equator. For example, the 3 high-Chl *a* stations associated with equatorial upwelling (0° to 1°S) at 140°W on EB05 averaged a C:Chl ratio of 96. In contrast, three stations with similarly high Chl *a* values associated with the tropical instability wave on the same cruise (0.5°N, 125-131°W) had mean mixed-layer ratios ranging narrowly from 57 to 59. Rapid physiological responses of cellular Chl *a* content to light and nutrient conditions often give exaggerated impressions of the carbon biomass response of phytoplankton. From the above comparison, however, it should also be noted that substantial differences in phytoplankton carbon response to

differing growth environments can be masked by the appearance of chlorophyll uniformity in satellite images or shipboard measurements.

Our calculated C:Chl ratios increased between the 1.0 and 0.1% light levels at all stations. We attribute this effect to the degradation of carbon content of cells, relative to biovolume, in the deep euphotic zone. The cells contained enough DNA (DAPI fluorescence) to appear viable and were counted by microscopy. However, process studies in this portion of the euphotic zone suggest that it is a stratum of negative growth and mineral regeneration (Krause et al., 2010; Landry et al., in review). Therefore, it seems unlikely that C:BV conversion factors derived for healthy and actively growing cells would be applicable in this portion of the euphotic zone.

Microplankton composition and size structure

Given the broad area covered in the sampling on two cruises, the most striking result of our study is the relative constancy of integrated community biomass, and to a slightly lesser extent, the biomass contributions of each functional group (Fig. 1.8). As a consequence, and despite some environmental variability evident in gradients of Fe concentration, TIW effects, proximity to upwelling and ENSO conditions (EB04 occurred during mild El Niño conditions; EB05 was ENSO neutral), the mean biomass profiles for different components of the microplankton community in Figure 1.11 suggest relatively robust regional patterns of light-depth relationships. Since most previous analyses of microplankton community biomass structure in the equatorial

Pacific have been based on samples from surface waters, these light-depth patterns may be useful in extrapolating surface stocks to the rest of the euphotic zone. One important point, for example, is the substantially slower decrease in biomass of heterotrophic protists with depth in the euphotic zone compared to autotrophs. This is consistent with the observation that the grazing impact of microzooplankton may still be quite high at depths where phytoplankton growth rate is severely diminished by low light (Landry et al., in review). Thus, inferences based on the coupling of growth and loss processes in the upper layers of high light may not reflect the balance of processes for the full euphotic zone (Landry et al., in review).

Previous studies of picophytoplankton populations in the tropical Pacific, which have involved the analysis of many hundreds of samples since high-precision flow cytometry was first applied to oceanographic research in the early 1990s, have shown them to be ubiquitous and important components of the microplankton assemblage (Landry and Kirchman, 2002). *Prochlorococcus*, in particular, has appeared broadly distributed at comparable densities in subtropical gyres, the western warm pool and the HNLC eastern sector of the Pacific, suggesting that it provides to the food web a stable base of small cells upon which the more dynamic populations of larger cells are overprinted (Landry and Kirchman, 2002). Consistent with this view, we found nanophytoplankton cells to dominate autotroph biomass in our mesotrophic study region, while *Prochlorococcus* alone often comprises half or more of phototrophic biomass in adjacent oligotrophic waters of the subtropical gyres (Karl, 1999; Kraay and Veldhuis, 2004). Interestingly, however, we found that PRO and

SYN also varied appreciably (factors of 4 and 3, respectively) along physiochemical gradients in the region. Selph et al. (2010) also observed a significant relationship between phytoplankton Chl *a* and Fe concentration along the equator that was almost entirely explained by the response of the DVChl *a* specific to *Prochlorococcus* rather than the MVChl *a* found in all other phytoplankton. PRO therefore seems to have greater relative variability within the phytoplankton than previously assumed. Rather than providing a constant base to the phytoplankton assemblage, both PRO and SYN varied with total eukaryotic photosynthetic biomass in our samples, showing similar to higher biomass responses in the hot spots of biological activity associated with TIW and upwelling just south of the equator at 140°W (Fig. 1.4). On a depth-integrated basis, PRO biomass was more variable as a percent of its mean value than A-Dino biomass, but less so than diatoms or SYN. We should keep in mind, however, that the variabilities observed for PRO and SYN are at the species level, or for a small number of eco-types that dominate different depth strata. Within the broader groups of our analysis, individual species may vary much more dynamically in their abundances at different stations.

Dinoflagellates were the dominant functional group in our samples, accounting on average for 27% of total microbial community biomass (including H-Bact), and 39% of the photoautotrophs. Consistent with previous studies, dinoflagellates in the nano-size class were the major contributors to both autotrophic and heterotrophic biomass (Vørs et al., 1995; Chavez et al., 1996; Stoecker et al., 1996; Verity et al., 1996; Mackey et al., 2002; Landry et al., 2003; Yang et al., 2004).

Diatoms, in contrast, comprised a small portion of autotrophic community biomass (~6%). Nano-size pennate forms dominated numerically and were a relatively consistent component of the community. Larger (>20 μm) diatoms were rare in general, but strongly enhanced in the areas of active upwelling and near the TIW-influenced area along the equatorial and 0.5ºN zonal transects (Fig. 1.9). Even larger forms (>40 μm) dominated the community response when Fe or Fe+Si were added in microcosm grow-out experiments conducted on shipboard during the cruises (Brzezinski et al., 2010). Diatoms thus display a pronounced size dependency in terms of their ability to respond to natural variability or deliberate manipulations of growth conditions (Fe and Si concentrations) in the HNLC equatorial Pacific.

Our results indicate an autotrophic to heterotrophic biomass ratio of ~1.2 in the EEP. Prokaryotes (PRO, SYN and H-Bact) comprise 60% of the living biomass and are major contributors to both the autotrophic and heterotrophic components of the A:H ratio. Including ciliates, protistan grazers average about 39% of autotrophic carbon and 20.5% of the combined biomass of phytoplankton and H-Bact, which comprise the bulk of living food resources. Landry and Calbet (2004) have noted that 2 to 3:1 biomass ratios for autotrophs and protistan grazers are typical of open-ocean ecosystems with high grazing turnover and similar growth rates of grazers and prey. These factors suggest a relatively tight coupling between primary production and grazer utilization within the microbial community, as found previously in the EEP as well as in companion experimental studies (e.g., Landry et al., 1997, 2010; Selph et al., 2010).

H-Dino <20-µm were major contributors to heterotrophic biomass, and their distributions consistently followed Chl *a* and autotrophic biomass. H-Dinos >20 µm were more variable in distribution and most conspicuous at locations where autotrophic biomass was enhanced. Given the dinoflagellate propensity for mixotrophic nutritional strategy, predatory feeding on more efficient competitors for Fe uptake may well explain how A-Dinos dominate autotroph carbon to such an extent. In addition, widespread phagotrophy among the A-Dinos would more than double the biomass of potential protistan grazers. Using fluorescently labeled bacteria (FLB) to track the uptake of bacterial-sized prey by pigmented and non-pigmented flagellates, Stukel et al. (2010) have estimated that about half of the grazing could be due to cells that we have characterized here as autotrophs.

Physical controls on phytoplankton communities

Despite the appearance of relative constancy in many biological properties, the eastern equatorial Pacific is a dynamic region with strong currents, upwelling and propagating waves. System perturbations occur on varying time scales with changes in the strength of the trade winds, TIWs, and El Niño/La Nina events effecting nutrient delivery to the euphotic zone, and therefore biomass and production. To the west of our study region, the nutrient-rich EUC generally resides too deep to influence the euphotic zone, but it shoals as it enters the eastern equatorial Pacific, where normal upwelling conditions bring the upper EUC to photic depths. In the present study, the Fe content from upwelled EUC waters was sharply depleted between 140° and 110°W

(Kaupp et al., 2010). That gradient is reflected in our findings of a W-E zonal decrease of Chl *a* and phytoplankton biomass along the equator (Fig. 1.2a). As noted above, Selph et al. (2010) determined that the Chl *a* response was largely explained by DVChl *a*, specific to *Prochlorococcus*. In contrast, the E-W carbon gradient is most apparent for larger phytoplankton, with A-Micro showing 3-fold higher biomass levels on the western portion of the equatorial transect (Table 1.1, Fig. 1.6). While cell abundances of PRO, SYN and A-Nano phytoplankton were also higher on the western side of the transect (135-140°W, Fig. 1.4), interpretations of their biomass variations on the eastern side of our transect were more confounded by passing TIWs than those for larger autotrophs.

TIWs are anticyclonic vortices of about 500-km diameter which propagate from east-to-west along the equator, creating localized areas of upwelling and downwelling, respectively, on their leading and trailing edges (Flament et al., 1996). During the equatorial transect on EB04, the broad band of relatively low biomass between our sampling stations at 120° and 127°W was an area of strong southern flow (ADCP currents), and therefore in the trailing edge of a TIW (Selph et al., 2010). Since we traveled in the direction of TIW propagation on this cruise, we likely sampled the same feature at different locations over several days. At 116°W, samples from the leading edge (northward flow) of an adjacent vortex showed strong enhancement of PRO (A-Pico) and A-Nano, but no effect on larger phytoplankton (Fig. 1.6a). Similarly, stations sampled in the leading edge of a TIW (northward currents of >50 cm s^{-1}) between 125° and 130°W on the 0.5°N transect during EB05

showed pronounced increases in Chl *a*, PRO, A-Pico, H-Nano and A-Nano, but A-Micro biomass was anomalously low (Figs. 2, 4 and 6). Larger diatoms (>20 μm) were highest at two locations of southerly flow (125°W on the EB04 equatorial line, and 132.5°W on the EB05 0.5°N line), presumably catching TIW trailing edges. These few observations suggest that smaller and larger size classes of phytoplankton have different areas of enhancement in the TIW flow field and may vary out-of-phase spatially. Dynamically, it is not clear how in situ growth versus advective processes determine these observed effects. This is an area where Lagrangian-based experimental process studies tracking the movement of water parcels would be very helpful in elucidating the temporal and spatial scales of variability in TIWs and their relationships to ocean ecology and biogeochemistry.

Advective processes clearly have important influences on distributional patterns off the equator. The expected symmetry in biomass distributions as upwelled waters diverge to either side of the equator is best illustrated for the EB04 transect along 110°W (Figs. 2, 4, 6, 10). Symmetry was not evident, however, in sampling along the 140°W transect, where strong southward flow at the time of sampling pushed the center of the upwelling divergence to about 1°S. It is interesting to note that biomass levels for most plankton groups showed local minima in the zone of active equatorial upwelling at 110°W, while the area of upwelling centered south of 140° on EB05 was the site of biological enhancement for the same groups (Figs. 2, 4, 6, 10). Small and large plankton size classes co-vary at these two sites, presumably in response to the E-W gradient of bioavailable Fe, but different from the spatial

separation of small and large cells in TIW flows. Selph et al. (2010) have suggested that variations in modes and rates of Fe delivery to the euphotic zone can impact the community structure of equatorial plankton in ways that are not expected from direct Fe fertilization of surface waters or shipboard microcosms (e.g., Coale et al., 1996). Our results further indicate that, even in a system renowned for its relative constancy, community responses to different drivers of physical variability do not necessarily follow the same pattern.

Conclusions

For 30 stations sampled over a broad area during two cruises in the eastern equatorial Pacific, the microplankton community displayed a remarkable constancy in integrated biomass, composition, size and depth structure, despite substantial environmental gradients and perturbations to the system from upwelling and TIWs. Nonetheless, the community was not everywhere the same, nor did it respond to environmental variability following a consistent pattern. Of particular note, *Prochlorococcus* exhibited surprising variability given its generally assumed role as a stable background species in the tropical oceans. Higher concentrations of *Prochlorococcus* generally defined the areas of enhanced autotrophic carbon and Chl *a*, more so, in the case of the leading edges of TIWs, than the biomass of larger phytoplankton. Such complexities and departures from conventional wisdom speak to the potential difficulties of interpreting the fine-scale dynamics of phytoplankton

community biomass and size structure from remotely sensed optical signals (e.g., Mouw and Yoder, 2005). Even when ambient standing stocks are directly measured, however, there are significant challenges remaining in understanding and modeling microbial community dynamics of the region. The present data, for example, do not elucidate the temporal and spatial scales of community responses to physical perturbations like upwelling and TIWs, which may have important implications for production processes, trophic coupling and biogeochemical cycling in the equatorial region. Future experimental studies need to be designed to understand community trajectories and underlying process rates in water parcels entrained in the equatorial flow field.

Acknowledgements

We thank the captain and crew of the R/V Roger Revelle for their professional and enthusiastic support of this project, and Mark Hodges, Michael Stukel, Darcy Taniguchi Daniel Wick and Emy Daniels for their help with the preparation and imaging of the samples. This work was funded by subcontracts to Scripps Institution of Oceanography and the University of Hawaii at Manoa from NSF Biocomplexity grant OCE 03-22074, administered through Oregon State University (D. Nelson, PI).

Chapter 1, in full, has been published in Deep-Sea Research II: Topical Studies in Oceanography: Taylor, A. G., Landry, M. R., Selph, K. E., Yang, E.- J., 2011. "Biomass, size structure and depth distributions of the microbial community in

the eastern equatorial Pacific." Deep-Sea Res. II **58:** 342-357. The dissertation author was the primary investigator and author of this paper.

Table 1.1. Mean station biomass concentrations of autotrophic bacterioplankton, *Prochlorococcus* (PRO) and *Synechococcus* (SYN); mean abundance and biomass of autotrophic eukaryotes by size class. A-Pico (0.2-2 μm), A-Nano (2-20 μm) and A-Micro (20-200 μm). Mean concentrations of total chlorophyll *a* (Chl), and mean autotrophic carbon to chlorophyll *a* ratio (C:Chl). Units are cells ml^{-1} for abundance, μg C L^{-1} for biomass, and μg Chl *a* L^{-1} for chlorophyll.

				Abundance (cells ml^{-1})			Biomass (μg C L^{-1})							
Cruise	Station	Lat	Lon (°W)	A-Pico	A-Nano	A-Micro	PRO	SYN	A-Pico	A-Nano	A-Micro	Chl	AC	C:Chl
EB04	3	3°N	110	160,000	3,400	13.3	4.7	1.0	0.12	7.0	1.7	0.25	14.5	61
	4	2°N	110	130,000	3,400	10.1	3.8	0.8	0.11	7.5	2.4	0.24	14.6	62
	5	1°N	110	60,000	3,800	12.3	1.6	0.7	0.14	7.0	2.9	0.20	12.3	62
	7	0°	110	60,000	3,000	13.0	1.8	0.6	0.13	5.6	1.6	0.23	9.8	54
	9	1°S	110	40,000	3,400	24.9	1.2	0.4	0.13	6.7	1.8	0.20	10.2	56
	10	2°S	110	120,000	3,500	9.2	3.6	0.6	0.09	7.5	1.1	0.20	12.8	66
	11	3°S	110	120,000	2,600	9.9	3.6	0.6	0.08	7.1	1.1	0.15	12.5	85
	12	4°S	110	160,000	2,800	12.7	4.9	0.5	0.09	7.1	1.4	0.14	14.0	101
	14	0°	116	170,000	3,200	16.8	5.2	0.9	0.10	8.3	1.6	0.21	16.1	76
	16	0°	120	50,000	2,700	26.3	1.5	0.7	0.10	6.9	1.6	0.18	10.9	59
	18	0°	122.5	80,000	2,600	18.7	2.2	0.9	0.09	7.8	2.4	0.20	13.3	67
	20	0°	125.3	100,000	2,800	11.0	3.0	0.5	0.13	4.4	2.0	0.21	10.0	38
	22	0°	128	80,000	3,400	24.9	2.2	0.7	0.11	8.0	2.1	0.23	13.2	59
	24	0°	131	60,000	2,600	14.0	1.8	0.8	0.10	6.3	2.3	0.19	11.3	62
	26	0°	135	150,000	3,500	29.3	4.6	0.8	0.11	7.5	2.8	0.24	15.9	64
	29	0°	140	150,000	4,000	13.7	4.3	1.3	0.10	9.3	4.2	0.29	19.1	67
EB05	1	4°N	140	180,000	1,200	5.4	5.4	1.0	0.33	3.7	2.2	0.23	12.6	58
	3	2.5°N	140	140,000	3,400	8.5	4.1	1.1	0.63	7.2	2.1	0.20	15.2	82
	5	1°N	140	120,000	3,800	18.7	3.4	0.9	0.07	9.6	1.8	0.22	15.8	74
	7	0.5°N	140	170,000	1,500	7.9	5.1	1.4	0.19	4.1	1.5	0.27	12.4	43
	9	0°	140	260,000	5,800	29.2	7.5	2.4	0.21	12.2	2.2	0.25	24.6	94
	11	0.5°S	140	270,000	3,800	15.4	8.0	2.4	0.85	8.6	4.7	0.39	24.4	60
	13	1°S	140	260,000	5,600	15.3	7.5	2.2	0.96	9.8	5.1	0.35	25.5	72
	15	2.5°S	140	150,000	3,900	32.5	4.4	1.4	0.08	7.8	2.3	0.24	16.0	67
	18	0.5°N	132.5	190,000	1,000	19.8	5.6	1.8	0.13	4.2	4.6	0.23	16.3	71
	19	0.5°N	130.5	180,000	800	16.8	5.3	1.6	0.11	2.8	2.6	0.26	12.3	45
	20	0.5°N	127.8	270,000	900	21.5	7.6	2.9	0.08	5.0	2.1	0.36	17.6	44
	21	0.5°N	125.7	230,000	1,000	54.7	6.5	2.5	0.14	2.9	1.7	0.31	13.7	44
	22	0.5°N	123.5	160,000	1,100	15.7	4.4	2.2	0.22	3.7	2.6	0.24	13.1	54
	23	1.75°N	125	150,000	2,500	11.9	4.1	2.2	0.37	7.4	1.8	0.23	15.8	68

Table 1.2. Mean station concentrations of heterotrophic bacteria (H-Bact) and ciliate (CIL) biomass, and heterotrophic eukaryote abundance and biomass by size class. H-Pico (0.2-2 μm), H-Nano (2-20 μm) and H-Micro (20-200 μm). H-Protist biomass is w/o CIL. Total heterotrophic biomass (HC) is w/CIL. Units are cells mL^{-1} for abundance, and μg C L^{-1} for biomass.

				Abundance (cells ml^{-1})			Biomass (μg C L^{-1})						
Cruise	Station	Lat	Lon (°W)	H-Pico	H-Nano	H-Micro	HBACT	H-Pico	H-Nano	H-Micro	Cilliates	H-Protist	HC
EB04	3	3°N	110	890,000	1,300	1.0	8.9	0.04	1.4	0.3	nd	1.8	10.7
	4	2°N	110	700,000	1,000	0.8	7.0	0.04	1.4	0.2	nd	1.6	8.6
	5	1°N	110	490,000	900	1.0	4.9	0.03	1.4	0.4	2.0	3.9	10.9
	7	0°	110	560,000	1,000	1.0	5.6	0.03	1.5	0.3	1.9	3.7	11.2
	9	1°S	110	430,000	1,000	1.1	4.3	0.05	1.5	0.4	1.9	3.8	10.1
	10	2°S	110	660,000	1,000	0.4	6.6	0.04	1.3	0.2	nd	1.5	8.2
	11	3°S	110	760,000	800	1.1	7.6	0.03	1.3	0.4	nd	1.7	9.3
	12	4°S	110	750,000	1,000	1.1	7.5	0.03	1.6	0.4	nd	2.1	9.5
	14	0°	116	750,000	900	1.8	7.5	0.03	1.9	0.6	nd	2.5	10.1
	16	0°	120	570,000	1,000	2.1	5.7	0.05	1.6	0.7	1.4	3.8	11.0
	18	0°	122.5	740,000	900	1.5	7.4	0.03	2.0	0.5	1.9	4.5	13.8
	20	0°	125.3	560,000	700	0.9	5.6	0.02	1.1	0.4	nd	1.5	7.1
	22	0°	128	510,000	800	0.9	5.1	0.03	1.9	0.2	2.5	4.5	12.0
	24	0°	131	590,000	800	2.3	5.9	0.03	1.9	0.8	2.0	4.5	11.6
	26	0°	135	620,000	1,100	2.7	6.2	0.03	2.7	0.9	nd	3.6	9.9
	29	0°	140	860,000	1,000	1.1	8.6	0.05	1.6	0.3	2.9	4.9	16.3
EB05	1	4°N	140	720,000	500	2.9	7.2	0.12	1.6	1.4	nd	3.1	10.4
	3	2.5°N	140	600,000	500	3.3	6.0	0.13	1.4	1.4	nd	2.9	8.9
	5	1°N	140	630,000	2,800	0.8	6.3	0.14	2.4	0.2	nd	2.8	9.1
	7	0.5°N	140	690,000	1,000	0.9	6.9	0.12	1.7	0.3	nd	2.1	9.0
	9	0°	140	830,000	6,800	2.1	8.3	0.16	7.0	0.9	nd	8.0	16.3
	11	0.5°S	140	800,000	1,900	2.9	8.0	0.44	4.2	1.0	nd	5.6	13.5
	13	1°S	140	860,000	1,600	1.5	8.6	0.42	2.6	0.5	nd	3.6	12.2
	15	2.5°S	140	850,000	3,000	2.8	8.5	0.10	4.3	1.1	nd	5.5	14.0
	18	0.5°N	132.5	720,000	1,200	3.1	7.2	0.22	2.4	1.6	nd	4.2	11.5
	19	0.5°N	130.5	730,000	1,000	4.3	7.3	0.13	2.3	1.4	nd	3.7	11.1
	20	0.5°N	127.8	690,000	1,600	5.3	6.9	0.23	3.4	1.9	nd	5.6	12.5
	21	0.5°N	125.7	760,000	1,800	3.8	7.6	0.24	3.6	1.3	nd	5.2	12.8
	22	0.5°N	123.5	770,000	1,300	3.6	7.7	0.22	2.4	1.6	nd	4.2	11.9
	23	1.75°N	125	890,000	1,600	3.1	8.9	0.32	3.6	0.9	nd	4.9	13.7

Table 1.3. Percentage contribution of each phytoplankton functional type to euphotic-zone integrated biomass of the autotrophic community along the 110ºW and equatorial transects (2004), and the 0.5ºN and 140ºW transects (2005). *Prochlorococcus (PRO*), *Synechococcus (SYN*), Diatom, autotrophic flagellate (A-Flag), Prymnisophyte (Prym), and autotrophic dinoflagellate (A-Dino). Data are means ± standard deviations.

Cruise	TRANSECT	PRO	SYN	A-Dino	Diatom	A-Flag	Prym
EB04	110°W	24.5	4.6	37.6	7.3	14.6	11.4
		± 7.9	± 0.9	± 4.7	± 3.7	± 2.8	± 1.5
	Equatorial	19.8	5.3	37.3	8.4	16.6	12.6
		± 6.5	± 1.7	± 7.3	± 3.6	± 4.0	± 3.4
EB05	140°W	31.5	8.4	44.8	2.9	12.3	nd
		± 6.6	± 2.0	± 7.7	± 1.7	± 3.9	
	0.5°N	40.4	13.8	33.1	6.9	5.8	nd
		± 5.1	± 2.9	± 4.9	± 5.6	± 3.7	

Table 1.4. Station values of euphotic-zone integrated biomass for each plankton functional type. *Prochlorococcus (PRO)*, *Synechococcus (SYN)*, autotrophic dinoflagellate (A-Dino), Diatom, autotrophic flagellate (A-Flag), prymnisophyte (Prym), heterotrophic prokaryotes (H-Bact), heterotrophic dinoflagellate (H-Dino), and heterotrophic flagellate (H-Flag) and ciliates (CIL). Total autotrophic carbon (AC), total heterotrophic carbon (HC), and total biomass (Biomass). Units are mg C m^{-2}.

				Depth Integrated Biomass mg C m^{-2}												
Cruise	Station	Lat	Lon (°W)	PRO	SYN	A-Dino	Diatom	A-Flag	Prym	HBACT	H-Dino	H-Flag	Cilliates	AC	HC	BM
EB04	3	3°N	110	430	83	580	65	130	130	940	140	66	nd	1,410	200	1,600
	4	2°N	110	400	77	600	159	190	170	860	120	94	nd	1,590	210	1,800
	5	1°N	110	210	69	580	212	210	180	640	180	84	240	1,450	510	2,000
	7	0°	110	230	67	420	85	180	160	650	160	81	220	1,140	470	1,600
	9	1°S	110	160	44	540	93	200	150	520	140	88	210	1,190	440	1,600
	10	2°S	110	400	58	450	85	260	170	730	60	108	nd	1,420	170	1,600
	11	3°S	110	390	57	480	39	200	140	820	100	83	nd	1,310	190	1,500
	12	4°S	110	560	52	500	76	240	160	840	120	110	nd	1,590	230	1,800
	14	0°	116	460	72	470	67	210	180	680	100	134	nd	1,460	230	1,700
	16	0°	120	140	60	350	66	180	120	530	100	108	140	910	350	1,300
	18	0°	122.5	240	87	560	113	200	150	750	170	95	210	1,340	470	1,800
	20	0°	125.3	80	10	200	131	210	160	180	80	87	nd	780	170	1,000
	22	0°	128	230	68	630	79	200	130	540	170	63	260	1,350	490	1,800
	24	0°	131	200	75	560	69	160	120	620	220	98	210	1,180	530	1,700
	26	0°	135	430	74	490	132	250	210	660	160	206	nd	1,580	370	2,000
	29	0°	140	410	116	660	193	260	170	790	120	86	260	1,810	460	2,300
EB05	1	4°N	140	600	112	630	13	100	nd	870	340	99	nd	1,460	430	1,900
	3	2.5°N	140	420	90	690	62	210	nd	580	130	139	nd	1,470	270	1,700
	5	1°N	140	310	83	920	77	100	nd	670	130	167	nd	1,480	300	1,800
	7	0.5°N	140	370	105	340	22	130	nd	650	100	98	nd	970	200	1,200
	9	0°	140	570	180	670	21	190	nd	730	230	313	nd	1,620	540	2,200
	11	0.5°S	140	600	175	850	33	230	nd	680	190	293	nd	1,890	480	2,400
	13	1°S	140	600	180	890	112	350	nd	780	220	155	nd	2,130	370	2,500
	15	2.5°S	140	410	125	630	38	250	nd	840	200	324	nd	1,450	530	2,000
	18	0.5°N	132.5	470	153	360	222	40	nd	610	220	197	nd	1,250	410	1,700
	19	0.5°N	130.5	430	107	320	76	50	nd	610	150	195	nd	980	340	1,300
	20	0.5°N	127.8	540	195	450	51	40	nd	550	220	293	nd	1,280	510	1,800
	21	0.5°N	125.7	510	185	290	60	50	nd	650	220	207	nd	1,090	430	1,500
	22	0.5°N	123.5	370	192	450	50	70	nd	730	100	255	nd	1,140	360	1,500

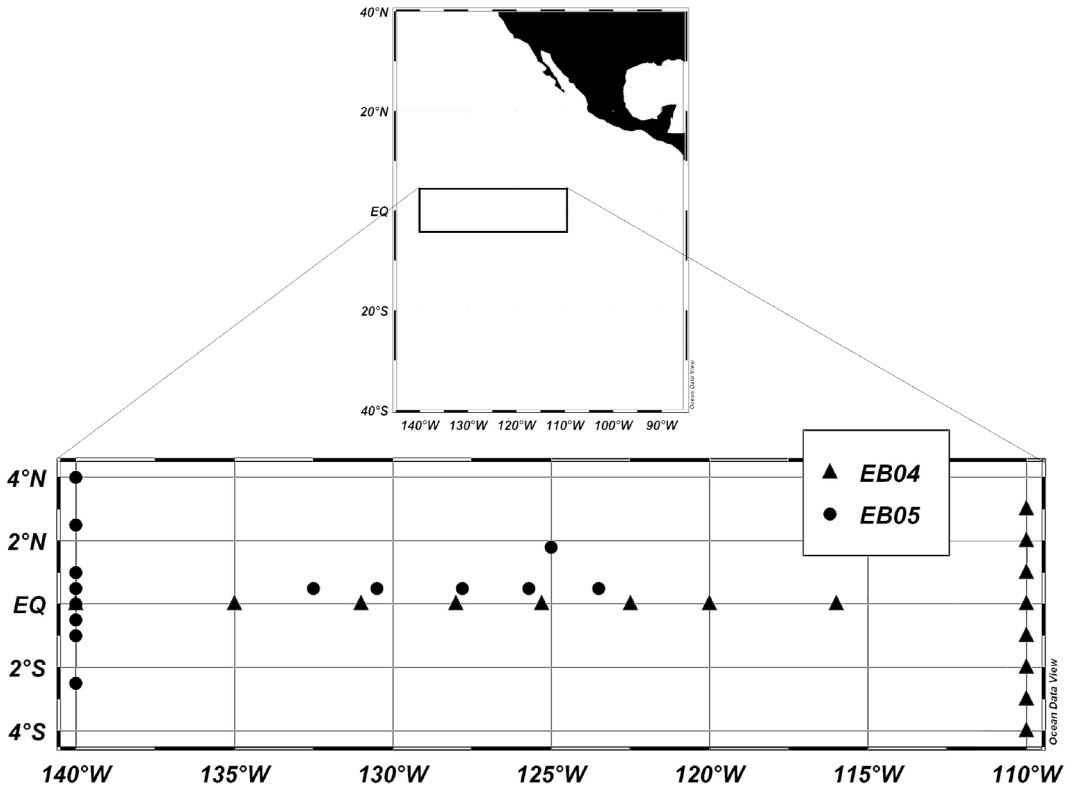

Figure 1.1. Station locations for cruises during December 2004 (EB04, triangles) and September 2005 (EB05, circles). Station order along meridional transects was north to south in both years, while zonal transects were sampled westward in 2004 and eastward in 2005).

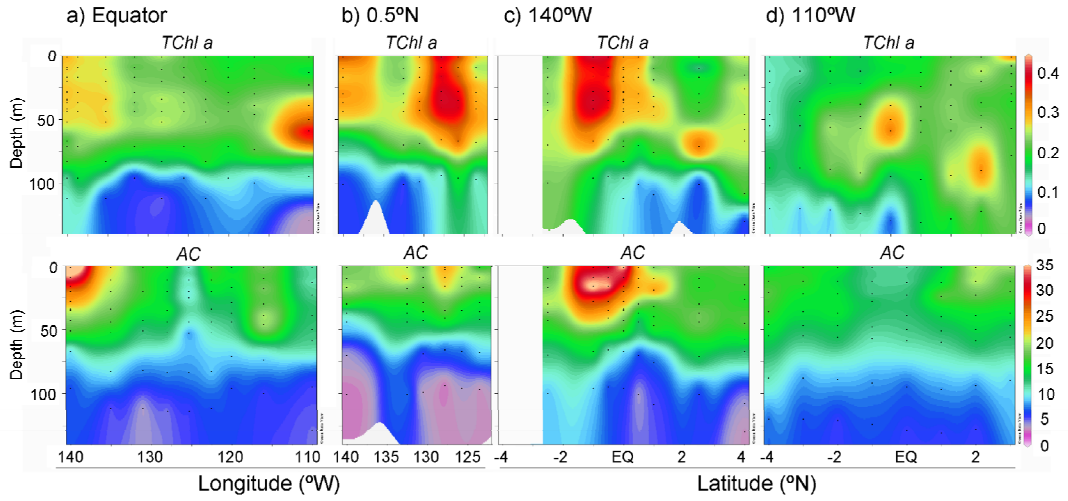

Figure 1.2. Distributions of chlorophyll *a* (TChl *a*) and total autotrophic carbon (AC) along the equatorial **(a)**, 0.5ºN **(b)**, 140ºW **(c)**, and 110ºW **(d)** transects. Units are µg Chl *a* L^{-1} for TChl *a* and µg C L^{-1} for AC.

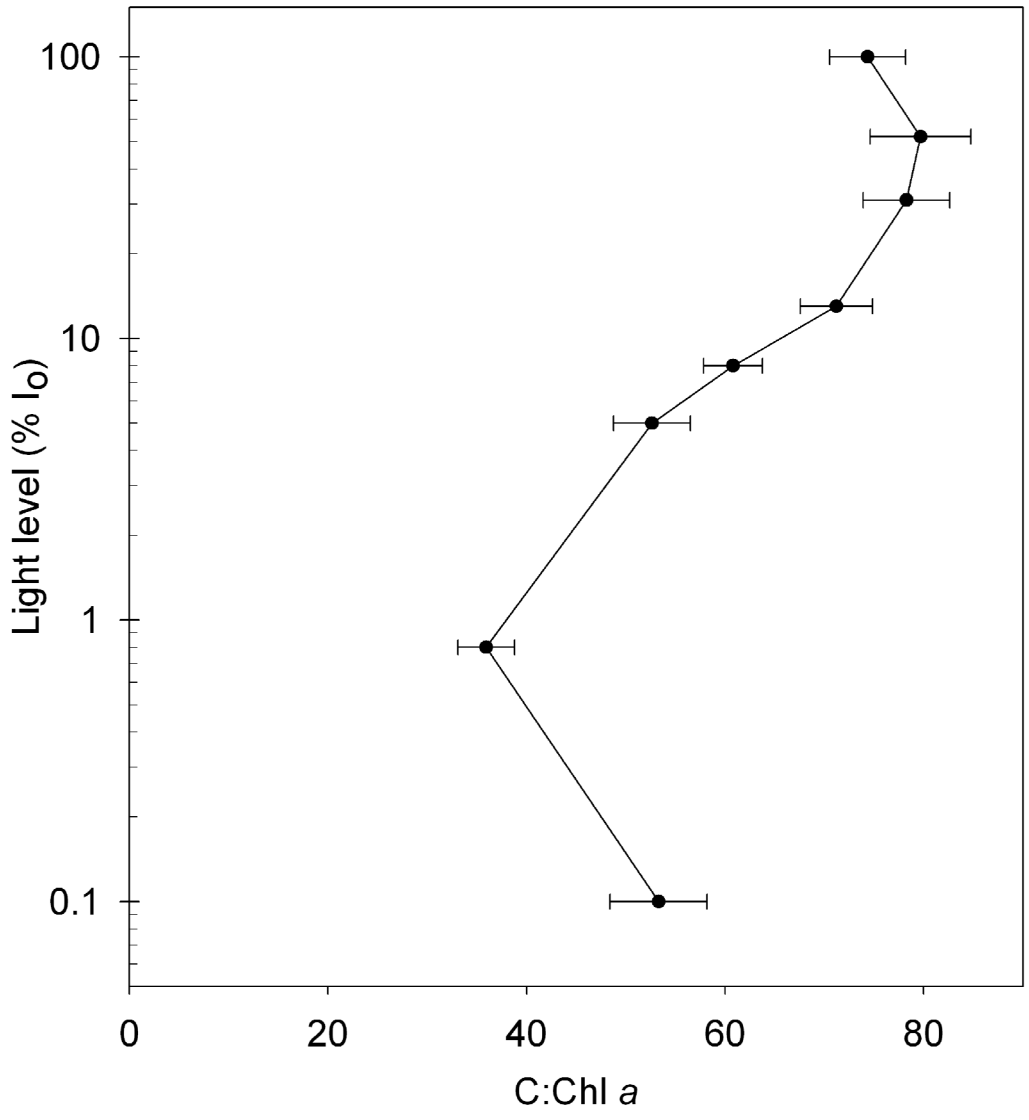

Figure 1.3. Mean autotrophic carbon to chlorophyll *a* ratios (C:Chl *a*) for the eastern equatorial Pacific study area. Error bars represent 95% confidence intervals.

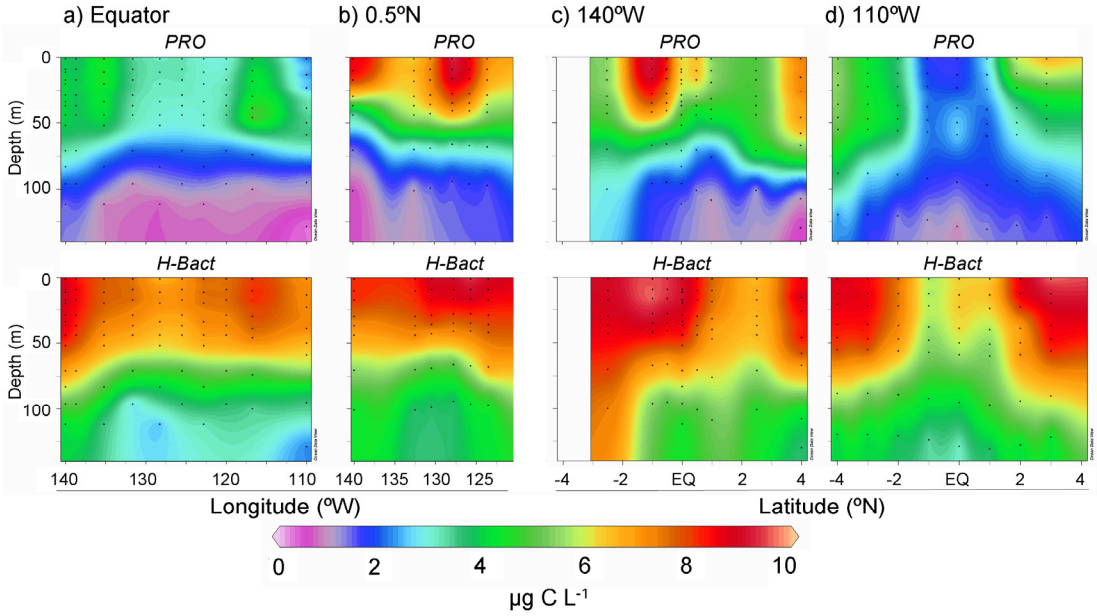

Figure 1.4. Contour plots of *Prochlorococcus* (PRO) and heterotrophic bacteria (H-Bact) biomass distributions along the equatorial **(a)**, 0.5ºN **(b)**, 140ºW **(c)**, and 110ºW **(d)** transects. Units are µg C L^{-1}, and scales are the same for all plots.

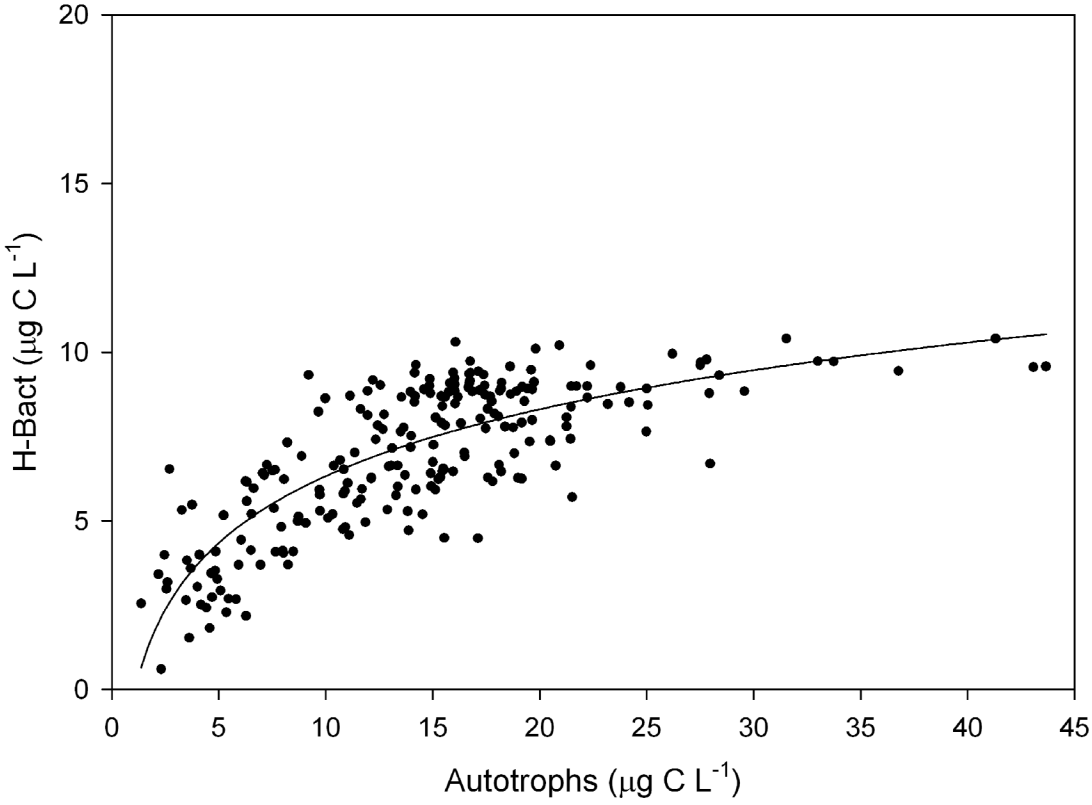

Figure 1.5. Relationship between total autotrophic carbon (Autotrophs) and heterotrophic bacteria (H-Bact) biomass for all samples collected. R^2= 0.63, $p<0.0001$.

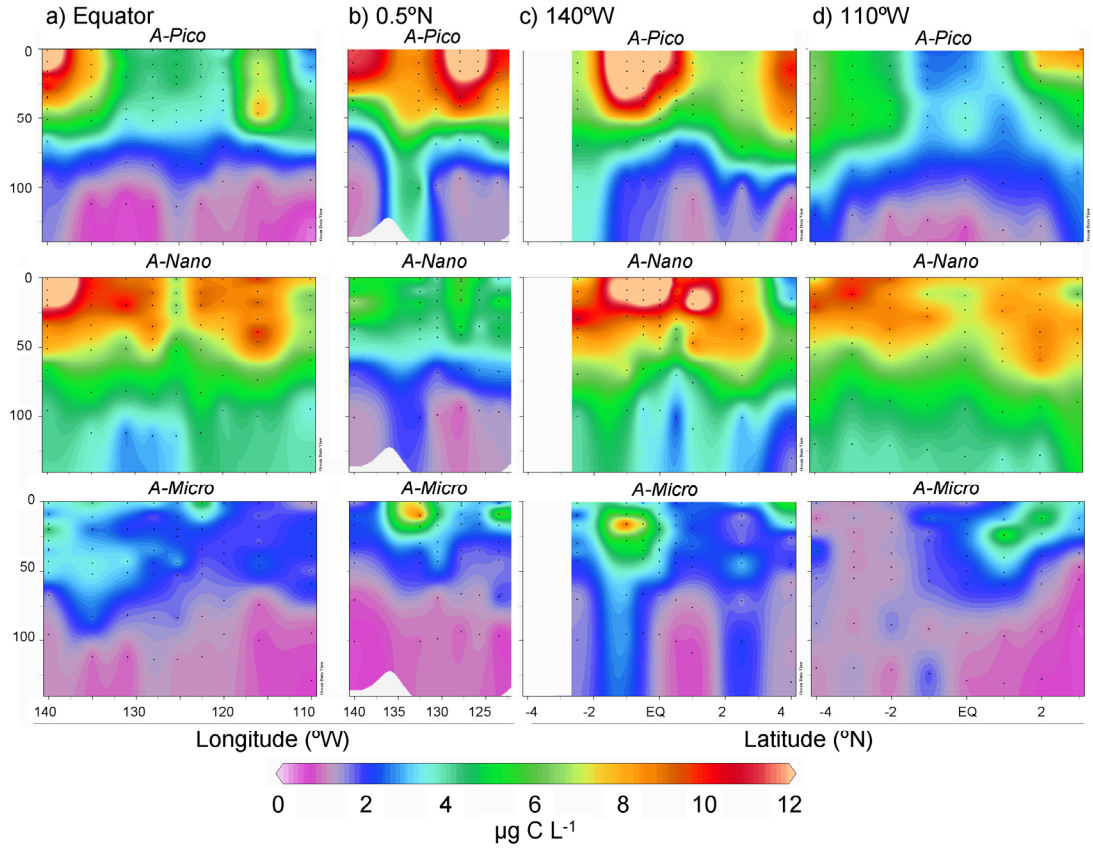

Figure 1.6. Contour plots of phytoplankton biomass distributions by size class along the equatorial **(a)**, 0.5ºN **(b)**, 140ºW **(c)**, and 110ºW **(d)** transects. A-Pico (0.2-2 µm), A-Nano (2-20 µm), and A-Micro (20-200 µm). Units are µg C L^{-1}, and scales are the same for all plots.

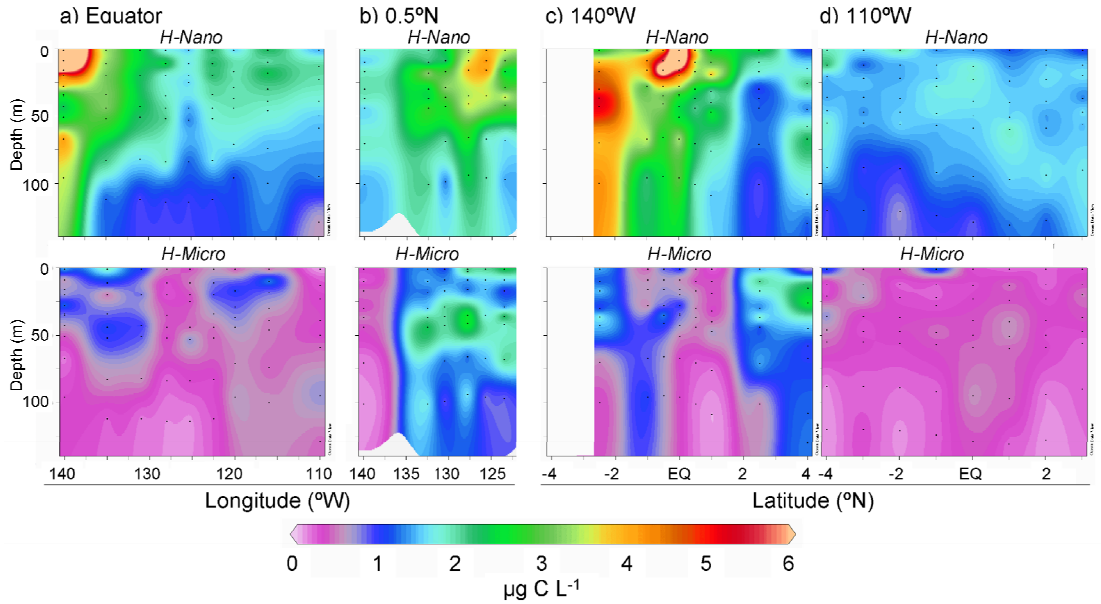

Figure 1.7. Contour plots of heterotrophic biomass distributions by size class along the equatorial **(a)**, 0.5ºN **(b)**, 140ºW **(c)**, and 110ºW **(d)** transects. H-Nano (2-20 µm) and H-Micro (20-200 µm). Units are µg C L^{-1}, and scales are the same for all plots.

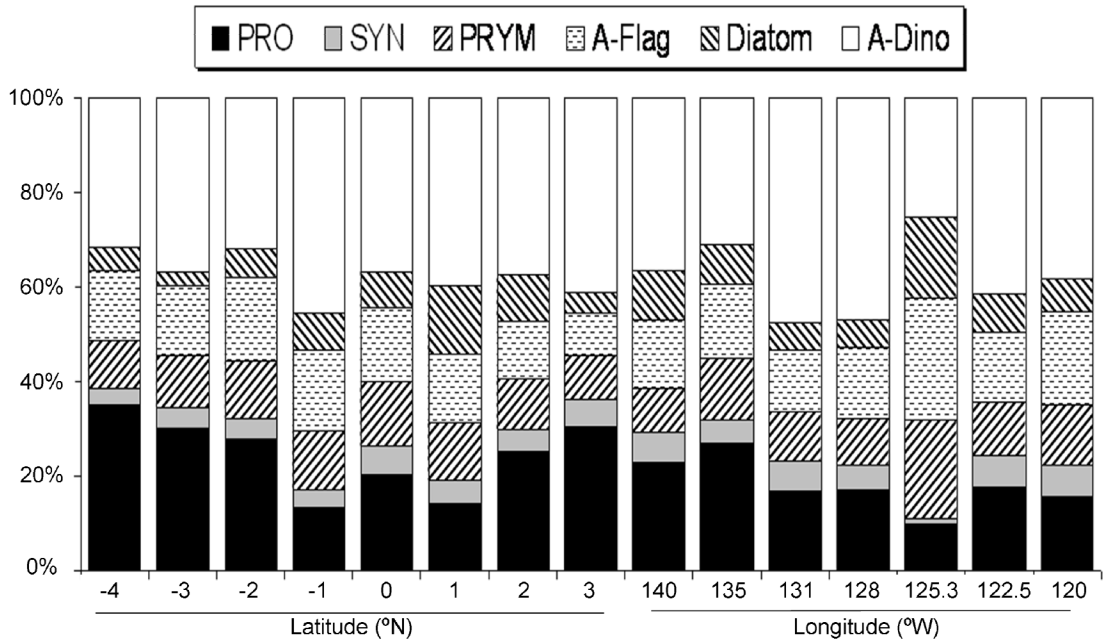

Figure 1.8. Percentage contributions of each phytoplankton functional type to total euphotic zone integrated autotrophic community biomass along the 110ºW and equatorial transects. *Prochlorococcus* (PRO), *Synechococcus* (SYN), prymnesiophytes (PRYM), autotrophic flagellates (A-Flag), diatoms, and autotrophic dinoflagellates (A-Dino).

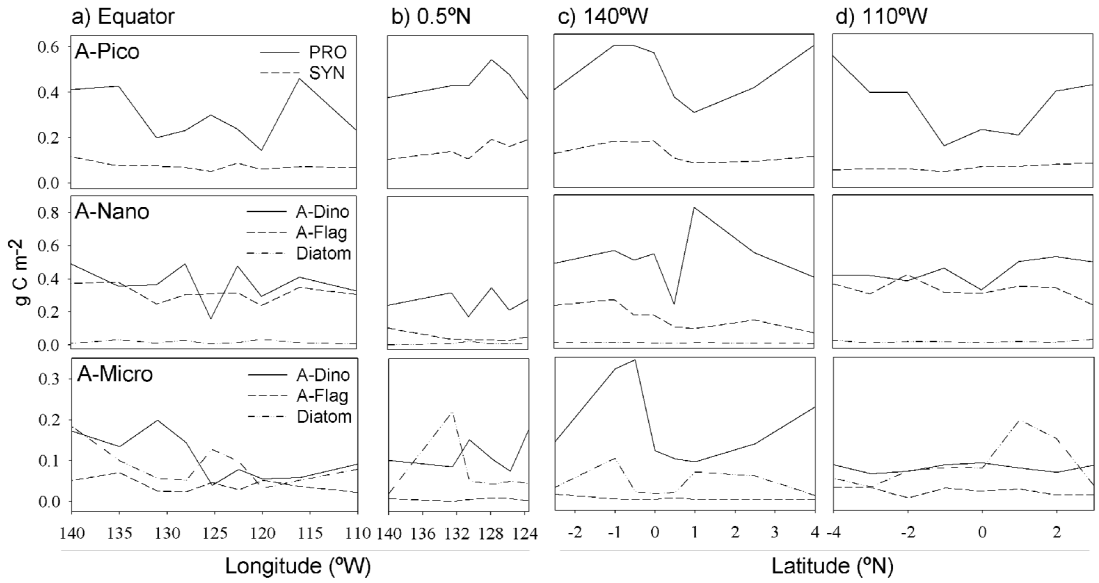

Figure 1.9. Euphotic-zone integrated (100-0.1% I_o) biomass of autotrophs by size class and functional type along the equatorial **(a)**, 0.5ºN **(b)**, 140ºW **(c)**, and 110ºW **(d)** transects. Units are g C m^{-2}.

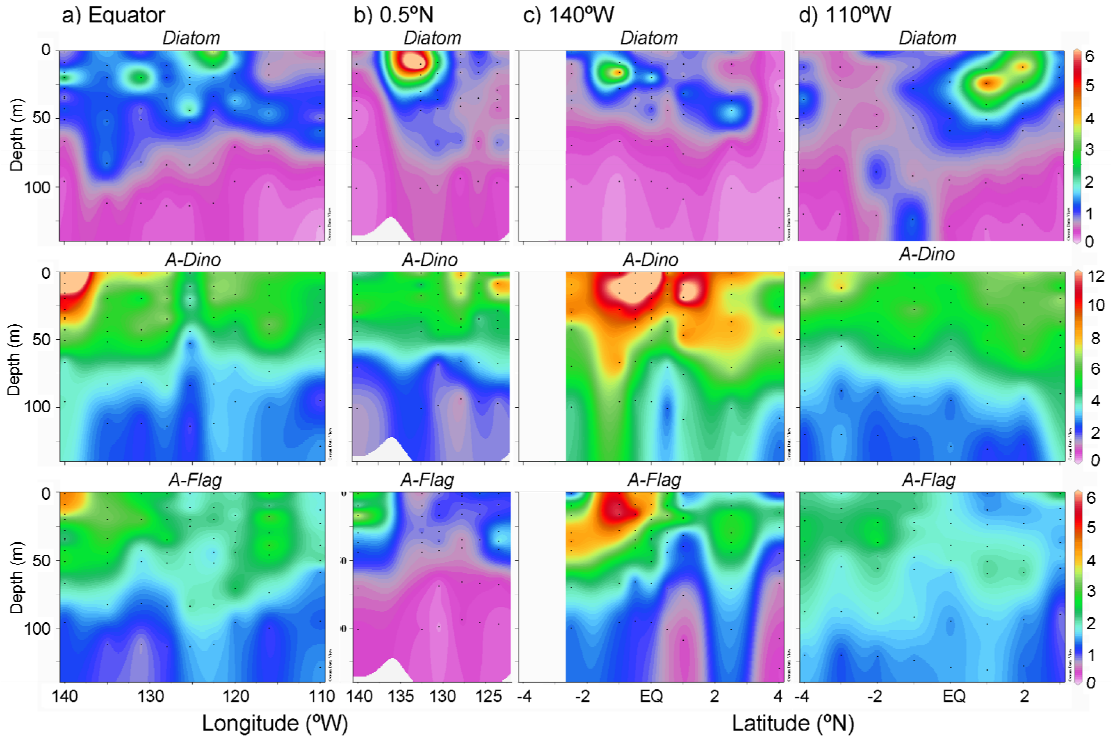

Figure 1.10. Biomass distributions of diatoms, autotrophic dinoflagellates (A-Dino) and autotrophic flagellates (A-Flag) along the equatorial **(a)**, 0.5ºN **(b)**, 140ºW **(c)**, and 110ºW **(d)** transects. Units are µg C L^{-1} and note that a different scale is used for A-Dino.

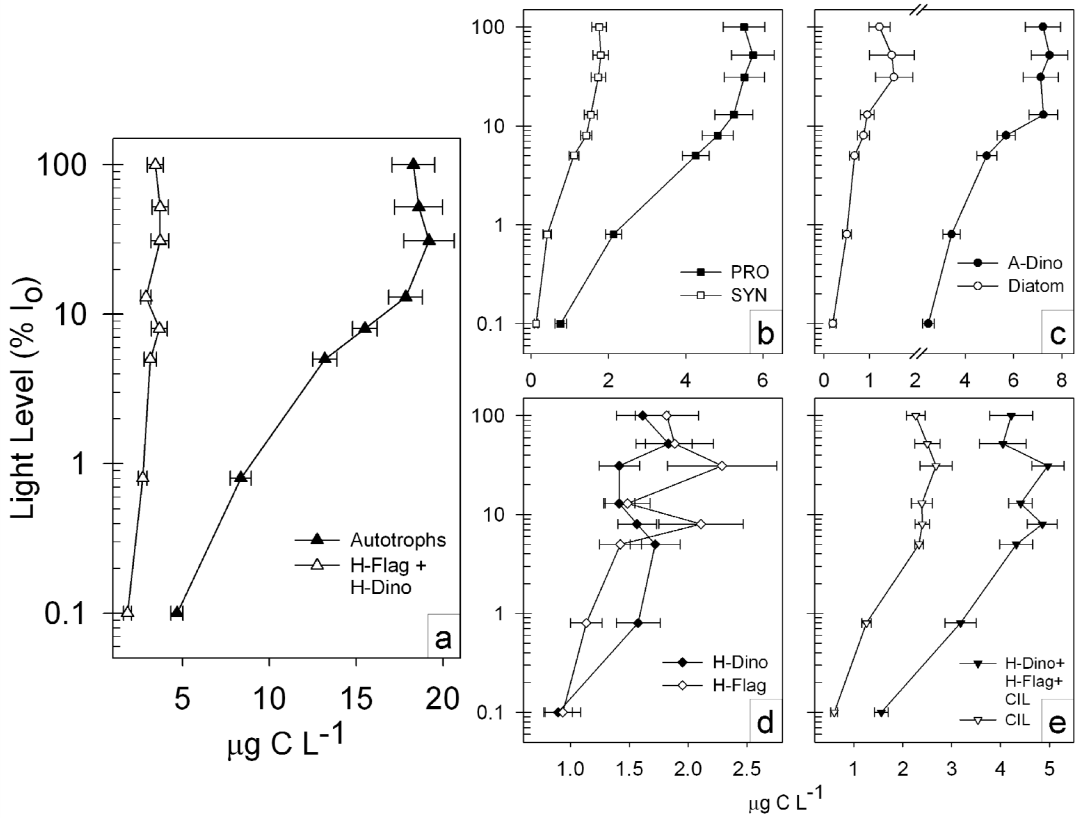

Figure 1.11. Mean depth profiles for total autotrophs and total heterotrophic protists (H-Dino + H-Flag) **(a)**, and various components of the autotrophic and heterotrophic assemblages in the eastern equatorial Pacific: *Prochlorococcus* (PRO) and *Synechococcus* (SYN) **(b)**, autotrophic dinoflagellates (A-Dino) and diatoms **(c)**, and heterotrophic dinoflagellates (H-Dino) and flagellates (H-Flag) **(d)**. Profiles a-d are the means for 30 stations. Profiles for cilliates (CIL) and total H-protists (H-Dino + H-Flag + CIL) **(e)** are the means of 8 stations where ciliates were analyzed by inverted microscopy of acid Lugol's preserved samples. Error bars represent 95% confidence intervals.

References

Balch, W.M., Poulton, A., Drapeau, D.T., Bowler, B.C., Windecker, L.A., Booth, E. S., 2010. Zonal and meridional patterns of phytoplankton biomass and carbon fixation in the Equatorial Pacific Ocean, between 110°W and 140°W. Deep-Sea Research II, this volume.

Binder, B.J., Chisholm, S.W., Olson, R.J., Frankel, S.L., Worden, A.Z., 1996. Dynamics of picophytoplankton, ultraphytoplankton and bacteria in the Central Equatorial Pacific. Deep-Sea Research II 43, 907-931.

Brown, S.L., Landry, M.R., Neveux, J., Dupouy, C., 2003. Microbial community abundance and biomass along a 180°W transect in the equatorial Pacific during an El Niño-Southern Oscillation cold phase. Journal of Geophysical Research 108(C12), 8139, doi:10.1029/2000JC000817.

Brown, S.L., Landry, M.R., Yang, E.J., Rii, Y.M., Bidigare, R.R., 2008. Diatoms in the desert: Plankton community response to a mesoscale eddy in the subtropical North Pacific. Deep-Sea Research II 55, 1321-1333.

Brzezinski, M.A., Baines, S., Balch, W.M., Beuchere, C., Chai, F., Dugdale, R.C., Krause, J.W., Landry, M.R., Marchii, A., Measures, C.I., Nelson, D.M., Parker, A., Poulton, A., Selph, K.E., Strutton, P., Taylor A.G., Twining, B.S., 2010. Co-limitation of diatoms by iron and silicic acid in the equatorial Pacific. Deep-Sea Research II, this volume.

Campbell, L., Vaulot, D., 1993. Photosynthetic picoplankton community structure in the subtropical North Pacific Ocean near Hawaii (station ALOHA). Deep-Sea Research I 40, 2043-2060.

Chavez, F.P., Buck, K.R., Coale, K.H., Martin, J.H., DiTullio, G.R., Welschmeyer, N.A., Jacobson, A.C., Barber, R.T., 1991. Growth rates, grazing, sinking, and iron limitation of equatorial Pacific phytoplankton. Limnology and Oceanography 36, 1816-1833.

Chavez, F.P., Buck, K.R., Service, S.K., Newton, J., Barber, R.T., 1996. Phytoplankton variability in the central and eastern tropical Pacific. Deep-Sea Research II 43, 835-870.

Coale, K.H., Johnson, K.S., Fitzwater, S.E., Gordon, R.M., Tanner, S., Chavez, F.P., Ferioli, L., Sakamoto, C., Rogers, P., Millero, F., Steinberg, P., Nightingale, P., Cooper, D., Cochlan, W.P., Landry, M.R., Constantinou, J., Rollwagen, G., Trasvina, A., Kudela, R., 1996. A massive phytoplankton bloom induced by an ecosystem-scale iron fertilization experiment in the equatorial Pacific Ocean. Nature 383, 495-501.

Décima, M., Landry, M.R., Rykaczewski, R., 2010. Broad-scale patterns in mesozooplankton biomass and grazing in the Eastern Equatorial Pacific. Deep-Sea Research II, this volume.

Dugdale, R.C., Wilkerson, F.P., 1998. Silicate regulation of new production in the Equatorial Pacific upwelling. Nature 391, 270-273.

Dugdale, R.C., Chai, F., Measures, C.I., Parker, A, Wilkerson, F.P., 2010. The regulation of equatorial Pacific pCO_2 by diatoms. Deep-Sea Research II, this volume.

Eppley, R.W., Reid, F.M.H., Strickland, J.D.H., 1970. Estimates of phytoplankton crop size, growth rate, and primary production. In: The ecology of the plankton off La Jolla California in the period April through September, 1967. In: Strickland, H.J.D. (Ed.), Bulletin of Scripps Institution of Oceanography, pp. 33-42.

Eppley, R.W., Chavez, F.P., Barber, R.T., 1992. Standing stocks of particulate carbon and nitrogen in the equatorial Pacific at 150°W. Journal of Geophysical Research 97, 655-661.

Feely, R.A., Boutin, J., Cosca, C.E., Dandonneau, Y., Etcheto, J., Inoue, H.Y., Ishii, M., Le Quere, C., Mackey, D.J., McPhaden, M., Metzl, N., Poisson, A., Wanninkhof, R., 2002. Seasonal and interannual variability of CO_2 in the equatorial Pacific. Deep-Sea Research II 49, 2443-2469.

Feely, R.A., Takahashi, T., Wanninkhof, R.H., McPhaden, M.J., Cosca, C.E., Sutherland, S.C., Carr, M.-E., 2006. Decadal variability of the air-sea CO_2 fluxes in the equatorial Pacific Ocean. Journal of Geophysical Research, Oceans 111, doi:10.1029/2005JC003129.

Flament, P.J., Kennan, S.C. Knox, R.A., Niiler, P.P. Bernstein, R.L., 1996. The three-dimensional structure of an upper ocean vortex in the tropical Pacific Ocean. Nature 383, 610-613.

Frost, B.W., Franzen, N.C., 1992. Grazing and iron limitation in the control of phytoplankton stock and nutrient concentration: A chemostat analogue of the Pacific equatorial upwelling zone. Marine Ecology Progress Series 83, 291-303.

Garrison, D.L, Gowing, M.M., Hughes, M.P., Campbell, L., Caron, D.A., Dennett, M.R., Shalapyonok, A., Olson, R.J., Landry, M.R., Brown, S.L., Liu, H., Azam, F., Steward, G.F., Ducklow, H.W., Smith, D.C., 2000. Microbial food web structure in the Arabian Sea: a US JGOFS study. Deep-Sea Research II 47, 1387-1422.

Holm-Hansen, O., Lorenzen, C., Holmes, R., Strickland, J., 1963. Fluorometric determination of chlorophyll. Journal du Conseil International pour l'Exploration de la Mer. 30, 3-15.

Iriarte, J.L., Fryxell, G.A., 1995. Micro-phytoplankton at the equatorial Pacific (140ºW) during the JGOFS EqPac Time Series studies: March to April and October 1992. Deep-Sea Research II 42, 559-583.

Ishizaka, J., Harada, K., Ishikawa, K., Kiyosawa, H., Furusawa, H., Watanabe, Y., Ishida, H., Suzuki, K., Handa, N., Takahashi, M., 1997. Size and taxonomic plankton community structure and carbon flow at the equator, 175°E during 1990-1994. Deep-Sea Research II 44, 1927-1949.

Johnson, G.C., Sloyan, B.M., Kessler, W.S., McTaggart, K.E., 2002. Direct measurements of upper ocean currents and water properties across the tropical Pacific during the 1990s. Progress in Oceanography 52, 31-61.

Karl, D.M., 1999. A sea of change: Biogeochemical variability in the North Pacific Subtropical Gyre. Ecosystems 2, 181-214.

Kaupp, L.J., Measures, C.I., Selph, K.E., Mackenzie, F.T., 2010. The distribution of dissolved Fe and Al in the upper waters of the eastern equatorial Pacific. Deep-Sea Research II, this volume.

Kirchman, D.L., Rich, J.H., Barber, R.T., 1995. Biomass and biomass production of heterotrophic bacteria along 140°W in the equatorial Pacific: Effect of temperature on the microbial loop. Deep-Sea Research II 42, 603-619.

Kraay, G.W., Veldhuis, M.J.W., 2004. Phytoplankton in the subtropical Atlantic Ocean: Towards a better assessment of biomass and composition. Deep-Sea Research I 51, 507-530.

Krause, J.W., Nelson, D.M., Brezinski, M.A., 2010. Biogenic silica production and diatoms' contribution to primary and new production in the eastern equatorial Pacific. Deep-Sea Research II, this volume.

Landry, M.R., Barber, R.T., Bidigare, R., Chai, F., Coale, K.H., Dam, H.G., Lewis, M.R., Lindley, S., McCarthy, J.J., Roman, M.R., Stoecker, D.K., Verity, P.G., White, J.R., 1997. Iron and grazing constraints on primary production in the central equatorial Pacific: An EqPac synthesis. Limnology and Oceanography 42, 405-418.

Landry, M.R., Ondrusek, M.E., Tanner, S.J., Brown, S.L., Constantinou, J., Bidigare, R.R., Coale, K.H., Fitzwater, S., 2000. Biological response to iron fertilization in the eastern equatorial Pacific (IronEx II). I. Microplankton community abundances and biomass. Marine Ecology Progress Series 201, 27-42.

Landry, M.R., Kirchman, D.L., 2002. Microbial community structure and variability in the tropical Pacific. Deep-Sea Research II 49, 2669-2693.

Landry, M.R., Brown, S.L., Neveux, J., Dupouy, C., Blanchot, J., Christensen, S., Bidigare, R.R., 2003. Phytoplankton growth and microzooplankton grazing in HNLC waters of the equatorial Pacific: Community and taxon-specific rate assessments from pigment and flow cytometric analyses. Journal of Geophysical Research 108(C12), 8142, doi:10.1029/2000JC000744.

Landry, M.R., Calbet, A., 2004. Microzooplankton production in the oceans. International Council for the Exploration of the Sea, Journal of Marine Science 61, 501-507.

Landry, M.R., Selph, K.E., Taylor, A.G., Décima, M., Balch, W.M., Bidigare, R.R., 2010. Phytoplankton growth, grazing and production balances in the HNLC equatorial Pacific. Deep Sea Research II, this volume.

Landry, M.R., Selph, K.E., Yang, E.-J., in review. Decoupled phytoplankton growth and microzooplankton grazing in the deep euphotic zone of the HNLC equatorial Pacific. Marine Ecology Progress Series.

Mackey, D.J., Blanchot, J., Higgins, H.W., Neveux, J., 2002. Phytoplankton abundances and community structure in the equatorial Pacific. Deep-Sea Research II 49, 2561-2582.

Martin, J.H., Gordon, R.M., Fitzwater, S.E., 1991. The case for iron. Limnology and Oceanography 36, 1793-1802.

McPhaden, M.J., Zhang, D., 2004. Pacific Ocean circulation rebounds. Geophysical Research Letters 31, L18301, doi:10.1029/2004GL020727.

Menden-Deuer, S., Lessard, E.J., 2000. Carbon to volume relationships for dinoflagellates, diatoms, and other protist plankton. Limnology and Oceanography 45, 569-579.

Monger, B.C., Landry, M.R., 1993. Flow cytometric analysis of marine bacteria with Hoechst 33342. Applied Environmental Microbiology 59, 905-911.

Mouw, C.B., Yoder, J.A., 2005. Inversion of remote sensing reflectance to obtain phytoplankton community size structure. EOS, Transactions of the American Geophysical Union, 87.

Murray, J.W., Barber, R.T., Roman, M.R., Bacon, M.P., Feely, R.A., 1994. Physical and biological controls on carbon cycling in the equatorial Pacific. Science 266, 58-65.

Price, N.M., Ahner, B.A., Morel, F.M.M., 1994. The equatorial Pacific ocean: Grazer-controlled phytoplankton populations in an iron-limited ecosystem. Limnology and Oceanography 39, 520-534.

Putt, M., Stoecker, D.K., 1989. An experimentally determined carbon: volume ratio for marine ‘‘oligotrichous’’ ciliates from estuarine and coastal waters. Limnology and Oceanography 34, 1097–1103.

Schlitzer, R., 2006. Ocean Data View, http://odv.awi.de.

Selph, K.E., Landry, M.R., Taylor, A.G., Yang, E.J., Measures, C.I., Yang, J., Stukel, M.R., Christensen, S., Bidigare, R.R., 2010. Spatially-resolved taxon-specific phytoplankton production and grazing dynamics in relation to iron distributions in the equatorial Pacific between 110 and 140°W. Deep-Sea Research II, this volume.

Sheridan, C.C., Landry, M.R., 2004. A 9-year increasing trend in mesozooplankton biomass at the Hawaii Ocean Time-Series Station ALOHA. ICES Journal of Marine Science 61, 457-463.

Sherr, E.B., Sherr, B.F., 1993. Preservation and storage of samples for enumeration of heterotrophic protists, in Handbook of Methods in Aquatic Microbial Ecology, edited by P. K. Kemp et al., pp. 207-212, CRC Press Boca Raton, Fla.

Stoecker, D.K., Gustafson, D.E., Verity, P.G., 1996. Micro- and mesoprotozooplankton at 140°W in the equatorial Pacific: Heterotrophs and mixotrophs. Aquatic Microbial Ecology 10, 273-282.

Strutton, P., Palacz, A., Chai, F., Dugdatle, R.C., Marchi, A., Hogue, V., Parker, A., 2010. The impact of equatorial Pacific tropical instability waves on hydrography and nutrients: 2004-2005. Deep-Sea Research II, this volume.

Verity, P.G., Langdon, C., 1984. Relationship between lorica volume, carbon, nitrogen, and ATP content of tintinnids in Narragansett Bay. Journal of Plankton Research 66, 859-868.

Verity, P.G., Stoecker, D.K., Sieracki, M.E., Nelson, J.R., 1996. Microzooplankton grazing of primary production at 140°W in the equatorial Pacific. Deep-Sea Research II 43, 1227-1255.

Vørs, N., Buck, K.R., Chavez, F.P., Eikrem, W., Hansen, L.E., Østergaard, J.B., Thomsen, H.A., 1995. Nanoplankton of the equatorial Pacific with emphasis on the heterotrophic protists. Deep-Sea Research II 42, 585-595.

Yang, E.J., Choi, J.K., Hyun, J.H., 2004. Distribution and structure of heterotrophic protist communities in the northeast equatorial Pacific Ocean. Marine Biology 146, 1-15.

CHAPTER 2

Sharp gradients in phytoplankton community structure across a frontal zone in the California Current Ecosystem

Andrew G. Taylor, Ralf Goericke, Michael R. Landry, Karen E. Selph,

Daniel A. Wick, Megan J. Roadman

Abstract

Spatial variability of plankton biomass, community composition and size structure were investigated across a strong frontal transition (A-Front) in the southern California Current Ecosystem (CCE) in October 2008. Depth profiles were taken across a 25-km transect of nine stations sampled semi-synoptically during one night and for 3 days following drifter arrays in the adjacent water masses. Community compositions are compared based on analyses by digital epifluorescence microscopy, flow cytometry and pigment composition by high-pressure liquid chromatography. Our results show three assemblages sharply delineated in space, with plankton at the front being compositionally distinct and biomass elevated relative to either of the adjacent water masses. Depth-averaged chlorophyll *a* (Chl *a*) varied by a factor of 2.3 (0.35-0.81 μg Chl *a* L^{-1}) and autotrophic carbon (AC) varied almost 3-fold (13.6-35.4 μg C L^{-1}) across the front. One of the most striking features was a sharp gradient in the distribution of *Prochlorococcus* (PRO) and *Synechococcus* (SYN), with PRO

located in the warmer oligotrophic waters on the south side of the front and SYN located in the cooler mesotrophic waters to the north. Both PRO and SYN had local biomass minima directly at the front. The peak in phytoplankton biomass at the front was dominated by large (>20 μm) diatom cells, comprising 71% of the total community biomass. In contrast to previous studies of frontal features in the southern California Current, our study of the A-Front shows strong frontal enhancement of phytoplankton biomass and a shift of phytoplankton size structure towards larger cells.

Introduction

Sharp gradients in physicochemical properties and currents at ocean fronts are known to alter the composition and structure of plankton communities, often resulting in zones of enhanced primary production and biomass (Boucher et al., 1987; Hood et al., 1991; Franks, 1992a,b; Claustre et al., 1994; Kemp et al., 2006). Similar patterns of biological response have been found for frontal features associated with tides, shelf breaks, upwelling and geostrophic currents in varying geographic locations (Pingree et al., 1978; Holligan, 1981; Houghton and Marra, 1983; Traganza et al., 1987; Fiala et al., 1994). Even within regions, however, results can be variable. Based on two cruises of sampling across a prominent front in the southern California Current off Ensenada, Mexico, for instance, Haury et al. and Venrick (Haury et al., 1993; Venrick, 2000) concluded that the front did not represent a biologically distinguishable feature in terms of chlorophyll, production or phytoplankton composition. In contrast, Hood et al. (Hood et al., 1991) found evidence of higher chlorophyll and larger phytoplankton in the vicinity of a front off northern California. Given such dissimilar findings, the nature of frontal systems and the extent to which they impact local ecology and regional productivity remain open and important questions for the California Current System, a highly productive eastern boundary region that is notably rich in mesoscale variability.

In the present study, we investigate the spatial patterns of phytoplankton and heterotrophic protists across a strong frontal feature that was sampled as part of the California Current Ecosystem, Long-Term Ecological Research (CCE-LTER)

program in October 2008. The feature, referred to as 'A-Front' in this and accompanying papers, was located in a region of eastward flow, 150 to 500 km due west of San Diego, California. The main frontal feature was evident in satellite color and temperature images (Landry et al., this issue). We used a complementary suite of methods -- digital epifluorescence microscopy, flow cytometry (FCM), and pigment analyses by high-pressure liquid chromatography (HPLC) -- to provide a comprehensive assessment of abundance, biomass, size structure and compositional changes across the front and in the adjacent water masses. Our results show three sharply delineated assemblages, with plankton at the front being compositionally distinct and biomass elevated relative to either of the adjacent water masses.

Methods

Sampling

On CCE-LTER process cruise P0810 on the R/V Melville, we sampled a transect of 9 stations spanning ~25 km across the frontal zone during the night of 24-25 October 2008. Sampling began in warm oligotrophic water to the south of the front (32.67°N, 120.56°W) at ~2100 local time and ended in cool eutrophic water to the north (32.90°N, 120.71°W) at ~ 0600 (Fig 2.1). All sampling was completed during darkness. At each station, we deployed a CTD rosette with 10-L Niskin bottles to collect discrete water samples from 7-8 depths through the euphotic zone to a depth of 80 m. The chlorophyll fluorescence profile was observed on the downcast, and bottles

were tripped "on-the-fly" on the upcast at variable depths that captured the mixed layer, the peak concentration of the subsurface chlorophyll maximum, if present, and the shoulders and breaks that defined those features. The Niskin bottles were sampled for analyses of total chlorophyll *a* (Chl *a*), phytoplankton accessory pigments by high performance liquid chromatography (HPLC), prokaryotic abundance and biomass by flow cytometry (FCM), and protistan community abundance and biomass by digital epifluorescence microscopy. In addition, we conducted similar sampling during experimental drifter studies in water masses to the north (Cycle 5; 22-24 October) and south (Cycle 6; 26-28 October) of the front (Fig. 2.1). For each of these experiments (described in Landry et al., this issue), we sampled the euphotic zone at 8 depths at the location of the satellite-tracked, drogued drifter at around 0300 each morning for 3 consecutive days.

HPLC analysis

Concentrations of lipophilic pigments, chlorophylls and carotenoids, were determined using high-pressure liquid chromatography (HPLC). For HPLC analysis, 2.2- or 4.4-L samples of seawater were filtered onto Whatman GF/F filters, stored in liquid nitrogen and extracted in acetone as described by Goericke (Goericke, 2002). An internal standard (canthaxanthin) was added to the samples, which were analyzed on an Agilent 1100 series HPLC system (Agilent Technologies, Santa Clara, CA, USA) with a Waters Symmetry C8 column (3.5-µm particle size, 4.6 x 150 mm, silica, reverse-phase; Waters, Milford, MA, USA). Pigments were eluted using a gradient

method with two solvents: (A) a mixture of methanol, acetonitrile and an aqueous pyridine solution (0.25 M, pH = 5) (50:25:25 v:v:v); and (B) a mixture of methanol, acetonitrile, and acetone (20:60:20 v:v:v), according to following times and proportions (time, %A, %B): (0, 100, 0), (12, 60, 40), (36, 0, 100), (38, 0, 100), (40, 100, 0). Contributions of chemotaxonomically defined taxa to total chlorophyll a (TChl a = chlorophyll a (Chl a1) plus divinyl-chlorophyll a (Chl a2)) were calculated as described previously (Goericke and Montoya, 1998; Goericke, 2002).

Picoplankton analysis by flow cytometry

We enumerated pico-phytoplankton and heterotrophic bacteria from 2-mL samples preserved with 0.5% paraformaldehyde (final concentration) and flash frozen in liquid nitrogen. On shore, the samples were stored at -80°C, then thawed in batches and stained with Hoechst 34442 (1 μg mL^{-1}, final concentration) immediately prior to analysis (Monger and Landry, 1993, Campbell and Vaulot, 1993). The analyses were conducted at the SOEST Flow Cytometry Facility (www.soest.hawaii.edu/sfcf) using a Beckman-Coulter Altra flow cytometer equipped with a Harvard Apparatus syringe pump for quantitative analyses and two argon ion lasers tuned to UV (200 mW) and 488 nm (1 W) excitation. Fluorescence signals were collected using filters for Hoechst-bound DNA, phycoerythrin and chlorophyll, all normalized to internal standards of 0.5- and 1.0-μm yellow-green (YG) polystyrene beads (Polysciences Inc., Warrington, PA). Listmode data files (FCS 2.0 format) of cell fluorescence and light-scatter properties were acquired with Expo32 software (Beckman-Coulter) and used

with FlowJo software (Tree Star, Inc., www.flowjo.com) to define populations of *Prochlorococcus* (PRO), *Synechococcus* (SYN), heterotrophic bacteria (H-Bact) and photosynthetic eukaryotic phytoplankton. PRO and SYN abundance estimates from flow cytometry (FCM) analyses were converted to biomass using mixed-layer estimates of 32 and 101 fg C $cell^{-1}$, respectively (Garrison et al., 2000; Brown et al., 2008).

Microscopical assessment of nano- and microplankton

Seawater samples were collected for analysis of the protistan eukaryote communities using advanced digital epifluorescence microscopy. Seawater samples of 500 mL were preserved according to a modified protocol of Sherr and Sherr (Sherr and Sherr, 1993), by adding 260 µL of alkaline Lugol's solution, 10 mL of buffered formalin and 500 µL of sodium thiosulfate sequentially to the samples and gently mixing between each addition. Preserved samples were allowed to sit and clear in the dark at room temperature for one hour. They were then stained with 1 mL of proflavin (0.33% w/v) and stored in the dark for an additional hour. Just prior to filtering, the samples were stained with 1 mL of DAPI (0.01 mg mL^{-1}). A 50-mL aliquot (small volume; SV) of the sample was filtered onto a 25-mm 0.8-µm pore size black polycarbonate filter, and the remaining 450 mL aliquot (large volume; LV) was filtered onto a 25-mm 8.0-µm pore size black polycarbonate filter. A 10-µm nylon backing filter was used under all polycarbonate filters to promote even cell

distribution, and all filtering was done under a gentle vacuum (< 100 mm Hg). Each filter was then mounted onto glass slides using immersion oil and a No. 2 cover slip.

Slides were digitally imaged using a Zeiss Axiovert 200M inverted compound microscope, equipped for epifluorescence microscopy and driven by Zeiss Axiovision software. The stage, filter set and focus drive were motorized to allow for automated image acquisition. Digital images were acquired with a Zeiss AxioCam HRc color CCD digital camera. Exposure times for each image were automatically determined by the software in order to avoid over exposure. SV samples (50 mL aliquots) were viewed at 630X magnification and LV samples (450 mL aliquots) were viewed at 200X magnification. A minimum of 20 random positions were imaged for each slide, with each position consisting of three to four fluorescent channels: Chl *a*, DAPI, FITC (SV and LV samples) and phycoerythrin (SV samples only). The separate channels were combined to form one composite 24-bit RGB image for each position.

The resulting images were processed and analyzed using ImagePro software to semi-automate the enumeration of eukaryotic cells larger than 1.5 µm in length. Whenever possible >300 cells were counted for each slide. Using a VBA script within the ImagePro software, a series of pre-processing steps were performed using the green channel, which corresponds to the fluorescence of proflavin staining of cell protein. The green channel was first extracted as an 8-bit gray scale image from the original 24-bit RGB image. A fast Fourier transform (FFT) was applied to remove background noise, followed by the application of a Laplace filter to improve the definition of the cell edge and to minimize the halo effect common in epifluorescent

images. Images that were out of focus or of poor quality were discarded. Cells were automatically segmented from the background and outlined, and the outlines are reapplied to the original 24-bit RGB image. User interaction was then required to check each image, split connected cells, outline cells that did not auto-segment from the background and delete artifacts and detritus that the software had incorrectly outlined.

Each cell was manually identified and grouped into seven plankton functional groups: diatoms, prymnesiophytes, autotrophic flagellates, heterotrophic flagellates, autotrophic dinoflagellates, heterotrophic dinoflagellates and ciliates. Autotrophic plankton was classified based on the presence of chlorophyll *a*, which autofluoresces red under blue light excitation. Cells were also grouped into three size catagories (Pico, <2 μm; Nano, 2-20 μm; Micro, 20-200 μm) based on the length of their longest axis. The size class for autotrophic picophytoplankton (A-Pico) also includes *Prochlorococcus* and *Synechococcus* cells measured by flow cytometry. Biovolumes (BV; μm^3) were calculated from the length (L) and width (W) measurements of each cell using the geometric formula of a prolate sphere (BV=0.524LWH). For the height of cells (H), which was unmeasured, we used H=W for diatoms and H=0.5W for flagellates (Taylor *et al.*, 2011). Biomass was calculated as carbon (C; pg $cell^{-1}$) using the equations of Menden-Deuer and Lessard (2000): $C = 0.288\ BV^{0.811}$ for diatoms, $C = 0.216\ BV^{0.939}$ for non-diatoms, and C = 0.190 BV for ciliates.

Nutrient analysis

Samples for the analysis of nitrate, nitrite, ammonium, phosphate, and silicate were collected from Niskin bottles into 45-mL plastic test tubes and stored frozen at -18°C until analysis ashore within 2 months of collection. Nutrients were analyzed by flow injection analysis at the nutrient laboratory of the University of California, Santa Barbara on a Lachat Instruments QuikChem 8000 using standard wet-chemistry methods (Gordon *et al*., 1992).

Contour plots

Contour plots were generated using Ocean Data View (Schlitzer, 2006). A VG gridding algorithm was used for variable resolution in a rectangular grid where grid spacing varied accordingly to data density.

Results

Hydrography and nutrients

In late October 2008, the A-Front was evident as a strong east-west orientated surface feature at ~ 32.8 °N, 121.8 °W in satellite color and temperature images (Landry et al., this issue). The 16°C isotherm clearly marked the location of the front at the surface. Several underway transects across the front conducted prior to the nighttime sampling showed that its location wandered slightly during the day (Ohman et al., this issue), perhaps reflecting tides or current undulations along its length.

Observed surface currents in the vicinity of the front (upper 60 m) flowed west-to-east at speeds of 20 to 30 cm sec^{-1} (Li et al., this issue). Currents north of the front were weaker, flowing in a northeasterly direction. Below the surface, the front was evident to 80-m depth, clearly delimited by the 33.4 isohaline (Landry et al., this issue). Water masses in the upper 100 m to the north of the front were saline and cool, as typical for the northern coastal area where upwelling occurs. South of the front, low salinity water of the California Current was evident at a depth of 60 m, subducted below higher salinity water, a mixture of the California Current and central Pacific subtropical waters that flow into the Southern California Bight from the south during summer. At the front (Stations 4 and 5), isotherms and isohalines broadened from 20-60 m, likely reflecting shear-induced mixing.

The depth where concentrations of nitrate reach values of 1 μM, i.e. the nitracline, increased gradually from 40 m south of the front to 30 m north of the front (Fig. 2.2). At the front, concentrations of nitrate were slightly elevated in the upper 30 m. Phosphate followed the distribution of nitrate (data not shown). Concentrations of ammonium in the upper 25 m (0.2-0.4 μM) did not vary systematically across the front. A subsurface ammonium maximum was observed at ~35 m at and north of the front. The average molar carbon to nitrogen ratio of particulate matter in the upper 45 m south of the front ranged from 6.5 to 7.7 and was substantially lower at the front (4.8) and to the north (5.3 to 6.5)**.**

Chlorophyll *a* and autotrophic biomass

Chlorophyll *a* distribution shows a strong subsurface maximum across the frontal transect, located between the 24.75 and 25.00 isopycnals (Fig. 2.3). The depth of this maximum shoaled from ~40 m on the southern side of the front to ~20 m on the northern side. Averaged over the upper 80 m of the water column at each station, Chl *a* concentrations varied from 0.35 to 0.81 μg Chl *a* L^{-1}, with a grand mean of 0.57 ± 0.15 μg Chl *a* L^{-1} for the transect (Table 2.1). The highest depth-averaged Chl *a* values (0.81 μg Chl *a* L^{-1}) were found at the front Stns. 4 and 5 while mean concentrations to the south and north were 0.4 and 0.6 μg Chl *a* L^{-1}, respectively. The three-day depth-averaged Chl *a* concentration for Cycle 5 north of the front (0.86 ± 0.13 μg Chl *a* L^{-1}) was 3 times higher than Cycle 6 south of the front (0.28 ± 0.01 μg Chl *a* L^{-1}) and about the same as at the front (0.81 μg Chl *a* L^{-1}). The highest Chl *a* concentrations observed were on the first and second days of cycle 5 (Table 2.1).

Following the general distribution pattern for Chl *a*, lower values of autotrophic carbon (AC), calculated from FCM and microscopy, were located south of the front and higher values to the north. The depth of the AC maximum also shoaled from south to north, though slightly shallower than the subsurface Chl *a* maximum due to pigment photoadaptation (i.e. increasing cellular Chl *a* content with depth) (Fig. 2.3). AC distribution differs from Chl *a* in the magnitude of subsurface enhancement at the front, as opposed to the more uniform Chl *a* depth profiles from the front to the most northern station sampled. That is, while both measurements showed local enhancements of phytoplankton standing stock at the front, AC more strongly defined

the subsurface biomass maximum (20-40 m) at the front relative to the adjacent water masses. Depth-averaged AC varied almost 3-fold, from 13.6 to 35.4 μg C L^{-1}, across the front, with a mean of 21.4 ± 8.0 μg C L^{-1} (Table 2.1). The highest values were found directly at the front (34.3 ± 1.5 μg C L^{-1}) compared to northern and southern station averages of 20.1 ± 2.9 and 14.6 ± 1.0 and μg C L^{-1}, respectively. Similarly, the mean AC concentration during the northern Cycle 5 experiments (22.8 ± 3.7 μg C L^{-1}) was substantially higher than during Cycle 6 (9.7 ± 0.4 μg C L^{-1}), but less than at the front.

Biomass estimates of phototrophic and heterotrophic prokaryotes

Biomass estimates of the phototrophic bacteria *Prochlorococcus* (PRO) and *Synechococcus* (SYN), enumerated by flow cytometry, showed very strong but opposing gradients across the frontal system (Fig. 2.4). PRO biomass was highest on the southern, oligotrophic side (mean depth-averaged station biomass 2.6 ± 0.8 μg C L^{-1}) and was almost zero on the northern, mesotrophic side (Table 2.1). The distribution of Chl a2, a unique biomarker for PRO, followed the pattern for PRO cell counts, except that the concentration maximum was deeper, reflecting changing carbon to Chl a2 ratios due to photoadaptation. In contrast to PRO, SYN biomass was highest on the northern side (mean depth-averaged station biomass 6.0 ± 1.3 μg C L^{-1}) and diminished greatly south of the front (Table 2.1). Similarly, PRO biomass was undetectable in the mesotrophic waters of Cycle 5, while SYN averaged 3.0 ± 1.1 μg

C L^{-1}. During Cycle 6, PRO biomass averaged 2.8 ± 0.66 μg C L^{-1} while SYN was 0.9 ± 0.16 μg C L^{-1}.

Another interesting feature of the front transect is that both PRO and SYN had local biomass minima directly at the front: for Stns. 4 and 5, PRO and SYN averaged 0.3 and 0.8 μg C L^{-1} respectively (Table 2.1). This result is confirmed by the distribution of zeaxanthin, a nonphotosynthetically active pigment marker for cyanobacteria, which also showed a local minimum at the front. For the most part, the bulk of PRO and SYN cells and pigments were contained within the upper 50 m depth of southern waters and the upper 30 m in the north.

Heterotrophic bacteria (H-Bact) also showed a strong gradient across the frontal system with highest mean 0-80 m biomass concentrations on the northern side of the front (15 ± 1.7 μg C L^{-1}) and lower values to the south (8.1 ± 0.4 μg C L^{-1}) (Table 2.2). H-Bact biomass averaged 15 ± 3.9 μg C L^{-1} during Cycle 5 and 6.9 ± 1.3 μg C L^{-1} during Cycle 6.

Biomass distributions of heterotrophic protists

Depth-averaged station estimates for heterotrophic protist biomass (H-Protist) varied by more than 2-fold across the front (from 2.3 to 5.5 μg C L^{-1}), with a mean value of 4.1 ± 1.2 μg C L^{-1} (Table 2.2). Station estimates were lowest on the south side of the front and increased towards the north, with the highest biomass at Stn. 7. Component assemblages of H-Flag and H-Dino ranged from 0.7 to 2.3 μg C L^{-1} (mean 1.2 ± 0.56 μg C L^{-1}) and from 1.6 to 4.1 μg C L^{-1} (mean 3.0 ± 0.8 μg C L^{-1}),

respectively. Nano-sized heterotrophic flagellates (H-Nano, 2-20 μm) comprised the majority (mean = 76%) of the biomass, while H-Pico (<2 μm) and H-Micro (20-200 μm) cells accounted for 0.6 and 27%, respectively (Table 2.2). H-Nano contributed 68% to H-Protist biomass in Cycle 5 and 71% in Cycle 6, while H-Micro contributed 31% in Cycle 5 and 29% in Cycle 6.

Biomass of ciliated protists are likely underestimated in our epifluorescence microscopy counts (Taylor et al., 2011), and is therefore not included in the estimates above for heterotrophic flagellates. Nevertheless, the relative concentrations of ciliates that we did enumerate were found to be highest directly on the front (Table 2.3).

Distributions of eukaryotic autotroph groups

Based on microscopy, diatoms dominated the maximum in autotroph carbon (AC) at front Stns. 4 and 5, contributing 78-86% of AC at the 20-40 m depths of their maximum concentrations (Fig. 2.5). The distribution of fucoxanthin, a pigment found primarily in diatoms, strongly supports the subsurface maximum of diatom biomass at the front. North of the front, the diatom contribution to total biomass decreased, ranging from 34% of AC in the subsurface Chl maximum to <13% in the mixed layer.

Dinoflagellates biomass showed an enriched area extending north from front Stns. 5 to 7, but the highest biomass was at the surface north of the front (Stn. 7; Fig. 2.5). Distribution of the pigment-marker peridinin diverged markedly from microscopically derived A-Dino carbon, reflecting changing pigment-biomass ratios

as a function of depth as well as the lack of peridinin in some dinoflagellate species. Prymnesiophyte biomass was highest primarily in near-surface waters north of the front, but their associated pigment marker, hexfucoxanthin, showed a subsurface maximum at 30-40 m south of the front.

Integrated community composition, biomass and size-structure

For the nine transect stations, depth-integrated autotrophic biomass (AC) varied 2.6-fold, ranging from 1,090 to 2,830 mg C m^{-2}, with a mean value of 1,720 ± 640 mg C m^{-2} (Table 2.3). The highest AC was found directly at the front (Stns. 4 and 5, 2,750 mg C m^{-2}), about double the mean concentration to the south and north (1,420 mg C m^{-2}). Diatoms dominated the phytoplankton community at the front, with 6.8 times higher biomass (1,951 ± 84 mg C m^{-2}) than the north-south station mean (286 ± 193 mg C m^{-2}) (Fig. 2.5). The average euphotic-zone integrated AC biomass for Cycle 5 (1,820 ± 300 mg C m^{-2}) was more than double the integrated biomass found for Cycle 6 (780 ± 28 mg C m^{-2}) (Fig. 2.6). For both cycles and the transect stations all euphotic-zone integrations were done to 80 m. While the transect was sampled at night, and we dot have any light measurements for these specific stations, we do have noon cast CTD profiles from cycles 5 and 6. These CTD casts show that 80 m depth is well below the 0.1% light level.

Biomass contributions of each phototrophic group were variable across the front, but organized into three community groups (Fig. 2.6A); the southern community (stations 1-3), a front community (stations 4 and 5) and the northern community

(stations 6-9). A principal component analysis was preformed using all of the phototrophic groups (PRO, SYN, diatoms, A-Dino, A-Flag and Prym), which also split the phototrophic community into these three groups (Fig. 2.7). The first two principal components, diatoms and SYN, accounted for 88% and 8.6% of the variance, respectively. The oligotrophic cluster was comprised of Cycle 6 and transect stations 1-3, the front cluster was transect stations 4 and 5, and the mesotrophic cluster was comprised of Cycle 5 and transect stations 6-9. The southern community was dominated by autotrophic dinoflagellates (A-Dino) which made up 35% of the total community biomass, followed by PRO (18%), prymnesiophyte (Prym; 13.5%), autotrophic flagellates (AF;12%), SYN (12%) and diatoms (9.2%) (Table 2.4). The front community was dominated by diatoms (71.3%), followed by A-Dino (14.9%), Prym (5.8%), AF (4.9%), SYN (2.1%) and PRO (0.9%). The northern frontal community was more diverse, with SYN (29.1%), diatoms (25.3%) and A-Dino (23.2%) comprising the bulk of the biomass, followed by Prym (11.3%), AF (10.8%) and PRO (0.2%). Diatoms comprised almost half (48.5%) of the autotrophic community biomass during the Cycle 5 experiments, followed by A-Dino (16%), A-Flag (16.3%), SYN (12.9%) and Prym (6.0%). During Cycle 6, PRO was the largest contributor (29 %) to AC; A-Dino (17.9%), Prym (16.9%) and A-Flag (16.2%) contributed roughly equal shares to comprise half of the total biomass, and diatoms (11.1%) and SYN (8.9%) made up the remainder.

Phytoplankton size class distributions were very similar on the northern and southern sides of the front, with nano-sized autotrophs (2-20 μm) comprising 44 and

49% of AC, respectively, and A-Micro accounting for 26 and 20%, respectively (Fig. 2.6B, Table 2.4). Pico-autotrophs (< 2 μm), primarily PRO south of the front and SYN north of the front, contributed the same fractions, 30 and 31%, respectively, to total AC. These proportions were markedly skewed to larger size classes at the front, where A-Pico, Nano and Micro contributed 3, 53 and 44% of total AC. During Cycle 5, the proportion of larger phytoplankton was higher (A-Micro = 38%) and smaller phytoplankton lower (A-Pico = 13%) than the average for the northern transect stations. For Cycle 6, the contribution of A-Micro was lower (18%) and A-Pico higher (38%) than the mean for the southern transect stations.

Discussion

For this study we used a complementary set of measurements from microscopy, flow cytometry (FCM) and HPLC pigment analysis to provide a comprehensive assessment of microbial community biomass, composition and size-structure changes across a frontal transition in the California Current System, or an Eastern Boundary Current. Overall, we observed generally good agreement between the biomass distributions of phytoplankton groups from microscopy and flow cytometry and the patterns of diagnostic marker pigments: fucoxanthin (diatoms), 19'-hexanoyloxyfucoxanthin (prymnesiophytes), divinyl Chl *a* (PRO) and zeaxanthin (cyanobacteria) (Figs. 4 and 5). While dinoflagellate biomass and peridinin values agreed reasonably well north and south of the front, that was not the case at front Stn.

5. This disparity suggests that the composition of dinoflagellates at the front may have included forms that lack or have substantially lower cell contents of the peridinin accessory pigment (c.f., Tangen and Bjornland, 1981; Jeffrey and Wright, 2005).

One of the most striking features of our A-Front crossing was the sharp discontinuity in abundances of the phototrophic bacteria, *Prochlorococcus* (PRO) and *Synechococcus* (SYN), with PRO located in the warm and oligotrophic waters to the south and SYN located in the cool and eutrophic waters to the north, and both groups showing depressed abundance directly at the front. The other major feature was the almost 7-fold increase in diatom biomass, attributed to micro-sized (>20 μm) cells at the front. Both patterns are similar to observations from upwelling and geostrophic fronts in the Alboran Sea (Claustre et al., 1994; Fiala et al., 1994; Reul et al., 2005) and a geostropic front in the western Mediterranean Sea (Jacquet et al., 2002). For the latter, Jacquet et al. (Jacquet et al., 2002) were able to distinguish a mesotrophic system in Atlantic waters dominated by eukaryotes and SYN and a more oligotrophic system in the Mediterranean Sea waters dominated by PRO. For the former, Fiala et al. (Fiala et al., 1994) found that Chl *a*, fucoxanthin and microscopy estimates of diatom abundance were 1-2 orders of magnitude higher in the frontal jet then in the surrounding waters, while pico- and nanoplankton were most abundant in the adjacent waters and consisted mostly of prymnesiophytes. At this front the distribution of Chl *a* concentrations at the depth of the chlorophyll maximum ranged from 0.2-2.6 μg Chl *a* L^{-1}, similar to the range that we found across the A-Front system, if we include Cycles 5 and 6 (0.47-2.0 μg Chl *a* L^{-1}). Fiala et al. (Fiala et al., 1994) reported similar

densities of >20-µm diatom cells (1-200 cells mL^{-1}) in the Chl *a* maximum of their frontal jet to what we found in our study area (10-220 cells mL^{-1}). The similarities in observations for these very different front-generating mechanisms suggest common patterns of community response to environmental perturbations at frontal transitions.

The commonalities in community changes at fronts are not so evident within the California Current System, however. For a front study off of Northern California, for example, Hood et al. (Hood et al., 1991) reported a significant increase in large phytoplankton on the cold eutrophic side of the water mass transition, rather than directly in the frontal jet. This observation was based on size-fractionated Chl *a*, with photomicrographs confirming qualitatively the increased abundance of chain-forming diatoms. In a study slightly to the south of our site, off of Ensenada, Mexico, Haury et al. and Venrick (Haury et al., 1993; Venrick, 2000) concluded that the front only marked the transition of water masses, with no evidence of local enhancement of biomass or altered community composition. These differences would lead us to believe that frontal formation mechanisms or community responses to fronts are sufficiently varied to require substantial additional research to understand their differences, as well as the overall contributions of fronts to regional productivity and local ecology.

In the present study, the altered structure of the phytoplankton community observed directly at the A-Front seems to have profound impacts on many aspects of local trophic ecology. These include enhanced microbial activity (Samo et al., this issue), enhanced physiological potential and PvE photosynthetic efficiency (Wang et

al., this issue), increased suspended particulates and altered composition and biomass of mesozooplankton (Ohman et al., this issue), and increased densities of acoustically estimated krill and fish (Lara Lopez et al., this issue). The area of highest diatom biomass directly on the front was also the area with the highest variable fluorescence (F_v/F_m) (Chekalyuk et al., this issue), a measure of the maximum quantum yield of photosynthesis that can be used as an indicator of nutrient stress. The high F_v/F_m found at the front, along with the substantial increase in large diatoms, suggests that the area was enriched with nutrients and highly productive. Along with the dramatic change in the community structure, this finding supports the hypothesis that the enhanced phytoplankton community at the front was the result of active in situ growth, rather than the passive accumulation of biomass in a zone of physical convergence. It is likely, however, that the assemblage observed in the frontal jet originated from upstream. As the California Current frontal jet makes its way down the coast, its community composition is affected by convergent flows and subduction from adjacent coastal surface waters (Hood et al., 1991) and by nutrient intrusions and wind forcing events along the way (Franks and Walstad, 1997). How the relative contributions of local growth enhancement processes versus upstream and advective effects to community composition change across California Current frontal features is an important question for future research.

Our observations of the phytoplankton community response across A-Front also bring into question how global climate change may impact the California Current Ecosystem. It is thought, for example, that a warming planet could lead to enhanced

thermal stratification of open-ocean waters, while at the same time intensifying winds, due to land-sea warming differences, that drive coastal upwelling (Bakun, 1990; Snyder et al., 2003). Consequently, the frequency and intensity of frontal features along the along eastern boundary current regions where open-ocean and coastal upwelling waters meet might reasonably increase. Indeed, Kahru et al. (Kahru et al., this issue) have shown increasing trends in the frequencies of thermal and chlorophyll fronts in the A-Front study area over the last decades. If enhancement of phytoplankton biomass and a community shift towards larger cells are common characteristics of such frontal features, as seen in this and other investigations, we can hypothesize that increased frontal frequency could lead to higher productivity, carbon export and food web transfer efficiency in the southern California Current Ecosystem.

Acknowledgements

We thank the captain and crew of the R/V Melville and all participants in the CCE-LTER process cruises. The A-Front study was supported by U. S. National Science Foundation grants OCE 04-17616 and 10-26607 for the CCE LTER Program.

Chapter 2, in full, has been published in Journal of Plankton Research: Taylor, A. G., Goericke, R., Landry, M. R., Selph, K. E., Wick, D. A., Roadman, M. J., 2012. "Sharp gradients in phytoplankton community structure across a frontal zone in the California Current Ecosystem." J. Plankton Res **34:** 778-789. The dissertation author was the primary investigator and author of this paper.

Table 2.1. Mean phytoplankton abundance and biomass estimates for the A-Front study. All estimates were first integrated, then averaged for the upper 80 m at each station. Categories are: autotrophic prokaryotes [*Prochlorococcus* (PRO) and *Synechococcus* (SYN)] from FCM analyses, and autotrophic eukaryotes by size class [A-Pico (0.2-2 μm), A-Nano (2-20 μm) and A-Micro (20-200 μm)] from epifluorence microscopy. Mean values of total chlorophyll a (Chl), total autotrophic biomass (AC = sum of prokaryotes and eukaryotes), and autotrophic carbon to chlorophyll a ratio (AC:Chl) are also given. Units are cells mL^{-1} for abundance, μg C L^{-1} for biomass and μg Chl a L^{-1} for chlorophyll.

		Lat (°N)	Lon (°W)	Abundance (cells mL^{-1})			Biomass (µg C L^{-1})					Chl	AC	AC:Chl
				A-Pico	A-Nano	A-Micro	PRO	SYN	A-Pico	A-Nano	A-Micro			
Cycle 6 (day)	1	32.60	120.56	200	2,000	15	2.1	0.8	0.06	4.2	2.3	0.27	9.5	35
	2	32.57	120.33	190	2,100	12	3.2	0.7	0.06	4.0	1.6	0.29	9.6	33
	3	32.49	120.11	80	1,600	10	3.2	1.0	0.02	4.6	1.3	0.28	10.1	36
A-Front (stn)	1	32.67	120.72	350	3,000	10	3.5	1.8	0.11	5.9	2.4	0.39	13.6	35
	2	32.70	120.71	380	4,000	20	2.1	1.7	0.12	7.9	2.6	0.35	14.4	41
	3	32.73	120.71	450	3,500	20	2.2	1.9	0.14	7.7	3.6	0.44	15.6	35
	4	32.75	120.71	230	2,500	100	0.6	0.9	0.07	18.7	13.0	0.68	33.3	49
	5	32.78	120.71	220	2,600	160	0.0	0.6	0.07	17.1	17.7	0.81	35.4	43
	6	32.80	120.71	100	2,700	60	0.0	6.3	0.03	10.4	5.9	0.66	22.7	34
	7	32.83	120.71	170	3,600	50	0.0	6.1	0.05	10.4	4.6	0.63	21.2	34
	8	32.85	120.71	180	2,800	40	0.0	7.2	0.05	7.7	5.7	0.55	20.8	38
	9	32.90	120.71	50	1,800	30	0.1	4.2	0.02	7.1	4.5	0.57	15.9	28
Cycle 5 (day)	1	32.92	120.90	120	2,500	80	0	4.2	0.04	11.6	8.3	0.98	24.1	25
	2	32.82	120.84	120	2,100	100	0	2.6	0.04	12.6	10.3	0.88	25.6	29
	3	32.85	120.57	90	1,600	70	0	2.1	0.03	8.9	7.5	0.72	18.6	26

Table 2.2. Mean abundance and biomass estimates of heterotrophs for the A-Front study. All estimates were first integrated, then averaged for the upper 80 m at each station. Categories are: heterotrophic bacteria (H-Bact) from FCM analyses, and heterotrophic eukaryote by size class. H-Pico (0.2-2 µm), H-Nano (2-20 µm) and H-Micro (20-200 µm) from epifluorescence microscopy. Heterotrophic carbon (HC) is the sum for all eukaryote size classes (i.e. protistan grazers), excluding H-Bact. Units are cells mL^{-1} for abundance, and µg C L^{-1} for biomass.

		Lat (°N)	Lon (°W)	Abundance (cells mL^{-1})			Biomass (µg C L^{-1})				HC
				H-Pico	H-Nano	H-Micro	H-Bact	H-Pico	H-Nano	H-Micro	
Cycle 6 (day)	1	32.60	120.56	50	800	2	6.1	0.02	1.9	1.0	2.9
	2	32.57	120.33	70	900	1	6.4	0.02	1.7	0.3	2.1
	3	32.49	120.11	10	500	2	8.2	0.00	2.0	1.0	3.0
A-Front (stn)	1	32.67	120.72	90	1,200	1	8.6	0.03	1.8	0.4	2.3
	2	32.70	120.71	110	1,500	1	7.7	0.03	2.6	0.3	3.0
	3	32.73	120.71	90	1,300	2	7.9	0.03	2.9	1.2	4.1
	4	32.75	120.71	80	1,100	2	8.5	0.02	2.4	1.2	3.6
	5	32.78	120.71	40	900	3	9.3	0.01	2.6	1.0	3.6
	6	32.80	120.71	110	1,800	3	14.9	0.03	4.2	1.4	5.6
	7	32.83	120.71	100	1,500	3	13.6	0.03	4.4	1.3	5.7
	8	32.85	120.71	60	1,200	3	17.1	0.02	3.1	2.0	5.2
	9	32.90	120.71	50	900	4	13.3	0.01	3.9	1.4	5.3
Cycle 5 (day)	1	32.92	120.90	90	1,400	2	19.7	0.03	3.4	1.2	4.7
	2	32.82	120.84	60	1,300	3	13.5	0.02	3.4	1.4	4.8
	3	32.85	120.57	60	1,000	3	12.5	0.02	2.8	1.8	4.7

Table 2.3. Station values of euphotic-zone integrated biomass (0-80 m) for all enumerated plankton taxa: *Prochlorococcus* (PRO), *Synechococcus* (SYN), autotrophic dinoflagellates (A-Dino), diatoms, autotrophic flagellates (A-Flag), prymnesiophytes (Prym), heterotrophic prokaryotes (H-Bact), heterotrophic dinoflagellates (H-Dino), heterotrophic flagellates (H-Flag) and ciliates (CIL). Total autotrophic carbon (AC) includes both prokaryotes and eukaryotes. Total heterotrophic carbon (HC) includes only eukaryotes. Total biomass =AC + HC, exclusive of H-Bact . Units are mg C m^{-2}.

		Lat (°N)	Lon (°W)	Depth Integrated Biomass (mg C m^{-2})										AC	HC	Biomass
				PRO	SYN	A-Dino	Diatom	A-Flag	Prym	H-Bact	H-Dino	H-Flag	CIL			
Cycle 6 (day)	1	32.60	120.56	170	70	150	120	100	150	500	160	80	0	760	240	1,000
	2	32.57	120.33	260	60	130	90	120	110	500	80	80	0	770	170	940
	3	32.49	120.11	260	80	130	50	160	130	700	160	80	0	810	240	1,050
A-Front (stn)	1	32.67	120.72	280	140	370	40	150	110	700	130	50	0	1,090	180	1,270
	2	32.70	120.71	170	130	430	110	130	180	600	170	60	0	1,150	240	1,390
	3	32.73	120.71	170	150	410	180	150	190	600	240	70	20	1,250	310	1,560
	4	32.75	120.71	40	70	380	1,900	120	150	700	200	60	30	2,660	260	2,920
	5	32.78	120.71	3	50	460	2,000	150	160	700	220	70	60	2,830	290	3,120
	6	32.80	120.71	1	500	380	580	180	160	1,200	260	150	40	1,810	410	2,220
	7	32.83	120.71	2	490	420	340	240	210	1,100	260	180	10	1,700	440	2,140
	8	32.85	120.71	4	580	310	450	150	160	1,400	330	90	0	1,660	420	2,080
	9	32.90	120.71	5	340	360	290	120	170	1,100	310	100	20	1,280	410	1,690
Cycle 5 (day)	1	32.92	120.90	3	330	310	780	370	120	1,600	250	120	0	1,930	380	2,310
	2	32.82	120.84	3	210	360	1,100	290	120	1,100	240	140	0	2,050	380	2,430
	3	32.85	120.57	2	160	230	780	220	90	1,000	250	120	0	1,480	370	1,850

Table 2.4. Percentage contribution of each phytoplankton taxa and size-class to euphotic-zone integrated biomass of the autotrophic community in cycles 5 and 6, and south front (stations 1-3), front (stations 4-5) and north front (stations 6-9). *Prochlorococcus* (PRO), *Synechococcus* (SYN), autotrophic dinoflagellate (A-Dino), Diatom, autotrophic flagellate (A-Flag) and prymnesiophyte (Prym). Pico-autotrophs (A-Pico; 0.2-2 μm), Nano-autotrophs (A-Nano; 2-20 μm) and Micro-autotrophs (A-Micro; 20-200 μm). Data are means ± standard deviations.

	Cycle 6	Station 1-3	Station 4-5	Station 6-9	Cycle 5
PRO	29 ± 6.7	18 ± 6.5	0.9 ± 1.1	0.2 ± 0.1	0.2 ± 0.0
SYN	9 ± 1.3	12 ± 0.7	2 ± 0.9	29 ± 3.2	13 ± 3.9
A-Dino	18 ± 2.1	35 ± 2.6	15 ± 0.9	23 ± 4.1	16 ± 1.1
Diatom	11 ± 5.0	9 ± 5.3	71 ± 0.4	25 ± 5.4	49 ± 7.0
A-Flag	16 ± 3.2	12 ± 1.6	5 ± 0.3	10 ± 2.0	16 ± 2.8
Prym	17 ± 2.5	14 ± 3.0	6 ± 0.3	11 ± 1.8	6.0 ± 0.3
A-Pico	38 ± 6	31 ± 7	3 ± 2	30 ± 3	13 ± 4
A-Nano	44 ± 2	49 ± 6	53 ± 5	45 ± 4	48 ± 1
A-Micro	18 ± 6	20 ± 3	44 ± 7	26 ± 3	38 ± 4

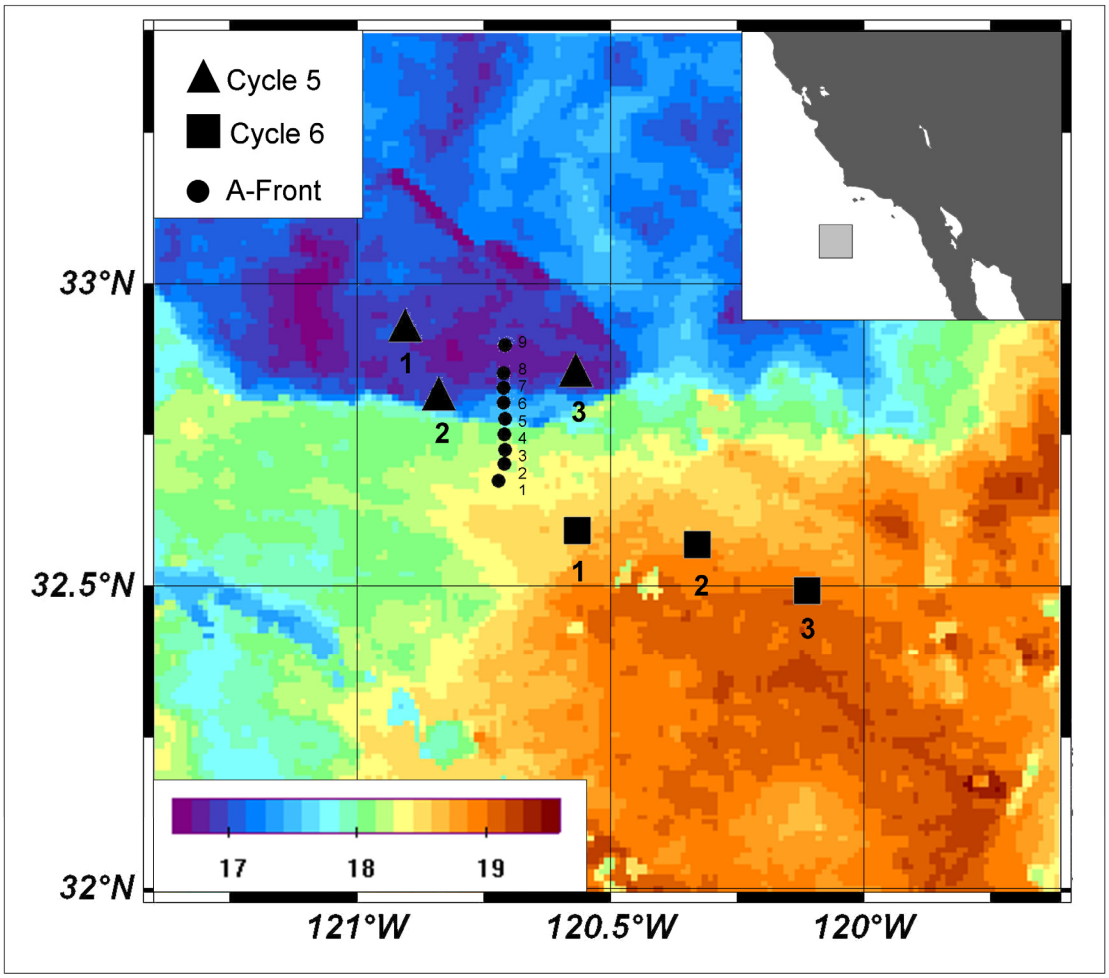

Figure 2.1. Map of A-Front station locations and satellite measured sea surface temperature (SST). Circles mark the nine transect sampling stations, triangles mark the three sampling days for Cycle 5, and squares mark the three sampling days for Cycle 6. Sampling for the A-Front transect crossing was conducted from south to north in a single night. Cycle 5 and 6 samplings were conducted from west to east following drifter flows. SST is merged from MODIS Aqua and Terra satellites from the period of 22-25 October, 2008. The color bar represents SST (°C).

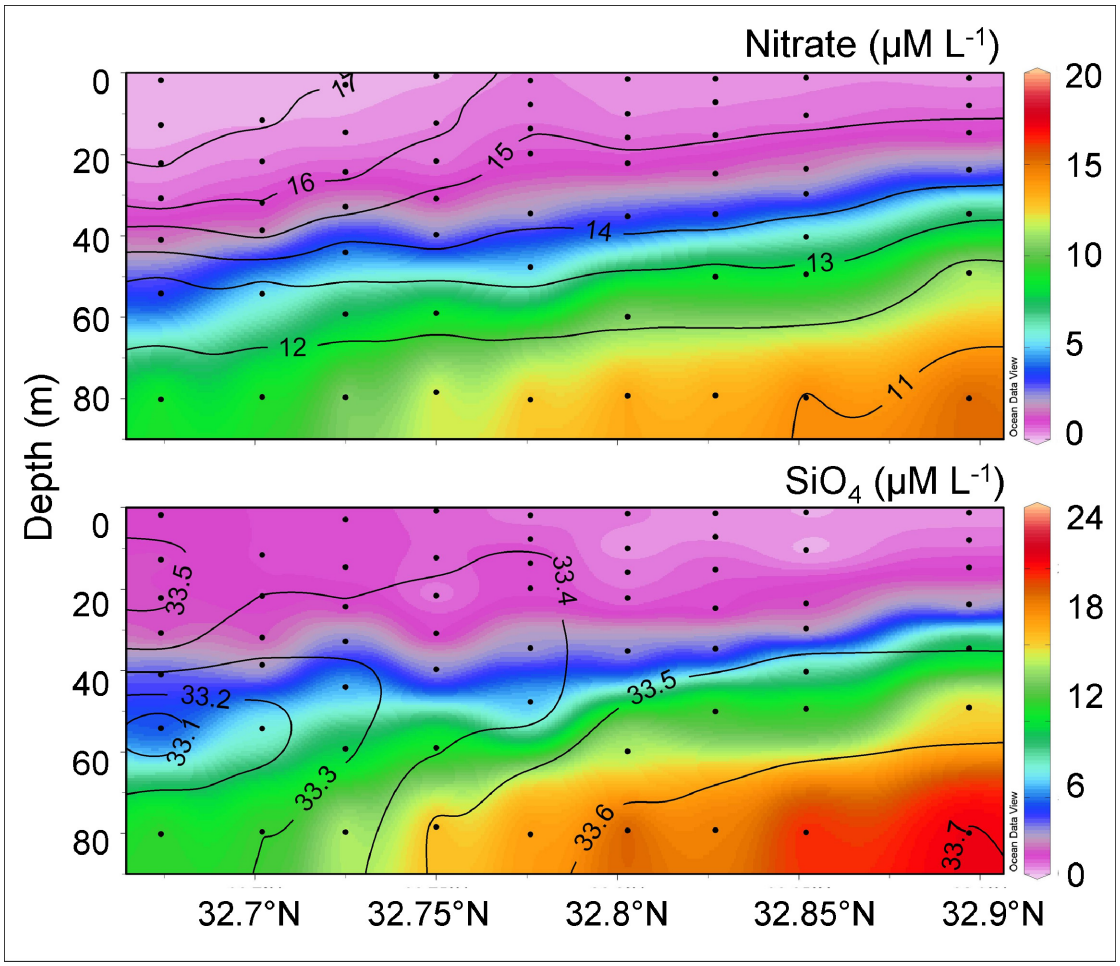

Figure 2.2. Distributions of nitrate and SiO_4 (µM L^{-1}) across A-Front. For the nitrate panel black lines are contours of isotherms (°C) and for the SiO_4 panel black lines are contours of isohalines (PSU).

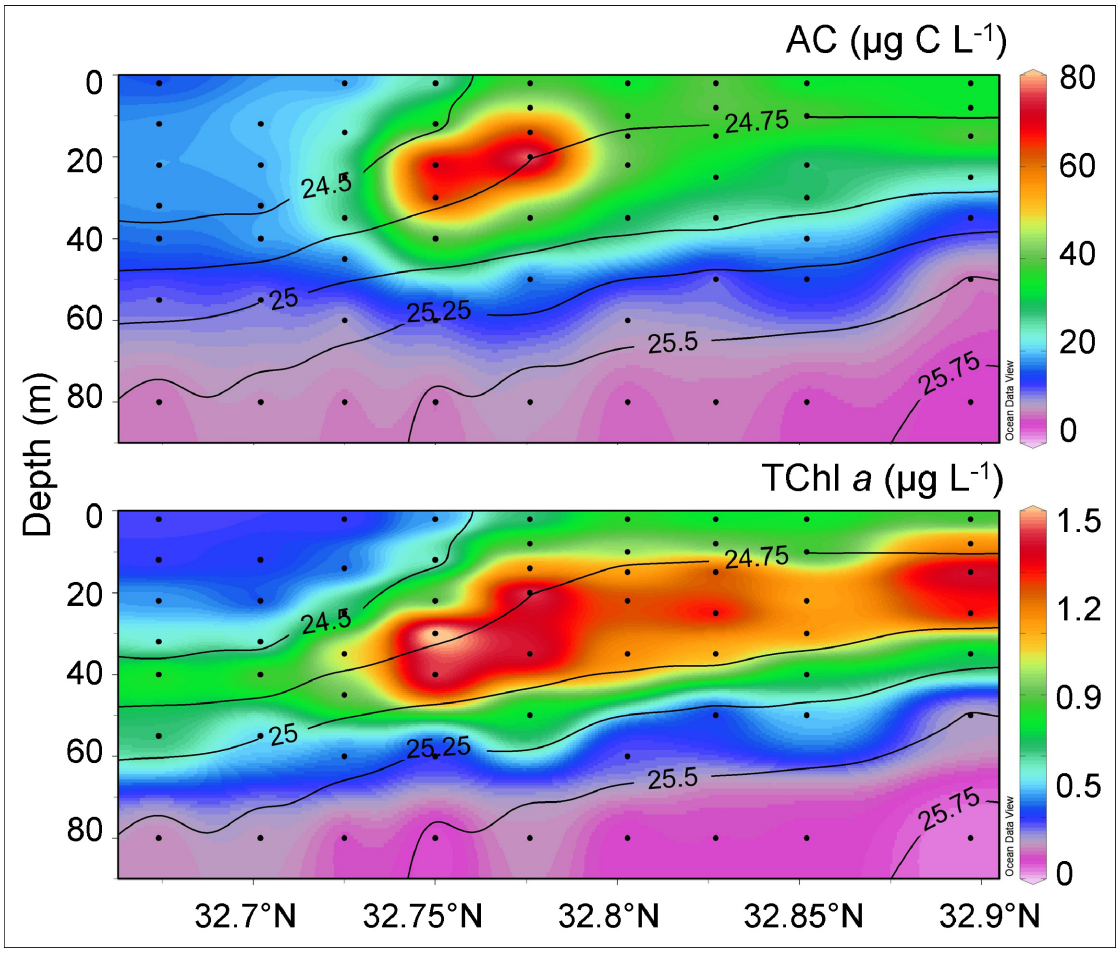

Figure 2.3. Distributions of total chlorophyll *a* (TChl *a* = µg Chl *a* L^{-1}) and total autotrophic carbon (AC = µg C L^{-1}) across A-Front. Black lines are contours of density surfaces (kg m^{-3}).

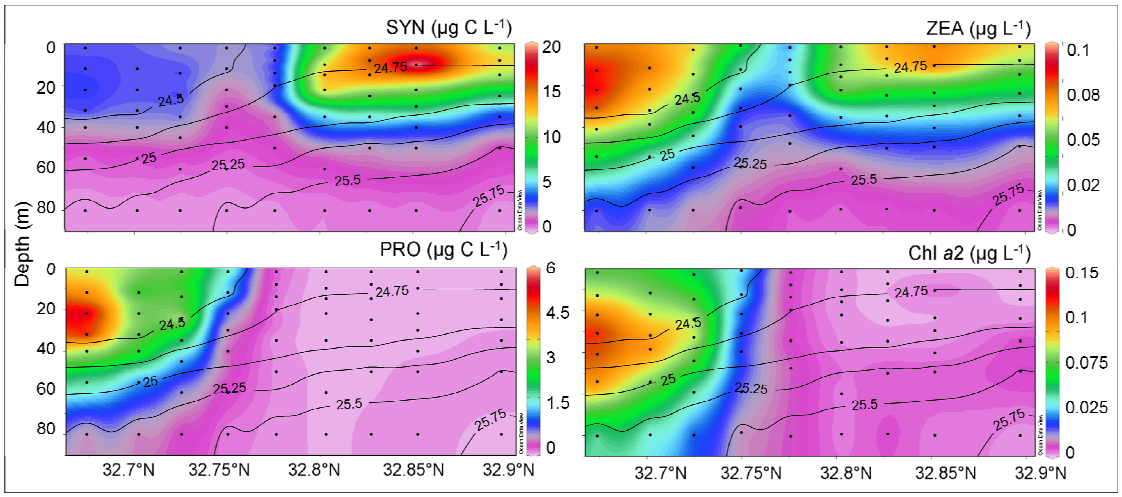

Figure 2.4. Distributions of phototrophic prokaryotes *Prochlorococcus* (PRO) and *Synechococcus* (SYN) across A-Front, as determined by flow cytometry. Units are µg C L^{-1}, and note that scales are different for each plot. Distributions of the PRO taxon-specific marker pigment divinyl chlorophyll *a* (Chl *a*2) and zeaxanthin (ZEA) which is specific to both SYN and PRO, as determined by HPLC. Units are µg pigment L^{-1}, and note that scales are different for each plot. Black lines are contours of density surfaces (kg m^{-3}).

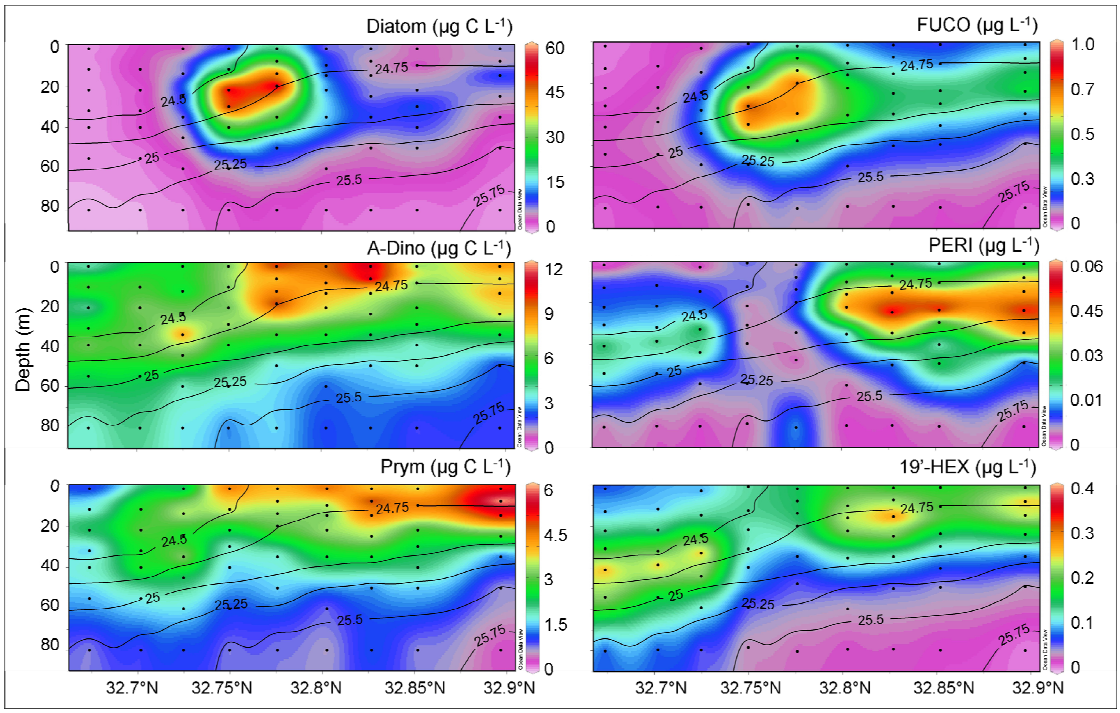

Figure 2.5. Distributions of select phytoplankton marker pigments and phytoplankton functional groups across A-Front. Fucoxanthin (FUCO), Peridinin (PERI), 19'-hexanoyloxyfucoxanthin (19'-HEX), as determined by HPLC; and Diatom, autotrophic dinoflagellates (A-Dino) and prymnesiophytes (Prym), as determined by microscopy. Units are µg pigment L^{-1} and µg C L^{-1}. Note the different scales used for each plot. Black lines are contours of density surfaces (kg m^{-3}).

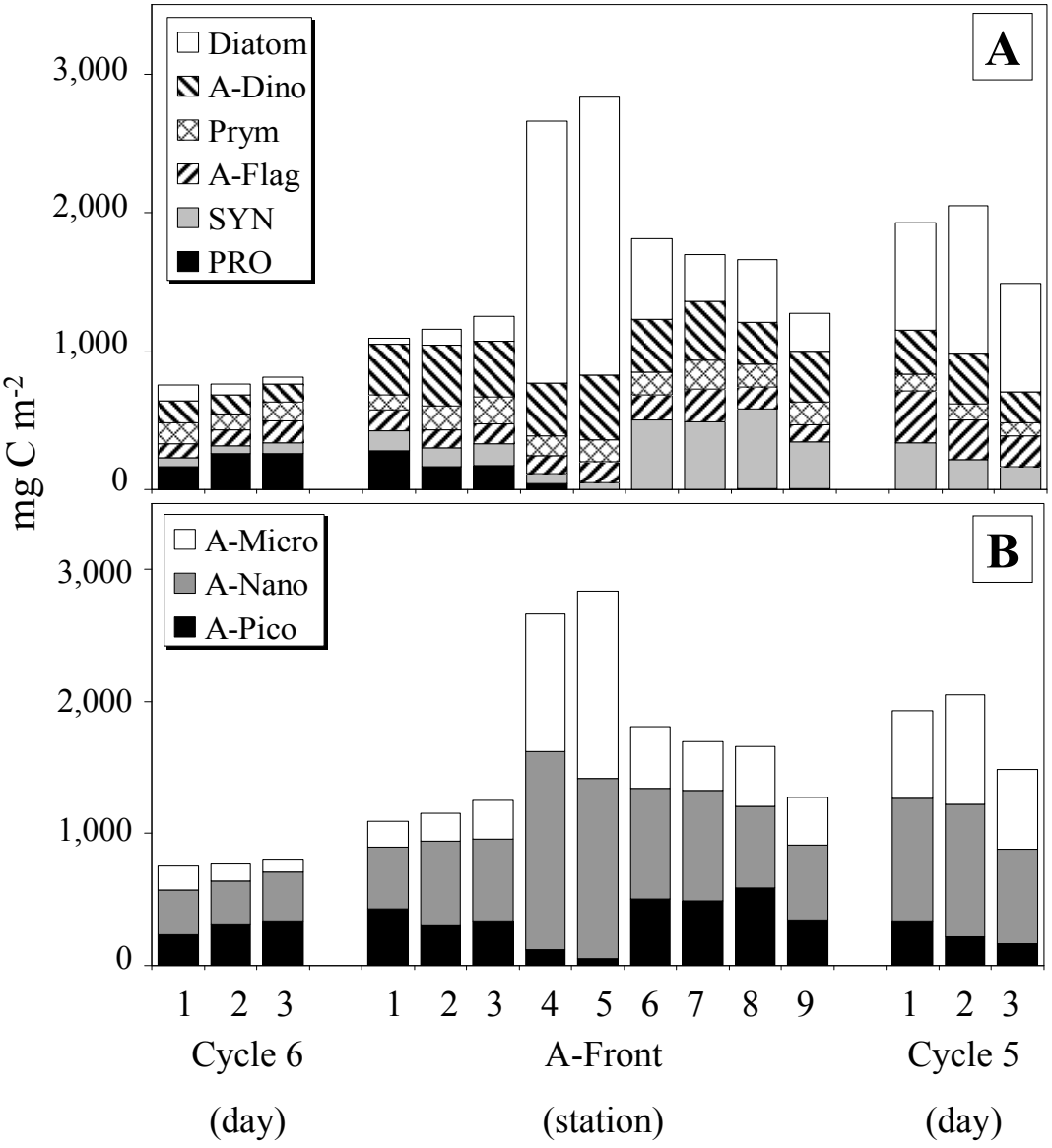

Figure 2.6. (A) Biomass contributions of phytoplankton functional groups to total euphotic-zone integrated autotrophic community biomass: Diatom, autotrophic dinoflagellate (A-Dino), prymnesiophytes (Prym), autotrophic flagellates (A-Flag), *Synechococcus* (SYN) and *Prochlorococcus* (PRO). (B) Biomass contributions of phytoplankton size classes to total euphotic-zone integrated autotrophic community biomass: A-Micro (20-200 µm), A-Nano (2-20 µm) and A-Pico (0.2-2 µm). Units are mg C m^{-2} for both plots; determined by microscopy and flow cytometry.

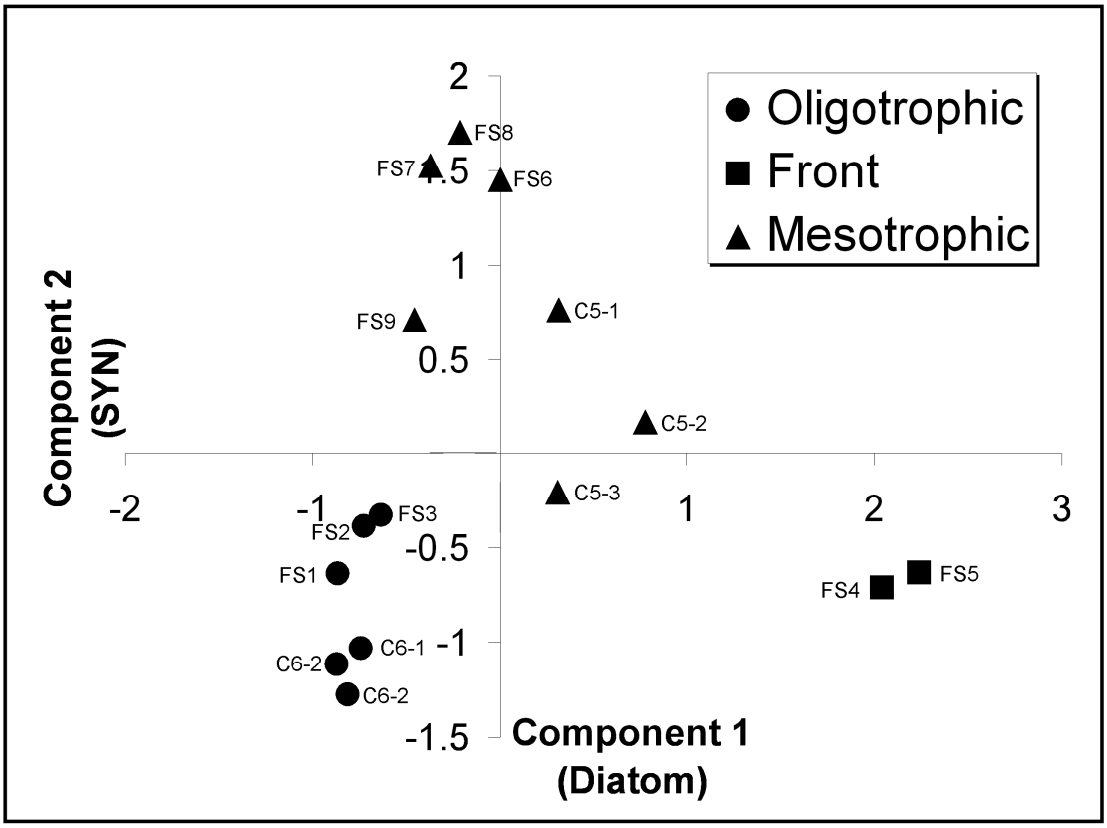

Figure 2.7. Results of a principal component analysis using all of the phytoplankton groups (*Prochlorocuccus* (PRO), *Synechococcus* (SYN), diatoms, autotrophic dinoflagellates, prymnesiophytes and autotrophic flagellates). The first two principal components, diatom and SYN, explained 88% and 8.6% of the variance, respectively. The oligotrophic cluster is Cycle 6 (C6-1, C6-2, C6-3) and transect stations 1-3 (FS1, FS2, FS3). The front cluster is transect stations 4-5 (FS4, FS5). The mesotrophic cluster is Cycle 5 (C5-1, C5-2, C5-3) and transect stations 6-9 (FS6, FS7, FS8, FS9).

References

Bakun, A. (1990) Global climate change and intensification of coastal ocean upwelling. *Science*, **247**, 198-201.

Boucher, J., Ibanez, F. and Prieur, L. (1987) Daily and seasonal variations in the spatial distribution of zooplankton populations in relation to the physical structure in the Ligurian front. *J. Mar. Res.*, **45**, 133–173.

Brown, S. L., Landry, M. R., Yang, E. J., Rii, Y. M., and Bidigare, R. R. (2008) Diatoms in the desert; plankton community response to a mesoscale eddy in the subtropical North Pacific. *Deep-Sea Res. II,* **55**, 1321-1333.

Campbell, L. and Vaulot, D. (1993) Photosynthetic picoplankton community structure in the subtropical North Pacific Ocean near Hawaii (station ALOHA). *Deep-Sea Res. I*, **40**, 2043-2060.

Chekalyuk, A. M, Landry, M. R., Goericke, R., Taylor, A. G. and Hafez, M. (in review) Laser fluorescence analysis of phytoplankton across a frontal zone in the California Current Ecosystem. *J. Plankton Res.*, this issue.

Claustre, H., Kerhervé, P., Marty, J. C., Prieur, L., Videau, C. and Hecq, J-H. (1994) Phytoplankton dynamics associated with a geostrophic front: ecological and biogeochemical implications. *J. Mar. Res.*, **52**, 711–742.

Fiala, M., Sournia, A., Claustre, H., Marty, L. C., Prieur, L., and Vétion, G. (1994) Gradients of phytoplankton abundance, composition and photosynthetic pigments across the Almeria-Oran front (SW Mediterranean Sea). *J. Mar. Syst.*, **5**, 223-233.

Franks, P. J. S. (1992a) Sink or swim: accumulation of biomass at fronts. *Mar. Ecol. Prog. Ser.*, **82**, 1–12.

Franks, P. J. S. (1992b) Phytoplankton blooms at fronts: patterns, scales and physical forcing mechanisms. *Rev. Aqua. Sci.*, **6**, 121–137.

Franks, P. J. S. and Walstad, L. J. (1997) Phytoplankton patches at fronts: a model of formation and response to wind events. *J. Mar. Res.*, **55**, 1-29.

Garrison, D. L., Gowing, M. M., Hughes, M. P., Campbell, L., Caron, D. A., Dennett, M. R., Shalapyonok, A., Olson, R. J., Landry, M. R., Brown, S. L., Liu, H., Azam, F., Steward, G. F., Ducklow, H. W. and Smith, D. C. (2000) Microbial food web structure in the Arabian Sea: a US JGOFS study. *Deep-Sea Res. II,* **47**, 1387-1422.

Goericke, R., Montoya, J. (1998) Estimating the contribution of microalgal taxa to chlorophyll *a* in the field - variations of pigment ratios under nutrient- and light-limited growth. *Mar. Ecol. Prog. Ser.* **169**, 97 - 112.

Goericke, R. (2002) Top-down control of phytoplankton biomass and community structure in the monsoonal Arabian Sea. *Limnol. Oceanogr.* **47**, 1307-1323.

Gordon, L. I., Jennings, J. C., Ross, A. A. and Krest, J. M. (1992) A suggested protocol for continuous flow automated analysis of seawater nutrients in the WOCE hydrographic program and the Joint Global Ocean Fluxes Study. Grp. Tech Rpt 92-1, OSU College of Oceanography Descr. Chem Oc.

Haury, L. R., Venrick, E. L., Fey, C. L., McGowan, J. A. and Niiler, P. P. (1993) The Ensenada Front: July 1985. *CalCOFI Reports*, **34**, 69–88.

Holligan, P. M. (1981) Biological implications of fronts on the northwest European continental shelf. *Phil. Trans. R. Soc. Lond.*, **A302**, 547-562.

Hood, R. R., Abbott, M. R. and Huyer, A. (1991) Phytoplankton and photosynthetic light response in the coastal transition zone off northern California in June 1987. *J. Geophys. Res.*, **96**, 14,769-14,780.

Houghton, R. W. and Marra, J. (1983) Physical/biological structure and exchange across the thermohaline shelf/slope front in the New York Bight. *J. Geophys. Res.*, **88**, 4467-4481.

Jacquet, S., Prieur, L., Avois-Jacquet, C., Lennon, J.-F. and Vaulot, D. (2002) Short-timescale variability of picophytoplankton abundance and cellular parameters in surface waters of the Alboran Sea (western Mediterranean) *J. Plankton Res.*, **24**, 635-651.

Jeffrey, S. W. and Wright, S. W. (2005) Photosynthetic pigments in marine microalgae. In: Subba Rao, D. V. (Ed), *Algal Cultures, Analogues of Blooms and Applications.* Science Publishers, New Hampshire, pp. 33-90.

Kahru, M., Di Lorenzo, E., Manzano-Sarabia, M. and Mitchell, B. G. (in review) Spatial and temporal statistics of sea surface temperature and chlorophyll fronts in the California Current. *J. Plank. Res.*, this issue.

Kemp, A. E. S., Pearce, R. B., Grigorov, I., Rance, J., Lange, C. B., Quilty, P. and Salter, I. (2006) Production of giant marine diatoms and their export at oceanic frontal zones: implications for Si and C flux from stratified oceans. *Global Biogeochem. Cycles*, **20**, GB4S04, doi:10.1029/2006GB002698.

Landry, M. R., Ohman, M. D., Goericke, R., Stukel, M. R., Barbeau, K., Bundy, R. and Kahru, M. (in review) Pelagic community responses to a deep-water frontal system in the California Current Ecosystem: Overview of the A-front study. *J. Plankton Res.*, this issue.

Lara Lopez, A. L., Davison, P. and Koslow, J. A. (in review) Abundance and community composition of micronekton across a frontal system off Southern California. *J. Plankton Res.*, this issue.

Li, Q. P., Franks, P. J. S., Ohman, M. D. and Landry, M. R. (in review) Enhanced nitrate fluxes and biological processes at a frontal zone in the southern California Current system. *J. Plankton Res.*, this issue.

Monger, B. C. and Landry, M. R. (1993) Flow cytometric analysis of marine bacteria with Hoechst 33342 *Appl. Environ. Microbiol.*, **59**, 905-911.

Ohman, M. D., Powell, J., Picheral, M. and Jensen, D. W. (in review) Mesozooplankton and particulate matter responses to a deep-water frontal system in the southern California Current System. *J. Plankton Res.*, this issue.

Pingree, R. D., Holligan, P. M. and Mardell, G. T. (1978) The effects of vertical stability on phytoplankton distributions in the summer on the northeast European shelf. *Deep-Sea Res.*, **25**, 1011-1028.

Reul, A., Rodríquez, V., Jiménez-Gómez, F., Blanco, J. M., Bautista, B., Sarhan, T., Guerrero, F., Ruíz, J. and García-Lafuente, J. (2005) Variability in the spatio-temporal distribution and size-structure of phytoplankton across an upwelling area in the NW-Alboran Sea, (W-Mediterranean) *Cont. Shelf Res.*, **25**, 589-608.

Samo, T. J., Pedler, B. E., Ball, I. G., Pasulka, A. L., Taylor, A. G., Aluwihare, L. I., Azam, F., Goericke, R. and Landry, M. R. (in review) Enhanced microbial processes at a water mass frontal zone in the California Current Ecosystem. *J. Plankton Res.*, this issue.

Schlitzer, R. (2006) Ocean Data View, <http://odv.awi.de>.

Sherr, E. B. and Sherr, B. F. (1993) Preservation and storage of samples for enumeration of heterotrophic protists In: Kemp, P. K. (Ed), *Handbook of Methods in Aquatic Microbial Ecology.* CRC Press, Boca Raton, Fl, pp. 207-212.

Snyder, M. A., Sloan, L. C., Diffenbaugh, N. S. and Bell, J. L. (2003) Future climate change and upwelling in the California Current. *Geophys. Res. Lett.*, **30**, dio:10.1029/2003GL017647.

Tangen, K., Björnland, T. (1981) Observations on pigments and morphology of *Gyrodinium aureolum* Hulburt, a marine dinoflagellate containing 19'-hexanoyloxyfucoxanthin as the main carotenoid. *J. Plankton Res.*, **3**, 389-401.

Taylor, A. G., Landry, M. R., Selph, K. E. and Yang, E. J. (2011) Biomass, size structure and depth distributions of the microbial community in the eastern equatorial Pacific. *Deep-Sea Res. II,* **58**, 342-357.

Traganza, E. D., Redalje, D. G. and Garwood, R. W. (1987) Chemical flux, mixed layer entrainment and phytoplankton blooms at upwelling fronts in the California coastal zone. *Cont. Shelf Res.*, **7**, 89-105.

Venrick, E. L. (2000) Summer in the Ensenada Front: the distribution of phytoplankton species, July 1985 and September 1988. *J. Plankton Res.*, **22**, 813–841.

Wang H., Schieber, B., Seegers, B. and Mitchell, B. G. (in review) Bio-optics and photo-physiology across a strong frontal gradient in the California Current Ecosystem. *J. Plankton Res.*, this issue.

CHAPTER 3

Temporal and spatial patterns of microbial community biomass and composition in the southern California Current Ecosystem

Andrew G. Taylor, Michael R. Landry, Karen E. Selph, John J. Wokuluk

Abstract

As part of the California Current Ecosystem Long Term Ecological Research (CCE-LTER) Program, samples for epifluorescence microscopy and flow cytometry (FCM) were collected at ten 'cardinal' stations on the California Cooperative Oceanic Fisheries Investigations (CalCOFI) grid during 25 quarterly cruises from 2004 to 2010 to investigate the biomass, composition and size-structure of microbial communities within the southern CCE. Based on our results, we divided the region into offshore, and inshore northern and southern zones. Mixed-layer phytoplankton communities in the offshore had lower biomass (16 ± 2 μg C L^{-1}; all errors represent the 95% confidence interval), smaller size-class cells and biomass was more stable over seasonal cycles. Offshore phytoplankton biomass peaked during the winter months. Mixed-layer phytoplankton communities in the northern and southern inshore zones had higher biomass (78 ± 22 and 32 ± 9 μg C L^{-1}, respectively), larger size-class cells and stronger seasonal biomass patterns. Inshore communities were often dominated by micro-size (20 – 200 μm) diatoms; however, autotrophic dinoflagellates dominated

during late 2005 to early 2006, corresponding to a year of delayed upwelling in the northern CCE. Biomass trends in mid and deep euphotic zone samples were similar to those seen in the mixed-layer, but with declining biomass with depth, especially for larger size classes in the inshore regions. Mixed-layer ratios of autotrophic carbon to chlorophyll *a* (AC:Chl *a*) had a mean value of 51.5 ± 5.3. Variability of nitracline depth, bin-averaged AC:Chl *a* in the mixed-layer ranged from 40 to 80 and from 22 to 35 for the deep euphotic zone, both with significant positive relationships to nitracline depth. Total living microbial carbon, including auto- and heterotrophs, consistently comprised about half of particulate organic carbon (POC).

Introduction

The California Current Ecosystem (CCE) is a productive eastern boundary current system where nutrient delivery by coastal upwelling, wind stress curl and mesoscale eddies support high plankton production and standing stocks (Huyer, 1983; Legaard and Thomas, 2006; Rykaczewski and Checkley, 2008; Mantyla et al., 2008; Thomas et al., 2009). The main core of the California Current flows equatorward along the west coast of North America, and is defined by cool, low salinity subarctic water (Hickey, 1979; Lynn and Simpson, 1987). In the southern portion of the CCE Point Conception marks a transition zone, as the primary orientation of the coast line abruptly shifts from north-south to east-west, becoming the northern portion of the Santa Barbara Basin (SBB). A poleward flowing California Undercurrent originates in the eastern tropical Pacific, bringing warm, saline water from offshore and the south and forming the Southern California eddy which is centered approximately near San Nicholas Island (Lynn and Simpson, 1987; Niiler et al., 1989; Bray et al., 1999). The interactions of these currents in the California Bight and offshore regions set up distinct floristic zones, defined by water masses and floral patterns, that can be used to split the region into northern and southern nearshore, and offshore regions (Hayward and Venrick, 1998; Venrick, 2002 and 2009).

To better understand pelagic ecosystem dynamics of the southern CCE, extensive modeling and remote sensing studies have been conducted to determine processes controlling chlorophyll *a* concentrations, primary production, phytoplankton growth rates, biomass and carbon to chlorophyll *a* ratios (Eppley et al., 1985; Peláez

and McGowan, 1986; Di Lorenzo et al., 2004; Gruber et al., 2006; Li et al., 2010; Kahru et al., 2012; Kahru et al., this issue). However, the success of such studies depends highly on quality *in situ* measurements for parameterization, algorithm development and validation.

The California Cooperative Oceanic Fisheries Investigations (CalCOFI) has conducted routine assessments of ocean hydrography and biology on a spatially extensive sampling grid pattern in the southern CCE region since 1949. Aside from regular chlorophyll *a* analyses and occasional taxonomic studies based on visual microscopy and HPLC pigment analysis (Hayward and Venrick, 1998; Venrick, 1992, 2002, 2009, 2012; Goericke, 2011), detailed investigations of microbial community biomass and structure have not been a part of the CalCOFI program. Beginning in November 2004, the California Current Ecosystem, Long Term Ecological Research (CCE-LTER) program has augmented core CalCOFI measurements in this area, using advanced high-throughput digital epifluorescence microscopy and flow cytometry (FCM), to assess microbial community biomass, size-structure and taxonomic composition.

Here we present for the first time a detailed examination of carbon biomass, size-structure and composition of CCE microbial communities, sampled on quarterly CalCOFI cruises from 2004 through 2010. The goal of the study is to establish baseline measurements for the southern CCE, that are relevant for documenting and investigating climate change impacts in the region, and that will facilitate the

development of ecosystem models and remote sensing algorithms that capture the natural variability in phytoplankton carbon biomass and functional group composition.

Materials and methods

Sample collection

We collected samples for analyses of microbial community abundance, biomass and composition during 25 quarterly CalCOFI cruises from November 2004 (cruise 200411) to November 2010 (cruise 201011). On each cruise, we sampled three depths with CTD rosette casts at each of 10 'cardinal' stations distributed onshore to offshore along Lines 80 and 90 of the standard CalCOFI grid pattern (Fig. 3.1). The locations of cardinal stations were selected so that at least two were located in each of the major floristic regions identified by Venrick (2002, 2009). The depths of sample collection were dependent upon the depth of the in vivo fluorescence maximum: Type I stations (0-50 m fluorescence max) were sampled at 10 m as well as the middle and bottom shoulder of the fluorescence layer; Type II stations (50-80 m fluorescence max) were sampled at 10 m, 40 m and the fluorescence max; and Type III stations (80-120 m fluorescence max) were sampled at 10 m, 62 m and the fluorescence max. From each depth sampled, aliquots were taken directly from the Niskin bottles for plankton community analyses by flow cytometry (FCM) and epifluorescence microscopy, as well as for concentrations of dissolved nutrients, chlorophyll *a* (Chl *a*)

and particulate organic carbon (POC) measurements made by the CalCOFI or CCE-LTER groups. Details of those methods are described below.

Analysis of eukaryotic nano- and microplankton by epifluorescence microscopy

Seawater samples (500 mL) for microscopical analysis were gently collected from the CTD and immediately preserved for slide preparation according to a modified protocol of Sherr and Sherr (1993). The samples were first preserved with 260 µL of alkaline Lugol's solution, immediately followed by 10 mL of buffered formalin and 500 µL of sodium thiosulfate, with gentle mixing between each addition. Preserved samples were shielded from light and left to rest at room temperature for 1 h. After the rest period, 1 mL of proflavin (0.33% w/v) was added and the samples were stored in the dark for an additional hour. Just prior to filtration, the preserved samples were stained with 1 mL of DAPI (0.01 mg mL^{-1}) and immediately transferred to the filtration manifold. A 50-mL aliquot (small volume, SV) of the sample was filtered through a 25-mm black polycarbonate filter with 0.8-µm pore size, and the remaining 450 mL aliquot (large volume, LV) was filtered through a 25-mm black polycarbonate filter with 8.0-µm pores. We placed a 10-mm nylon backing filter under all polycarbonate filters to promote even cell distribution, and filtered the samples under gentle vacuum pressure (<100 mm Hg). Each filter was then mounted onto glass slides with one drop of Type DF immersion oil and a No. 2 cover slip, and the prepared slides were frozen at -80°C for later analysis in the lab.

Slides were digitally imaged using a Zeiss Axiovert 200 M inverted compound microscope equipped for high-throughput epifluorescence microscopy with a motorized focus drive, stage, objective and filters. Digital images were acquired with a Zeiss AxioCam MRc black and white 8-bit CCD camera. All microscope functions were controlled by Zeiss Axiovision software, and images were collected using automated image acquisition. Exposure times for each image were automatically determined by the Axiovision software to avoid over exposure. SV samples (50 mL aliquots) were viewed at 630X magnification, and LV samples (450 mL aliquots) were viewed at 200X magnification. A minimum of 20 random positions were imaged for each slide, with each position consisting of three to four fluorescent channels: Chl *a*, DAPI, FITC (SV and LV samples) and phycoerythrin (SV samples only). In addition, 5 to 10 z-plane images were acquired at each position and for each fluorescence channel. The resulting z-stack images were subsequently combined using an extended depth of field algorithm to produce an entirely in-focus image from each position channel for Chl *a*, DAPI and FITC. These were then false colored (Chl *a* = red, DAPI = blue and FITC = green) and combined to form a single composite 24-bit RGB image for each position (Fig. 3.2).

The combined images were processed and analyzed using ImagePro software to semi-automate the enumeration of eukaryotic cells larger than 1.5 μm in length (Taylor et al., 2012). Whenever possible, 20 positions and >300 cells were counted for each slide. With a VBA script routine in the ImagePro software, a series of preprocessing steps were performed using the green channel, proflavin staining of cell

protein, to extract the cells from the background for measurement. The green channel was first extracted as an 8-bit gray scale image from the combined 24-bit RGB image. A fast Fourier transform was then applied to remove background noise, followed by the application of a Laplace filter to improve the definition of cell edges and to minimize the halo effects common in epifluorescent images. Poor quality images were discarded. Cells were automatically segmented from the background and outlined, and the outlines were reapplied to the original 24-bit image. User interaction was then required to check each image, split connected cells, outline cells that did not auto-segment from the background and delete artifacts and detritus that the software had incorrectly outlined.

Each cell was manually identified and grouped into seven plankton functional groups: autotrophic dinoflagellates (A-Dino), autotrophic flagellates (A-Flag), cryptophytes (Crypto), diatoms, prymnesiophytes (Prym), heterotrophic dinoflagellates (H-Dino) and heterotrophic flagellates (H-Flag). Autotrophic cells were identified by the presence of chlorophyll *a* (red autofluorescence under blue light excitation), generally clearly packaged in defined chloroplasts, and obvious heterotrophic cells with recently consumed prey were manually excluded from the autotroph classification. Although mixotrophy is a common nutritional strategy in pelagic microbial communities (Sanders, 1991; Jones, 2000; Stukel et al., 2011), mixotrophic cells are grouped with autotrophs in the present analysis. It should also be noted that because our preservation and slide-making protocols are inadequate for ciliates, they are not included in the resulting estimates of heterotrophic protist carbon

(HC). As a consequence, reported HC values should be viewed as conservative estimates of protistan grazer biomass in the CCE.

Analyzed cells were grouped into three size categories (Pico, <2 μm; Nano, 2-20 μm; Micro, 20-200 μm) based on the lengths of their longest axis. The size class for autotrophic picophytoplankton (A-Pico) is dominated numerically by photosynthetic bacteria, *Prochlorococcus* (PRO) and *Synechococcus* (SYN) enumerated by FCM, but microscopy included the small eukaryotes in this size category. Biovolumes (BV; μm^3) were calculated from the length (L) and width (W) measurements of each cell using the geometric formula of a prolate sphere (BV = 0.524*LWH), assuming H = W. Biomass was calculated as carbon (C; pg $cell^{-1}$) using the equations of Menden-Deuer and Lessard (2000): $C = 0.288\ BV^{0.811}$ for diatoms and $C = 0.216\ BV^{0.939}$ for non-diatoms. These microscopical estimates of community abundance, biomass and composition are available for individual cruises at the CCE-LTER DataZoo database (http://oceaninformatics.ucsd.edu/datazoo/).

Analysis of bacterial populations by flow cytometry

Samples (2 mL) for FCM analysis of phototrophic bacteria, PRO and SYN, and heterotrophic bacteria (H-Bact) were preserved with 0.5% paraformaldehyde (final concentration) and flash frozen in liquid nitrogen. On shore, the samples were stored at -80°C, then thawed in batches and stained with Hoechst 34442 (1 μg mL^{-1}, final concentration) immediately prior to the analysis (Campbell and Vaulot, 1993; Monger and Landry, 1993). The analyses were conducted at the SOEST Flow

Cytometry Facility (www.soest.hawaii.edu/sfcf) using a Beckman-Coulter Altra flow cytometer equipped with a Harvard Apparatus syringe pump for quantitative analyses and two argon ion lasers tuned to UV (200 mW) and 488 nm (1 W) excitation. Fluorescence signals were collected using filters for Hoechst-bound DNA, phycoerythrin and chlorophyll, all normalized to internal standards of 0.5- and 1.0-µm yellow-green (YG) polystyrene beads (Polysciences Inc., Warrington, PA, USA). Listmode data files (FCS 2.0 format) of cell fluorescence and light-scatter properties were acquired with Expo32 software (Beckman-Coulter) and used with FlowJo software (Tree Star, Inc., www.flowjo.com) to define populations based on DNA signal (all cells), absence of photosynthetic pigments (H-Bact), presence of Chl *a* (PRO and SYN), presence of phycoerythrin (SYN), and forward angle light scatter (relative size). Abundance estimates from FCM analyses were converted to biomass using mixed-layer estimates of 11, 32 and 101 fg C $cell^{-1}$ for H-Bact, PRO and SYN, respectively (Garrison et al., 2000; Brown et al., 2008). FCM estimates of bacterial abundance and biomass are available for individual cruises at http://oceaninformatics.ucsd.edu/datazoo/.

Chlorophyll a and POC analysis

Samples for Chl *a* and POC analyses were taken from the same hydrocasts and Niskin bottles as used for the microscopy and flow cytometry analyses.

Chlorophyll *a* values in the present dataset were obtained from the CalCOFI database (http://calcofi.org/data/ctddata.html). Analyses were done by the standard

CalCOFI chlorophyll protocol (http://www.calcofi.org/references/ccmethods/292-art-chlorophyllmethods.html), which is based on methods of Yentsch and Menzel (1963), Holm-Hansen et al. (1965) and Lorenzen (1967). Briefly, seawater samples of 50-250 ml were filtered under vacuum (< 500 mm Hg) on to 25-mm GF/F filters. The filters were placed in 10-ml screw top culture tubes, and the pigment was extracted in 8.0 ml of 90% acetone at -20°C in the dark for 24 to 48 h. Prior to analysis, the tube contents were agitated and allowed to equilibrate to room temperature in the dark. The filters were then removed from the tubes and Chl *a* fluorescence measured on a Turner Model 10AU fluorometer.

Particulate Organic Carbon (POC) values were obtained from the CCE-LTER DataZoo database (http://oceaninformatics.ucsd.edu/datazoo/). Seawater samples (0.5 to 4 L) for POC analysis were filtered onto pre-combusted 25-mm GF/F filters under low vacuum (< 40 mm Hg) and stored in liquid nitrogen. In the lab, samples were acidified with fuming HCl in a desiccator, then dried for 48 hours at 60°C. Half of the filter was then placed into a 9 x 10-mm tin capsule and analyzed on a ESC 4010 CHNSO analyzer at 1000°C, along with combusted GF/F blank and seven standards.

Data analyses and regional grouping

Based upon a preliminary comparison of community structure in mixed-layer samples for the ten cardinal sampling stations in Figure 3.1, which agreed largely with previously established floral patterns for the southern CCE (Hayward and Venrick, 1998; Venrick, 2002, 2009), we grouped the stations into southern inshore (Stas..

90.37 and 90.53), northern inshore (Stas. 82.47 and 80.55) and offshore (Stas. 90.70, 90.90, 90.120, 80.70, 80.80, and 80.100) zones. Data from these station groupings were averaged for the 25 cruises of our study period to assess temporal variability in regional mixed-layer averages of phytoplankton community carbon biomass, size-structure, taxonomic composition and pigment concentration.

Results

General seasonal and spatial trends

Averaged over the six-year study period and for all mixed-layer depths sampled at each cardinal station, total biomass and composition of the phytoplankton community show the strongest seasonal differences and the highest variability between northern (Line 80) and southern (Line 90) areas at the stations closest to the coast (Figs. 3 and 4). Along Line 80 (Fig. 3.3), the upwelling region off Point Conception (Stn. 80.55, ~ 32 km offshore) had higher mean biomass during summer and fall than winter and spring cruises, while biomass in waters overlying the Santa Barbara Basin (Stn. 82.47) was higher during winter and especially springtime cruises. Along Line 90 (Fig. 3.4), biomass was most elevated during spring and summer cruises, with the biomass peak more typically at Stn 90.53, rather than closer to shore (Stn 90.37). The pattern at Stn. 90.53 likely reflects the influence of advective transport of waters from Pt. Conception upwelling to the south (Stn 90.53, Fig. 3.1), as seen generally in satellite images, as well as the northward transport of subtropical

waters to the innermost stations of the Southern California Bight, especially during later summer and fall (Lynn and Simpson, 1987; Venrick, 2002). Biomass at the three offshore stations along each line typically declined seaward without marked seasonal blooms, although some compositional variability was evident.

Diatoms are small contributors to biomass in the offshore stations along each line, consistent with the lack of observed seasonal blooms in these areas. Conversely, at the more inshore stations, diatoms contribute significantly to biomass, particularly during the seasons when highest total biomass for a station is observed. Diatoms, however, do not account for all of the seasonal variability observed at the more inshore stations. Notably, dinoflagellates contribute comparably or more to total biomass, on average, for most of the inshore stations and for most of the year, including the seasons of high biomass (Figs. 3 and 4). Prymnesiophytes and other flagellates also make significant contributions at times, but never clearly dominate the inshore phytoplankton assemblage at any time of the year.

As would be expected from the inshore-offshore differences in phytoplankton community composition (Figs. 3 and 4), which reflect proximity to nutrient inputs, larger cells (A-Micro, 20-200 μm) are the dominant contributors to total community biomass near the coast, and particularly near the Pt. Conception upwelling center in the north and the Santa Barbara Basin (Fig. 3.5). At these stations (82.55 and 80.47, respectively), A-Micro comprises 57% of total autotrophic biomass, on average, followed by A-Nano (2-20 μm cells; 38%) and A-Pico (<2-μm cells; 5%). The inshore stations on Line 90, which are substantially further offshore than their

counterparts to the North, have a distinctly different size structure in which A-Nano cells typically comprise more biomass than A-Micro (Fig. 3.5). A-Pico cells notably maintain similar mean biomass levels (3-7 μg C L^{-1}) throughout the region, while larger cells decline significantly with distance from shore, though more so for micro- than nano-sized cells. As a consequence, A-Nano increase in relative biomass contribution, typically comprising the dominant size class (~60% of total AC), on average, at all stations except 80.55 and 82.47.

The size-structure trends for mixed-layer phytoplankton along Lines 80 and 90 are also very similar for mid and deep euphotic zone samples, although with declining carbon biomass with depth (Fig. 3.5). In mid-euphotic zone samples, mean biomass and size composition are almost identical to mixed-layer values at most stations, except for proportionally reduced size categories at 82.47 and 80.55. In the deep euphotic zone samples, the prominent peaks in nano- and micro-sized cells seen in the upper layers at coastal stations are greatly reduced relative to the size distributions at offshore stations.

Microbial carbon relationships to POC and chlorophyll

For all depths and stations sampled, estimates of total microbial carbon based on analyses by FCM and microscopy (MC; including all phytoplankton, heterotrophic protists and heterotrophic bacteria) account, on average, for half of the measured concentration of particulate organic carbon (POC) (Fig. 3.6). Very few of the microbial biomass estimates exceed measured POC, and then only by relatively small

amounts. Similarly, few of the microbial biomass estimates fall significantly below 25% of POC. An ordinary least squares regression indicates that MC is related to POC by the equation MC = 0.46 x (POC), (Pearson Correlation of 0.75; $p < 0.0001$).

Ratios of autotrophic carbon to chlorophyll *a* (AC:Chl *a*) for mixed-layer phytoplankton average 51.5 ± 5.3 (all errors are 95% confidence level unless otherwise noted) for the region and study period. However, mean AC:Chl *a* in the mixed layer varies significantly with the depth of the nitracline, defined as the depth at which nitrate concentration first reaches 1 μM, for the data binned in 20-m depth intervals (Fig. 3.7). An ordinary least squares regression yields the relationship AC:Chl *a* = 0.35 x (Nitracline depth bin) + 33.48, ($R^2 = 0.90$). On average, therefore, our estimates indicate a systematic 2-fold variability in mixed-layer AC:Chl *a* ratios between the typically nearshore, upwelling influenced waters with shallow nitraclines (AC:Chl *a* ≈ 40) and the typically offshore, oligotrophic waters with deep nitraclines (AC:Chl *a* ≈ 80). For individual samples, however, the differences can be much greater.

Similar increasing trends of AC:Chl *a* ratio with nitracline depth are also evident for samples collected routinely in the mid and deep euphotic zone (Fig. 3.7), although the slopes and intercepts decline progressively with increasing depth of collection (decreasing light level, and generally higher nutrient concentrations). Like the mixed-layer, AC:Chl *a* values for the mid euphotic zone vary 2-fold, on average, from 23 to 47 for shallow and deep nitraclines, respectively. AC:Chl *a* values for the

deep euphotic zone are less variable, with averages ranging from 22 to 33 from typical onshore to offshore conditions.

Temporal variability of phytoplankton biomass and composition

Over the study period, total autotrophic carbon (AC) and total chlorophyll *a* (TChl *a*) for the southern inshore CCE region each varied by about one order of magnitude, with AC ranging from 10 to 100 μg C L^{-1} (mean 32 ± 9 μg C L^{-1}), and TChl *a* concentrations ranging from 0.18 to 3 μg Chl *a* L^{-1} (mean 0.81 ± 0.25 μg Chl *a* L^{-1}) (Table 3.1 and Fig. 3.8A). The highest concentrations of AC were measured in July 2005 and the highest TChl *a* were measured in April 2006, while the lowest values were found in October 2006 (AC) and November 2004 (TChl *a*). For the northern inshore CCE region AC and TChl *a* also varied by about one order of magnitude, with AC ranging from 22 to 229 μg C L^{-1} (mean 78 ± 22 μg C L^{-1}), and TChl *a* ranging from 0.64 to 11 μg Chl *a* L^{-1} (mean 3.0 ± 0.95 μg Chl *a* L^{-1}) (Table 3.1 and Fig. 3.8A). The highest concentrations of AC and TChl *a* were measured in April 2010, while the lowest values of AC were found in January 2010, and November 2005 (TChl *a*). Biomass concentrations were distinctly lower and less variable in the offshore zone, ranging from 8.0 to 32.0 μg C L^{-1} (mean 16.4 ± 2.4 μg C L^{-1}) for AC (Fig. 3.8A) and from 0.15 to 0.80 μg Chl *a* L^{-1} (mean 0.40 ± 0.07 μg Chl *a* L^{-1}) for TChl *a* (Table 3.1).

Community composition by taxonomic groups differed substantially between the inshore and offshore environments. For the northern inshore stations,

phytoplankton biomass was dominated by autotrophic dinoflagellates (A-Dino) and diatoms (Table 3.1 and Fig. 3.8B), which comprised an average of 39% and 36% of AC, respectively. Temporally, dinoflagellates were the most dominant group earlier in the study period, particularly during 2005 and 2006, while diatoms predominated later (Fig. 3.8B). Other contributors to autotrophic carbon biomass varied temporally in the northern inshore zone, but decreased on average in order from autotrophic flagellates (A-Flag; 13%), prymnesiophytes (Prym; 7%), *Synechococcus* (SYN; 5%), cryptophytes (Crypto; 2%) to *Prochlorococcus* (PRO; <1%).

Among the southern inshore stations, phytoplankton biomass was dominated by diatoms and A-Dino (Table 3.1 and Fig. 3.8C), which comprised 26% and 23% of AC, respectively, on average. A-Dino were also the most dominant group earlier in the study period for the southern inshore zone, particularly during 2005 and 2006, while diatoms predominated later (Fig. 3.8C). Other contributors to AC biomass varied temporally in the southern inshore zone, but decreased on average from A-Flag (18%) to Prym (16%), SYN (12%), PRO (3%) and Crypto (2%). Phytoplankton community biomass in the offshore region of the CCE was more evenly distributed among the functional groups, with AF comprising 26%, Prym 19%, A-Dino 17%, SYN 15%, PRO 12%, diatoms 11% and Crypto 1% of mixed-layer AC biomass (Table 3.1).

Temporal variability of heterotrophic protists

The distributions of heterotrophic protists (HC) assessed by epifluorescence microscopy, comprised of heterotrophic dinoflagellates (H-Dino) and heterotrophic flagellates (H-Flag), generally follow the biomass patterns for AC, except from late 2005 to early 2006 (Fig 9A). As noted previously, since biomass of mixotrophs and ciliates are not included in our estimates of heterotrophic protist carbon, the reported values are conservative. For the northern inshore stations, HC varied by a factor of 18, with a mean concentration of 17.8 ± 6.1 μg C L^{-1} (Fig. 3.9B). The highest concentrations (61.2 μg C L^{-1}) were found during October 2006, while the lowest concentrations (3.3 μg C L^{-1}) were during July 2007. The ratio of total AC to HC for these stations ranged from 1 to 29, with a mean value of 6.8 ± 2.6.

For the southern inshore zone of the CCE, HC varied by a factor of 9, averaging 9.2 ± 1.9 μg C L^{-1} (Fig. 3.9C). The highest HC concentration (24.1 μg C L^{-1}) was in April 2006, while the lowest (2.6 μg C L^{-1}) was in April 2007. The ratio of total AC to HC for the southern onshore stations averaged 3.6 ± 0.8 and was less variable than the northern onshore zone, ranging from 1 to 10.

For the offshore regions of the CCE, HC was slightly more stable, varying by a factor of 5.8, and had a mean concentration of 6.8 ± 1.2 μg C L^{-1} (Fig. 3.9A). The highest HC value (15.3 μg C L^{-1}) was found during January 2009, while the lowest (2.6 μg C L^{-1}) was in October 2006. The ratio of AC to HC in the offshore CCE ranged from 1 to 6, with a mean value of 2.6 ± 0.4.

Discussion

Seasonal phytoplankton trends

Coastal upwelling and wind stress curl are major drivers of the nutrient inputs that support phytoplankton production and biomass in the southern CCE (Legaard and Thomas, 2006; Rykaczewski and Checkley, 2008; Mantyla et al., 2008; Thomas et al., 2009). Nutrient mixing by winter storms, followed by periods of relative calm and sunshine, can also fuel significant wintertime production in the latitudinal range (30-35°N) of the CalCOFI grid. These seasonal and areal differences in nutrient delivery mechanisms, along with relatively consistent year-round ocean conditions, lead to a poorly defined seasonal bloom cycle for the southern CCE as a whole. In addition, a recent weakening of spring blooms in the region, as noted by the shift to more summer phytoplankton maxima after the major El Niño event in 1997-98 (Venrick, 2012), might contribute to reduced seasonality in the present data.

A spring biomass maximum is only evident for station 82.47 overlying the Santa Barbara Basin, which also has relatively high biomass in the winter (Table 3.1 and Fig. 3.3). Large April blooms of diatoms in this area have long been known (Allen, 1945a,b). However,at Stn. 80.55, 32 km off Pt. Conception, which is more strongly influenced by the seasonal cycle of coastal upwelling favorable winds, biomass is highest during the summer and fall. Spring-summer differences are less well defined in the south, although mean phytoplankton biomasses for both of the shoreward stations on Line 90 increase during the summer (Table 3.1 and Fig. 3.4).

This area is enriched by wind-stress curl, by advective transport from Pt. Conception upwelling, and by eddies, fronts and meanders of the California Current jet, which takes an eastward turn toward the coast in this vicinity (Lynn and Simpson, 1987; Hayward et al., 1995; Pelaez and McGowan, 1986, Thomas and Strub, 1990; Haury et al., 1993; Venrick, 2000; Taylor et al., 2012).

Generally, mean phytoplankton biomass in the offshore stations is highest during wintertime, although the enhancement is no greater than a factor of two compared to other seasons (Figs. 3 and 4). In subtropical North Pacific waters to the west, a winter maximum in surface chlorophyll concentration has long been noted (Letelier at al., 1993; Venrick, 1993; Winn et al., 1995), though largely ascribed to a photoadaptive response of cellular pigment to lower seasonal light (Letelier et al., 1993). Additionally, Yuras et al. (2005) have reported a winter increase in chlorophyll concentration in the offshore surface waters in the southern Pacific off the coast of Chile. Our current study, as well as a recent similar analysis of phytoplankton samples collected by the Hawaii Ocean Time-series Program at Station ALOHA (Pasulka et al., 2013), document that the winter chlorophyll maximum is more than a pigment response, but an actual seasonal, though modest, increase in carbon biomass of the plankton community.

Microbial carbon relationships to POC

Particulate organic carbon (POC) measurements provide an upper-limit constraint on estimates of total microbial carbon (MC; including all phytoplankton,

heterotrophic protists and heterotrophic bacteria) from our microscopy and FCM analyses. For all stations, depths and cruises, our samples of MC average one half of POC, and only a few of the MC samples were less than 25% of POC. One conclusion that we can draw from this result is that the carbon:biovolume conversion factors used in our analyses do not produce large and obvious systematic errors in plankton biomass estimates. It is also apparent that relationships among living organisms (MC), non-living particles (detritus) and total POC are surprisingly consistent across quite variable environmental conditions in the CCE.

Cho and Azam (1990) observed a similar constancy between POC estimates and phytoplankton and bacterial carbon in environments ranging from the oligotrophic North Pacific gyre to the coastal Southern California Bight. However, their study did not include heterotrophic protists, and it used a carbon to chlorophyll *a* conversion of 47-50 to estimate phytoplankton carbon. Using similar microscopy-based assessments of protistan biomass to those used here, Landry et al. (2002) also noted that plankton carbon estimates in the Southern Ocean were consistently around a mean of 58% of POC for varying conditions, from open ocean to ice-edge blooms. In addition, Claustre et al. (1999) estimated that detrital material contributed between 43 and 55% of total euphotic-layer in the tropical Pacific, using particle attenuation as a proxy for POC, relative to chlorophyll *in situ* fluorescence. Such results suggest that there exist, at least on regional scales, a general balance of living and non-living particulate carbon across a broad range of system states.

Autotrophic carbon to chlorophyll ratios

The mean autotrophic carbon to chlorophyll *a* (AC:Chl *a*) value of 51.5 ± 5.3 determined in this study is only slightly lower than the widely used value of 58 derived by Eppley et al. (1992) from the slope of the regression of POC versus total chlorophyll *a* (TChl *a*) for samples taken in the equatorial Pacific. While is it reassuring to see that these estimates are not much different, the value of the present data is not in validating a mean number, but in guiding appropriate usage of variable AC:Chl *a* values in experimental, modeling and remote sensing studies of the CCE. Many factors affect AC:Chl *a* values, including light, nutrients, temperature, taxonomic composition, growth rate and time of day (Eppley et al., 1971; Eppley, 1972; Cullen, 1982; Geider, 1987). In addition, methodological imprecisions, notably from inadequate counts of large rare cells with high individual carbon contents, introduce substantial errors into the ratio calculations. Since such errors balance out in large data sets, our results are best viewed as providing broad mean estimates of how the ratio varies spatially within the southern CCE region, rather than precise individual estimates of ratio variability.

Mean trends in the CCE data show strong associations between AC:Chl *a* and nitracline depth for all depth strata sampled (Fig. 3.7). The taxonomic and size-class composition of the different communities of the CCE also play a role in these AC:Chl *a* trends. For example, diatoms have lower AC:Chl *a* values than autotrophic dinoflagellates, and larger cells typically have lower AC:Chl *a* than smaller cells (Chan, 1980; Falkowski et al., 1985; Geider, 1987). Therefore, coastal communities

dominated by large diatoms are expected to have lower AC:Chl *a* values. Although the mean values of AC:Chl *a* largely reflect variability along environmental gradients from the eutrophic nearshore (shallow nitracline) to oligotrophic offshore (deep nitracline), they also predict how values might respond, for example, to depression of the nitracline during El Niño events, or to temporal variability at a given location due to local processes or advective transport of water by jets, eddies, current meanders or other mechanisms. In general, variations in nitracline depth within the CCE lead to a factor of two difference in mixed-layer AC:Chl *a* values. There is another 2-fold difference, on average, between near-surface and deep euphotic zone values at a given location (Fig. 3.7).

Although AC:Chl *a* is rarely measured, both its values and its variability are important for estimating carbon flows from pigment-based experimental rate determinations (e.g., Landry et al., 2009; Stukel et al. 2013), for modeling of ocean ecosystem dynamics (Morel, 1988; Taylor et al., 1991; Sathyendranath et al., 2009; Wang et al., 2009) and for interpreting biomass and production distributions with remote sensing techniques (Eppley et al., 1985; Falkowski, 1994; Antoine et al., 1996; Behrenfeld et al., 2005). Using CCE-LTER data, for example, Li et al. (2010) have successfully parameterized models that effectively capture observed spatial and depth variability in phytoplankton biomass, AC:Chl *a* and growth rates across inshore and offshore regions of the southern CCE. In more general usage, values in the range of 20 to 80, appropriate for the conditions measured (Fig. 3.7), will better account for the natural variability of AC:Chl *a* encountered in the southern CCE region.

Community composition

Microbial communities of the CCE vary by location and season from low biomass, mixed communities of small pico- and nano-sized cells to high biomass assemblages dominated by large microplankton, often a single taxon or functional group. The former, characteristic of the offshore region, has greater taxonomic evenness than the inshore sampling stations and greater relative contribution (28%) of phototrophic bacteria (Fig. 3.3 and 3.4). In terms of size-structure and composition, the offshore CCE assemblages resemble those in oligotrophic regions of the central Pacific, although with higher biomass concentrations and substantially reduced dominance of cells in the pico-phytoplankton size class. Nonetheless, taxonomic analysis of larger cells by Venrick (1992, 2002 and 2009) has shown that species composition in offshore CCE waters is very similar to that of the North Pacific subtropical gyre (NPSG). Additionally, using the same methods as the current study, Pasulka et al. (2013) found similar phytoplankton community composition at station ALOHA in the NPSG, which would reasonably constitute the oligotrophic end-member of CCE variability.

For the inshore regions of the CCE, high nutrient delivery by coastal upwelling (Huyer, 1983; Jones et al., 1983), results in blooms of diatoms or A-Dinos, which overprint the ubiquitous background assemblage of smaller taxa (Fig. 3.3, 3.4 and 3.8B). Diatoms dominate the northern inshore phytoplankton community during most years and seasons. However, autotrophic dinoflagellates were especially prevalent in

our data from late 2004 and mid 2005 to mid 2006 (Fig. 3.8B). While conditions in the CalCOFI-CCE study area during this time period were not extraordinary, and near their long-term averages, the upwelling season in the northern California Current was markedly delayed, creating unusually warm sea surface temperatures through the spring and early summer months (Hickey et al., 2006; Peterson et al., 2006; Schwing et al., 2006; Barth et al., 2007). High dinoflagellate biomass during this period was not just a local phenomenon for the inshore region of the southern CCE. Dominant toxin-producing algal species in central California shifted from diatoms to dinoflagellates (Jester et al., 2009), and there were also reports of reduced zooplankton biomass, reduced seabird fecundity and altered marine mammal foraging in more northern waters (Peterson et al., 2006; Sydeman et al., 2006; Weise et al., 2006). Additionally, northern anchovy densities decreased significantly from 2005-2006 off the Oregon and Washington coast, and fatty acid biomarkers of northern anchovy, Pacific herring and whitebait smelt indicated that the food web in 2005 was mainly based on dinoflagellates, switching back to diatoms in 2006 (Litz, 2008; Litz et al., 2008).

Our present study of the microbial community biomass, size-structure and composition is the first of its kind for the CCE region. While the resulting six-year dataset is too short to detect long-term trends, it nevertheless establishes baseline measurements that will help to document and resolve temporal trends in future CCE and CalCOFI sampling. The present study also provides a robust dataset to facilitate the development and testing of ecosystem models at the level of phytoplankton

functional groups and to improve algorithms for extracting community biomass and composition information from satellite remote sensing measurements. Future climate changes in the southern CCE region are projected to include increased thermal stratification (Rykaczewski and Dunne, 2010), increased delivery of nitrate to coastal areas by upwelling (Bakun, 1990; Snyder et al., 2003; Aknes and Ohman, 2009), and increased number and intensity of ocean frontal systems (Kahru et al., 2012), each capable individually of significantly impacting productivity, standing stocks and composition of the food web base, though their effects will likely differ spatially. Continued monitoring as well as experimental and modeling studies are needed to elucidate how such changes will combine to alter biogeochemical cycling and trophic coupling within the southern CCE region.

Acknowledgments

We would like to thank the CCE-LTER technicians Megan Roadman and Shonna Dovel for collecting samples during the quarterly CalCOFI/CCE-LTER cruises, and the CalCOFI team for providing chlorophyll, POC and hydrographic data. Additionally, we gratefully acknowledge James Conners and the CCE-LTER DataZoo team for their help in putting together the large dataset used for this study. This work was funded by U. S. National Science Foundation grants OCE 04-17616 and 10-26607 for the CCE-LTER Program.

Chapter 3, in full, has been submitted for publication of the material as it may appear in Deep-Sea Research II: Topical Studies in Oceanography: Taylor, A.G., Landry, M.R., Selph, K.E., Wokuluk, J.J., 2013. "Temporal and spatial patterns of microbial community biomass and composition in the southern California Current Ecosystem." Deep-Sea Res. II. The dissertation author was the primary investigator and author of this paper.

Table 3.1. Mean biomass estimates, total chlorophyll *a* (TChl) and carbon to chlorophyll (C:Chl) of northern inshore (stations 82.47 and 80.55), southern inshore (stations 90.37 and 90.53) and offshore (stations 80.70, 80.80, 80.100, 90.70, 90.90 and 90.120) zones from mixed-layer depths for each cruise. Diatom, autotrophic dinoflagellates (A-Dino), prymnesiophytes (Prym), cryptophytes (Crypto), autotrophic flagellates (A-Flag), *Prochlorococcus* (PRO) and *Synechococcus* (SYN). Total autotrophic carbon (AC) is the sum of all autotrophic groups. Biomass units are µg C L^{-1} and TChl units are µg Chl L^{-1}. Errors are ± the 95% confidence interval. Cruises are listed as year and month. (Continued next two pages)

Region	Cruise	Biomass (µg C L-1)							AC	TChl	AC:Chl
		Diatom	A-Dino	Prym	Crypto	A-Flag	PRO	SYN			
Northern	2004-11	11±2.2	120±98	3.2±0.3	-	4.7±0.4	-	1.3±0.2	100±79	2.3±1.0	49±20
Inshore	2005-01	1.1±0.5	22±14	6.2±1.2	-	7.8±5.8	0.5±0.0	1.7±0.2	34±18	1.8±0.4	21±5.5
	2005-04	82±36	7.5±4.8	19±5.0	-	4.5±1.2	1.4±1.4	0.4±0.1	110±36	8.0±4.8	18±6.5
	2005-07	29±5.4	2.9±0.6	2.6±0.3	-	7.8±4.0	-	0.1±0.0	42±2.2	1.1±0.3	42±8.9
	2005-11	12±7.6	160±21	2.8±0.1	1.4±1.4	4.0±0.3	-	0.5±0.0	180±29	0.6±0.2	310±70
	2006-02	11±8.1	150±8.1	5.2±1.3	0.7±0.2	7.5±2.3	-	2.3±0.3	170±3.8	3.2±0.2	55±2.6
	2006-04	13±12	29±24	12±1.3	-	6.0±4.3	-	3.6±2.9	63±36	3.5±2.6	23±6.7
	2006-07	19±17	71±38	13±5.6	10±7.6	41±11	-	3.7±0.6	160±45	3.0±1.1	56±6.5
	2006-10	9.1±6.2	37±22	2.5±0.2	0.5±0.5	3.4±1.1	0.8±0.5	3.9±1.7	57±32	1.4±0.5	37±9.0
	2007-01	28±3.9	11±8.5	2.7±0.4	2.0±1.9	5.4±1.7	-	0.3±0.0	49±1.3	2.8±0.4	18±3.0
	2007-04	15±10	0.7±0.1	5.4±1.4	1.7±0.1	2.7±0.2	-	0.3±0.1	25±9.4	1.8±1.0	16±4.0
	2007-07	17±15	31±29	4.4±0.6	3.1±1.2	1.7±0.5	0.3±0.1	3.0±1.2	61±46	1.2±0.7	42±15
	2007-11	2.9±1.3	11±0.8	10±3.8	2.0±2.0	15±8.1	1.3±0.2	9.2±3.1	51±15	2.1±1.1	28±7.5
	2008-01	1.4±1.3	4.9±1.8	6.3±3.6	1.4±0.6	7.8±0.4	0.4±0.1	3.1±0.2	25±5.2	1.4±0.3	18±0.8
	2008-04	58±29	31±25	3.3±0.5	0.3±0.3	4.9±0.7	-	0.9±0.1	98±54	5.2±2.6	18±1.1
	2008-08	2.5±2.5	0.9±0.6	3.6±0.9	0.6±0.6	13±1.8	0.5±0.4	5.6±2.3	27±3.7	1.6±0.4	18±1.6
	2008-10	4.0±3.4	0.7±0.3	2.8±2.5	-	16.3±0.1	-	7.4±2.2	31±8.5	0.9±0.5	43±13
	2009-01	0.7	13.0	11.0	1.2	13.0	1.8	12.0	52.0	1.0	51.0
	2009-03	75±68	4.6±0.6	1.2±0.8	3.3±2.5	14±3.6	-	1.2±0.6	99±72	5.5±3.6	17±2.4
	2009-07	55±3.6	3.2±1.5	5.8±3.0	7.2±7.0	7.2±1.9	-	3.4±0.4	81±17	2.3±1.2	43±15
	2009-11	12±8.2	4.0±2.5	2.5±0.2.0	1.0±0.8	7.2±1.4	0.2±0.2	5.8±1.0	33±7.4	3.0±2.2	20±12
	2010-01	3.5±2.9	2.7±0.6	3.4±0.1	0.8±0.1	10±5.2	-	1.6±0.1	22±8.8	1.0±0.2	21±3.9
	2010-04	180±150	30±12	4.6±0.2	0.5±0.5	15±4.8	0.3±0.3	0.3±0.2	230±170	11±8.2	21±0.1
	2010-08	15±8.8	6.3±1.4	8.7±4.2	1.0±0.9	17±3.9	-	15±6.3	63±1.8	5.1±2.7	17±8.9
	2010-11	51±1.7	3.4±1.0	2.4±0.6	1.8±1.8	6.3±2.1	-	2.0±0.8	67±1.3	3.2±0.2	21±0.6
Southern	2004-11	0.9±0.8	1.8±1.0	2.6±0.6	-	2.5±0.4	2.6±0.0	0.7±0.3	11±1.1	0.2±0.0	63±4.3
Inshore	2005-01	0.6±0.1	0.3±0.2	3.8±0.4	-	3.4±1.4	3.1±0.4	3.0±0.9	14±1.9	0.6±0.1	24±2.2
	2005-04	25±20	1.2±0.1	2.3±0.6	-	3.5±0.3	0.4±0.4	4.8±4.2	37±15	0.7±0.4	59±10
	2005-07	33±24	56±16	7.0±0.7	-	1.7±0.1	-	1.9±1.4	99±9.1	1.0±0.5	120±54
	2005-11	-	-	-	-	-	-	-	-	-	-
	2006-02	0.3±0.1	2.8±0.6	9.6±1.9	0.1±0.1	6.8±0.3	1.4±1.2	2.9±1.2	24±0.4	0.6±0.2	53±24
	2006-04	18±11	41±16	9.7±2.5	2.9±0.3	8.4±6.5	-	0.9±0.2	81±13	3.0±0.2	27±6.2
	2006-07	2.5±1.3	30±23	12±4.9	3.0±2.9	9.6±6.4	1.1±0.4	17±14	75±6.1	1.2±0.8	110±71
	2006-10	0.1±0.0	2.1±0.3	1.7±1.2	-	3.0±1.4	2.1±0.6	0.6±0.1	9.5±0.2	0.2±0.0	45±6.1
	2007-01	3.9±3.1	2.7±0.9	1.7±0.2	0.5±0.5	2.9±1.8	-	1.3±0.9	13±7.4	0.5±0.3	24±2.2
	2007-04	0.8±0.1	0.6±0.2	8.7±3.9	1.0±1.0	5.2±2.3	-	2.2±0.6	19±6.9	0.8±0.5	32±11
	2007-07	28±23	2.2±0.9	5.5±1.4	2.8±2.8	6.5±0.1	0.6±0.2	3.5±0.8	49±27	1.9±1.5	37±14
	2007-11	0.9±0.7	6.6±3.7	5.0±2.7	1.1±0.7	5.7±3.9	-	3.2±1.6	23±13	1.1±0.5	18±4.3
	2008-01	1.2±0.6	5.0±1.0	8.3±4.2	1.1±1.1	13±7.3	0.4±0.1	6.5±1.2	35±11	1.2±0.6	32±6.7
	2008-04	10±6.7	1.6±1.1	4.0±2.0	1.1±0.1	6.0±1.7	-	1.5±1.1	24±0.6	1.5±0.0	16±0.1
	2008-08	0.3±0.1	-	1.7±0.2	-	5.4±1.9	0.8±0.8	1.6±0.1	9.9±1.5	0.3±0.0	37±0.9
	2008-10	34±30	-	1.9±0.3	-	6.4±0.2	-	2.7±1.7	45±31	0.7±0.5	67±1.6
	2009-01	3.3±0.3	11±7.4	7.0±2.2	0.2±0.2	9.4±2.3	0.4±0.4	7.3±1.5	39±10	0.8±0.1	50±4.2
	2009-03	0.5±0.1	2.1±1.0	2.4±0.9	-	6.0±0.5	2.3±1.2	6.7±1.8	20±1.7	0.5±0.1	44±4.2
	2009-07	24±9.9	2.4±0.6	3.1±0.7	-	3.0±1.2	0.2±0.2	2.1±1.1	35±9.5	0.4±0.1	96±4.3
	2009-11	-	0.8±0.7	3.0±2.1	-	3.3±1.5	1.0±0.2	4.6±1.8	13±6.4	0.3±0.1	35±8.3
	2010-01	0.1±0.0	0.8±0.0	2.9±0.6	0.4±0.4	3.8±1.0	0.8±0.2	6.1±4.8	15±6.5	0.4±0.1	35±11
	2010-04	1.5±1.3	4.1±1.8	6.3±1.8	0.5±0.5	7.9±0.3	1.5±0.4	4.4±1.9	26±4.6	0.5±0.1	54±0.8
	2010-08	1.0±0.9	1.1±0.7	5.2±2.0	-	6.0±1.5	0.3±0.3	5.5±2.4	19±6.0	0.5±0.0	36±8.4
	2010-11	8.0±4.6	1.6±0.3	11±3.9	-	9.0±0.4	2.5±0.6	3.4±1.9	36±0.9	0.7±0.1	50±8.0

Table 3.1 continued

Region	Cruise	Biomass (µg C L-1)							AC	TChl	AC:Chl
		Diatom	A-Dino	Prym	Crypto	A-Flag	PRO	SYN			
Offshore	2004-11	2.7±2.2	1.4±0.3	2.0±0.5	-	9.8±5.7	2.9±0.7	1.7±0.7	20±6.1	0.5±0.2	72±18
	2005-01	0.6±0.3	4.6±1.3	2.2±0.5	-	3.8±0.6	3.0±0.5	4.9±1.8	19±3.3	0.5±0.2	48±7.7
	2005-04	1.4±0.7	3.4±1.1	3.1±0.7	-	1.5±0.2	1.2±0.4	0.8±0.3	11±2.7	0.2±0.0	130±47
	2005-07	0.1±0.0	2.1±0.6	4.2±0.7	-	1.4±0.6	2.4±0.6	1.0±0.6	11±1.8	0.4±0.1	30±5.8
	2005-11	0.1±0.1	2.0±0.7	3.8±1.0	0.1±0.1	2.3±0.6	2.1±0.3	2.7±1.8	13±3.8	0.4±0.1	33±4.1
	2006-02	-	1.6±0.3	3.5±0.6	-	1.9±0.5	1.7±0.5	1.0±0.4	9.7±1.3	0.3±0.1	40±7.4
	2006-04	0.3±0.1	2.9±1.2	4.0±0.8	-	1.7±0.5	1.9±0.6	1.8±0.8	13±2.0	0.2±0.0	85±18
	2006-07	0.3±0.1	1.4±0.4	1.9±0.7	-	1.8±0.5	3.4±0.9	2.4±1.5	11±2.5	0.3±0.1	56±12
	2006-10	0.2±0.1	0.9±0.2	1.4±0.4	-	2.2±0.3	3.0±0.4	0.4±0.1	8.0±1.0	0.2±0.0	60±13
	2007-01	15±14	3.4±1.1	2.7±0.9	0.8±0.4	4.6±1.5	2.9±0.6	2.0±0.9	32±13	0.8±0.2	40±6.8
	2007-04	1.4±0.8	1.4±0.5	4.1±0.6	0.2±0.2	2.6±0.7	1.4±0.9	1.1±0.4	12±2.2	0.4±0.1	50±13
	2007-07	1.3±0.5	1.2±0.4	3.7±0.8	-	2.4±0.4	2.7±0.6	0.3±0.1	12±1.5	0.2±0.1	100±18
	2007-11	1.4±0.7	4.2±1.6	2.8±0.7	0.3±0.3	3.2±0.9	1.9±0.5	3.7±1.5	18±4.4	0.4±0.1	48±9.4
	2008-01	0.7±0.3	3.2±1.5	5.0±0.7	0.3±0.1	4.6±0.9	1.3±0.7	3.0±1.1	18±3.8	0.6±0.1	32±4.6
	2008-04	7.6±4.1	3.7±0.9	3.8±0.6	0.3±0.1	5.0±0.8	0.9±0.5	1.8±0.5	23±4.2	0.8±0.3	44±9.0
	2008-08	0.5±0.2	0.8±0.5	1.2±0.2	0.1±0.0	4.6±1.1	0.2±0.2	1.9±0.4	9.4±1.5	0.2±0.0	44±6.0
	2008-10	3.2±1.6	0.8±0.4	1.8±0.4	-	6.6±2.1	-	1.5±0.5	14±4.6	0.3±0.1	47±4.5
	2009-01	0.6±0.3	8.6±3.2	5.7±0.7	0.3±0.2	5.9±1.0	1.8±0.2	4.1±1.3	27±5.5	0.5±0.1	53±3.9
	2009-03	1.1±0.4	1.2±0.5	2.2±0.4	-	6.5±1.8	1.1±0.2	1.5±0.3	14±2.8	0.3±0.1	40±3.4
	2009-07	0.3±0.1	4.4±1.2	2.7±0.7	0.1±0.1	3.8±0.5	0.9±0.2	2.1±0.7	14±2.8	0.2±0.0	79±4.9
	2009-11	0.3±0.2	1.0±0.3	3.2±1.5	0.5±0.2	4.5±1.2	1.4±0.3	2.9±1.0	14±3.9	0.5±0.2	36±4.9
	2010-01	-	1.5±0.6	2.4±1.0	-	9.1±2.8	1.7±0.1	3.7±1.2	18.5±5	0.4±0.1	44±3.3
	2010-04	3.8±3.3	6.0±2.4	2.8±0.4	0.2±0.2	5.6±1.2	0.8±0.3	5.3±2.1	24±6.5	0.7±0.4	59±8.7
	2010-08	0.7±0.6	1.6±1.2	2.4±0.5	0.3±0.3	4.5±1.6	3.1±0.8	4.2±2.4	17±4.9	0.3±0.1	64±6.6
	2010-11	0.7±0.6	5.2±2.1	4.7±1.3	0.5±0.3	7.4±3.2	3.3±0.6	5.0±2.2	27±8.6	0.5±0.2	64±6.6

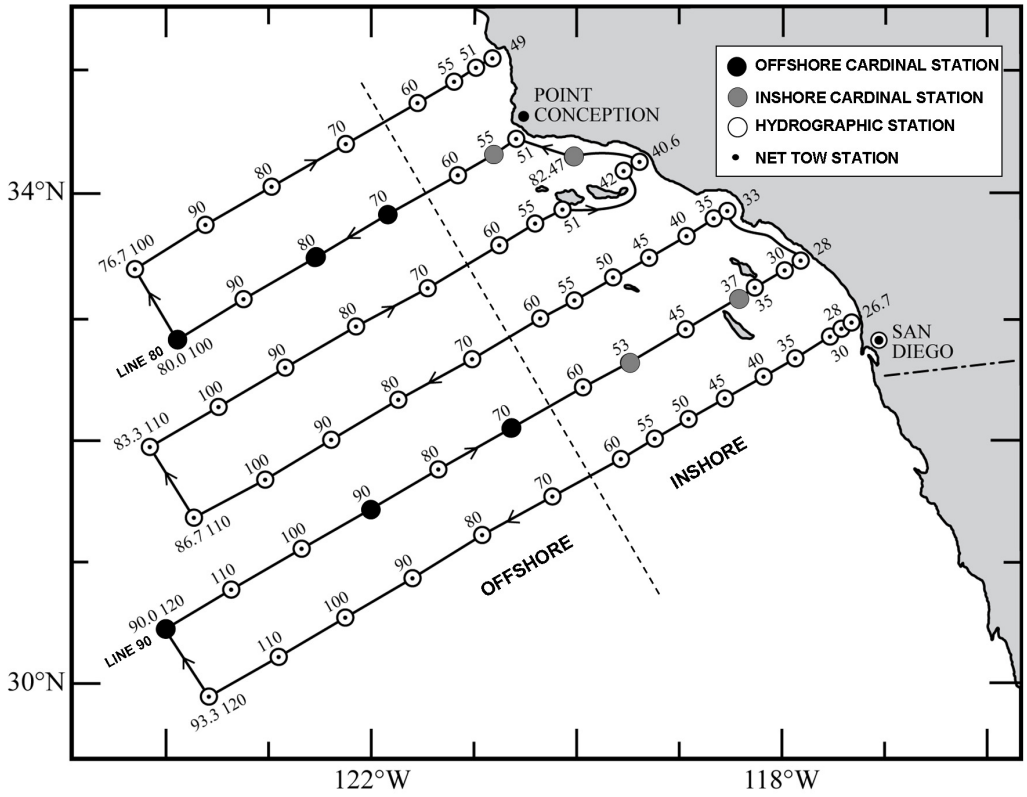

Figure 3.1. Map of the CCE region showing the standard cruise tracks and station position of the CalCOFI sampling grid. The ten cardinal stations are depicted with filled in solid circles. Coastal cardinal stations are solid grey, offshore cardinal stations are solid black. Open circles are the other standard CalCOFI hydrographic stations. Map adapted from calcofi.org.

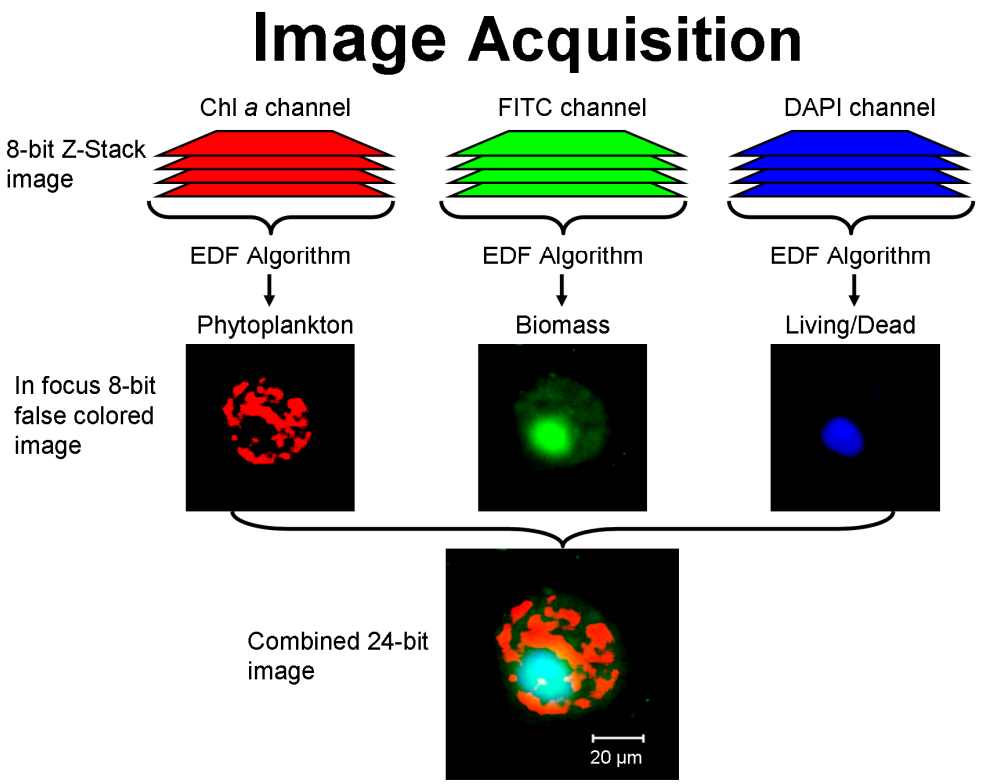

Figure 3.2. A graphical illustration of the automated image acquisition process, for a single slide position using the advanced epifluorescence microscopy method. Chlorophyll *a* channel is Chl *a* autofluorescence, FITC channel is proflavin stained protein fluorescence, and DAPI channel is DAPI stained DNA fluorescence. The actual image shown the in focus 8-bit false colored image is an autotrophic dinoflagellate under each channel, and the combined 24-bit image is three separate channels put together.

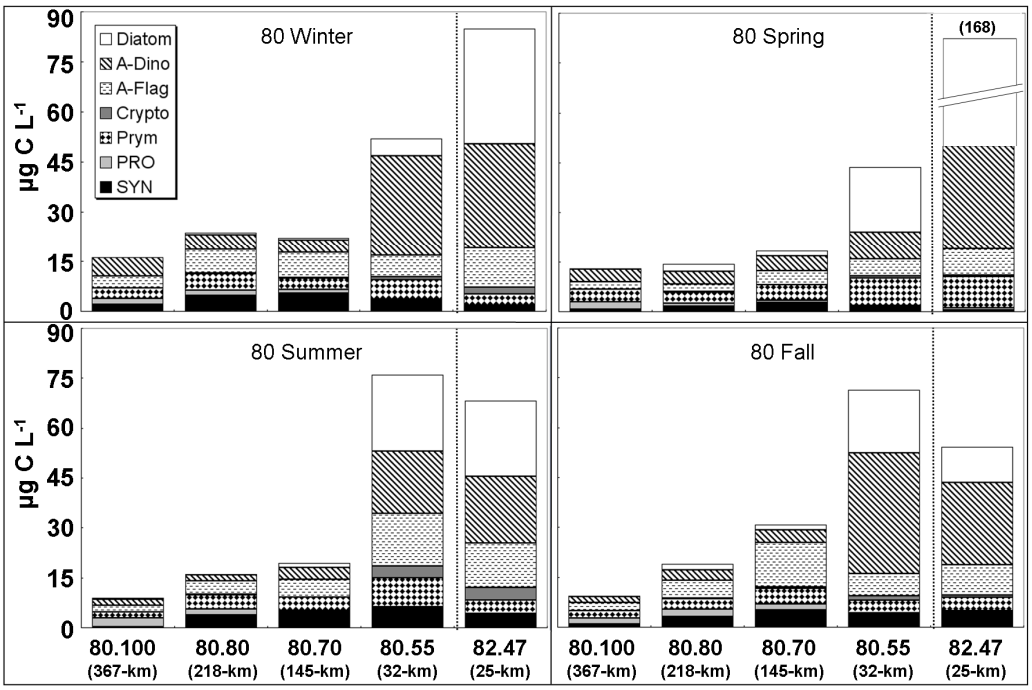

Figure 3.3. Mean seasonal variations of mixed-layer phytoplankton taxa along Line 80. Diatom, autotrophic dinoflagellates (A-Dino), autotrophic flagellates (A-Flag), cryptophytes (Crypto), prymnesiophytes (Prym), *Prochlorococcus* (PRO) and *Synechococcus* (SYN). Units are µg C L^{-1}. Station numbers and distance from shore are given on the x-axis. Note that the bar for station 82.47 has been reduced in the spring to fit on this axis. The actual biomass concentration reached an average of 168 µg C L^{-1}, with diatoms comprising 118 µg C L^{-1} of the total community biomass. A dotted line separates the Santa Barbara Basin (station 82.47) from the rest of line 80.

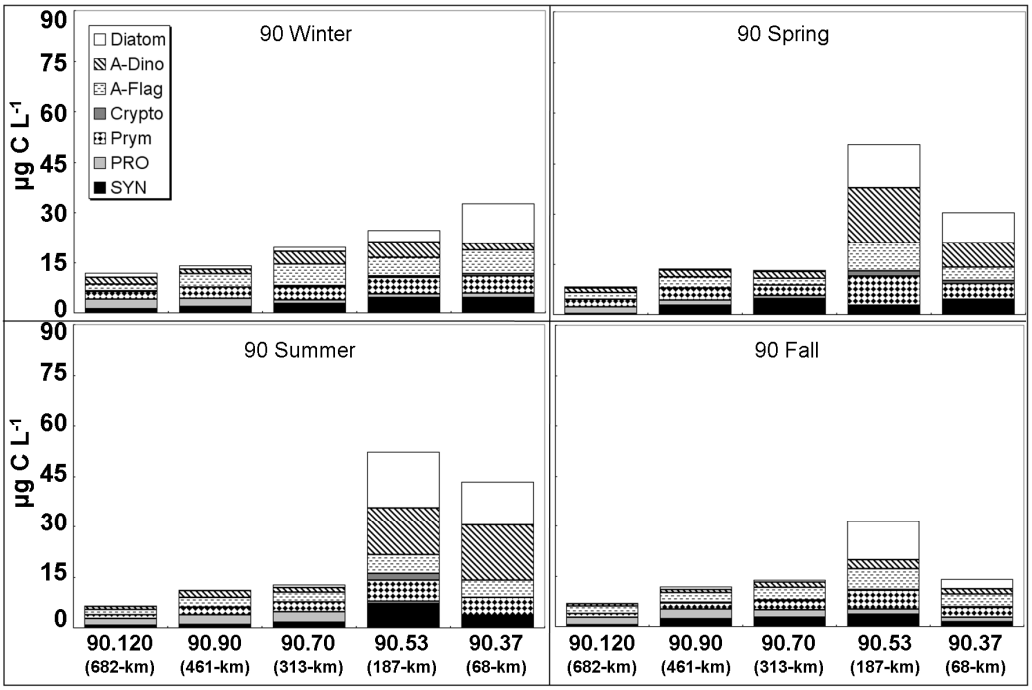

Figure 3.4. Mean seasonal variations of mixed-layer phytoplankton taxa along Line 90. Diatom, autotrophic dinoflagellates (A-Dino), autotrophic flagellates (A-Flag), cryptophytes (Crypto), prymnesiophytes (Prym), *Prochlorococcus* (PRO) and *Synechococcus* (SYN). Units are µg C L^{-1}. Station numbers and distance from shore are given on the x-axis.

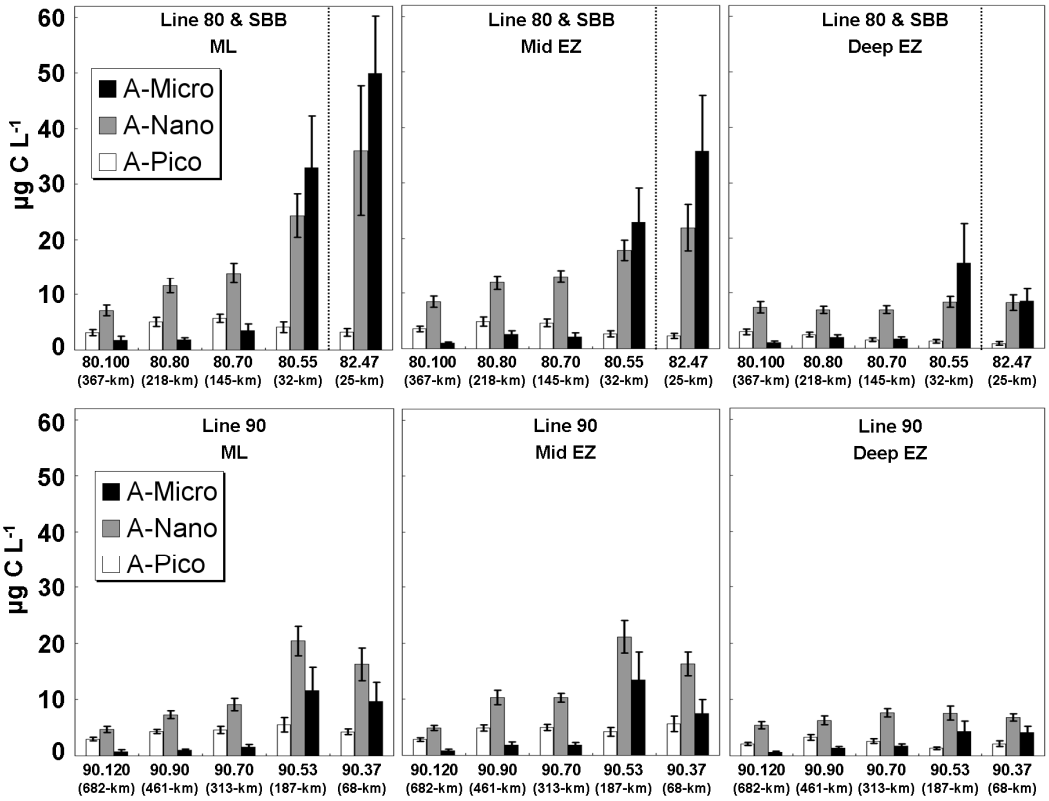

Figure 3.5. Mean autotrophic community size-class structure from the mixed-layer (ML), mid euphotic zone (Mid EZ) and deep euphotic zone (Deep EZ) for the ten cardinal stations sampled during quarterly cruises from November 2004 to October 2010. Size-classes are based on the longest cell axis measured: A-Pico (0.2 – 2 µm), A-Nano (2 – 20 µm) and A-Micro (20 – 200 µm). Units are µg C L^{-1} and error bars represent the 95% confidence level. Station numbers and distance from shore are given on the x-axis. A dotted line separates the Santa Barbara Basin (station 82.47) from the rest of line 80.

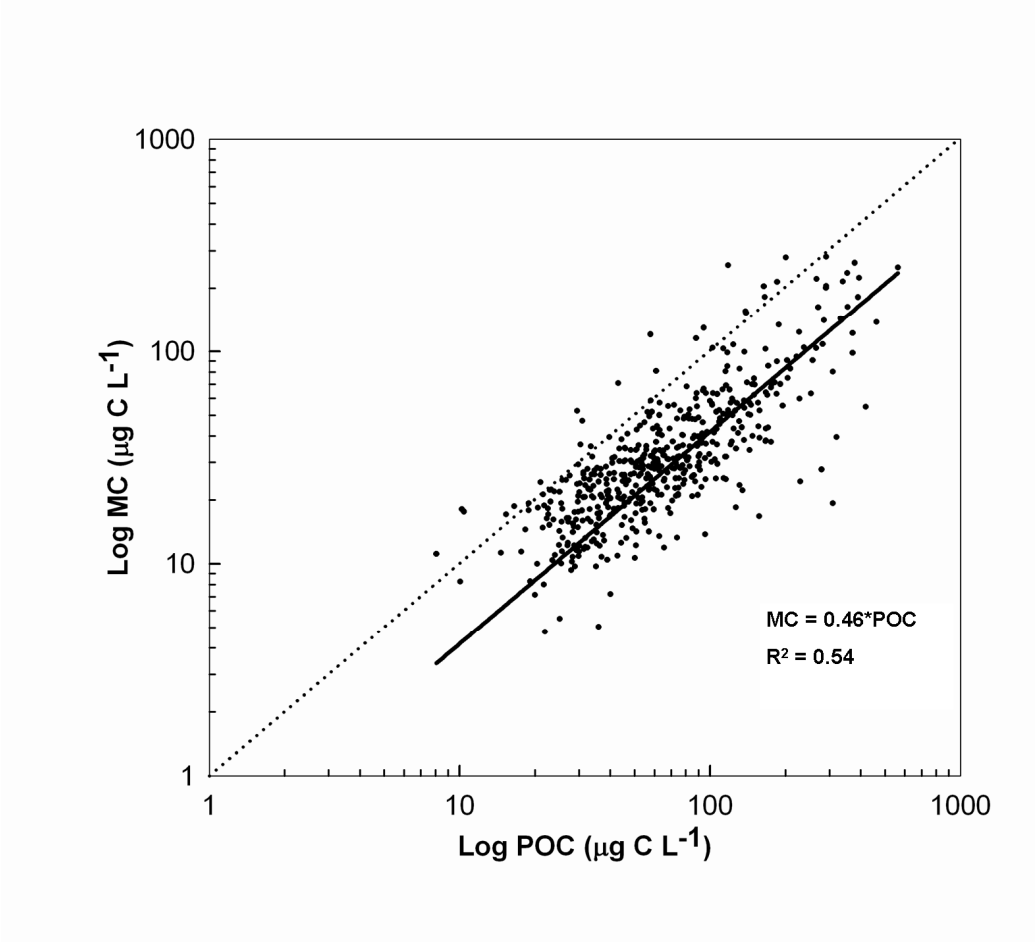

Figure 3.6. Relationship between POC and total microbial carbon (MC) for all stations, depths and cruises. MC is the sum of *Prochlorococcus*, *Synechococcus*, diatom, autotrophic dinoflagellates, autotrophic flagellates, cryptophytes, prymnesiophytes, heterotrophic dinoflagellates, heterotrophic flagellates and heterotrophic bacteria. Ordinary least squares regression, $y = 0.46x$, ($R^2 = 0.54$). The dotted line represents the 1:1 relationship.

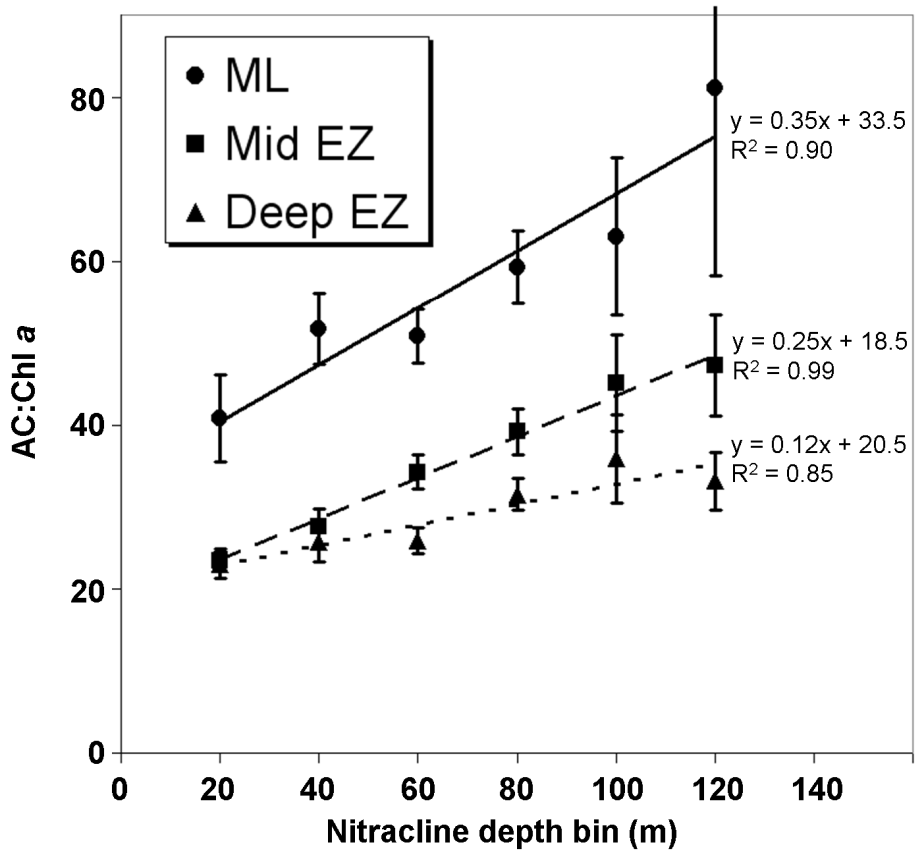

Figure 3.7. Mixed layer (ML), mid euphotic zone (Mid EZ) and deep euphotic zone (Deep EZ) autotrophic carbon:chlorophyll *a* ratios (AC:Chl) as a function of nitracline depth bin for all cardinal stations sampled from November 2004 to October 2010. The solid line represents an ordinary least squares (OLS) regression for the ML, the dashed line represents an OLS regression for the Mid EZ and the dotted line represents an OLS regression for the Deep EZ. Equations and R^2 values for each regression are shown next to the regression line on the plot.

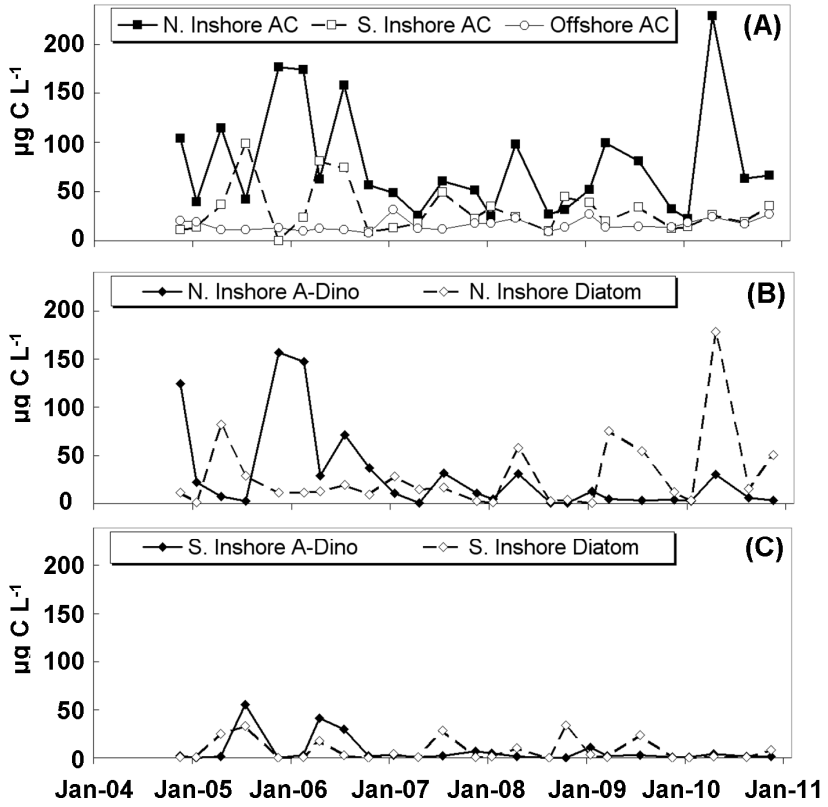

Figure 3.8. (A) Mixed-layer biomass of total autotrophic carbon (AC) from November 2004 to October 2010. Offshore stations, northern inshore stations (N.) and southern inshore stations (S.). (B) Mixed-layer biomass of northern inshore autotrophic dinoflagellates (A-Dino) and diatoms. (C) Mixed-layer biomass of southern inshore A-Dino and diatoms. Units are µg C L^{-1}.

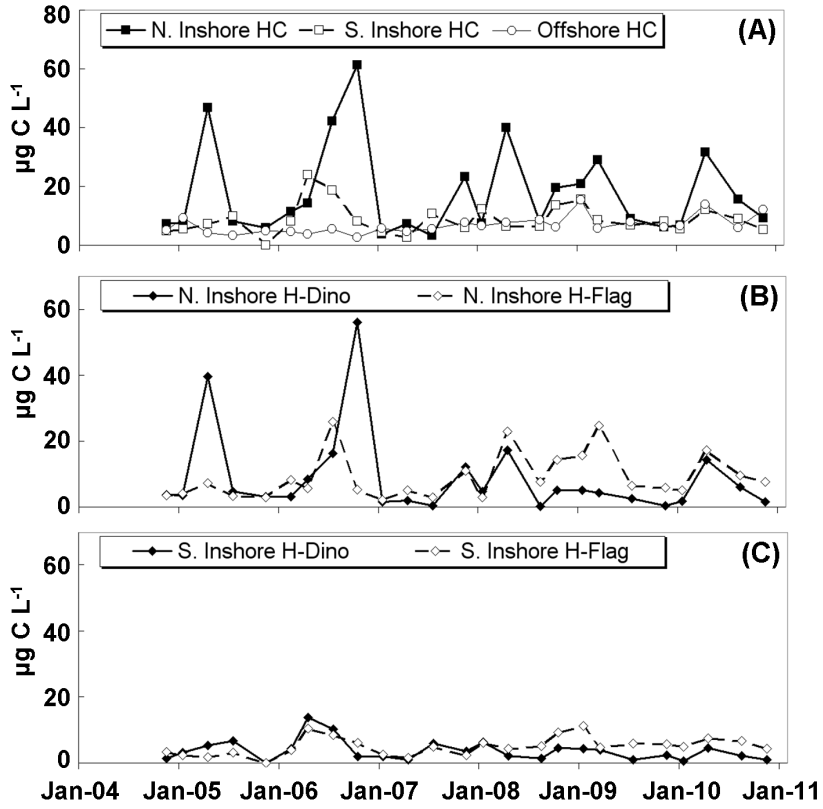

Figure 3.9. (A) Mixed-layer biomass of total heterotrophic protist carbon (HC) from November 2004 to October 2010. Offshore stations, northern inshore stations (N.) and southern inshore stations (S.). (B) Mixed-layer biomass of northern inshore heterotrophic dinoflagellates (H-Dino) and heterotrophic flagellates (H-Flag). (C) Mixed-layer biomass of southern inshore H-Dino and H-Flag. Units are µg C L^{-1}.

References

Aksnes, D.L., Ohman, M.D., 2009. Multi-decadal shoaling of the euphotic zone in the southern sector of the California Current System. Limnology and Oceanography 54, 1272-1281

Allen, W.E., 1945a. Seasonal occurrence of marine plankton diatoms of Southern California in 1938. Contributions of Scripps Institution of Oceanography, New Series, No. 45, pp. 293-334.

Allen, W.E., 1945b. Vernal distribution of marine plankton diatoms offshore in Southern California in 1940. Contributions of Scripps Institution of Oceanography, New Series, No. 2585, pp. 335-369.

Antoine, D., André, J.-M., Morel, A., 1996. Oceanic primary production 2. Estimation at global scale from satellite (coastal zone color scanner) chlorophyll. Global Biogeochemical Cycles 10, 57-69.

Bakun, A., 1990. Global climate change and intensification of coastal ocean upwelling. Science 247, 198-201.

Barth, J.A., Menge, B.A., Lubchenco, J., Chan, F., Bane, J.M., Kirincich, A.R., McManus, M.A., Nielsen, K.J., Pierce, S.D., Washburn, L., 2007. Delayed upwelling alters nearshore coastal ocean ecosystems in the northern California current. Proceedings of the National Academy of Sciences 104, 3719-3724.

Behrenfled, M.J., Boss, E., Siegel, D.A., Shea, D.M., 2005. Carbon-based ocean productivity and phytoplankton physiology from space. Global Biogeochemical Cycles 19, GB1006. doi:10.1029/2004GB002299.

Bray, N. A., Keyes, A., Morawitz, W. M. L., 1999. The California Current system in the Southern California Bight and the anta Barbara Channel. Journal of Geophysical Research 104, 7695-7714.

Brown, S.L., Landry, M.R., Yang, E.J., Rii, Y.M., Bidigare, R.R., 2008. Diatoms in the desert: plankton community response to a mesoscale eddy in the subtropical North Pacific. Deep-Sea Research II 55, 1321-1333.

Campbell, L., Vaulot, D., 1993. Photosynthetic picoplankton community structure in the subtropical North Pacific Ocean near Hawaii (station ALOHA). Deep-Sea Research I 40, 2043-2060.

Chan, A.T., 1980. Comparative physiological study of marine diatoms and dinoflagellates in relation to irradiance and cell size. II. Relationship between photosynthesis, growth, and carbon/chlorophyll *a* ratio. Journal of Phycology 16, 428-432.

Cho, B.C., Azam, F., 1990. Biogeochemical significance of bacterial biomass in the ocean's euphotic zone. Marine Ecology Progress Series 63, 253-259.

Claustre, H., Morel, A., Babin, M., Cailliau, C., Marie, D., Martym J-C., Tailliez, D., Vaulot, D., 1999. Variability in particle attenuation and chlorophyll fluorescence in the tropical Pacific: Scales, patterns, and biogeochemical implications. Journal of Geophysical Research 104, 3401-3422.

Cullen, J.J., 1982. The deep chlorophyll maximum: Comparing vertical profiles of chlorophyll *a*. Canadian Journal of Fisheries and Aquatic Sciences 39, 791-803.

Di Lorenzo, E., Miller, A.J., Neilson, D.J., Cornuelle, B.D., Moisan, J.R., 2004. Modelling observed California Current mesoscale eddies and the ecosystem response. International Journal of Remote Sensing 25, 1307-1312.

Eppley, R.W., Carlucci, A.F., Holm-Hansen, O., Kiefer, D., McCarthy, J.J., Venrick, E., Williams, P.M., 1971. Phytoplankton growth and composition in shipboard cultures supplied with nitrate, ammonium, or urea as the nitrogen source. Limnology and Oceanography 16, 741-751.

Eppley, R.W., 1972. Temperature and phytoplankton growth in the sea. Fishery Bulletin (U.S.) 70, 1063-1085.

Eppley, R.W., Stewart, E., Abbott, M.R., Heyman, U., 1985. Estimating ocean primary production from satellite chlorophyll. Introduction to regional differences and statistics for the Southern California Bight. Journal of Plankton Research 7, 57-70.

Eppley, R.W., Chavez, F.P., Barber, R.T., 1992. Standing stocks of particulate carbon and nitrogen in the equatorial Pacific at 150°W. Journal of Geophysical Research 97, 655-661.

Falkowski, P.G., Dubinsky, Z., Wayman, K., 1985. Growth-irradiance relationships in phytoplankton. Limnology and Oceanography 30, 311-321.

Falkowski, P.G., 1994. The role of phytoplankton photosynthesis in global biogeochemical cycles. Photosynthesis Research 39, 235-258.

Garrison, D.L., Gowing, M.M., Hughes, M.P., Campbell, L., Caron, D.A., Dennett, M.R., Shalapyonok, A., Olson, R.J., Landry, M.R., Brown, S.L., Liu, H., Azam, F., Steward, G.F., Ducklow, H.W., Smith, D.C., 2000. Microbial food web structure in the Arabian Sea: a US JGOFS study. Deep-Sea Research II 47, 1387-1422.

Geider, R.J., 1987. Light and temperature dependence of the carbon to chlorophyll *a* ratio in microalgae and cyanobacteria: Implications for physiology and growth of phytoplankton. New Phytologist 106, 1-34.

Goericke, R., 2011. The structure of marine phytoplankton communities – Patterns, rules and mechanisms. CalCOFI Reports 52, 182-197.

Gruber, N., Frenzel, H., Doney, S.C., Marchesiello, P., McWilliams, J.C., Moisan, J.R., Oram, J.J., Plattner, G.-K., Stolzenbach, K.D., 2006. Eddy-resolving simulation of plankton ecosystem dynamics in the California Current System. Deep-Sea Research I 53, 1483-1516.

Haury, L.R., Venrick, E.L., Fey, C.L., McGowan, J.A., Niiler, P.P., 1993. The Ensenada front: July 1985. CalCOFI Reports 34, 69-88.

Hayward, T.L., Venrick, E.L., 1998. Nearsurface pattern in the California Current: coupling between physical and biological structure. Deep-Sea Research II 45, 1617-1638.

Hayward, T.L., Cayan, D.R., Franks, P.J.S., Lynn, R.J., Mantyla, A.W., McGowan, J.A., Smith, P.E., Schwing, F.B., Venrick, E.L., 1995. The state of the California Current in 1994-1995: a period of transition. CalCOFI Reports 36, 19-39.

Hickey, B., 1979. The California Current system—hypotheses and facts. Progress in Oceanography 8, 191-279.

Hickey, B., MacFadyen, A., Cochlan, W., Kudela, R., Bruland, K., Trick, C., 2006. Evolution of chemical, biological, and physical water properties in the northern California Current in 2005: Remote or local wind forcing? Geophysical Research Letters 33, L22S02. doi:10.1029/2006GL026782.

Holm-Hansen, O., Lorenzen, C.J., Holms, R.W., Strickland, J.D.H., 1965. Fluorometric determination of chlorophyll. Journal du Conseil International pour l'Exploration de la Mer. 30, 3-15.

Huyer, A., 1983. Coastal upwelling in the California Current System. Progress in Oceanography 12, 259-284.

Jester, R., Lefebvre, K., Langlois, G., Vigilant, V., Baugh, K., Silver, M.W., 2009. A shift in the dominant toxin-producing algal species in central California alters phycotoxins in food webs. Harmful Algae 8, 291-298.

Jones, B.H., Brink, K.H., Dugdale, R.C., Stuart, D.W., Ven Leer, J.C., Blasco, D., Kelley, J.C., 1983. Observations of a persistent upwelling center off Point Conception, California. In: Suess, E., Thiede, J. (eds) Coastal upwelling, its sediment record. Part A: Responses of the sedimentary regime to present coastal upwelling. Plenum Press, New York, p 37-60.

Jones, R.I., 2000. Mixotrophy in planktonic protists: an overview. Freshwater Biology 45, 219-226.

Kahru, M., Di Lorenzo, E., Manzano-Sarabia, M., Mitchell, G.B., 2012. Spatial and temporal statistics of sea surface temperature and chlorophyll fronts in the California Current. Journal of Plankton Research 34, 749-760.

Kahru, M., Lee, Z., Kudela, R.M., Manzano-Sarabia, M., Mitchell, G.B., this issue. Multi-satellite time series of inherent optical properties in the California Current. Deep-Sea Research II (this issue).

Landry, M.R., Ohman, M.D., Goericke, R., Stukel, M.R., Tsyrklevich, K., 2009. Lagrangian studies of phytoplankton growth and grazing relationships in a coastal upwelling ecosystem off Southern California. Progress in Oceanography 83, 208-216.

Landry, M.R., Selph, K.E., Brown, S.L., Abbott, M.R., Measures, C.I., Vink, S., Allen, C.B., Calbet, A., Christensen, S., Nolla, H., 2002. Seasonal dynamics of phytoplankton in the Antarctic Polar Front region at 170°W. Deep-Sea Research II. 49, 1843-1865.

Legaard, K.R., Thomas, A.C, 2006. Spatial patterns in seasonal and interannual variability of chlorophyll and sea surface temperature in the California Current. Journal of Geophysical Research 111, C06032. doi:10.1029/2005JC003282.

Letelier, R.M., Bidigare, R.R., Hebel, V., Ondrusek, M., Winn, C.D., Karl, D.M., 1993. Temporal variability of phytoplankton community structure based on pigment analysis. Limnology and Oceanography 38, 1420-1437.

Li, Q.P., Franks, P.J.S., Landry, M.R., Goericke, R., Taylor, A.G., 2010. Modeling phytoplankton growth rates and chlorophyll to carbon ratios in the California coastal and pelagic ecosystems. Journal of Geophysical Research 115, 1-12.

Litz, M.N.C., 2008. Ecology of the northern subpopulation of northern anchovy (*Engraulis mordax*) in the California Current Large Marine Ecosystem. (Master's thesis). Retrieved from http://hdl.handle.net/1957/8313

Litz, N.M.C., Heppell, S.S., Emmett, R.L., Brodeur, R.D., 2008. Ecology and distribution of the northern subpopulation of northern anchovy (*Engraulis mordax*) off the U.S. west coast. CalCOFI Report 49, 167-182.

Lorenzen, C.J., 1967. Determination of chlorophylls and phaeopigments: spectrophotometric equations. Limnology and Oceanography 12, 343-346.

Lynn R.J., Simpson, J.J., 1987. The California Current system: The seasonal variability of its physical characteristics. Journal of Geophysical Research 92, 12947-12966.

Mantyla, A.W., Bograd, S.J., Venrick, E.L., 2008. Patterns and controls of chlorophyll *a* and primary productivity cycles in the Southern California Bight. Journal of Marine Systems 73, 48-60.

Menden-Deuer, S., Lessard, E.J., 2000. Carbon to volume relationships for dinoflagellates, diatoms and other protist plankton. Limnology and Oceanography 45, 569-579.

Monger, B.C., Landry, M.R., 1993. Flow cytometric analysis of marine bacteria with Hoechst 33342. Applied Environmental Microbiology 59, 905-911.

Morel, A., 1988. Optical modeling of the upper ocean in relation to its biogenous matter content (Case I Waters). Journal of Geophysical Research 93, 10,749-10,768.

Niiler, P. P., Poulain, P.-M., Haury, L. R., 1989. Synoptic three-dimensional circulation in an onshore-flowing filament of the California Current. Deep-Sea Research 36, 385-405.

Pasulka, A.L., Landry, M.R., Taniguchi, D.A.A., Taylor, A.G., Church, M.J., 2013. Temporal dynamics of phytoplankton and heterotrophic protists at station ALOHA. Deep-Sea Research II, http://dx.doi.org/10.1016/j.dsr2.2013.01.007

Peláez, J., McGowan, J.A., 1986. Phytoplankton pigment patterns in the California Current as determined by satellite. Limnology and Oceanography 31, 927-950.

Peterson, B., Emmett, R., Goericke, R., Venrick, E., Mantyla, A., Bograd, S.J., Schwing, F.B., Ralston, S., Forney, K.A., Hewitt, R., Lo, N., Watson, W., Barlow, J., Lowry, M., Lavaniegos, B.E., Chavez, F., Sydeman, W.J., Hyrenbach, D., Bradley, R.W., Warzybok, P., Hunter, K., Benson, S., Weise, M., Harvey, J., 2006. The state of the California current, 2005–2006: warm in the north, cool in the south. California Cooperative Oceanic Fisheries Investigations Reports 47, 30–74.

Rykaczewski, R.R., Checkley, D.M., 2008. Influence of ocean winds on the pelagic ecosystem in upwelling regions. Proceedings of the National Academy of Sciences 105, 1965-1970. http://dx.doi.org/10.1073/pnas.0711777105.

Rykaczewski, R.R., Dunne, J.P., 2010. Enhanced nutrient supply to the California Current Ecosystem with global warming and increased stratification in an earth system model. Geophysical Research Letters 37, L21606, doi:10.1029/2010GL045019.

Sanders, R.W., 1991. Mixotrophic protists in marine and fresh-water ecosystems. Journal of Protozoology 38, 76-81.

Sathyendranath, S., Stuart, V., Nair, A., Oka, K., Nakane, T., Bouman, H., Forget, M.-H., Maass, H., Platt, T., 2009. Carbon-to-chlorophyll ratio and growth rate of phytoplankton in the sea. Marine Ecology Progress Series 383, 73-84.

Schwing, F.B., Bond, N.A., Bograd, S.J., Mitchell, T., Alexander, M.A., Mantua, N., 2006. Delayed coastal upwelling along the U.S. West Coast in 2005: A historical perspective. Geophysical Research Letters 33, L22S01. doi:10.1029/2006GL026911.

Sherr, E.B., Sherr, B.F., 1993. Preservation and storage of samples for enumeration of heterotrophic protists. In: Kemp, P.K. (Ed.), Handbook of Methods in Aquatic Microbial Ecology. CRC Press, Boca Raton, FL, pp. 207-212.

Snyder, M.A., Sloan, L.C., Diffenbaugh, N.S., Bell, J.L., 2003. Future climate change and upwelling in the California Current. Geophysical Research Letters 30, doi:10.1029/2003GL017647.

Stukel, M.R., Landry, M.R., Selph, K.E., 2011. Nanoplankton mixotrophy in the eastern equatorial Pacific. Deep-Sea Research II 58, 378-386.

Stukel, M.R., Décima, M., Selph, K.E., Taniguchi , D.A.A., Landry, M.R., 2013. The role of *Synechococcus* in vertical flux in the Costa Rica upwelling dome. Progress in Oceanography, http://dx.doi.org/10.1016/j.pocean.2013.04.003.

Sydeman, W.J., Bradley, R.W., Warzybok, P., Abraham, C.L., Jahncke, J., Hyrenbach, K.D., Kousky, V., Hipfner, J.M., Ohman, M.D., 2006. Planktivorous auklet *Ptychoramphus aleuticus* responds to ocean climate 2005, Unusual atmospheric blocking? Geophysical Research Letters 33, LS22S09. doi:10.1029/2006GL026736.

Taylor, A.G., Goericke, R., Landry, M.R., Selph, K.E., Wick, D.A., Roadman, M.J., 2012. Sharp gradients in phytoplankton community structure across a frontal zone in the California Current Ecosystem. Journal of Plankton Research 34, 778-798.

Taylor, A.H., Watson, A.J., Ainsworth, M., Robertson, J.E., Turner, D.R., 1991. A modeling investigation of the role of phytoplankton in the balance of carbon at the surface of the north Atlantic. Global Biogeochemical Cycles 5, 151-171.

Thomas, A.C., Strub, P.T., 1990. Seasonal and interannual variability of pigment concentrations across a California Current frontal zone. Journal of Geophysical Research 95, 13023-13042.

Thomas, A.C., Brickley, P., Weatherbee, R., 2009. Interannual variability in chlorophyll concentrations in the Humboldt and California Current systems. Progress in Oceanography 83, 386-392.

Venrick, E.L., 1992. Phytoplankton species structure in the central North Pacific: Is the edge like the center? Journal of Plankton Research 14, 665-680.

Venrick, E.L., 1993. Phytoplankton seasonality in the central North Pacific: The endless summer reconsidered. Limnology and Oceanography 38, 1135-1149.

Venrick, E.L., 2000. Summer in the Ensenada Front: the distribution of phytoplankton species, July 1995 and September 1988. Journal of Plankton Research 22, 813-841.

Venrick, E.L., 2002. Floral patterns in the California Current System off southern California: 1990-1996. Journal of Marine Research 60, 171-189.

Venrick, E.L., 2009. Floral patterns in the California Current: the coastal-offshore boundary zone. Journal of Marine Research 67, 89-111.

Venrick, E.L., 2012. Phytoplankton in the California Current system off southern California: Changes in a changing environment. Progress in Oceanography 104, 46-58.

Wang, X., Le Borgne, R., Murtugudde, R., Busalacchi, A.J., Behrenfeld, M., 2009. Spatial and temporal variability of the phytoplankton carbon to chlorophyll ratio in the equatorial Pacific: A basin-scale modeling study. Journal of Geophysical Research 114, C07008. doi:10.1029/2008JC004942.

Weise, M.J., Costa, D.P., Kudela, R.M., 2006. Movement and diving behavior of male California sea lion (*Zalophus californianus*) during anomalous oceanographic conditions of 2005 compared to those of 2004. Geophysical Research Letter 33, LS22S10. doi:10.1029/2006GL027113.

Winn, C.D., Campbell, L., Christian, J.R., Letelier, R.M., Hebel, D.V., Dore, J.E., Fujieki, L., Karl, D.M., 1995. Seasonal variability in the phytoplankton community of the North Pacific Subtropical Gyre. Global Biogeochemical Cycles 9, 605-620.

Yentsch, C.S., Menzel, D.W., 1963. A method for the determination of phytoplankton chlorophyll and phaeophytin by fluorescence. Deep-Sea Research 10, 221-231.

Yuras, G., Ulloa, O., Hornazábal, S., 2005. On the annual cycle of coastal and open ocean satellite chlorophyll off Chile (18°-40°S). Geophysical Research Letters 32, L23604. doi:10.1029/2005GL023946.

CHAPTER 4

Patterns and variability in phytoplankton size structure, biomass and community composition across the southern California Current and adjacent ocean ecosystems

Andrew G. Taylor, Michael R. Landry

Abstract

We used a combination of digital epifluorescence microscopy and flow cytometry to investigate the variability of phytoplankton community biomass, composition, and size structure across gradients of ocean system richness and to test three conflicting predictions about the biomass response of picophytoplankton to increasing trophic state . Samples were collected from four ocean systems in the northern Pacific Ocean -- the southern California Current Ecosystem, the eastern Equatorial Pacific, the Costa Rica Dome, and the subtropical north Pacific gyre at station ALOHA. Relative system richness was represented by total phytoplankton carbon biomass and by total chlorophyll *a*. All size classes increased in biomass up to total autotrophic biomass of ~50 μg C L^{-1}, beyond which the the nanophytoplankton (2-20-μm) eventually leveled off and picophytoplankton (< 2-μm) declined in both relative and absolute terms. Microphytoplankton (> 20-μm) increased monotonically with system richness, resulting in their strong dominance at high total community biomass. Differences in response patterns were also evident in the compositions of

taxonomic groups within and between size classes and among samples collected in the four regions. Significantly reduced biomass of picophytoplankton in richer coastal waters was consistent with a previously proposed hypothesis linking *Prochlorococcus* decline to enhanced grazing pressure on heterotrophic bacteria. Over the 3 orders-of-magnitude of autotrophic carbon biomass in our data, biomass of heterotrophic nanoflagellates, the presumptive consumers of bacteria, increase 5 fold, while turnover estimates of bacteria based on measured biomass and production-chlorophyll relationships increase 4 fold. Both indicate a significantly enhanced microbial loop driven mainly by organic substrates from large-phytoplankton productivity, and thus decoupled from the density-dependent dynamics of picophytoplankton per se. Our results suggest that density-independent grazing pressure may be a strong driver of picophytoplankton selection across trophic gradients, with implications for potentially interesting strategy trade-offs in growth rate and grazing resistance as well as representation of mortality relationships in marine ecosystem models..

Introduction

Many of the key processes in ocean carbon cycling and biogeochemistry, such as primary production, new production, nutrient and trace element limitation, and carbon export from the euphotic zone, are strongly related to the biomass structure and composition of phytoplankton communities (Eppley and Peterson 1979; Longhurst 1991; Falkowski et al. 2000). In addition, the size-structure of phytoplankton communities directly impacts food-web length and trophic efficiency, with nutrient-rich regions typically supporting larger phytoplankton and fewer food web steps to higher-level consumers than found in poorer system (Ryther 1969; Fenchel 1988; Iverson 1990). Because phytoplankton structure is important for understanding and modeling such processes, many attempts have been made to assess phytoplankton community biomass, structure and production based on a few key, remotely sensed parameters, such as water temperature and total chlorophyll *a* (Chl *a*) (Platt 1986; Morel and Berthon 1989; Behrenfeld et al. 2005). These remain somewhat elusive goals because large field data sets of quantitatively measured phytoplankton biomass remain relatively sparse.

It is broadly understood that phytoplankton communities are influenced both by physical/chemical (bottom-up, macro- and micro-nutrient/light limitation) and by biological/trophic (top-down, grazing) forcing (Tilman 1977; Tilman et al. 1982; Hecky and Kilham 1988; 1998; Goericke 2002; Calbet and Landry 2004). Several hypotheses have emerged to explain how such mechanisms may interact to determine community composition and biomass. One of these, which we term the *step-addition*

hypothesis, envisions the community response to increasing nutrient inventory as creating new niches for larger cells to be added to a stable foundation of smaller cells (Chisholm 1992; Thingstad 1998). According to this view, grazing controls set upper limits on the biomass that can be achieved by smaller competitive dominants for nutrients, and larger taxa are laid sequentially on top as the resource base expands. Smaller size classes are predicted to achieve a maximum biomass in relatively low nutrient systems and remain relatively constant in biomass as system richness increases. Alternatively, the recent *rising tide* hypotheses of Barber and Hiscock (2006) predicts that all phytoplankton size classes should benefit from and increase in response to improved nutrient conditions for growth. According to this hypothesis, smaller size classes of cells increase steadily in biomass as system richness increases, though larger cells increase disproportionately. Barber and Hiscock (2006) specifically contrast the rising tide hypothesis with expectations from succession/replacement theory, in which size classes or functional groups replace one another, all or in part, as conditions vary from oligotrophic to eutrophic.

Although no general hypothesis has been advanced to predict a broad biomass decline of small phytoplankton with increasing system richness, several studies have noted that certain populations like *Prochlorococcus* (PRO) may be driven by grazing pressure linked to the dynamics of comparably sized heterotrophic bacteria. Kuipers and Witte (2000), for instance, observed that PRO grazing mortality in the chlorophyll maximum of the subtropical North Atlantic was correlated with the loss rates of heterotrophic bacteria and independent of PRO abundance, growth rate or time of cell

division. These results supported their hypothesis that PRO was taken mainly as a by-catch of small grazers feeding on bacteria and not separately regulated by density-dependent interactions with its own suite of consumers. Coupled grazing dynamics of PRO and heterotrophic bacteria, stimulated by increased supply of dissolved organic carbon (DOC) from bloom-forming phytoplankton to bacteria, have also been speculated to explain observed population responses to iron fertilization in the equatorial Pacific (Landry and Kirchman 2002). Goericke (2011a) has further advanced this hypothesis to explain the observed decline of PRO across the California Current and in other coastal ecosystems as a result of increased grazing pressure tied to the enhanced growth environment for heterotrophic bacteria. Such a mechanism could also reasonably apply to all phytoplankton in the pico-size (<2 μm) range, which share common predators with bacteria. It thus provides a mechanistic basis for a third prediction – small phytoplankton will decline with increasing system richness – in the present study.

Recent pigment-based studies in the California Current have shown contrasting results with respect to relationships, or rules, describing the variability of phytoplankton structure with increasing trophic richness (Goericke 2011a, b). Based on size-fractionation of chlorophyll a (Chl a), for instance, Goericke (2011b) found some evidence supporting biomass thresholds or upper limits for intermediate sizes of phytoplankton as predicted by theory (Thingstad 1998). Notably, however, with regard to the grazing hypothesis developed above, size-fractioned Chl *a* data did not show a general decline of small (<3-μm) phytoplankton in richer systems (Goericke

2011b). Nonetheless, analyses of phytoplankton marker pigments by high-pressure liquid chromatography (HPLC) did reveal distinct patterns in the variability of phytoplankton functional groups with total Chl *a* (Goericke 2011a). Such patterns are useful because they can be applied to other large data sets based on pigment analyses or remote sensing. They are clearly limited, however, in what they can tell us about size-structure carbon biomass because pigment-carbon relationships vary substantially with light level, nutrients and among phytoplankton groups, and because cell size is not expressly addressed as a measured parameter.

In the present study, we investigate the variability of phytoplankton community composition, biomass and size structure in response to increasing system richness, measured as total autotrophic biomass or chlorophyll *a*. The data consists of 1,944 carbon-based community analyses by combined digital epifluorescence microscopy and flow cytometry. Samples were collected throughout the euphotic zone from four diverse oceanic systems in the central and eastern North Pacific, including coastal upwelling, oligotrophic subtropical, and open-ocean high-nitrate, low-chlorophyll (HNLC) regions. Across these regions, we demonstrate a coherent pattern of size-class variability, with monotonically increasing microphytoplankton, leveling off of nanophytoplankton and declining picophytoplankton biomass in richer coastal conditions. We also reveal compositional and structural differences among the four investigated regions over the biomass spectrum where they overlap. Lastly, we explore the proposed grazing mechanism for picophytoplankton decline, using two ways to quantify the relative change in the mortality environment for small cells in

coastal environments – the increasing biomass of nanoflagellate grazers, and enhanced turnover rate of bacteria based on bacterial production : Chl *a* relationships and measured bacterial biomass.

Methods

Study areas and sampling

Data were collected over a six-year period (2004-2010) from four areas and research projects in the central to eastern North Pacific Ocean (Table 4.1, Fig. 4.1): the California Current Ecosystem, Long Term Ecological Research (CCE-LTER) program off of southern California (Ohman et al. 2013); the Hawaii Ocean Time-series (HOT) program at ocean station ALOHA (Karl and Lukas 1996); the Equatorial Biocomplexity (EB) project in the eastern equatorial Pacific between 110° and 140°W (Nelson and Landry 2011) and the FLUx and Zinc Experiment (FLUZiE; Stukel et al. 2013) in the Costa Rica Dome (CRD) . These studies cover a broad range of phytoplankton growth conditions in tropical-to-temperate marine ecosystems of the Pacific Ocean, including eutrophic coastal upwelling (CCE), oligotrophic open-ocean and subtropical downwelling (HOT), high-nitrate, low-chlorophyll (HNLC) waters associated with chronic iron limitation (EB), and highly stratified waters overlying a shallow oxygen minimum zone (CRD). CCE data come both from designed experimental process studies over a range of coastal to offshore conditions, as well as from sampling at 10 cardinal stations along lines 80 and 90 of the California

Cooperative Oceanic Fisheries Investigations (CalCOFI) during 25 quarterly cruises from November 2004 to October 2010. On all cruises, samples for microscopy, flow cytometry and chlorophyll *a* analyses were collected from CTD-rosette bottle casts. Eight depths were typically sampled on each hydrocast from the surface to the bottom of the euphotic zone (depth of penetration of ~0.1% of incident solar radiation). On the CalCOFI cruises, however, we only sampled three depths, corresponding to the mixed-layer, the mid- and the deep-euphotic zone (Taylor et al. in review).

Analysis of eukaryotic plankton by epifluorescence microscopy

Seawater samples were prepared very similarly for epifluorecence microscopical analyses in the four research projects, but with slight differences in some details. For example, in EB and HOT collections and in CCE sampling prior to October, 2008, we analyzed a separate 50-mL sample preserved with paraformaldehyde (0.5% final concentration) to assess nanoplankton (small-volume, SV, samples, below). In later cruises, and after negligible differences were found between preservation treatments, nanoplankton slides were prepared from 50-mL subsamples of the water preserved for microplankton analyses (large-volume, LV, samples). For the latter, 500-mL samples were gently collected from the CTD and immediately preserved according to a modified protocol of Sherr and Sherr (1993). The samples were first preserved with 260 μL of alkaline Lugol's solution, immediately followed by 10 mL of buffered formalin and 500 μL of sodium thiosulfate, with gentle mixing between each addition. Preserved samples were

shielded from light and left to rest at room temperature for 1 h. After this fixation period, 1 mL of proflavin (0.33% w/v) was added, and the samples were stored in the dark for an additional hour. Immediately prior to filtration, the preserved samples were stained with 1 mL of 4',6-diamidino-2-phenylindole (DAPI) (0.01 mg mL^{-1}). Cells in the 50-mL SV aliquots (or separate paraformaldehyde-preserved samples with comparable proflavin and DAPI staining) were filtered onto 25-mm black polycarbonate filters with 0.8-μm pores. The remaining 450-mL LV aliquots, often less when plankton concentrations were visibly high on the SV filters, were concentrated onto 25-mm black polycarbonate filters with 8.0-μm pores. We placed a pre-wetted 10-µm nylon backing filter under all polycarbonate filters to promote even cell distribution, and filtered the samples under gentle vacuum pressure (<100 mm Hg). Each filter was then mounted onto glass slides with one drop of Type DF immersion oil and a No. 2 cover slip, and the prepared slides were frozen at -80°C for later analysis in the lab.

Slides were digitally imaged using a Zeiss Axiovert 200 M inverted compound microscope equipped for high-throughput epifluorescence microscopy with a motorized focus drive, stage, objective and filters. Digital images were acquired with a Zeiss AxioCam MRc black and white 8-bit CCD camera (Zeiss AxioCam HRc color CCD camera for EB and HOT). All microscope functions were controlled by Zeiss Axiovision software, and images were collected using automated image acquisition. Exposure times for each image were automatically determined by the Axiovision software to avoid over exposure. SV samples (50 mL aliquots) were viewed at 630X

magnification, and LV samples (450 mL aliquots) were viewed at 200X magnification. A minimum of 20 random positions were imaged for each slide, with each position consisting of three to four fluorescent channels: Chl *a*, DAPI, FITC (SV and LV samples) and phycoerythrin (SV samples only).

The combined images were processed and analyzed using ImagePro software to semi-automate the enumeration of eukaryotic cells larger than 1.5 μm in length (Taylor et al. submitted). Whenever possible, 20 positions and >300 cells were counted for each slide. Poor quality images were discarded. Cells were automatically segmented from the background and outlined; user interaction was then required to check each image, split connected cells, outline cells that did not auto-segment from the background and delete artifacts and detritus that the software had incorrectly outlined.

Each cell was manually identified and grouped into seven plankton functional groups: diatoms, autotrophic dinoflagellates (A-Dino), prymnesiophytes (Prym), cryptophytes (Crypto), autotrophic flagellates (A-Flag), heterotrophic dinoflagellates (H-Dino) and heterotrophic flagellates (H-Flag). The A- and H-Flag categories contained all cells that could not be clearly placed into the taxon-defined functional groups, which makes the biomass estimates for those groups conservative (i.e., some dinoflagellates and prymnesiophytes with ambiguous characteristics were likely included in the flagellate groups). Autotrophic cells were identified by the presence of chlorophyll *a* (red autofluorescence under blue light excitation), generally clearly

packaged in defined chloroplasts. Obvious heterotrophic cells with recently consumed prey were manually excluded from the autotroph classification.

Cells were also grouped into three size categories (Pico, <2 μm; Nano, 2-20 μm; Micro, 20-200 μm) based on the lengths of their longest axis. Microscopical size analysis alone defines the composition of Nano and Mico categories. However, the size class for autotrophic picophytoplankton (A-Pico) also includes contributions from the photosynthetic bacteria, *Prochlorococcus* (PRO) and *Synechococcus* (SYN), and < 1.5-μm pico-autotrophic eukaryotes (P-Euk) enumerated by flow cytometry (described below), in addition to the autotrophic eukaryotic cells between 1.5 and 2.0 µm measured by epifluorescence microscopy.

For all size categories, biovolumes (BV; μm^3) were calculated from the length (L) and width (W) measurements of each cell using the geometric formula of a prolate sphere (BV = 0.524*LWH), assuming H = W, except for the EB study where it was found that H = 0.5W for non-diatom cells (Taylor et al. 2011). Biomass was calculated as carbon (C; pg $cell^{-1}$) using the equations of Menden-Deuer and Lessard (2000): $C = 0.288\ BV^{0.811}$ for diatoms and $C = 0.216\ BV^{0.939}$ for non-diatoms.

Picoplankton analysis by FCM

Samples (2 mL) for flow cytometry (FCM) analysis of phototrophic bacteria, *Prochlorococcus* (PRO) and *Synechococcus* (SYN), heterotrophic bacteria (H-Bact) and pico-eukaryotes (P-Euk) were preserved with 0.5% paraformaldehyde (final concentration) and flash frozen in liquid nitrogen. On shore, the samples were stored

at -80°C, then thawed in batches and stained with Hoechst 34442 (1 μg mL^{-1}, final concentration) immediately prior to the analysis (Campbell and Vaulot 1993; Monger and Landry 1993). The analyses were conducted at the SOEST Flow Cytometry Facility (www.soest.hawaii.edu/sfcf) using a Beckman-Coulter Altra flow cytometer equipped with a Harvard Apparatus syringe pump for quantitative analyses and two argon ion lasers tuned to UV (200 mW) and 488 nm (1 W) excitation. Fluorescence signals were collected using filters for Hoechst-bound DNA, phycoerythrin and chlorophyll, all normalized to internal standards of 0.5- and 1.0-μm yellow-green (YG) polystyrene beads (Polysciences Inc., Warrington, PA, USA). Listmode data files (FCS 2.0 format) of cell fluorescence and light-scatter properties were acquired with Expo32 software (Beckman-Coulter) and used with FlowJo software (Tree Star, Inc., www.flowjo.com) to define populations based on DNA signal (all cells), absence of photosynthetic pigments (H-Bact), presence of Chl *a* (P-Euk, PRO and SYN), presence of phycoerythrin (SYN), and forward angle light scatter (FALS; relative size).

Abundance estimates PRO, SYN and H-Bact from FCM analyses were converted to carbon biomass using carbon per cell conversions estimated for each taxonomic group, and by depth and cruise, using bead-normalized forward-angle light scattering (FALS) as a relative measure of cell biovolume (Linacre et al. 2010, 2012). Estimates of cell carbon content were made using mean open-ocean, mixed-layer estimates of 10, 32 and 101 fg C cell^{-1} as a starting point for H-Bact, PRO and SYN, respectively (Garrison et al. 2000; Brown et al. 2008). Then, using the scaling factor

$FALS^{0.55}$ (Binder et al. 1996; Landry et al. 2003), the carbon:cell content was determined for each category and for each cruise and depth from the taxon-specific mean cell carbon values and the FALS ratio $(FALS_{sample}:FALS_{mean})^{0.55}$.

Eukaryotic autotrophic picoplankton less than 1.5 μm in length were estimated from P-Euks measured by FCM and added to A-Pico measured by microscopy. Since we are unable to distinguish the relative size of P-Euks measured by FCM, and in order not to double count cells measured by microscopy, we assumed that the cells counted by the flow cytometer were < 5 μm in length. Then, we summed up the number of cells between 1.5 and 5 μm in length counted by microscopy and subtracted this from the total number of P-Euks measured by FCM. This gives the number of pico-autotrophic cells less than 1.5 μm in length. For these cells we assumed the average cell size would be between 0.8 and 1.5 μm and applied the BV:C equations of Menden-Deuer and Lessard (2000) for non-diatom cells to arrive at a C:Cell conversion of 192 fg C $cell^{-1}$ to use for picoautotrophic cells < 1.5 μm in length. These were then combined with A-Pico biomass measured by microscopy and SYN and PRO measured from FCM to get total A-Pico biomass.

Specific growth rates of heterotrophic bacteria

As part of our analysis to explain why pico-phytoplankton might decline in more eutrophic systems, we wanted to assess the likely magnitude of increasing H-Bact growth rate with increasing trophic state. For this, FALS-adjusted estimates of H-Bact carbon biomass (μg C L^{-1}) were computed for each sample analyzed and

binned according to total chlorophyll. For each sample, a corresponding estimate of H-Bact production (BP; μg C L^{-1} d^{-1}) was calculated from the Cole et al. (1988) relationships of BP to chlorophyll concentration, $BP = CF * [2.218192(Chl)^{0.618}]$, where CF (= 1.59) is the factor that corrects for antilog transformation bias when converting to linear terms. The BP rate was then divided by H-Bact biomass to give an estimate of H-Bact specific growth rate for each sample.

Data analysis

Biomass and abundance estimates of microbial community size-class, composition and H-Bact specific growth rates were binned using either total chlorophyll *a* (Chl, μg Chl L^{-1}) or total autotrophic carbon (AC, μg C L^{-1}; the biomass sum of PRO, SYN, Diatom, A-Dino, A-Flag, Prym and Crypto) as a proxy for system richness. A total of 17 bins were used for each of the Chl and AC groupings for the trophic state proxies. Given the wide range of values within our dataset, bin cutoffs were set so that the bins would contain, within reason, a similar number of samples. Chl bins ranged from < 0.07 to > 6.01 μg Chl L^{-1}, and were set to increase by 35% for each increment. AC bins ranged from < 1 to > 438 μg C L^{-1}, and were set to increase by 50% for each increment. In different analyses, we averaged data on size classes and composition in the four study areas separately and combined together. All errors (±) referred to in the text or shown on figure plots are 95% confidence intervals for the mean values computed for the Chl- or AC-binned data.

Results

Autotrophic biomass and size trends

Whether the data are organized in terms of increasing total autotrophic carbon (AC, Fig. 4.2 top) or increasing total chlorophyll (Chl *a*, Fig. 4.2 bottom), they show similar gross features of phytoplankton size-structure variation with increasing biomass. The smallest size class (A-Pico) first increases with increasing total biomass, then decreases in absolute as well as relative biomass at the highest levels. A-Nano and A-Micro both increase strongly with total biomass, but A-Nano levels off somewhat at higher levels while the A-Micro increase is more rapid and monotonic, resulting in A-Micro dominance at high biomass. Some details vary notably, however, between the Chl *a* and AC plots. For instance, the initial increase, the decline, and the mid-biomass peak for A-Pico are substantially sharper for the data binned by AC. AC binning also shows that A-Nanos dominate at low total biomass, while Chl binning has A-Pico and A-Nano more nearly equal and co-dominant at low biomass. These differences reflect variations in cellular C:Chl ratios within the dataset and their relation to habitat-depth associations in the systems studied. For example, the lowest Chl *a* values typically occur near the sea surface under oligotrophic open-ocean conditions, and these are conditions where picophytoplankton, especially PRO, have their greatest competitive advantage (Raven 1986). In contrast, data in the lowest AC biomass categories more generally come from the lower euphotic zone, where light is limiting, C:Chl values low, and A-Nano relatively abundant (Eppley et al. 1988,

Pasulka et al. 2013). Variable C:Chl also influences the ranges of the biomass data represented, with AC-binning giving a > 3 order-of-magnitude difference between mean values in the smallest and largest biomass bins (0.61 ± 0.07 versus 786 ± 140 μg C L^{-1}, respectively) while the difference between the smallest and largest Chl bins is < 2 orders of magnitude (3.8 ± 0.4 versus 318 ± 53 μg C L^{-1}).

On the AC scale, the peak biomass of A-Pico (10.7 ± 0.71 μg C L^{-1}) occurs at around 50 µg C L^{-1} of total phytoplankton biomass before declining by a factor of 4 (2.43 ± 0.28 μg C L^{-1}) at higher levels. Interestingly, at low AC before reaching its peak, the A-Pico contribution to total AC varies approximately around 30%, if not increasing slightly, while A-Nano contribution varies generally in the range of 48-60% of total AC, and A-Micro contribution increases from about 10 to 18% (Table 4.2). In other words, for much of the biomass scale, the size fractions increase at roughly comparable rates with increasing biomass and therefore maintain relatively similar proportionalities. Beyond this point, however, the changes with increasing biomass steps are rapid, with A-Micro comprising 94% of total AC, A-Nano 6% and A-Pico < 0.3% among samples in the highest biomass category (Table 4.2).

Trends in phytoplankton composition

The composition of taxonomic groups within phytoplankton size classes provides added insight into the structural changes that occur with increasing AC biomass (Fig. 4.3). Within the A-Pico size class, the phototrophic bacteria *Prochlorococcus* (PRO) dominates at low AC, while *Synechococcus* (SYN) and

picoeukaryotes (P-Euk) co-dominate at high AC, where PRO disappears. The transition, where declining PRO biomass is overtaken by rising SYN and P-Euk, occurs at approximately the AC concentration where total A-Pico biomass peaks (Fig. 4.2). In the A-Nano size class, small indistinguishable cells (A-Flag) are the major category at low AC, while diatoms increase disproportionately to the other groups at higher AC. Among A-Micro, dinoflagellates (A-Dino) and diatoms contribute roughly similarly to biomass in the AC-binned averages, except for the very high biomass samples, which A-Dino dominate (Table 4.3).

Inter-regional comparisons

To compare size-structured biomass and composition among the different areas that were sampled in this study, we focus on the lower portion of the AC-binned biomass averages where there are data for each region (Figs. 4 and 5). The four sampling regions show modest, though statistically significant differences in relative size-class contributions and taxonomic composition within size-class (Table 4.4 and 4.5). For instance, A-Micro biomass contributions within AC bins are lower in HOT and CRD than for the CCE and EB regions (one way ANOVA, $F(3, 34) = 6.708$, $p = 0.001$; Tukey post-hoc comparisons was statistically significant at $p < 0.05$). A-Nano biomass contributions are higher for CCE and HOT than for CRD and EB (one way ANOVA, $F(3, 34) = 6.119$), $p = 0.002$; Tukey post-hoc comparisons was statistically significant at $p < 0.05$). In addition, A-Pico biomass is higher for the CRD than for the CCE (one way ANOVA, $F(3, 34) = 4.071$, $p = 0.014$; Tukey post-hoc comparisons

was statistically significant at $p < 0.05$). However, over the portion of the biomass spectrum where the open-ocean systems can be compared, they all show strongly increasing biomass trends (the rising-tide prediction) for all size classes with increasing AC biomass (Fig. 4.4).

Within size classes, the four sampling regions exhibit more profound differences in functional group composition (Fig. 4.5). For instance, PRO markedly dominates A-Pico in datasets from the subtropical (HOT) and high-nitrate, low-chlorophyll, (HNLC) equatorial Pacific (EB) (averaging 97% and 67%, respectively), but SYN dominates (56% on average) in the Costa Rica upwelling dome (CRD). Moreover, A-Pico biomass is more evenly distributed over the groups (35% PRO, 34% SYN and 29% P-Euk) in the southern California Current (CCE). For A-Nano composition assigned at the class level (i.e., neglecting cells in the uncertain A-Flag category), Prym are especially important in the HOT samples (45% of A-Nano biomass, compared to 22%, 21% and 7% for CRD, CCE and EB, respectively), while A-Dinos dominate in the EB region (68% of A-Nano, compared to 38%, 16%, and > 1% for CRD, CCE and HOT). Within the truncated AC biomass range examined in Figure 4.5, dinoflagellates contribute more than diatoms to A-Micro biomass in EB (64% versus 31%) and CRD data (81% versus 8%), while their contributions are more even (35% versus 47%) in the CCE. For HOT, in particular, there is major uncertainty in the taxonomic composition of A-Micro because the biomass is mainly comprised (73%) of cells enumerated as A-Flag.

Heterotrophic protists

For all data combined, H-Pico protists (i.e. exclusive of prokaryotes) are typically negligible while H-Nano and H-Micro both increase with total AC biomass (Fig. 4.6). Total biomass of heterotrophic protists increases by a factor of ~58 across the AC-averaged bins, from 3.6 ± 0.89 to 186 ± 52 μg C L^{-1} (Table 4.6). H-Nano biomass is typically double H-Micro biomass across a broad range of low to intermediate levels to total AC. However, at AC concentrations exceeding 100 µgC L^{-1}, H-Micro biomass rapidly increases to several times higher than H-Nano. The ratio of autotrophic to heterotrophic biomass (AC:HC) is less than 1.0 (0.2 – 0.7) at the lowest AC concentrations, but increases to ~4.5 at high AC. However, these analyses neglect the contributions of ciliated protozoa to total heterotrophs and to H-Micro, in particular, because ciliates are poorly preserved by the epifluorescence slide-making protocol (Taylor et al. 2011).

Heterotrophic bacteria

Mean biomass of heterotrophic bacteria (H-Bact, inclusive of all non-pigmented prokaryotes) also increases with increasing AC (Fig. 4.7A). However, the increase is only about one order of magnitude (1.9 ± 0.15 to 24 ± 1.9 μg C L^{-1}), thus not as dramatic as those for other biomass categories. In Figure 4.7B, the variability of H-Bact with AC is modeled as a logarithmic relationship: H-Bact = -1.64 + 3.43 * ln(AC), with reasonable predictive capability (R^2 = 0.92).

Using the Cole et al. (1988) relationship between bacterial production (BP) and chlorophyll concentration, calculated estimates of BP varied by a factor of ~28 (0.46 ± 0.01 to 12.6 ± 0.51 μg C L^{-1} d^{-1}) across our range of phytoplankton biomass (data not shown). When this production calculation was done for each sample with measured values of both H-Bact biomass and Chl *a*, specific growth rates of H-Bact could be computed (BP/H-Bact biomass) and averaged for each Chl *a* bin (Fig. 4.8). The results of this analysis suggest that specific growth rates of H-Bact are expected to vary by about a factor of 4 (0.28 ± 0.04 to 1.1 ± 0.34 d^{-1}) over the range of our phytoplankton biomass conditions (Fig. 4.8). The power function that defines this relationship is: H-Bact specific growth rate (d^{-1}) = 0.575 $(Chl)^{0.298}$ (R^2 = 0.98).

Discussion

The present study demonstrates coherent trends in phytoplankton size structure with increasing biomass across environmental gradients in the southern California Current Ecosystem and adjacent open-ocean regions. Biomass of larger phytoplankton increases dramatically, as expected, under rich coastal upwelling conditions. We find, however, a significant decrease of picophytoplankton that is not predicted either by step-addition theory (Thingstad 1998) or by the rising tide (Barber and Hiscock 2006) hypothesis. Furthermore, we find that all functional groups of picophytoplankton (*Prochlorococcus*, *Synechococcus*, and pico-eukaryotes) decrease in the richest trophic environments. Based on estimates of nano-heterotrophic grazers

and specific growth rate of bacteria, these declines of individual pico-phytoplankton populations and the group as a whole are consistent with the mechanism of DOC-enhanced bacterial growth and heterotrophic nanoflagellate grazing, as hypothesized for *Prochlorococcus* by Goericke (2011a). Interregional comparisons further show variability in size-class dominance and composition at comparable biomass levels. These differences are considered below with respect to mechanisms that may alter growth and grazing conditions within and between regions.

As illustrated in Figure 4.2, the general patterns of size variability are robust whether Chl *a* or total autotrophic carbon (AC) is used as an index of trophic state. For samples collected over the full depth range of euphotic zone, however, the choice of the index affects data binning, leading to different perceptions of pico- and nano-phytoplankton contributions to community biomass at the lowest levels of trophic state. These differences occur as a consequence of systematic variations in C:Chl and taxonomic and size-class habitat affinities relative to the upper (nutrient limited) and lower (light limited) euphotic zones. Chl *a* is often a useful proxy for system trophic state because it is easily measured, available as global or regional sea surface products (Morel and Berthon 1989; Behrenfeld and Falkowski 1997; Perez et al. 2005), and positively related to nutrient status (Eppley 1992; Claustre 1994). However, because the relationship between Chl *a* and carbon biomass can vary greatly with light, nutrients, taxonomic composition and growth rate (Eppley 1972; Cullen 1982; Geider 1987), estimates of total phytoplankton carbon biomass provide a more consistent basis for comparing data among regions and depths. As noted by Dodds and Cole

(2007), trophic state of aquatic systems is most appropriately measured as primary productivity, or combined production and heterotrophic respiratory processes, rather than as biomass proxies. Such rate-based definitions may, however, apply better to system comparisons on an areal basis rather than as discrete depth samples. Nonetheless, the typical sharp drop-off of primary productivity with depth compared to either pigment or carbon biomass concentrations means that a productivity-based index of trophic state would likely reveal a pattern similar to AC binning, i.e. with nanoplankton dominance at the low end of the scale.

Phytoplankton size structure

The biomass structure of phytoplankton communities is determined by a complex interplay of bottom-up influences on the physical/chemical growth environment (micro- and macro- nutrients availability) and top-down trophic impacts and loss rates (Tilman at al. 1982; Hutchins and Bruland 1998; Calbet and Landry 2004). At vanishingly low nutrient concentrations, theory predicts that very small cells with high surface-volume ratios will be the strongest competitors for nutrient uptake (Raven 1986; Chisholm 1992). Even with increasing nutrient input, such competitive dominants are assumed to keep ambient nutrients at levels that limit biomass accumulation of less efficient phytoplankton, until the dominants achieve maximum growth rates and their concentration is ultimately controlled by their grazers (Thingstad 1998). Thresholds have been observed for some taxa based on HPLC diagnostic marker pigments (Goericke, 2011b), consistent with the step-addition

hypothesis. While such a mechanism may hold in simple culture systems at very low nutrients, our data from natural systems, plotted against Chl *a* or total AC, fail to show a clear separation of pico- and nano-phytoplankton at the low end of the biomass spectrum, as would be predicted. This inconsistency with theory might be explained, in part, by the functional complexity of phytoplankton, e.g. mixotrophic nano-phytoplankton that do not compete directly with A-Pico for uptake of dissolved inorganic nutrients. In addition, sampling from both the shallow nutrient- and deeper light-limited habitats of the water column contributes to broad overlap of A-Pico and A-Nano at the low biomass levels in our dataset.

Where the step-addition (Thingstad 1998) and rising-tide hypotheses (Barber and Hiscock 2006) clearly differ is in the expected behavior of pico-phytoplankton with increasing trophic state. According to the former view, biomass of competitively dominant picoautotrophs should rise quickly to a dynamic steady-state balance (i.e., a constant upper limit) where maximum growth rate is offset by losses to their nano-zooplankton grazers, which can respond rapidly to perturbations in prey biomass. Larger cells are only added to the system once the "quotas" for the smaller size classes are filled (Raimbault et al. 1988). In the contrasting rising tide hypothesis, all types and size classes of phytoplankton are expected to benefit from increased nutrient availability during bloom events because none are assumed to have achieved their maximum growth rates under typical ambient open-ocean conditions. All therefore increase under favorable conditions, though the rate of increase is far greater for larger cells due to their higher unused growth potential and slower-responding

mesozooplankton consumers. Barber and Hiscock (2006) demonstrated that the rising tide hypothesis adequately explained the observed dynamics (enhanced growth rate and modestly increased abundance) of *Prochlorococcus* in response to the IronEx II iron-fertilization experiment in the equatorial Pacific. Such a result would also be expected from Figure 4.2, since the initial ambient biomass for the IronEx experiment (AC ≈ 25 μg C L^{-1}) lies to the left of the picophytoplankton biomass peak, and total AC only increased modestly, by a factor of 5, with iron fertilization (Landry et al. 2000). Nonetheless, neither step-addition nor rising tide predictions anticipate a decline of picophytoplankton beyond intermediate levels of phytoplankton biomass.

Figure 4.3 extends this conclusion to component groups of the picophytoplankon. Among *Prochlorococcus* spp., *Synechococcus* spp. and pico-eukaryotes, none show a tendency to increase or to level off at maximum concentrations at phytoplankton concentrations typical of the rich coastal environment. That is, even as phototrophic bacteria decline in coastal waters, there is no compensatory replacement of their role in community size structure by tiny eukaryotes. In contrast, A-Nano as a group appear to maintain relative constancy over a substantial increase of total biomass in coastal waters (Fig. 4.2). This portion of the size structure response conforms most closely with expectations of the step-addition theory (Thingstad 1998). However, individual functional-group components of the nano-phytoplankton show varying patterns of increase (flagellates, diatoms except at the highest biomass, which may be anomalous) or decrease (prymnesiophytes, cryptophytes, small dinoflagellates) with increasing total AC biomass (Fig. 4.3).

Regional differences in community structure

Although the regions examined in this study are ecologically distinct, they reside in relatively close proximity in the southeastern sector of the North Pacific with fluid boundaries and current systems that should allow for relatively easy population seeding and exchange among them. The California Undercurrent, for example, brings water of eastern tropical Pacific origin north into the southern CCE region (Lynn and Simpson 1987). Waters with flora of clear subtropical origin occur on the western edge of the California Current and also move well inshore during summertime due to circulation of the southern California eddy in the southern California Bight (Venrick 2000, 2002, 2009). Given the many potential routes of population exchange, the differences that arise in community structure and composition can reasonably be interpreted as reflecting differences in the relative selective pressures of the respective environments. Although mechanisms that lead to regional variations in structure and composition are poorly understood and likely complex, here we make an attempt to infer some possibilities from the similarities and differences that we observe.

Landry and Kirchman (2002) previously noted that the equatorial Pacific is similar to subtropical waters of the North Pacific gyre with respect to pico-phytoplankton dominance by *Prochlorococcus* (PRO). The main difference is that the more productive waters of the equatorial region have higher standing stocks of *Synechococcus* (SYN) and pico-eukayotes (P-euk) superimposed upon the similar concentrations of PRO (Landry 2002), as would be expected from step-addition theory

(Thingstad 1998). These observations also apply to the present comparisons of HOT and EB data (Fig. 4.5), which were not part of the previously analyzed dataset. The HOT and EB regions are contrasting physical-chemical systems in many respects (iron-sufficient, oligotrophic downwelling versus chronically iron-limited, open-ocean upwelling). Yet, these differences appear to have minimal effect on dominance structure of the pico-phytoplankton in the two areas. In contrast, at similar concentrations of total AC, pico-phytoplankton compositions differ substantially in the CCE and CRD regions. As discussed more fully below, increased grazing pressure due to enhanced activity of the microbial loop might explain the reduced abundance of PRO in these two systems. Mechanistically, the strong, shallow oxygen zone underlying the CRD upwelling system could be a source of substantial dissolved organic input into the euphotic zone to stimulate microbial activity. Similarly, rapid lateral advective transport by coastal jets, filaments and mesoscale eddies in the CCE region (Pelaez and McGowan 1986; Thomas and Strub 1990) are mechanisms with potential to bring significant subsidies of dissolved substrates from productive coastal upwelling cells to waters 100s of kilometers offshore. In addition, the unique dominance pattern and very high abundances of *Synechococcus* in the CRD region (see also Li et al. 1983; Saito et al. 2005) argue for a different resource environment than the iron and macro-nutrient limited waters of the equatorial and subtropical Pacific, where PRO predominates. Copper and cadmium effects (Saito et al. 2005) and zinc-iron co-limitation (Franck et al. 2003) have been proposed as possible

explanations of CRD phytoplankton structure, but definitive demonstrations of their effects have not been made.

One interesting characteristic of the three upwelling regions is the enhanced relative proportion of dinoflagellates to autotrophic biomass compared to samples from the subtropical Pacific (Fig. 4.5). For EB and CRD regions, A-Dinos dominate both nano- and micro-sized phytoplankton. In CCE samples, A-Dinos are more important in the larger size category, where they dominate or co-dominate (with diatoms) at especially the higher biomass values (Fig. 4.3). This contrasts with recent findings for the same system based HPLC pigment-based analyses, which suggest that A-Dinos contribute about 10-fold less to biomass than diatoms at high Chl *a* values (Goericke 2011 a). Similarly, very low concentrations of peridinin were found in the same EB samples where A-Dinos averaged 38% of all phytoplankton carbon (Selph et al. 2011; Taylor et al. 2011), indicating that their role in open-ocean phytoplankton communities may generally be underestimated by pigment markers.

Dinoflagellates are generally slow growing but often benefit from mixotrophic functionality, especially the ability to prey on other organisms (Sanders 1991; Jacobson and Anderson 1996; Stoecker 1999). Given demonstrated iron-limitation in the EB and coastal CCE regions (Coale et al. 1998; King and Barbeau 2007; Brzezinski et al. 2011) and likely trace-element limitation in the CRD (Franck et al. 2003), acquisition of trace resources by phagotrophy may help to explain the relative success of A-Dinos in these three systems. Their lesser importance under major-nutrient (nitrogen or phosphorous) limited conditions in the subtropical Pacific (HOT)

could mean that the mixotrophic strategy is less efficient in satisfying bulk nutrient requirements for growth, or that a significant subset of the potential prey (e.g., *Trichodesmium*) is resistant to being consumed. Alternatively, many dinoflagellates may simply have gone unrecognized in the enumeration of HOT samples and be part of the A-Flag category.

Among our four regions, samples from HOT are clearly distinct in the presence of nitrogen-fixing cyanobacteria, notably *Trichodesmium*, which has major biogeochemical roles in new production, export and driving the annual production cycle of the subtropical Pacific (e.g., Letelier and Karl 1996; Dore et al. 2002). Over the 5-year period of the present (~monthly) observations, however, we did not sample waters of exceptional phytoplankton biomass, as might be associated with occasional bloom concentrations of *Trichodesmium* or diazotrophy-associated diatoms during the summertime (Letelier and Karl 1996). Phytoplankton size structure and composition at HOT, especially the relative contributions of diatoms, therefore remain somewhat ambiguous at the upper end of the biomass levels achieved in that region. In contrast, our observations of relatively low diatom biomass in the CRD is consistent with previous reports, as well as the prospect that iron, zinc or a combination of the two strongly limit biomass accumulation of diatoms in this upwelling system (Franck et al. 2003).

The biomass decrease of picoautotrophs

It is difficult to imagine individual phytoplankton species capable of thriving across the broad range of environmental and trophic conditions from which our data are drawn. We therefore envision a scenario in which changing conditions, from oligotrophic open-ocean to coastal eutrophic, select for a succession of species or ecotypes that replace others in the same functional roles. Previous studies with flow cytometry and taxon-specific pigments in the California Current have documented offshore maxima and in-shore declines of photosynthetic bacteria, PRO and SYN (Collier and Palenik 2003; Goericke 2011a). Similar patterns have also been noted across strong environmental gradients in the Arabian Sea (Campbell et al. 1998). In addition, Taylor et al. (2012) have demonstrated fine-scale distributions of PRO and SYN across an enriched mesoscale front in the CCE, which essentially capture much of size-structure and compositional variability in Figures 4.2 and 4.3 over a few kilometers. What is remarkable and new about the present results is the apparent lack of a compensatory increase in pico-eukaryotes to fill the declining biomass niche of photosynthetic bacteria as trophic state becomes richer. In fact, biomass of pico-eukaryotes as a group, which comprises diverse taxa and capabilities, is also observed to decline (Fig. 4.2). This indicates that the mechanism leading to the pico-autotroph decline in richer coastal waters is more fundamental than the unique adaptations or tolerances of specific taxa, like PRO and SYN. Here we suggest that the decline of all groups of pico-phytoplankton is driven by the ramping up of grazing pressure due to

enhanced microbial loop activity with increasing system eutrophy (Landry and Kirchman 2002; Goericke 2011a).

As originally defined, the microbial loop, consisting of heterotrophic prokaryotes (nominally H-Bact) and associated grazers, is that part of food web that recaptures dissolved organic carbon (DOC) produced by food-web process and feeds into a protist-dominated consumer chain (Azam et al. 1983). Activity of the microbial loop, measured as the rate of bacterial carbon production, is thus directly influenced by primary productivity and processes that generate labile DOC. Nonetheless, bacterial production also scales across trophic states with phytoplankton biomass (e.g., Cole et al. 1988; White et al. 1991), a relationship that we use, along with estimates of bacterial carbon biomass, to derive first-order assessments of relative specific growth rates of bacteria (Fig. 4.8). The 10-fold difference observed in our estimates of bacterial carbon biomass (Fig. 4.7) thus translates roughly to a 4-fold range in rates of bacterial growth (Fig. 4.8).

If we assume that production and losses are balanced in steady-state turnover at any point along the trophic gradient, the corresponding 4-fold increase in bacterial mortality must be partitioned between losses to grazing, viral lysis and other processes. How this is done is unknown, although we note across our gradient a 5 to 6-fold increase in heterotrophic nanoplankton (Fig. 4.6), the presumptive grazers of bacteria, which is consistent with a largely proportional increase in grazing pressure with increased growth rate of bacteria. The many assumptions and uncertainties about conversion factors in the measurements of bacterial production and biomass caution

against taking the absolute values of derived growth rates in Figure 4.8 too seriously. Nonetheless, it is instructive to observe that pico-phytoplankton like PRO or SYN could comfortably accommodate grazing losses of 0.25 d^{-1} in oligotrophic waters (e.g. Vaulot et al. 1995; Liu et al. 1998) while being highly challenged by grazing turnover rates of 1.0 d^{-1} in coastal waters, even given optimal resource conditions for growth. The calculated bacterial growth and turnover estimates are therefore not entirely unrealistic as grazing rate impacts.

An important point about stimulated microbial activity along trophic gradients is the separation of cause and effect with respect to the picophytoplankton. DOC production comes from the whole food web, which in richer habitats is increasingly dominated on the autotrophic side by larger phytoplankton (A-Micro). However, the grazing mortality associated with larger stocks and higher turnover rates of heterotrophic bacteria impacts mainly the autotrophic cells of small size that share common grazers with bacteria. In effect, the grazing environment for picophytoplankton is driven principally by the dynamics of heterotrophic bacteria as a response to the production of large phytoplankton. It should consequently not exhibit the behaviors expected of strongly coupled predator-prey systems, such as predator decline if picophytoplankton are temporarily, or even permanently, overgrazed (Kuipers and Wille 2000; Goericke 2011a).

Hypothetically, picophytoplankton could meet the challenge of increasing grazer biomass and activity by growing faster, up to their maximum potential, or by adopting strategies that reduce grazing vulnerability. Examples of the latter strategies,

involving alteration of the cell-surface properties or defensive chemicals, have been demonstrated for cultured isolates of PRO, SYN and other small autotrophs (e.g., Monger et al. 1999; Apple et al. 2011; Strom et al. 2003, 2012). However, the extent of their occurrence and overall effects in natural ecosystems are largely unknown. Still, one can imagine a broad array of evolved growth-rate and grazing-defense characteristics among small phytoplankton species and ecotypes of coastal marine ecosystems, given the heightened predatory environment that must occur there. The diminished biomass of pico-phytoplankton in the richest environments (i.e., the lack of super-picos) suggests that there are physiological/energetic limitations or trade-offs between optimal strategies for growth and grazing. This would clearly be an important and exciting topic to explore across strong coastal gradients in microbial activity with methods that are able to resolve taxon-specific differences in growth and grazing mortality rates, as well as the genetic flexibility that species or clades may have to optimize strategic trade-offs.

Improved mechanistic understanding of predator-prey interactions at the base of the marine food web would also help to achieve more accurate representations of food web dynamics in marine ecosystem models. For instance, most models designed to investigate the interplay of bottom-up and top-down processes in shaping the size structure of plankton communities (e.g. Armstrong 1999; Poulin and Franks 2010) ignore the microbial loop entirely or parameterize only its nutrient remineralization function. Similarly, self-assembly models of phytoplankton community composition determine outcomes principally from trade-offs in the physiological capabilities of

light and nutrient utilization by competing phytoplankton ecotypes (e.g. Dutkiewicz et al. 2009, 2013; Goebel et al. 2012; see also Irwin et al. 2006). Mortality, assigned as simple or fixed functions, is typically given no dynamical role in such models, even though the resource competition theory upon which the models are based gives equal weighting to mortality and growth terms in setting the equilibrium concentrations of competing species (Tilman 1977, 1982). Here, we note that accounting for a dynamic ~4-fold variability in mortality pressure on picophytoplankton that scales with total primary productivity would likely provide new insights or explanations for distributional patterns, especially in coastal environments, that are poorly understood or previously ascribed to physiology. More clearly needs to be learned experimentally about mortality pressures and mitigating strategies of natural populations, but at the same time, the sensitivities of models to reasonable scenarios in mortality dynamics should also be examined.

Acknowledgements

We thank many colleagues who contributed to the collection and analysis of this dataset: John Wokuluk, Daniel Wick, Alexis Pasulka, Michael Stukel, Darcy Taniguchi, Mark Hodges, Daniel Lee, Lorena Linacre and Emy Daniels helped with preparation and imaging of the slide samples; Karen Selph analyzed flow cytometry samples; Shonna Dovel and Megan Roadman collected samples on CalCOFI survey cruises; and Blake Watkins collected samples on Hawaii Ocean Time-series (HOT)

cruises. We also thank the captains and crews of the numerous research vessels involved. This work was funded by U.S. National Science Foundation grants 0417616 and 1026607 (CCE-LTER Program), 0322074 (Equatorial Biocomplexity), 0324666 and 0926766 (HOT), and 0826626 (Costa Rica Dome, Flux and Zinc Experiments).

Chapter 4, in full, is currently in preparation for submission to Limnology and Oceanography: Taylor, A.G., Landry, M.R. "Patterns and variability in phytoplankton size structure, biomass and community composition across the southern California Current and adjacent ocean ecosystems." The dissertation author was the primary investigator and author of this paper.

Table 4.1. Summary of the four research projects and study areas used for the current study. Projects are Equatorial Biocomplexity (EB) project, California Current Ecosystem, Long Term Ecological Research (CCE-LTER) program along with the California Cooperative Oceanic Fisheries Investigations (CalCOFI) component, FLUx and Zinc Experiment in the Costa Rica Dome (CRD), and the Hawaii Ocean Time-series (HOT) program.

Project	Location	Cruise	Sampling plan	No. samples
EB	eastern equatorial Pacific	Dec 2004 & Sep 2005	transect sampling	228
CCE-LTER	southern California Current	May 2006, Apr 2007, Oct 2008	process cruises	553
CalCOFI/CCE-LTER	CalCOFI station grid	Nov 2004 - Oct 2010	quarterly cruises, station grid	710
CRD	Costa Rica Dome upwelling region	Jun/Jul 2010	process cruise	116
HOT	station ALOHA	Oct 2004 - Jan 2009	monthly cruises, fixed station	337

Table 4.2.: Mean biomass estimates and percent contributions of autotrophic size-classes for all studies binned by total autotrophic carbon (AC). Units are μg C L^{-1} for biomass and % for contribution. Size-classes are A-Pico (0.2 – 2 μm), A-Nano (2 – 20 μm) and A-Micro (20 – 200 μm). All ± errors represent the 95% confidence interval.

	Biomass			Percent contribution		
AC bin	A-Pico	A-Nano	A-Micro	A-Pico	A-Nano	A-Micro
< 1	0.2 ± 0.05	0.4 ± 0.08	< 0.1 ± 0.02	35	59	6
1.5	0.3 ± 0.06	0.7 ± 0.06	0.2 ± 0.03	25	61	14
2.25	0.3 ± 0.05	1.4 ± 0.07	0.2 ± 0.03	14	76	10
3.38	0.6 ± 0.06	1.8 ± 0.07	0.4 ± 0.05	21	65	13
5.06	1.1 ± 0.09	2.6 ± 0.10	0.5 ± 0.06	27	62	11
7.59	1.8 ± 0.09	3.7 ± 0.08	0.8 ± 0.07	29	59	12
11.4	3.8 ± 0.12	4.7 ± 0.10	1.1 ± 0.07	40	49	11
17.1	5.3 ± 0.13	6.9 ± 0.12	1.8 ± 0.09	38	49	13
25.6	7.7 ± 0.21	9.9 ± 0.20	3.3 ± 0.16	37	48	16
38.4	9.8 ± 0.39	15.0 ± 0.37	6.2 ± 0.36	32	48	20
57.7	10.7 ± 0.71	22.4 ± 0.69	13.8 ± 0.84	23	48	29
86.5	8.7 ± 1.04	32.7 ± 1.41	28.1 ± 1.64	13	47	40
130	6.2 ± 1.42	40.1 ± 3.42	55.1 ± 3.58	6	40	54
195	4.1 ± 0.38	56.4 ± 4.15	103 ± 5.43	2	34	63
292	5.3 ± 0.72	60.2 ± 6.48	168 ± 8.40	2	26	72
438	2.3 ± 0.78	81.0 ± 23.82	264 ± 23.0	1	23	76
> 438	2.4 ± 0.28	44.6 ± 0.86	739 ± 141	0	6	94

Table 4.3.: Mean biomass estimates of taxonomic groups within each autotrophic size-class for all studies binned by total autotrophic carbon (AC). Units are μg C L^{-1}. Size-classes are A-Pico (0.2 – 2 μm), A-Nano (2 – 20 μm) and A-Micro (20 – 200 μm). Groups are *Prochlorococcus* (PRO), *Synechococcus* (SYN), autotrophic flagellates (A-Flag), diatom, autotrophic dinoflagellates (A-Dino), prymnesiophytes (Prym) and cryptophytes (Crypto). Not shown: Prym never > 0.01 μg C L^{-1} in A-Micro size-class.

AC bin	A-Pico PRO	SYN	A-Flag	A-Nano Diatom	A-Dino	A-Flag	Prym	Crypto	A-Micro Diatom	A-Dino	A-Flag
< 1	0.16	0.01	>0.01	0.01	0.01	0.29	0.05	0	0.01	0.01	0.02
1.5	0.25	0.01	>0.01	>0.01	0.04	0.58	0.13	0	0.05	0.05	0.06
2.25	0.18	0.03	>0.01	0.01	0.10	1.03	0.23	0	0.04	0.05	0.08
3.38	0.42	0.06	>0.01	0.03	0.19	1.25	0.32	0.01	0.11	0.11	0.13
5.06	0.71	0.22	0.10	0.05	0.44	1.26	0.82	0.01	0.12	0.20	0.13
7.59	1.24	0.23	0.20	0.12	0.57	1.83	1.18	0.03	0.26	0.32	0.18
11.4	2.92	0.44	0.33	0.11	0.73	2.27	1.47	0.03	0.31	0.47	0.27
17.1	3.49	0.90	0.77	0.24	1.67	3.10	1.83	0.06	0.65	0.76	0.35
25.6	3.24	2.25	2.05	0.50	2.87	4.27	2.10	0.17	1.31	1.41	0.55
38.4	3.24	3.58	2.71	0.94	3.76	7.72	2.31	0.22	2.89	2.14	1.17
57.7	2.25	4.91	3.29	2.86	4.87	11.77	2.66	0.29	6.16	4.90	2.78
86.5	0.94	4.94	2.56	5.87	6.12	17.68	2.63	0.44	12.46	11.75	3.86
130	0.78	2.61	2.64	10.90	5.58	19.39	3.16	1.03	21.06	27.73	6.31
195	0.46	1.99	1.57	26.01	5.61	21.25	2.83	0.73	53.42	43.95	5.82
292	0.95	2.46	1.82	28.90	4.99	24.57	0.80	0.94	58.33	100.80	5.59
438	0	1.16	0.87	40.46	7.15	32.93	0.44	0	50.46	203.93	9.44
> 438	0	1.12	1.05	6.24	5.22	33.17	0	0	25.50	676.46	36.81

Table 4.4. Results of one way ANOVA with Tukey post-hoc tests of the relative size-class composition of autotrophic biomass between regions for the range of trophic states that overlap between regions. P values are shown when the difference between regions is significant ($p < 0.05$), while a dash represents no statically significant difference. Size-class groups are A-Pico (0.2 – 2 μm), A-Nano (2 – 20 μm) and A-Micro (20 – 200 μm). Regions are the California Current Ecosystem (CCE), Hawaii Ocean Time-series (HOT), Equatorial Biocomplexity project (EB) and the Costa Rica Dome (CRD).

	% A-Pico			**% A-Nano**			**% A-Micro**		
	HOT	**EB**	**CRD**	**HOT**	**EB**	**CRD**	**HOT**	**EB**	**CRD**
EB	–			0.022			0.001		
CRD	–	–		0.010	–		–	0.044	
CCE	–	–	0.009	–	–	0.028	0.031	–	–

Table 4.5. Results of one way ANOVA with Tukey post-hoc tests of the relative biomass contribution of taxonomic groups within the pico autotrophic size class (A-Pico; 0.2 – 2 μm) between regions for the range of trophic states that overlap between regions. P values are shown when the difference between regions is significant ($p < 0.05$), while a dash represents no statically significant difference. Taxonomic groups are *Prochlorococcus* (PRO), *Synechococcus* (SYN) and autotrophic flagellates (A-Flag). Regions are the California Current Ecosystem (CCE), Hawaii Ocean Time-series (HOT), Equatorial Biocomplexity project (EB) and the Costa Rica Dome (CRD).

	% PRO			**% SYN**			**% A-Flag**		
	HOT	**EB**	**CRD**	**HOT**	**EB**	**CRD**	**HOT**	**EB**	**CRD**
EB	0.004			–			0.005		
CRD	< 0.001	0.007		< 0.001	0.009		< 0.001	–	
CCE	< 0.001	< 0.001	–	< 0.001	0.046	–	< 0.001	< 0.001	0.006

Table 4.6. Mean biomass estimates of heterotrophic size-classes and taxonomic composition within each size-class, and heterotrophic bacteria (H-Bact) for all studies binned by total autotrophic carbon (AC; μg C L^{-1}). All units are μg C L^{-1}. Size-classes are H-Pico (0.2 – 2 µm), H-Nano (2 – 20 µm) and H-Micro (20 – 200 µm). Groups are heterotrophic flagellates (H-Flag) and heterotrophic dinoflagellates (H-Dino).

		H-Pico	H-Nano		H-Micro	
AC bin	H-Bact		H-Flag	H-Dino	H-Flag	H-Dino
< 1	1.9	0.07	2.3	0.1	0.9	0.3
1.5	1.8	0.03	2.2	0.2	0.9	0.1
2.25	1.8	0.05	2.0	0.2	0.9	0.1
3.38	2.3	0.03	2.3	0.3	1.0	0.3
5.06	3.4	0.03	1.9	0.6	0.6	0.4
7.59	4.2	0.04	2.3	0.8	0.7	0.8
11.4	5.4	0.04	2.8	0.9	0.7	0.8
17.1	6.3	0.05	2.8	1.2	0.7	0.9
25.6	7.9	0.06	3.1	1.8	0.6	1.3
38.4	9.2	0.10	4.0	2.6	1.1	2.2
57.7	11.3	0.06	4.7	3.1	0.9	2.4
86.5	12.8	0.05	5.1	3.9	0.9	3.3
130	14.8	0.07	7.1	3.6	2.7	12.1
195	17.2	0.05	10.7	5.2	3.0	21.3
292	18.7	0.06	8.9	4.2	4.3	22.9
438	20.0	0.17	9.2	8.2	1.3	63.0
> 438	23.9	0.13	10.7	8.6	2.6	163.7

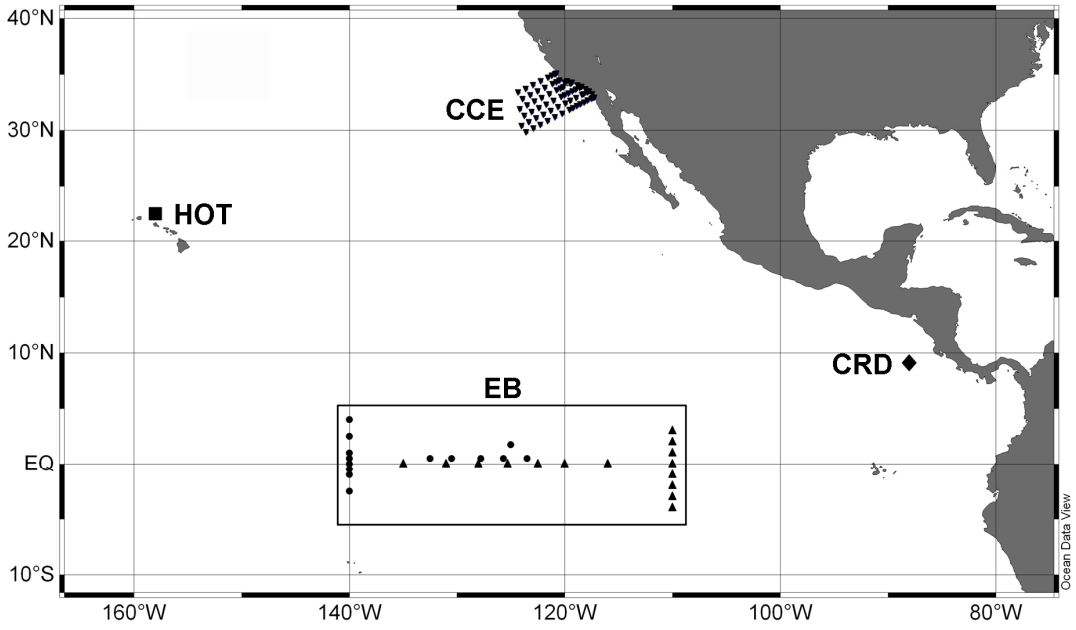

Figure 4.1. Map showing the different study areas and projects used for this study. California Current Ecosystem (CCE), Hawaii Ocean Time-series (HOT), Equatorial Biocomplexity project (EB) and the Costa Rica Dome (CRD). Inverted triangle symbols for the CCE region represent the CalCOFI sampling grid. Square symbol represents station ALOHA for HOT. Circles represent sampling stations for EB 2005 and triangles represent sampling stations for EB 2004. Diamond symbol represents the lagrangian drifter study area for CRD.

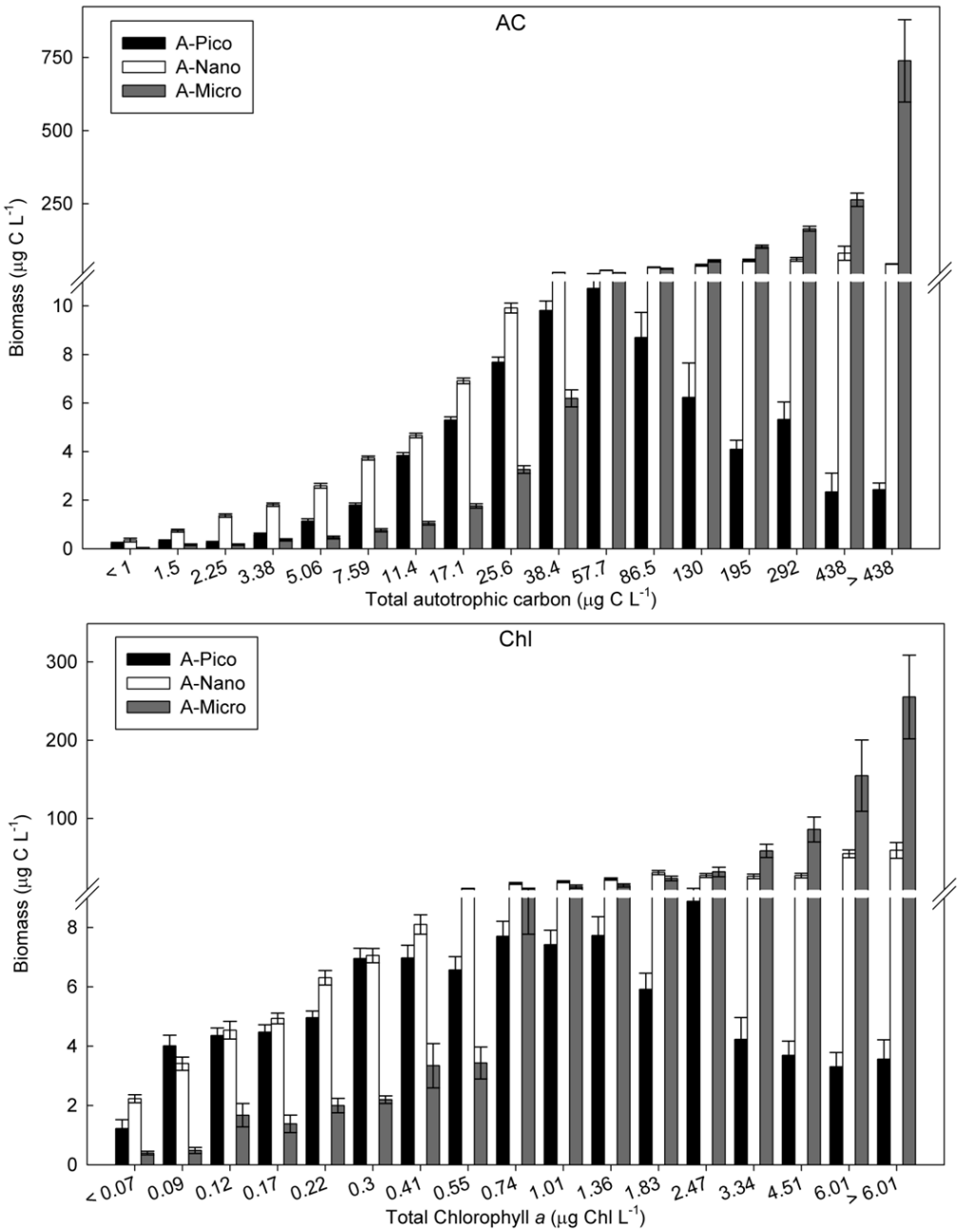

Figure 4.2. Mean biomass (μg C L^{-1}) estimates of total autotrophic biomass size-classes from all studies binned by total autotrophic carbon (AC, μg C L^{-1}) and total chlorophyll (Chl, μg Chl L^{-1}). Size-classes are A-Pico (0.2 – 2 µm), A-Nano (2 – 20 µm) and A-Micro (20 – 200 µm). Error bars represent the 95% confidence interval. Note that the y-axis is broken and that a different scale is used after the break on both plots.

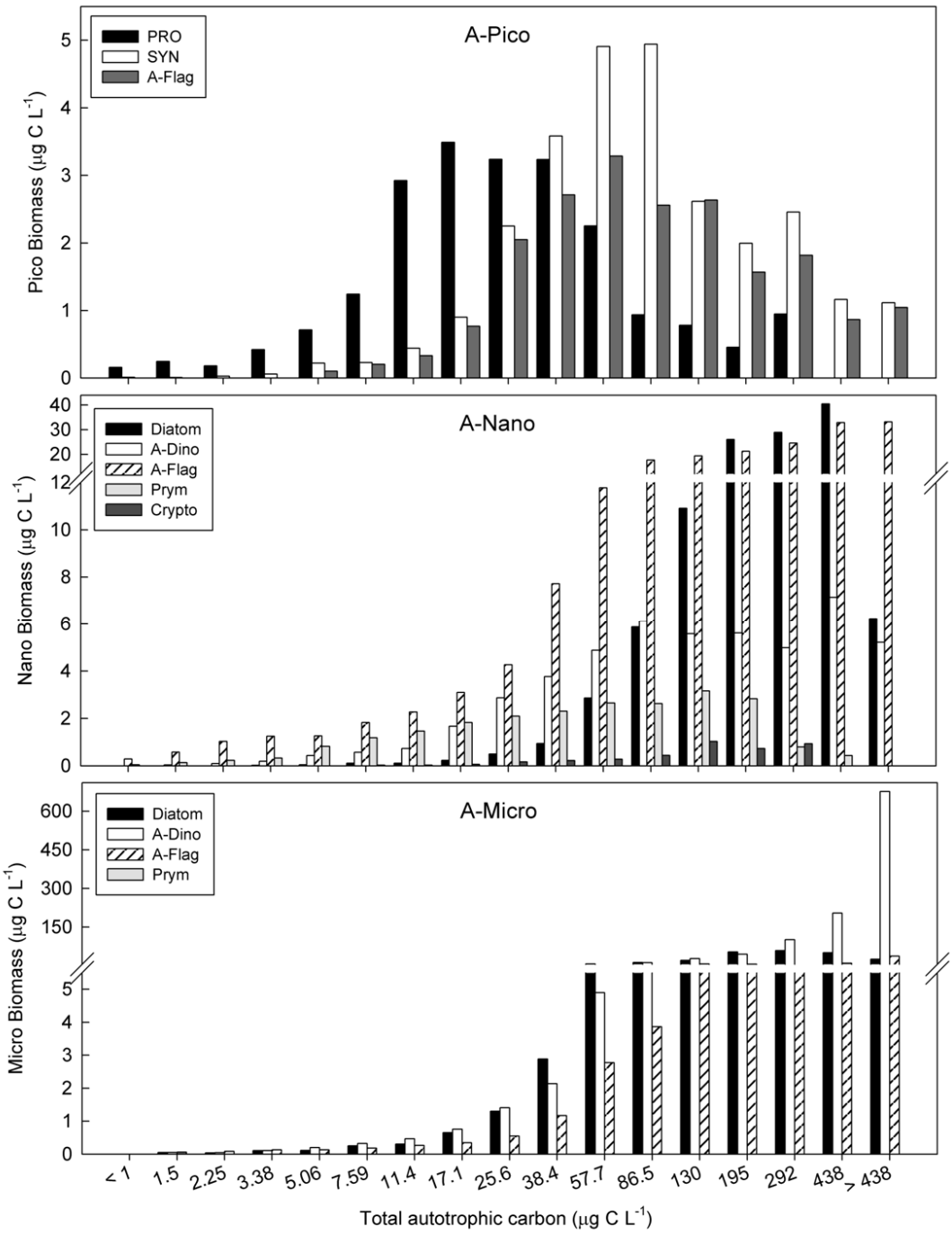

Figure 4.3. Mean biomass (μg C L^{-1}) estimates of taxonomic groups within each size-class from all studies binned by total autotrophic carbon (μg C L^{-1}). *Prochlorococcus* (PRO), *Synechococcus* (SYN), autotrophic flagellates (A-Flag), diatom, autotrophic dinoflagellates (A-Dino), prymnesiophytes (Prym) and cryptophytes (Crypto). Note that all plots have a different scale on the y-axis and that the y-axis is broken for A-Nano and A-Micro and a different scale is used after the break.

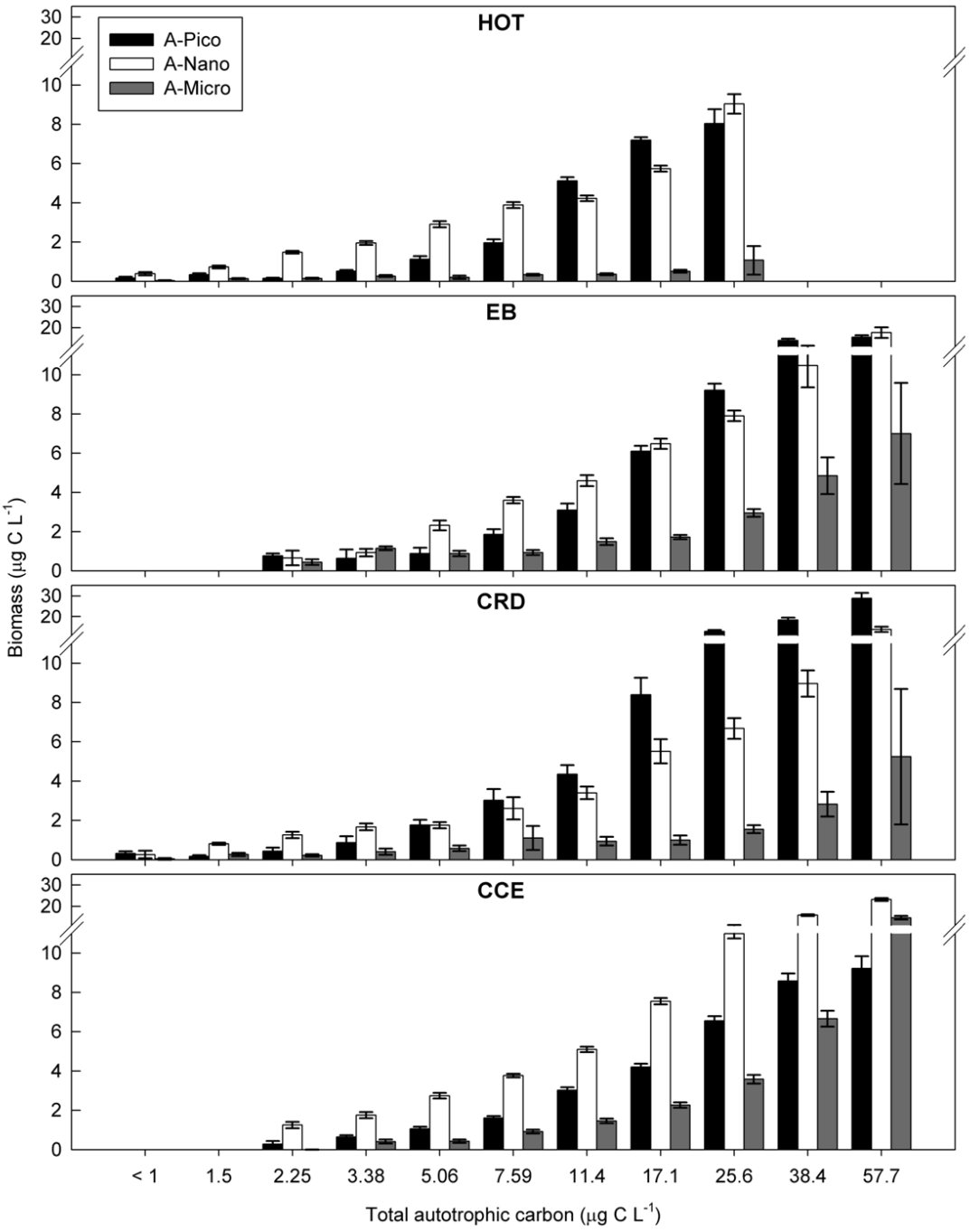

Figure 4.4. Mean biomass (μg C L^{-1}) estimates of total autotrophic biomass size-classes from each study region binned by total autotrophic carbon (μg C L^{-1}). Hawaii Ocean Time-series (HOT), Equatorial Biocomplexity project (EB), Costa Rica Dome (CRD) and the California Current Ecosystem (CCE). Size-class groups are A-Pico (0.2 – 2 μm), A-Nano (2 – 20 μm) and A-Micro (20 – 200 μm). Error bars represent the 95% confidence interval. Note that all plots are have the same y-axis and also the y-axis is broken and a different scale is used after the break.

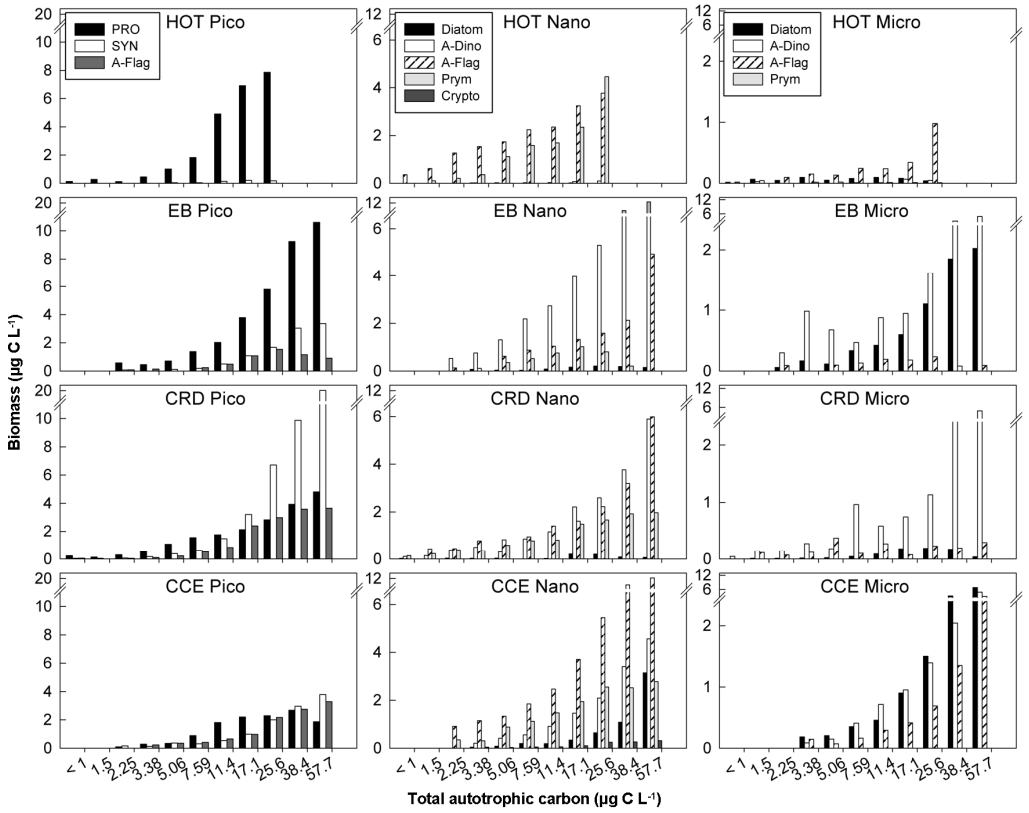

Figure 4.5. Mean biomass (μg C L^{-1}) estimates of taxonomic group composition within each size class for each study region binned by total autotrophic carbon (μg C L^{-1}). Hawaii Ocean Time-series (HOT), Equatorial Biocomplexity project (EB), Costa Rica Dome (CRD) and the California Current Ecosystem (CCE). Size-class groups are A-Pico (0.2 – 2 µm), A-Nano (2 – 20 µm) and A-Micro (20 – 200 µm). Taxonomic groups are *Prochlorococcus* (PRO), *Synechococcus* (SYN), autotrophic flagellates (A-Flag), diatom, autotrophic dinoflagellates (A-Dino), prymnesiophytes (Prym) and cryptophytes (Crypto). Note that y-axis is different for each size-class and that the y-axis is broken and a different scale is used after the break.

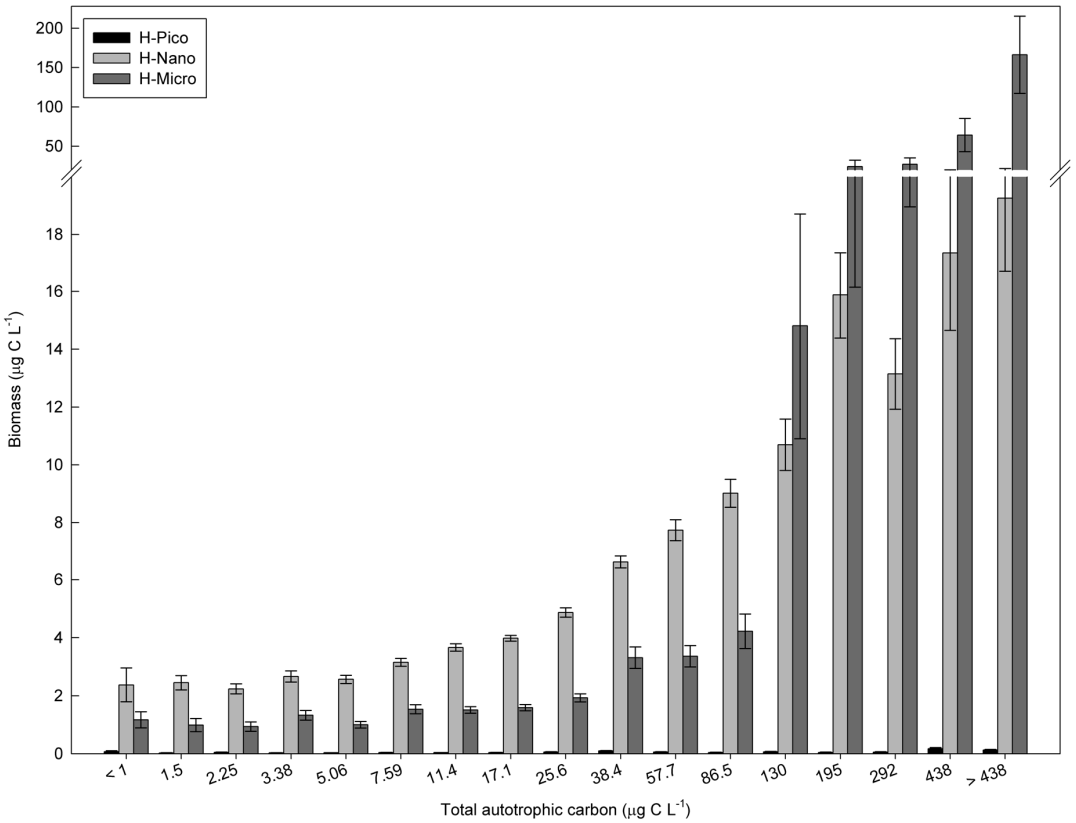

Figure 4.6. Mean biomass (μg C L^{-1}) estimates of total heterotrophic biomass size-classes from all studies binned by total autotrophic carbon (μg C L^{-1}). Size-class groups are H-Pico (0.2 – 2 µm), H-Nano (2 – 20 µm) and H-Micro (20 – 200 µm). Error bars represent the 95% confidence interval. Note that the y-axis is broken and a different scale is used after the break.

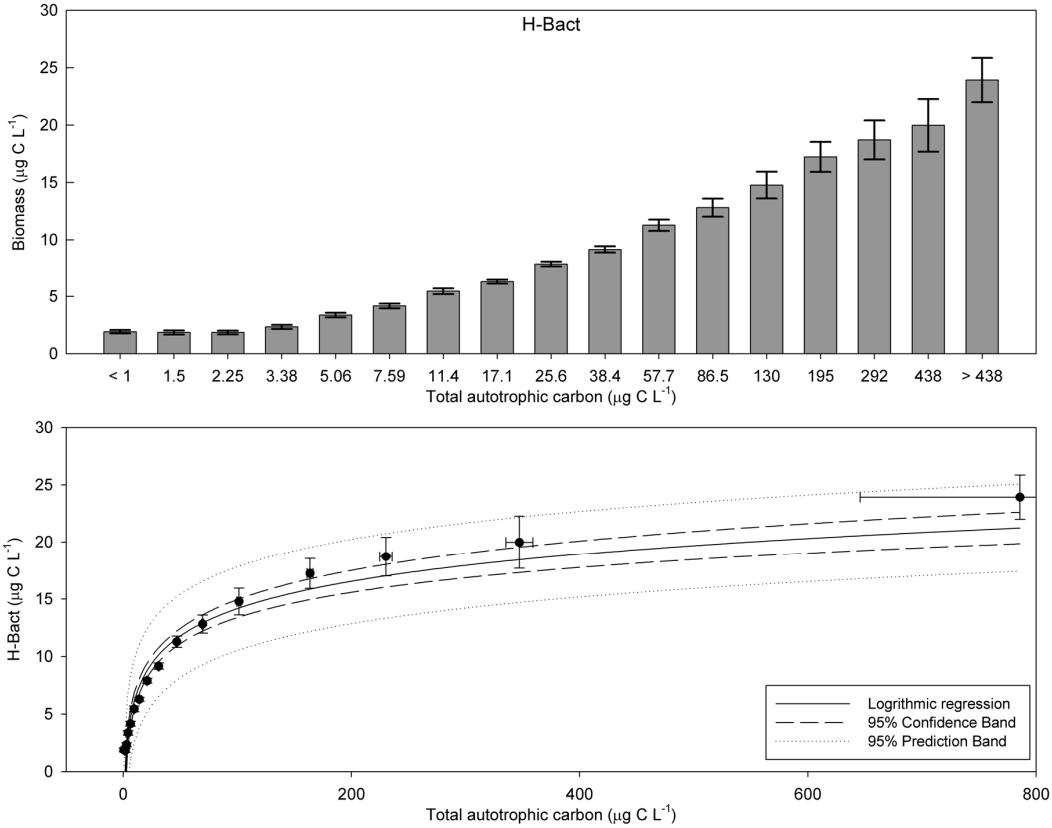

Figure 4.7. (*Top*) Mean biomass (μg C L^{-1}) estimates of heterotrophic bacteria (H-Bact) from all studies binned by total autotrophic carbon (μg C L^{-1}). (*Bottom*) relationship between mean H-Bact biomass and mean total autotrophic carbon (μg C L^{-1}) for all studies. Solid line is a logarithmic regression ($R^2 = 0.92$), dashed line is the 95% confidence band and the dotted line is the 95% prediction band from the regression. All error bars represent the 95% confidence interval.

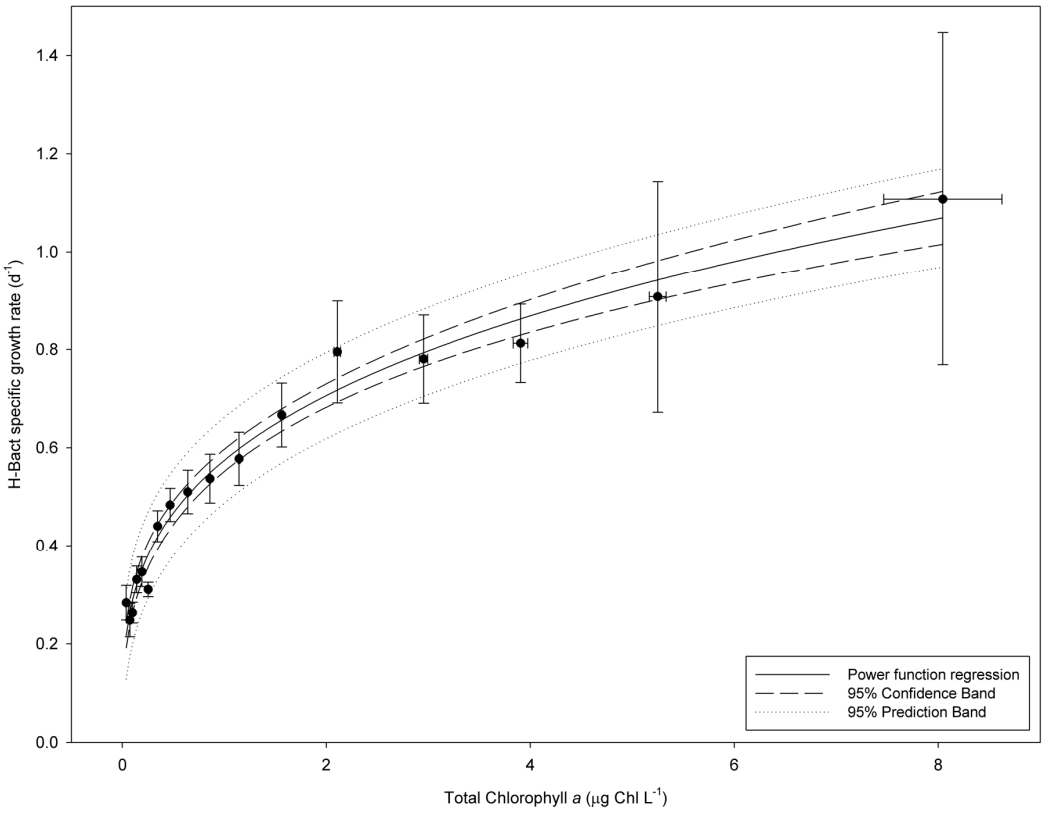

Figure 4.8. Mean specific growth rate (d^{-1}) of heterotrophic bacteria (H-Bact) as a function of mean chlorophyll concentration (μg Chl L^{-1}) for all studies. Solid line is a power function of the regression ($R^2 = 0.95$), dashed line is the 95% confidence band and the dotted line is the 95% prediction band from the regression. All error bars represent the 95% confidence interval.

References

Apple, J. K., S. L. Strom, B. Palenik, and B. Brahamsha. 2011. Variability in protists grazing and growth on different marine *Synechococcus* isolates. Appl. Environ. Microbiol. **77:** 3074-3084.

Armstrong, R. A. 1999. Stable model structures for representing biogeochemical diversity and size spectra in plankton communities. J. Plankton Res. **21**: 445–464.

Azam. F., T. Fenchel, J. G. Field. J. S. Grey. L. A. Meyer-Reil, and F. Thingstad. 1983. The ecological role of water-column microbes in the sea. Mar. Ecol. Prog. Ser. **10**: 257–263.

Barber, R. T., and M. R. Hiscock. 2006. A rising tide lifts all phytoplankton: growth response of other phytoplankton taxa in diatom-dominated blooms. Global Biogeochem. Cycles **20:** GB4S03, doi:10.1029/2006GB002726

Behrenfeld, M. J., E. Boss, D. A. Siegel, and Shea, D. M. 2005. Carbon-based ocean productivity and phytoplankton physiology from space. Global Biogeochem. Cycles **19:** 1-14, doi:10.1029/2004GB002299

Behrenfeld, M. J., and P. G. Falkowski. 1997. Photosynthetic rates derived from satellite-based chlorophyll concentration. Limnol. Oceanogr. **42:** 1-20.

Binder, B., S. W. Chisholm, R. J. Olson, S. L. Frankel, and A. Z. Worden. 1996. Dynamics of picophytoplankton, ultraphytoplankton and bacteria in the central equatorial Pacific. Deep-Sea Res. II **43:** 907-931.

Brown, S. L., M. R. Landry, E. J. Yang, M. R. Yoshimi, and R. R. Bidigare. 2008. Diatoms in the desert: Plankton community response to a mesoscale eddy in the subtropical North Pacific. Deep-Sea Res. II **55:** 1321-1333, doi:10.1016/j.dsr2.2008.02.012

Brzezinski, M. A., S. B. Baines, W. M. Balch, C. P. Beucher, F. Chai, R. C. Dugdale, J. W. Krause, M. R. Landry, A. Marchi, C. I. Measures, D. M. Nelson, A. E. Parker, A. J. Poulton, K. E. Selph, P. G. Strutton, A. G. Taylor, and B. S. Twining. 2011. Co-limitation of diatoms by iron and silicic acid in the equatorial Pacific. Deep-Sea Research II **58:** 493-511, http://dx.doi.org/10.1016/j.dsr2.2010.08.005

Calbet, A., and M. R. Landry. 2004. Phytoplankton growth, microzooplankton grazing, and carbon cycling in marine systems. Limnol. Oceanogr. **49:** 51-57, dio:10.4319/lo.2004.49.1.0051

Campbell, L., M. R. Landry, J. Constantinou, H. A. Nolla, S. L. Brown, H. Liu, and D. A. Caron. 1998. Response of microbial community structure to environmental forcing in the Arabian Sea. Deep-Sea Res. II **45**: 2301-2325.

Campbell, L., and D. Vaulot. 1993. Photosynthetic picoplankton community structure in the subtropical North Pacific Ocean near Hawaii (station ALOHA). Deep-Sea Res. I **40:** 2043-2060, http://dx.doi.org/10.1016/0967-0637(93)90044-4

Chisholm, S. W. 1992. Phytoplankton size. p. 213-237. *In* Falkowski, P. G. and A. D. Woodhead [eds.], Primary Productivity and Biogeochemical Cycles in the Sea. Plenum.

Claustre, H. 1994. The trophic status of various oceanic provinces as revealed by phytoplankton pigment signatures. Limnol. Oceanogr. **39:** 1206-1210.

Coale, K. H., K. S. Johnson, S. E. Fitzwater, S. P. G. Blain, T. P. Stanton, and T. L. Coley. 1998. IronEx-I, an *in situ* iron-enrichment experiment: experimental design, implementation and results. Deep-Sea Res. II **45:** 919-945, http://dx.doi.org/10.1016/S0967-0645(98)00019-8

Cole, J. J., S. Findlay, and M. L. Pace. 1988. Bacterial production in fresh and saltwater ecosystems: A cross-system overview. Mar. Ecol. Prog. Ser. **43:** 1-10.

Collier J. L., and B. Palenik. 2003. Phycoerythrin-containing picoplankton in the Southern California Bight. Deep-Sea Res. II **50**: 2405-2422.

Cullen, J. J. 1982. The deep chlorophyll maximum: Comparing vertical profiles of chlorophyll *a*. Can. J. Fish. Aquat. Sci. **39:** 791-803.

Dodds, W. K., and J. J. Cole. 2007. Expanding the concept of trophic state in aquatic ecosystems: It's not just the autotrophs. Aquat. Sci. **69:** 427-439.

Ducklow, H. 2000. Bacterial production and biomass in the oceans. *In* Kirchmann, D. L. [ed.], Microbial ecology of the oceans. Liss/Wiley.

Dutkiewicz, S., M. J. Follows, and J. G. Bragg. 2009. Modeling the coupling of ocean ecology and biogeochemistry. Global Biogeochem. Cycles **23**: GB4017, doi:10.1029/2008GB003405.

Dutkiewicz, S., J. R. Scott, and M. J. Follows. 2013. Winners and losers: Ecological and biogeochemical changes in a warming ocean. Global Biogeochem. Cycles **27**: 463–477, doi:10.1002/gbc.20042.

Eppley, R. W. 1972. Temperature and phytoplankton growth in the sea. Fish. Bull. **70:** 1063-1085.

Eppley, R. W. 1992. Chlorophyll, photosynthesis and new production in the Southern California Bight. Prog. Oceanog. **30:** 117-150, doi:10.1016/0079-6611(92)90010-W

Eppley, R. W., and B. J. Peterson. 1979. Particulate organic matter flux and planktonic new production in the deep ocean. Nature **282:** 677-680, doi:10.1038/282677a0

Eppley, R. W., E. Swift, D. G. Redalje, M. R. Landry, and L. W. Haas. 1988. The subsurface chlorophyll maximum in August-September, 1985 in the CLIMAX area of the North Pacific. Mar. Ecol. Prog. Ser. 42: 289-301.

Falkowski, P., R. J. Scholes, E. Boyle, J. Canadell, D. Canfield, J. Elser, N. rubber, K. Hibbard, P. Hŏgberg, S. Linder, F. T. Mackenzi, B. Moore III, T. Pedersen, Y. Rosenthal, S. Seitzinger, V. Smetacek, and W. Steffen. 2000. The global carbon cycle: A test of our knowledge of earth as a system. Science **290:** 291-296, doi:10.1126/science.290.5490.291

Fenchel, T. 1988. Marine plankton food chains. Ann. Rev. Syst. **19:** 19-38.

Fiedler, P. C. 2002. The annual cycle and biological effects of the Costa Rica Dome. Deep-Sea Res. I **49:** 321-338, doi:10.1016/S0967-0637(01)00057-7

Franck, V. M., K. W. Bruland, D. A. Hutchins, and M. A. Brzezinski. 2003. Iron and zinc effects on silicic acid and nitrate uptake kinetics in three high-nutrient, low-chlorophyll (HNLC) regions. Mar. Ecol. Prog. Ser. **252:** 15-33.

Geider, R. J. 1987. Light and temperature dependence of the carbon to chlorophyll *a* ratio in microalgae and cyanobacteria: Implications for physiology and growth of phytoplankton. New Phytologist **106:** 1-34.

Garrison, D. L., M. M. Gowing, M. P. Hughes, L. Campbell, D. A. Caron, M. R. Dennett, A. Shalapyonok, R. J. Olson, M. R. Landry, S. L. Brown, H.- B. Liu, F. Azam, G. F. Steward, H. W. Ducklow, and D. C. Smith. 2000. Microbial food web structure in the Arabian Sea: a US JGOFS study. Deep-Sea Res II **47:** 1387-1422.

Goebel, N. A., C. A. Edwards, J. P. Zehra, M. J. Follows, and S. G. Morgan. 2013. Modeled phytoplankton diversity and productivity in the California Current System. Ecol. Model. **264**: 37-47.

Goericke, R. 2002. Top-down control of phytoplankton biomass and community structure in the monsoonal Arabian Sea. Limnology and Oceanography **47:** 1307-1323.

Goericke, R. 2011a. The structure of marine phytoplankton communities—patterns, rules and mechanisms. CalCOFI Reports **52:** 182-197.

Goericke, R. 2011b. The size structure of marine phytoplankton—what are the rules? CalCOFI Reports **52:** 198-204.

Hecky, R. E., and P. Kilham. 1988. Nutrient limitation of phytoplankton in freshwater and marine environments: a review of recent evidence on the effects of enrichment. Limnol. Oceanogr. **33:** 796-822.

Hickey, B. 1979. The California Current System – hypotheses and facts. Prog. Oceanogr. **8:** 191-279.

Hutchins, D. A., and K. W. Bruland. 1998. Iron-limited diatom growth and Si:N uptake ratios in a coastal upwelling regime. Nature **393:** 561-564, doi:10.1038/31203

Iverson, R. L. 1990. Control of marine fish production. Limnol. Oceanogr. **35:** 1593-1604.

Jacobson, D. M. and D. M. Anderson. 1996. Widespread phagocytosis of ciliates and other protists by marine mixotrophic and heterotrophic thecate dinoflagellates. J. Phycol. **32:** 279-285.

Karl, D. M., and R. Lukas. 1996. The Hawaii Ocean Time-series (HOT) program: Background, rationale and field implementation. Deep Sea-Res. II **43**: 129-156.

Kaupp, L. J., C. I. Measures, K. E. Selph, and F. T. Mackenzie. 2011. The distribution of dissolved Fe and Al in the upper waters of the Eastern Equatorial Pacific. Deep-Sea Res. II **58:** 296-310, dio:10.1016/j.dsr2.2010.08.009.

King, A. L. and K. Barbeau. 2007. Evidence for phytoplankton iron limitation in the southern California Current System. Mar. Ecol. Prog. Ser. **342:** 91-103.

Kuipers, B. R., H. J. Witte. 2000. Prochlorophytes as secondary prey for heterotrophic nanoflagellates in the deep chlorophyll maximum layer of the (sub)tropical North Atlantic. Mar. Ecol. Prog. Ser. **204:** 53-63.

Landry, M. R. 2002. Integrating classical and microbial food web concepts: Evolving views from the open-ocean tropical Pacific. Hydrobiologia, 480: 29-39.

Landry, M. R., S. L. Brown, J. Neveux, C. Dupouy, J. Blanchot, S. Christensen, and R. R. Bidigare. 2003. Phytoplankton growth and microzooplankton grazing in high-nutrient, low-chlorophyll waters of the equatorial Pacific: Community and taxon-specific rate assessments from pigment and flow cytometric analyses. J. Geophys. Res. **108:** 8142, doi:10.1029/2000JC000744

Landry, M. R., and D. L. Kirchman. 2002. Microbial community structure and variability in the tropical Pacific. Deep-Sea Res. II 49: 2669-2694.

Landry, M. R., M. E. Ondrusek, S. J. Tanner, S. L. Brown, J. Constantinou, R. R. Bidigare, K. H. Coale, and S. Fitzwater. 2000. Biological response to iron fertilization in the eastern equatorial Pacific (IronEx II). I. Microplankton community abundances and biomass. Mar. Ecol. Prog. Ser. 201: 27-42.

Letelier, R. M., and D. M. Karl. 1996. Role of *Trichodesmium* spp. in the productivity of the subtropical North Pacific Ocean. Mar. Ecol. Prog. Ser. **133**: 263-273.

Linacre, L. P., M. R. Landry, J. R. Lara-Lara, J. M. Hernández-Ayón, and C. Bazán-Guzmán. 2010. Picoplankton dynamics during contrasting seasonal oceanographic conditions at a coastal upwelling station off Northern Baja California, Mexico. J. Plankton Res. **32:** 539-557, doi:10.1093/plankt/fbp148

Linacre, L. P., M. R. Landry, R. Cajal-Medrano, J. R. Lara-Lara, J. M. Hernández-Ayón, R. R. Mouriño-Pérez, E. García-Mendoza, and C. Bazán-Guzmán. 2012. Temporal dynamics of carbon flow trhough the microbial plankton community in a coastal upwelling system off northern Baja California, Mexico. Mar. Ecol. Prog. Ser. **461:** 31-46, doi:10.3354/meps09782

Li, W. K. W., D. V. Subba Rao, W. G. Harrison, J. C. Smith, J. J. Cullen, B. Irwin, and T. Platt. 1983. Autotrophic picoplankton in the tropical ocean. Science **219:** 292-295.

Liu, H., H. A. Nolla, and L. Campbell. 1997. *Prochlorococcus* growth rate and contribution to primary production in the equatorial and subtropical North Pacific Ocean. Aquat. Microb. Ecol. **12:** 39-47.

Liu, H., L. Campbell, M. R. Landry, H. A. Nolla, S. L. Brown, and J. Constantinou. 1998. *Prochlorococcus* and *Synechococcus* growth rates and contributions to production in the Arabian Sea during the 1995 Southwest and Northeast monsoons. Deep-Sea Res. II **45:** 2327-2352, http://dx.doi.org/10.1016/S0967-0645(98)00073-3

Longhurst, A. R. 1991. Role of the marine biosphere in the global carbon cycle. Limnol. Oceanogr. **36:** 1507-1526.

Lynn, R. J., and J. J. Simpson. 1987. The California Current System: the seasonal variability of its physical characteristics. J. Geophys. Res. **92:** 12,947-12,966.

McClain, C. R., J. R. Christian, S. R. Signorini, M. R. Lewis, I. Asanuma, D. Turk, and C. Dupont-Douchement. 2002. Satellite ocean-color observations of the tropical Pacific Ocean. Deep-Sea Res. II **49:** 2533-2560.

Menden-Deuer, S., and E. J. Lessard. 2000. Carbon to volume relationships for dinoflagellates, diatoms and other protist plankton. Limnol. Oceanogr. **45:** 569-579, doi:10.4319/lo.2000.45.3.0569

Monger, B. C., and M. R. Landry. 1993. Flow cytometric analysis of marine bacteria with Hoechst 33342. Appl. Environ. Microbiol. **59:** 905-911.

Monger, B. C., M. R. Landry, and S. L. Brown. 1999. Feeding selection of heterotrophic marine nanoflagellates based on the surface hydrophobicity of their picoplankton prey. Limnol. Oceanogr. **44**: 1917-1927.

Morel, A., and J-F. Berthon. 1989. Surface pigments, algal biomass profiles, and potential production of the euphotic layer: relationships reinvestigated in view of remote-sensing applications. Limonol. Oceanogr. **34:** 1545-1562.

Nelson, D. M., and M. R. Landry. 2011. Regulation of phytoplankton production and upper-ocean biogeochemistry in the eastern equatorial Pacific: Introduction to results of the Equatorial Biocomplexity project. Deep-Sea Res. II, 58: 277-283.

Ohman, M. D., K. A. Barbeau, P. J. S. Franks, R. Goericke, M. R. Landry, and A. J. Miller. 2013. Ecological transitions in a coastal upwelling ecosystem. Oceanogr. (in press)

Pasulka, A. L, M. R. Landry, D. A. A. Taniguchi, A. G. Taylor, and M. J. Church. 2013. Temporal dynamics of phytoplankton and heterotrophic protists at Station ALOHA. Deep-Sea Res II. 93: 44-57.

Pelaez, J., and J. A. McGowan. 1986. Phytoplankton pigment patterns in the California Current as determined by satellite. Limnol. Oceanogr. **31:** 927-950.

Platt, T. 1986. Primary productin of the ocean water column as a function of surface light intensity: algorithms for remote sensing. Deep-Sea Res. I **33:** 149-163.

Poulin, F., and P. J. S. Franks. 2010. Size-structured plankton ecosystems: constraints, controls and assembly instructions. J. Plankton. Res. 32: 1121-1130.

Raimbault, P., M. Rodier, and I. Taupier-Letage. 1988. Size fraction of phytoplankton in the Ligurian Sea and the Algerian Basin (Mediterranean Sea): Size distribution versus total concentration. Mar. Microb. Food Webs **3:** 1-7.

Raven, J. A. 1986. Physiological consequences of extremely small size for autotrophic organisms in the sea. *In.* T. Platt and W. K. W. Li [eds.], Photosynthetic picoplankton. Can. Bull. Fish. Aquat. Sci. **214:** 1-70.

Ryther, J. H. 1963. Components of ecosystems. p. 25. *In.* Riley [ed.], Marine Biology I. Am. Ins. Of Biol. Sci.

Ryther, J. H. 1969. Photosynthesis and fish production in the sea. The production of organic matter and its conversion to higher forms of life vary throughout the world ocean. Nature **166:** 72-78.

Saito, M. A., G. Rocap, and J. W. Moffett. 2005. Production of cobalt binding ligands in a *Synechococcus* feature at the Costa Rica upwelling dome. Limol. Oceanogr. **50:** 279-290.

Sanders, R. W. 1991. Mixotrophic protists in marine and freshwater ecosystems. Journal of Protozoology **38:** 76-81.

Selph, K. E., M. R. Landry, A. G. Taylor, E. -J. Yang, C. I. Measures, J. J. Yang, M. R. Stukel, S. Christensen, and R. R. Bidigare. 2011. Spatially-resolved taxon-specific phytoplankton production and grazing dynamics in relation to iron distributions in the Equatorial Pacific between 110 and 140°W. Deep-Sea Res. II **58**: 358-377.

Sherr, E. B., and B. F. Sherr. 1993. Preservation and storage of samples for enumeration of heterotrophic protists. p. 207-212. *In* P. Kemp [ed.], Handbook of Methods in Aquatic Microbial Ecology. Lewis.

Stoecker, D. K. 1999. Mixotrophy among dinoflagellates. J. Eukaryot. Microbiol. **46:** 397-401.

Strom S. L., B. Brahamsha, K. A. Fredrickson, J. K. Apple, and A. G. Rodriguez. 2012. A giant cell surface protein in *Synechococcus* WH8102 inhibits feeding by a dinoflagellate predator. Environ. Microbiol. **14:** 807-816.

Strom S., G. Wolfe, A. Slajer, S. Lambert, and J. Clough. 2003. Chemical defense in the microplankton. II. Inhibition of protist feeding by β–dimethylsulfoniopropionate (DMSP). Limnol. Oceanogr. **48**: 230–237.

Taylor, A. G., M. R. Landry, K. E. Selph, and E.-J. Yang. 2011. Biomass, size structure and depth distributions of the microbial community in the eastern equatorial Pacific. Deep-Sea Res. II **58:** 342-357, doi:10.1016/j.dsr2.2010.08.017

Taylor, A. G., R. Goericke, M. R. Landry, K. E. Selph, D. A. Wick, and M. J. Rodman. 2012. Sharp gradients in phytoplankton community structure across a frontal zone in the California Current Ecosystem. J. Plankton Res. **34:** 778-789, doi:10.1093/plankt/fbs036

Taylor, A. G., M. R. Landry, K. E. Selph, and J. J. Wokuluk. In review. Temporal and spatial patterns of microbial community biomass and composition in the southern California Current Ecosystem. Deep-Sea Res. II.

Thingstad, T. F. 1998. A theoretical approach to structuring mechanisms in the pelagic food web. Hydrobiologia **363:** 59-72.

Thomas, A. C., and P. T. Strub. 1990. Seasonal and interannual variability of pigment concentrations across a California Current frontal zone. J. Geophys. Res. **95:** 13,023-13,042.

Tilman, D. 1977. Resource competition between planktonic algae: An experimental and theoretical approach. Ecology **58**: 338-348.

Tilman, D. 1982. Resource Competition and Community Structure. Monogr. in Pop. Biol., **17**: 296 pp., Princeton Univ. Press, Princeton, N. J

Tilman, D., S. S. Kilham, and P. Kilham. 1982. Phytoplankton community ecology: the role of limiting nutrients. Ann. Rev. Ecol. Syst. **13:** 349-372.

Vaulot, D., M. Dominique, R. J. Olson, and S. W. Chisholm. 1995. Growth of *Prochlorococcus*, a photosynthetic prokaryote, in the Equatorial Pacific Ocean. Science **9:** 1480-1482, doi:10.1126/science.268.5216.1480

Venrick, E. L. 2000. Summer in the Ensenada Front: the distribution of phytoplankton species, July 1985 and September 1988. J. Plankton Res. **22**: 813–841.

Venrick, E. L. 2002. Floral patterns in the California Current System off southern California: 1990-1996. J. Mar. Res. **60:** 171-189.

Venrick, E. L. 2009. Floral patterns in the California Current: the coastal-offshore boundary zone. J. Mar. Res. **67:** 89-111, http://dx.doi.org/10.1357/002224009788597917

White, P. A., J. Kalff, J. B. Rasmussen, and J. M. Gasol. 1991. The effect of temperature and algal biomass on bacterial production and specific growth rate in freshwater and marine habitats. Microb. Ecol. **21:** 99-118, doi:10.1007/BF0253914

CONCLUSIONS

Understanding phytoplankton community biomass, structure and composition

One major challenge in the field of biological oceanography is investigating plankton processes occurring over large-spatial and small-time scales. Shipboard measurements are currently the only way to directly estimate the standing stocks and production rates of phytoplankton communities throughout the entire water column. Yet, due to constraints of ship speed and amount of area covered in a study, these types of measurements are greatly limited in their ability to resolve large-scale processes in a synoptic manner. Furthermore, direct observations are challenged by high operational costs, limited ship-time availability, and the high cost and long time required for sample processing. Because the phytoplankton base is central to understanding and modeling many processes in marine ecosystems, various attempts have been made to assess phytoplankton community biomass, structure and production based on a few key, remotely sensed parameters, such as total chlorophyll *a* (TChl) and water temperature (Platt, 1986; Morel and Berthon, 1989; Behrenfeld and Falkowski, 1997; Behrenfeld et al., 2005; Perez et al., 2005). While much progress has been made in these assessments, field data sets of direct measurements are relatively sparse for quantitatively testing or refining results from such approaches.

My dissertation provides quantitative observations that relate the phytoplankton community structure and composition, throughout the euphotic zone, to environmental parameters as well as a new mechanistic hypothesis to explain the

relationship between phytoplankton community size-structure and trophic state. These can help refine and test current methods used to estimate and model the phytoplankton community from remotely sensed platforms in the California Current Ecosystem (CCE) and adjacent ocean systems.

For my dissertation, I developed and applied an automated digital epifluorescence microscopy system, and semi-automated digital analysis system, to estimate the biomass, composition and size-structure of the microbial community in a high-throughput manor. Combined with flow cytometry (FCM), this system allowed me to make a fairly complete assessment of community biomass and structure. Using these methods, I was able to make carbon-based assessments of microbial communities, throughout the euphotic zone, in the CCE region, the eastern Equatorial Pacific (EEP) region, and across a strong frontal zone in the CCE. Lastly, I combined microbial community data from the CCE, EEP, Costa Rica Dome (CRD) upwelling region and eastern North Pacific Ocean (Stn. ALOHA) to investigate interregional commonalities and differences, and to test hypothesized relationships between phytoplankton size structure and total phytoplankton biomass along trophic gradients.

Variability in phytoplankton community structure with trophic state

Phytoplankton communities can be organized in terms of cell size, where it is understood that the structure is controlled by the complex interaction of physical/chemical (bottom-up, macro- and micro-nutrient/light limitation) and biological/trophic (top-down, grazing) forcing (Tilman et al., 1982; Hecky and

Kilham, 1988; Hutchins and Bruland, 1998; Calbet and Landry, 2004). Furthermore, the size structure and composition of phytoplankton communities has direct effects on food-web length and trophic transfer (Ryther, 1969; Fenchel, 1988; Iverson, 1990), and many biogeochemical processes, such as primary production, new production, carbon export from the euphotic zone and trace-element limitation (Eppley and Peterson, 1979; Longhurst, 1991; Falkowski, 1993; Falkowski et al., 2000; Turner, 2002; Behrenfeld et al., 2006). Hypotheses such as *step addition* (Chisholm, 1992; Thingstad, 1998) and *rising tide* (Barber and Hiscock, 2006) have emerged to provide mechanistic explanations for the observed patterns of phytoplankton community biomass and size structure across trophic states. Many size-structured ecosystem models have also been developed to help us better understand how the size structure and composition of these communities function presently, and how they may be altered by future environmental change (Moloney and Field, 1991; Armstrong, 1999; Poulin and Franks, 2010; Ward et al., 2013).

While these idealized theories and models do a relatively good job of explaining many observations of phytoplankton community size structure, they fail to capture all of the size-dependent patterns that I observed when investigating the variability of the phytoplankton community biomass, composition and size structure in response to increasing system richness. Most notably, in Chapter 4, I demonstrated a coherent pattern of decreasing picophytoplankton biomass over the range from poorer to richer trophic conditions, which I linked mechanistically to increasing activity of the microbial loop. This advances the recent suggestion of Goericke (2011) that the

coastal CCE decline of *Prochlorococcus* is due to increased grazing as well as previous experimental studies that have linked variability in picophytoplankton grazing dynamics to heterotrophic bacteria (e.g., Calbet and Landry, 1999; Landry and Kirchman, 2002; Brown et al., 2002). Current models do not capture this result because they either ignore the microbial loop or parameterize only its nutrient remineralization function. Therefore, they do not account for the additional grazing pressure on small picophytoplankton prey that can come into play when the microbial loop is stimulated by high primary production in richer environments. Including this variability in future models could provide further insights into the functioning of microbial food webs, especially in the richest environments, where this portion of the food web is considered relatively less important than in the open ocean.

Autotrophic carbon:chlorophyll a

Autotrophic carbon:chlorophyll *a* (C:Chl) ratios are highly variable and are affected by many factors, including light, nutrients, temperature, taxonomic composition, growth rate and time of day (Eppley et al., 1971; Eppley, 1972; Cullen, 1982; Geider, 1987). While C:Chl is rarely measured, both its values and its variability are important for modeling ocean ecosystem dynamics (Morel, 1988; Taylor et al., 1991; Sathyendranath et al., 2009; Wang et al., 2009), for interpreting biomass and production distributions with remote sensing techniques (Eppley et al., 1985; Falkowski, 1994; Antoine et al., 1996; Behrenfeld et al., 2005), and for estimating carbon flows from pigment-based experimental rate determinations (e.g.,

Landry et al., 2009; Stukel et al. 2013). Yet many investigations simply pick a published C:Chl value and apply it to samples collected throughout the water column or across spatially distinct regions.

In Chapter 1, I show that there was a coherent pattern of C:Chl variability with depth in the Eastern Equatorial Pacific (EEP) region and between cruises in two years. Furthermore, in Chapter 3, I found strong associations between C:Chl and nitracline depth for all depth strata sampled in the CCE region. Variations in nitracline depth within the CCE lead to a factor of two difference in mixed-layer C:Chl values, and another 2-fold difference, on average, between near-surface and deep euphotic zone values at a given location. Using these relationships, and applying the appropriate C:Chl value for the conditions in question, future modeling and remote sensing studies will be able to better account for the natural spatial and depth variability of phytoplankton community biomass, C:Chl and growth rates in the southern CCE region.

Diagnostic marker pigments and phytoplankton communities

Information on class-specific accessory pigments derived from high-pressure liquid chromatography (HPLC) analysis are another way to quantify the composition of phytoplankton communities (Jeffrey et al., 1997a; Jeffrey et al., 1997b). HPLC has the advantage of measuring larger volumes of water (liters) and, therefore, includes the contributions of rare forms that might be missed in microscopic analyses. Additionally, HPLC analysis is also more rapid, more precise, and more cost effective,

at least compared to microscopy. It is therefore often used in place of microscopy to compare phytoplankton compositions among different regions and their temporal changes. Microscopy-normalized, HPLC analyses have also become the standard for making class-specific inferences of phytoplankton growth and microzooplankton grazing rates from dilution experiments (e.g., Selph et al., 2011; Landry et al., 2011).

Using taxon-specific biomarkers, such as fucoxanthin for diatoms, peridinin for dinoflagellates and 19'-hexanolyoxyfucoxanthin for prymnesiophytes, HPLC analyses indicates which phytoplankton types are present and important in the community. To determine how each taxonomic group contributes to TChl, however, a matrix factorization program, such as CHEMTAX, must be employed (Mackey et al., 1996; Mackey et al., 1998). These iterative methods work by applying a user-supplied starting matrix of pigment:chlorophyll ratios for all of the plankton taxa one wishes to identify from the field data and then finds the minimum error between the starting matrix and the matrix of field data.

Such methods are prone to errors in several areas. First, they are extremely sensitive to the choice of starting matrix ratios, typically based on laboratory studies or literature values. Second, they assume that the starting matrix represents a defined phytoplankton community with the same physiological state and light history (Mackey et al., 1996). Third, they assume that the ratios of taxon-specific pigments to TChl are constant. Since physiological state and composition are common variables of interest in phytoplankton community studies, the above assumptions are almost impossible to meet or confirm in most applications (Goericke and Montoya, 1998).

Additionally, while pigment methods generally assume that given markers are specific for given taxa (e.g. peridinin for dinoflagellates and fucoxanthin for diatoms), diagnostic pigments are not present in all species for a group, nor is the pigment:chlorophyll ratio likely to be constant within taxa. For example, not all prasinophytes contain the diagnostic pigment prasinoxanthin (Egeland et al., 1995), and some prymnesiophytes do not contain19'-hexanoyloxyfucoxanthin (Jeffrey and Wright, 1994). Moreover, some species with given taxa may not contain the group-specific pigment, or contain the diagnostic pigments of other groups. For example, some dinoflagellates contain 19'-hexanolyoxyfucoxanthin instead of the dinoflagellate marker pigment peridinin (Tangen and Bjornland, 1981), and some dinoflagellates, haptophytes, chrysophytes, rphidophytes and bolidophytes have been shown to contain fucoxanthin, which was once considered unique to diatoms (Jeffrey and Wright, 2005). Lastly, while taxon-specific biomarkers can give inferences about the composition of phytoplankton communities, they provide little information about the size structure and biomass of the community due to variability in biomass:TChl ratios (Geider et al., 1996; Goericke and Montoya, 1998).

Because of these limitations, HPLC pigment-based analyses can sometimes underestimate dinoflagellates, which can be an important component of phytoplankton communities in many systems. For example, in the eastern Equatorial Pacific region my microscopy-based estimates indicate that dinoflagellates comprise an average of 38% of total phytoplankton carbon, while concentrations of peridinin were very low compared to fucoxanthin (3% vs. 8% of total monovinyl chlorophyll *a*, respectively)

(Selph et al., 2011). Additionally, in my Chapter 3 and 4, microscopy based estimates of phytoplankton biomass show that dinoflagellates can sometimes be a large fraction of the biomass in the CCE region where they dominate, or co-dominate with diatoms, at higher Chl *a* values. Yet findings from HPLC pigment-based analyses for the same system suggest that dinoflagellates contribute about 10-fold less to biomass than diatoms at high Chl *a* values (Goericke 2011). These contradictory results highlight the need to use caution when making assessments of the phytoplankton community based on pigments alone.

Going forward

Despite shortcomings of matrix-factorization methods, HPLC datasets still have many advantages that compliment microscopy and FCM analysis. One original goal that I had in this dissertation was to explore relationships between microscopy-based estimates of phytoplankton community biomass and contemporaneous CCE estimates from taxon-specific marker pigments that might be useful for predicting biomass and composition from combined pigment and FCM measurements. That remains a goal that I wish to pursue in post-doctoral research. Since I have now a data set that includes epifluorescence microscopy, FCM and HPLC data from many CCE/CalCOFI cruises, the next step will be to partition total chlorophyll *a* among the phytoplankton groups for which carbon biomass has been determined (*Prochlorococcus, Synechococcus,* diatoms, dinoflagellates, prymnesiophytes, cryptophytes, and "other"). This will be accomplished using the red fluorescence data

(RED), which represents chlorophyll *a* per cell that is collected and measured from each cell analyzed by digital micrographs and flow cytometry. By summing the amount of RED per taxonomic group and size class, in terms of biomass, I will be able to partition the percentage contribution of each group to TChl to test relationships between Chl *a* and taxon-specific accessory pigments for each group. For microscopy, fluorescence measurements are normalized to the exposure time of the image. For FCM, fluorescence is normalized to standardized beads. Using normalized RED to biomass relationships obtained by FCM for specific taxa, PRO and SYN, I will have estimates of how C:Chl ratios change with depth at given sampling stations, from which I hope to assess how the marker pigments for these groups change with depth (pigment:chlorophyll and pigment:carbon). Then, by making the assumption that C:Chl ratios vary systematically across all groups, I can begin to apply these relationships to eukaryotic phytoplankton to determine total community biomass based on TChl.

Once this work is finalized, the relationships derived from carbon estimates obtained from digital microscopy and FCM, which come from a subset of 10 of the 77 CalCOFI grid stations, will be applied to the full-station HPLC pigment data set, to investigate broad-scale spatial and seasonal patterns of phytoplankton biomass and composition in the CalCOFI grid. The hope for the future is this will provide a more rapid approach for assessing total phytoplankton community biomass across the entire CCE region without the need to sustain a large effort in microscopical analysis. Additionally, any meaningful relationships derived from this method might be usefully

applied to historical samples from the CalCOFI program when microscopy samples were not taken, to investigate relationships and changes of phytoplankton community biomass to past environmental conditions in the CCE.

References

Antoine, D., André, J.-M., Morel, A., 1996. Oceanic primary production 2. Estimation at global scale from satellite (coastal zone color scanner) chlorophyll. Global Biogeochemical Cycles 10, 57-69.

Armstrong, R.A., 1999. Stable model structures for representing biogeochemical diversity and size spectra in plankton communities. Journal of Plankton Research 21, 445-464.

Barber, R.T., Hiscock, M.R., 2006. A rising tide lifts all phytoplankton: growth response of other phytoplankton taxa in diatom-dominated blooms. Global Biogeochemical Cycles 20, GB4S03. doi:10.1029/2006GB002726.

Behrenfeld, M.J., P.G. Falkowski. 1997. Photosynthetic Rates Derived from Satellite-Based Chlorophyll Concentration. Limnology and Oceanography 42, 1-20.

Behrenfeld, M.J., Boss, E., Siegel, D.A. Shea, D.M., 2005. Carbon-based ocean productivity and phytoplankton physiology from space. Global Biogeochem. Cycles 19, 1-14.

Behrenfeld, M.J., O'Malley, R.T., Siegel, D.A., McClain, C.R., Sarmiento, J.L., Feldman, G.C., Milligan, A.J., Falkowski, P.G., Letelier, R.M., Boss, E.S., 2006. Climate-driven trends in contemporary ocean productivity. Nature 444, 752-755.

Brown, S.L., Landry, M.R., Christensen, S., Garrison, D., Gowing, M.M., Bidigare, R.R., Campbell, L., 2002. Microbial community dynamics and taxon-specific phytoplankton production in the Arabian Sea during the 1995 monsoon seasons. Deep-Sea Research II 49, 2345-2376.

Calbet, A., Landry, M.R., 1999. Mesozooplankton influences on the microbial food web: Direct and indirect trophic interactions in the oligotrophic open ocean. Limnology and Oceanography 44, 1370-1380.

Calbet, A., Landry, M.R., 2004. Phytoplankton growth, microzooplankton grazing, and carbon cycling in marine systems. Limnology and Oceanography 49, 51-57.

Chisholm, S.W., 1992. Phytoplankton size. In: Falkowski, P. G., Woodhead, A. D. (Eds.), *Primary Productivity and Biogeochemical Cycles in the Sea.* Plenum, New York, pp. 213-237.

Cullen, J.J., 1982. The deep chlorophyll maximum: Comparing vertical profiles of chlorophyll a. Canadian Journal of Fisheries and Aquatic Sciences 39, 791-803.

Egeland, E.S., Eikrem, W., Throndesn, J., Wilhelm, C., Zapata, M. Liaaen-Jenson, S., 1995. Carotenoids from further prasinophytes. Biochem. Syst. Ecol. 23, 747-755.

Eppley, R.W., Carlucci, A.F., Holm-Hansen, O., Kiefer, D., McCarthy, J.J., Venrick, E., Williams, P.M., 1971. Phytoplankton growth and composition in shipboard cultures supplied with nitrate, ammonium, or urea as the nitrogen source. Limnology and Oceanography 16, 741-751.

Eppley, R.W., 1972. Temperature and phytoplankton growth in the sea. Fishery Bulletin (U.S.) 70, 1063-1085.

Eppley, R.W., Stewart, E., Abbott, M.R., Heyman, U., 1985. Estimating ocean primary production from satellite chlorophyll. Introduction to regional differences and statistics for the Southern California Bight. Journal of Plankton Research 7, 57-70.

Eppley, R.W., Peterson, B.J., 1979. Particulate organic matter flux and planktonic new production in the deep ocean. Nature 282, 677-680.

Falkowski, P.G., 1993. The role of phytoplankton photosynthesis in global biogeochemical cycles. Photosynthesis Research 39, 235-258.

Falkowski, P.G., 1994. The role of phytoplankton photosynthesis in global biogeochemical cycles. Photosynthesis Research 39, 235-258.

Falkowski, P.G., Scholes, R.J., Boyle, E., Canadell, J., Canfield, D., Elser, J., Gruber, N., Hibbard, K., Hogberg, P., Linder, S., Mackenzie, F.T., Morre III, B., Pedersen, T., Rosenthall, Y., Seitzinger, S., Smetacek, V., Steffen, W., 2000. The global carbon cycle: a test of our knowledge of earth as a system. Science 290, 291-296.

Fenchel, T., 1988. Marine plankton food chains. Ann. Rev. Syst. 19, 19-38.

Geider, R.J., 1987. Light and temperature dependence of the carbon to chlorophyll a ratio in microalgae and cyanobacteria: Implications for physiology and growth of phytoplankton. New Phytologist 106, 1-34.

Geider, R.J, McIntyre, H.L., Kana, T.M., 1996. Dynamic model of phytoplankton growth and acclimation: responses of the balanced growth rate and the chlorophyll a : carbon ratio to light, nutrient-limitation and temperature. Marine Ecology progress Series 148, 187-200.

Goericke, R., Montoya, J., 1998. Estimating the contribution of microalgal taxa to chlorophyll a in the field - variations of pigment ratios under nutrient- and light-limited growth. Marine Ecology Progress Series 169, 97 - 112.

Goericke, R., 2011. The structure of marine phytoplankton communities—patterns, rules and mechanisms. CalCOFI Reports 52, 182-197.

Hecky, R.E., Kilham, P., 1988. Nutrient limitation of phytoplankton in freshwater and marine environments: a review of recent evidence on the effects of enrichment. Limnology and Oceanography 33, 796-822.

Hutchins, D.A., Bruland, K.W., 1998. Iron-limited diatom growth and Si:N uptake ratios in a coastal upwelling regime. Nature 393, 561-564.

Iverson, R.L., 1990. Control of marine fish production. Limnology and Oceanography 35, 1593-1604.

Jeffrey, S.W., Wright, S.W., 1994. Photosynthetic pigments in the Haptophyta. In: Green J.C., Leadbeater, B.S.C. (Eds), The haptophyte algae. Clarendon Press, Oxford, pp. 111-132.

Jeffrey, S.W., Mantoura, R.F.C., Wright, S.W., 1997a, (eds) Phytoplankton pigments in oceanography: guidelines to modern methods. UNESCO, Paris.

Jeffrey, S.W., Mantours, R.F.C., Bjornland, T., 1997b. Data for the identification of 47 key phytoplankton pigments. In: Jeffrey, S.W., Mantoura, R.F.C., Wright, S.W. (eds), Phytoplankton pigments in oceanography: Guidelines to modern methods., UNESCO, Paris, pp. 447.

Jeffrey, S.W. and Wright, S.W., 2005. Photosynthetic pigments in marine microalgae. In: Subba Rao, D.V. (Ed), *Algal Cultures, Analogues of Blooms and Applications.* Science Publishers, New Hampshire, pp. 33-90.

Landry, M.R., Kirchman, D.L., 2002. Microbial community structure and variability in the tropical Pacific. Deep-Sea Research II 49, 2669-2693.

Landry, M.R., Ohman, M.D., Goericke, R., Stukel, M.R., Tsyrklevich, K., 2009. Lagrangian studies of phytoplankton growth and grazing relationships in a coastal upwelling ecosystem off Southern California. Progress in Oceanography 83, 208-216.

Landry, M.R., Selph, K.E., Taylor, A.G., Decima, M., Balch, W.M., Bidigare, R.R., 2011. Phytoplankton growth, grazing and production balances in the HNLC equatorial Pacific. Deep-Sea Research II 58, 524-535.

Longhurst, A.R., 1991. Role of the marine biosphere in the global carbon cycle. Limnology and Oceanography 36, 1507-1526.

Mackey, M.D., Mackey, D.J., Higgins, H.W., Wright, S.W., 1996. CHEMTAX—a program for estimating class abundances from chemical markers: application to HPLC measurements of phytoplankton. Marine Ecology Progress Series 144, 265-283.

Mackey, D.J., Higgins, H.W., Mackey, M.D., Holdsworth, D., 1998. Algal class abundances in the western equatorial Pacific: Estimation from HPLC measurements of chloroplast pigments using CHEMTAX. Deep-Sea Research I 45, 1441-1468.

Moloney, C.I., Field, J.G., 1991. The size-based dynamics of plankton food webs I. A simulation model of carbon and nitrogen flows. Journal of Plankton Research 13, 1003-1038.

Morel, A., 1988. Optical modeling of the upper ocean in relation to its biogenous matter content (Case I Waters). Journal of Geophysical Research 93, 10,749-10,768.

Morel, A., Berthon, J.-F., 1989. Surface Pigments, Algal Biomass Profiles, and Potential Production of the Euphotic Layer: Relationships Reinvestigated in View of Remote-Sensing Applications. Limnology and Oceanography 34, 1545-1562.

Perez, V., Fernandez, E., Maranon, E., Serret, P., Garcia-Soto, C., 2005. Seasonal and interannual variability of chlorophyll a and primary production in the Equatorial Atlantic: in situ and remote sensing observations. Journal of Plankton Research 27, 189-197.

Platt, T., 1986. Primary production of the ocean water column as a function of surface light intensity: algorithms for remote sensing. Deep-Sea Research 33, 149-163.

Poulin, F.J., Franks, P.J.S., 2010. Size-structured planktonic ecosystems: constraints, controls and assembly instructions. Journal of Plankton Research 32, 1121-1130.

Ryther, J.H., 1969. Photosynthesis and fish production in the sea. The production of organic matter and its conversion to higher forms of life vary throughout the world ocean. Nature 166, 72-78.

Sathyendranath, S., Stuart, V., Nair, A., Oka, K., Nakane, T., Bouman, H., Forget, M.-H., Maass, H., Platt, T., 2009. Carbon-to-chlorophyll ratio and growth rate of phytoplankton in the sea. Marine Ecology Progress Series 383, 73-84.

Selph, K.E., Landry, M.R., Taylor, A.G., Yang, E.-J., Measures, C.I., Yang, J., Stukel, M.R., Christensen, S., Bidigare, R.R., 2011. Spatially-resolved taxon-specific phytoplankton production and grazing dynamics in relation to iron distributions in the Equatorial Pacific between 110 and 140°W. Deep-Sea Research II 58, 358-377.

Stukel, M.R., Décima, M., Selph, K.E., Taniguchi , D.A.A., Landry, M.R., 2013. The role of Synechococcus in vertical flux in the Costa Rica upwelling dome. Progress in Oceanography, http://dx.doi.org/10.1016/j.pocean.2013.04.003.

Tangen, K. and Bjornland, T., 1981. Observations on pigments and morphology of Gyrodinium aureolum Hulburt, a marine dinoflagellate containing 19'-hexanoyloxyfucoxanthin as the main carotenoid. Journal of Plankton Research 3, 389-401.

Taylor, A.H., Watson, A.J., Ainsworth, M., Robertson, J.E., Turner, D.R., 1991. A modeling investigation of the role of phytoplankton in the balance of carbon at the surface of the north Atlantic. Global Biogeochemical Cycles 5, 151-171.

Thingstad, T.F., 1998. A theoretical approach to structuring mechanisms in the pelagic food web. Hydrobiologia 363, 59-72.

Tilman, D., Kilham, S.S., Kilham, P., 1982. Phytoplankton community ecology: the role of limiting nutrients. Ann. Rev. Ecol. Syst. 13, 349-372.

Turner, J.T., 2002. Zooplankton fecal pellets, marine snow and sinking phytoplankton blooms. Aquatic Microbial Ecology 27, 57-102.

Wang, X., Le Borgne, R., Murtugudde, R., Busalacchi, A.J., Behrenfeld, M., 2009. Spatial and temporal variability of the phytoplankton carbon to chlorophyll ratio in the equatorial Pacific: A basin-scale modeling study. Journal of Geophysical Research 114, C07008. doi:10.1029/2008JC004942.

Ward, B., Dutkiewicz, S., Follows, M.J., 2013. Modeling spatial and temporal patterns in size-structured marine plankton communities: top-down and bottom-up controls. Journal of Plankton Research, doi:10.1093/plankt/fbt097.